ADVANCES IN
QUANTUM CHEMISTRY

RECENT ADVANCES IN COMPUTATIONAL CHEMISTRY

EDITOR-IN-CHIEF

PER-OLOV LÖWDIN

PROFESSOR EMERITUS

DEPARTMENT OF QUANTUM CHEMISTRY
UPPSALA UNIVERSITY
UPPSALA, SWEDEN

AND

QUANTUM THEORY PROJECT
UNIVERSITY OF FLORIDA
GAINESVILLE, FLORIDA

EDITORS

JOHN R. SABIN AND MICHAEL C. ZERNER

QUANTUM THEORY PROJECT
UNIVERSITY OF FLORIDA
GAINESVILLE, FLORIDA

GUEST EDITORS

JACEK KARWOWSKI

DEPARTMENT OF PHYSICS
NICHOLAS COPERNICUS UNIVERSITY
TORUN, POLAND

MATI KARELSON

DEPARTMENT OF CHEMISTRY
UNIVERSITY OF TARTU
TARTU, ESTONIA

VOLUME 28

ACADEMIC PRESS

A Division of Harcourt Brace & Company

San Diego London Boston New York Sydney Tokyo Toronto

This book is printed on acid-free paper. ♾

Academic Press
a division of Harcourt Brace & Company
525 B Street, Suite 1900, San Diego, California 92101-4495, USA
http://www.apnet.com

Academic Press Limited
24-28 Oval Road, London NW1 7DX, UK
http://www.hbuk.co.uk/ap/

International Standard Book Number: 0-12-034828-4

PRINTED IN THE UNITED STATES OF AMERICA
97 98 99 00 01 02 QW 9 8 7 6 5 4 3 2 1

Contributors

Numbers in parentheses indicate the pages on which the authors' contributions begin.

Ad van der Avoird (119) Institute of Theoretical Chemistry, NSR Center, University of Nijmegen, Nijmegen, The Netherlands

Maria Barysz (257) Max-Planck-Institut für Astrophysik, Garching, Germany

Borislava Batandjieva (219) Department of Physical Chemistry, Faculty of Science, Comenius University, SK-84215 Bratislava, Slovakia

Dorota Bielińska-Wąż (159) Instytut Fizyki, Uniwersytet Mikolaja Kopernika, 87-100 Torun, Poland

Sylvio Canuto (89) Instituto de Física, Universidade de São Paulo, 05389-970 São Paulo, Brazil

Ivan Cernušák (219) Department of Physical Chemistry, Faculty of Science, Comenius University, SK-84215 Bratislava, Slovakia

J. Collis (319) Department of Computer Science, The Queen's University, BelfastBT7 1NN, Northern Ireland

Kaline Coutinho (89) Instituto de Física, Universidade de São Paulo, 05389-970 São Paulo, Brazil

G. H. F. Diercksen (189) Max-Plank Institut für Astrophysik, D-85740 Garching, Germany

Włodzisław Duch (329) Department of Computer Methods, Nicholas Copernicus University, 87-100 Torun, Poland

P. W. Fowler (247) Department of Chemistry, University of Exeter, Exeter 4QD, United Kingdom

J. M. García de la Vega (189) Departamento de Química Física Aplicada, Facultad de Ciencias, Universidad Autonoma de Madrid, 28049 Madrid, Spain

Tino G. A. Heijmen (119) Institute of Theoretical Chemistry NSR Center, University of Nijmegen, Nijmegen, The Netherlands

Kenneth Irving (293) MTC-Lab, University of Uruguay, 11800 Montevideo, Uruguay

Rudolf Janoschek (235) Institut für Theoretische Chemie, Karl-Franzens-Universitüt Graz, A-8010 Graz, Austria

Bogumił Jeziorski (171) Department of Chemistry, University of Warsaw, 02-093 Warsaw, Poland

Mati Karelson (141) Department of Chemistry, University of Tartu, Tartu EE2400, Estonia

Jacek Karwowski (159) Instytut Fizyki, Uniwersytet Mikolaja Kopernika, 87-100 Torun, Poland

R. Kelterbaum (273) UPR 139 du CNRS, Laboratoires de Chimie Théorique et de Chimie Quantique, Université Louis Pasteur, 67008 Strasbourg, France

Martina Kieninger (293) MTC-Lab, University of Uruguay, 11800 Montevideo, Uruguay

P. L. Kilpatrick (345) Department of Computer Science, The Queen's University of Belfast, Belfast BT7 1NN, Northern Ireland

S. Klein (273) UPR 139 du CNRS, Laboratoires de Chimie Théorique et de Chimie Quantique, Université Louis Pasteur, 67008 Strasbourg, France

M. Klobukowski (189) Department of Chemistry, University of Alberta, Edmonton, Alberta T6G 2G2, Canada

Jacek Kobus (1) Instytut Fizyki, Uniwersytet Mikolaja Kopernika, 87-100 Torun, Poland

E. Kochanski (273) UPR 139 du CNRS, Laboratoires de Chimie Théorique et de Chimie Quantique, Université Louis Pasteur, 67008 Strasbourg, France

Tatiana Korona (171) Department of Chemistry, University of Warsaw, 02-093 Warsaw, Poland

C. Lavín (205) Departamento de Química Física, Facultad de Ciencias, Universidad de Valladolid, 47005 Valladolid, Spain

A. C. Legon (247) Department of Chemistry, University of Exeter, Exeter 4QD, United Kingdom

Xiangzhu Li (15) Department of Applied Mathematics, University of Waterloo, Waterloo, Ontario N2L 3G1Canada

S. Loughlin (319) Department of Computer Science, The Queen's University, Belfast BT7 1NN, Northern Ireland

I. Martin (205) Departamento de Química Física, Facultad de Ciencias, Universidad de Valladolid, 47005 Valladolid, Spain

Ingrid Miadoková (219) Department of Physical Chemistry, Faculty of Science, Comenius University, SK-84215 Bratislava, Slovakia

D. Moncrieff (47) Supercomputer Computations Research Institute, Florida State University, Tallahassee, Florida, 32306

Robert Moszynski (119, 171) Department of Chemistry, University of Warsaw, 02-093 Warsaw, Poland

Florian Müeller-Plathe (81) Laboratorium für Physikalische Chemie, Eidgenössische Technische Hochschule, Zürich, CH-8092 Zürich, Switzerland

Josef Paldus (15) Department of Applied Mathematics, University of Waterloo, Waterloo, Ontario N2L 3G1, Canada

S. A. Peebles (247) Department of Chemistry, University of Exeter, Exeter 4QD, United Kingdom

E. Pérez-Romero (33) Departamento de Química Física, Universidad de Salamanca, Salamanca, 37008, Spain

A. Rahmouni (273) UPR 139 du CNRS, Laboratoires de Chimie Théorique et de Chimie Quantique, Université Louis Pasteur, 67008 Strasbourg, France

M. M. Rohmer (273) UPR 139 du CNRS, Laboratoires de Chimie Théorique et de Chimie, Quantique, Université Louis Pasteur, 67008 Strasbourg, France

John R. Sabin (107) Department of Physics, University of Florida, Gainesville, Florida, 32611

N. S. Scott (345) Department of Computer Science, The Queen's University of Belfast, Belfast BT7 1NN, Northern Ireland

F. J. Smith (319) Department of Computer Science, The Queen's University of Belfast, Belfast BT7 1NN, Northern Ireland

M. Sullivan (319) Department of Computer Science, The Queen's University of Belfast, Belfast BT7 1NN, Northern Ireland

B. T. Sutcliffe (65) Department of Chemistry, University of York, Heslington, England, York YO1 5DD

L. M. Tel (33) Departamento de Química Física, Universidad de Salamanca, Salamanca, 37008 Spain

Miroslav Urban (257) Department of Physical Chemistry, Comenius University, 84215 Bratislava, Slovak Republic

C. Valdemoro (33) Instituto de Matemáticas y Física Fundamental, Consejo Superior de Investigaciones Científicas, Madrid, 28006 Spain

Oscar N. Ventura (293), MTC-Lab, University of Uruguay, 11800 Montevideo, Uruguay

S. Wilson (47) Rutherford Appleton Laboratory, Chilton, Oxfordshire OX11 0QX, England

Paul E. S. Wormer (119) Institute of Theoretical Chemistry, NSR Center, University of Nijmegen, Nijmegen, The Netherlands

B. G. Wybourne (311) Instytut Fizyki, Uniwersytet Mikolaja Kopernika, 87-100 Torun, Poland

Preface

This volume collects papers written to honor Geerd H. F. Diercksen on his 60th birthday. Most of the papers were presented at the symposium Recent Advances in Computational Quantum Chemistry (Munich, 29–30 March 1996) organized by a group of friends of Geerd and attended by 33 of his present and former collaborators.

Geerd Diercksen belongs to the small group of scientists who managed to grasp the ideas developed mainly by physicists and mathematicians during the first three decades after the creation of quantum mechanics and to apply them to the interpretation of the fundamental problems of chemistry. Thus, according to standard classification schemes, he should be considered one of the founders of quantum chemistry. In fact, most of his nearly 200 published papers are concerned with quantum chemistry. Geerd's research includes studies on the structure and stability of hydrogen-bonded and Van der Waals dimers and small clusters, vibrational and rotational spectra of diatomic and triatomic molecules, static electric properties of molecules, properties and dynamics of atoms and molecules in their excited (especially Rydberg) states, and properties of molecules in solutions and adsorbed on surfaces. His results are essential in molecular and atomic physics, astrophysics, and biochemistry. For example, his highly accurate calculations of the nuclear quadrupole moment of beryllium led to a reassignment of the beryllium abundance in the universe, with consequences for the model of the early universe; his astrophysically stimulated studies on the rotational spectrum of HCO^+ led to correct identification of some lines in the microwave spectrum of interstellar molecular clouds and, further, to the search and discovery of some other molecules both in the laboratory and in interstellar space.

No simple classification schemes apply in the case of Geerd Diercksen. His scientific activity, driven, as in the case of the Renaissance scholars, by a real research curiousity, covers a very broad range of human knowledge, from the photodynamic therapy of cancer to artificial intelligence, computational physics, and computer science. In particular, his contribution to this last area is of high significance. He was the first to combine the methods of quantum chemistry, neural networks, and symbolic and numerical computation to build "intelligent software," a user-friendly environment in computational molecular physics. This system, called OpenMol (Open Molecular Software), is currently being developed under his guidance.

Geerd Diercksen's most valuable contribution, however, is in organizing the quantum chemistry community into its present shape. In 1969, with a group of young quantum chemists who even then appreciated the importance of large-

scale computations for development of quantum chemistry, he organized the first Strassbourg Seminar on Computational Problems in Quantum Chemistry. Since then, the seminars, held every second year, have continued to record and stimulate the development of quantum chemistry. A strong belief that the development of computational methods is the most significant factor in the progress of science pushed Geerd toward founding *Computer Physics Reports*, acting as the principal editor of *Computer Physics Communications*, and being a member of the editorial board of *Physics Reports*. Among his other achievements in creating conditions for an exchange of scientific ideas, one should mention his organizing six NATO Advanced Study Institutes. In addition, he has had seven Alexander von Humboldt fellows in his group, and four senior scientists received the Alexander von Humboldt award on his nomination. His high scientific qualifications have been recognized by the world scientific community. The international awards he has received include the Canada–Germany Research (Av Humboldt) Award in 1993/1994 and that of the Japan Society for the Promotion of Science in 1987.

Nearly all of his scientific life, Geerd has been associated with the Max-Planck-Institut für Astrophysik in Garching and has taken full advantage of the conditions offered by this institution to a scientist. Among his visitors were always many Eastern Europeans. For several decades, when the degree of isolation of Eastern Europe from the rest of the world was difficult to imagine for colleagues living in open Western societies, dozens of scientists from Poland, Slovakia, Bohemia, Estonia, Lithuania, and Latvia were supported by Geerd's personal grants, were encouraged to use the rich facilities of the Max Planck Institute, and were given opportunities to make direct contact with the leading scientists in their field in order to integrate with the external world, grasp new ideas, and absorb Western culture. And all of this was given for nothing, no one was asked to do anything specific. Scientists could work on their own projects, join projects run by others, start common projects, or just exchange ideas. Most of the visitors have never published a single paper with Geerd, but everyone was enriched by the experience.

Geerd has managed to combine the best of the traditional teachers and modern managers of science. His teaching activity extends far beyond professional issues. By his own example he has demonstrated the importance of personal integrity in scientific achievement. This was experienced directly by all his visitors. All of us, independent of our status, enjoyed innumerable visits to the Diercksen's house. And here we should pay tribute to Christel, Geerd's wife, for her unlimited hospitality, for her ability to bring together people with such diverse traditions and cultural backgrounds, and, last but not least, for the delicious meals.

JACEK KARWOWSKI AND JOHN R. SABIN

Conference Participants

Maria Barysz, Silesian University, Institute of Chemistry, Katowice, Poland
Ivan Cernusak, Katedra Fyzikalnej Chemie, Prirodovedeckej Fakulty UK, Bratislava, Slovakia
Geerd H. F. Diercksen, Max-Planck-Institut für Astrophysik, Garching bei München, Germany
Włodzisław Duch, Department of Computer Methods, Nicholas Copernicus University, Toruń, Poland
Norbert Flocke, Institute of Physics, Nicholas Copernicus University, Toruń, Poland
Patrick Fowler, Department of Chemistry, University of Exeter, Exeter, England
Karol Grudziński, Max-Planck-Institut für Astrophysik, Garching bei München, Germany
Bernd Hess, Institut für Physikalische Chemie, Universität Bonn, Bonn, Germany
Bogumił Jeziorski, Department of Chemistry, University of Warsaw, Warsaw, Poland
Mati Karelson, Department of Chemistry, University of Tartu, Tartu, Estonia
Jacek Karwowski, Institute of Physics, Nicholas Copernicus University, Toruń, Poland
Vladimir Kellöe, Department of Physical Chemistry, Comenius University, Bratislava, Slovakia
Mariusz Kłobukowski, Department of Chemistry, University of Alberta, Edmonton, Alberta, Canada
Jacek Kobus, Institute of Physics, Nicholas Copernicus University, Toruń, Poland
Elise Kochanski, Institut de Chimie, Universite Louis Pasteur, Strasbourg, France
Wolfgang Krämer, Max-Planck-Institut für Astrophysik, Garching bei München, Germany
Leif Laaksonen, Finnish State Computer Centre, Centre for Scientific Computing, Espoo, Finland
Robert G. Moszyński, Department of Chemistry, University of Warsaw, Warsaw, Poland
Florian Müller-Plathe, Laboratorium für Physikalische Chemie, ETH Zentrum, Zurich, Switzerland
Willem C. Nieuwpoort, Laboratory of Chemical Physics, University of Gröningen, Gröningen, Holland
Jens N. Oddershede, Department of Chemistry, Odense University, Odense, Denmark

Björn O. Roos, University of Lund, Chemical Center, Theoretical Chemistry, Lund, Sweden

John R. Sabin, University of Florida, Quantum Theory Project, Gainesville, Florida, USA

Andrzej J. Sadlej, Chemical Center, Theoretical Chemistry, University of Lund, Lund, Sweden

Stephan P. Sauer, Department of Chemistry, Odense University, Odense, Denmark

Erich Schreiner, Max-Planck-Institut für Astrophysik, Garching bei München, Germany

N. Stan Scott, The Queen's University of Belfast, Department of Computer Science, Belfast, Northern Ireland

F. Jack Smith, MRIA, The Queen's University of Belfast, School of Electrical Engineering and Computer Science, Belfast, Northern Ireland

Brian T. Sutcliffe, University of York, Department of Chemistry, Heslington, York, England

Miroslav Urban, Comenius University, Department of Physical Chemistry, Bratislava, Slovakia

Carmela Valdemoro, Instituto de Ciencia de Materiales, CSIC, Madrid 6, Spain

Oscar N. Ventura, Universidad de la Republica, Facultad de Quimica, Montevideo, Uruguay

Stephen Wilson, Computing and Information Systems Department, Rutherford Appleton Laboratory, Chilton, England

Introductory Remarks

At an occasion like this there are many things that should not be said, there are some things that may be said, and there is one thing that must be said: THANK YOU.

I would like to start by thanking my colleagues who are responsible for talking me into having this symposium on the occasion of my 60th birthday and for organizing it: Drs. Maria Barysz and Jacek Karwowski have taken care of the organization of the scientific part, Erich Schreiner has looked after the local arrangements, and Angelika Fröschl is responsible for the arrangement at this place.

I would like to say a deeply felt thank you to all of you for taking the time and effort to participate in this symposium and for contributing to it. Both Christel and I very much enjoy having you here.

There are institutions and individuals to whom I owe my thanks. The research has been funded for over thirty years by the Max-Planck-Gesellschaft. A very creative research environment has been provided by the Max-Planck-Institut für Astrophysik. The credit for the work is shared by many individuals: technical staff members, research students, postdoctoral fellows, and many colleagues. The research would not have been possible without their inspiration, encouragement, and hard work.

Basic research is sponsored by society, by the rich and the poor alike, for no immediate return. We should be aware of it always, we should be thankful for it, and we should respond to it as we are expected. As Nicolas Copernicus expressed it in *On the Revolutions, Book One*, ". . .men [and women] of learning. . .applying ourselves to seeking out the truth in the things as far as that has been permitted by God to human reason."

My strongest supporter for more than thirty years is my wife. I am very grateful to her for taking care, day by day, of the things most important to both of us, namely our family, and for providing me, most of the time, with the freedom to pursue my hobby: exploring nature.

Finally, let us be reminded: Research can be carried on by others, often even more successfully, and, if it is good research, it will be. But life is limited, and often much too limited. Therefore: let's enjoy both work and life, and life and work, at the right time and in proper proportion.

GEERD H. F. DIERCKSEN
MUNICH, MARCH 1996

Diatomic Molecules: Exact Solutions of HF Equations

Jacek Kobus

Instytut Fizyki
Uniwersytet Mikołaja Kopernika
ul. Grudziądzka 5/7, 87-100 Toruń, Poland

Abstract

An overview of the development of the finite difference Hartree-Fock method is presented. Some examples of it are given: construction of sequences of highly accurate basis sets, generation of exact solutions of diatomic states, CI with numerical molecular orbitals, Dirac-Hartree-Fock method based on a second-order Dirac equation.

ADVANCES IN QUANTUM CHEMISTRY, VOLUME 28

0065-3276/97 $25.00

1. Introduction

A decade ago Laaksonen *et al.* published a paper giving an outline of the finite difference (FD) (or numerical) Hartree-Fock (HF) method for diatomic molecules and several examples of its application to a series of molecules (1). A summary of the FD HF calculations performed until 1987 can be found in (2). The work of Laaksonen *et al.* can be considered a second attempt to solve numerically the HF equations for diatomic molecules exactly. The earlier attempt was due to McCullough who in the mid 1970s tried to tackle the problem using the partial wave expansion method (3). This approach had been extended to study correlation effects, polarizabilities and hyperfine constants and was extensively used by McCullough and his coworkers (4–6). Heinemann *et al.* (7–9) and Sundholm *et al.* (10,11) have shown that the finite element method could also be used to solve numerically the HF equations for diatomic molecules.

The success of quasirelativistic (QR) methods in accounting for major one-particle relativistic effects in atoms (12–15) made it tempting to describe the relativity in molecules in a similar fashion . Because of the complicated form of the quasirelativistic potential the exact solution of the molecular QR HF equations could not be performed using an algebraic approach but a fully numerical scheme was required. That was the prime motivation of the present author in getting interested (in the late 1980s) in the FD HF method in order to turn it into a QR HF method for diatomic molecules. From the computational point of view the FD HF method is a rather demanding one. Thus in order to tackle the QR problem an efficient scheme for solving the nonrelativistic HF equations for systems containing heavy, relativistic, atoms had to be addressed first.

This paper gives an overview of the developments of the FD HF method and some examples of its application. It is organized as follows. The current state of the FD HF method is given in section 2. Its application to the development of sequences of *even-tempered* gaussian basis sets is discussed in section 3. Section 4 shows the possibility of performing configuration interaction (CI) calculations using numerical one-particle basis sets composed of exact numerical HF orbitals augmented by a corresponding set of virtual orbitals. In section 5 the Th_2^{179+} one-electron system is used to show the influence of the finite charge distribution of the nuclei on the potential energy curve. Also the usefulness of the exact numerical solver of the one-electron diatomic systems for the development of the exchange-correlation potential functions of the density functional theory is mentioned. The possibility of using the FD HF machinery to solve exactly the Dirac-Hartree-Fock equations for diatomic molecules and devising a FD HF method for the linear polyatomic molecules is discussed in section 6.

2. FD HF method development

In general the Hartree-Fock equations for any molecular system form a set of 3-dimensional partial differential equations for orbitals, Coulomb and exchange potentials. In the case of diatomic molecules the prolate spheroidal coordinate system can be used to describe the positions of electrons and one of the coordinates (the azimuthal angle) can be treated analytically. As a result one is left with a problem of solving second order partial differential equations in the other two variables. (η and ξ).

Within the FD approach high order finite difference formulae are used to discretize the partial differential equations and transform them into a set of linear equations with large and sparse matrices. Thus the efficiency of the scheme depends primarily on the efficacy of the linear equation solver used and on the number of the unknowns, i.e. the values of the orbitals and the potential functions at the grid points. The linear equations are solved using the successive overrelaxation (SOR) iterative method or its vectorizable/paralellizable variant, namely, the multicolour SOR (MCSOR) method. Both methods have proved to be stable and efficient (Table 1) (16, 17). Davstad has shown that a multigrid conjugate residual method can also be used as the solver of such a system of equations (18).

Table 1
Performance of the (MC)SOR algorithm on a range of computers. A single processor CPU times (in seconds) required to perform 100 (MC)SOR iterations on a 294×298 grid are given with the corresponding MFLOPS rates in parentheses. Note that the MCSOR scheme should not be used for calculations performed on a single scalar processor.

	Cray $Y-MP$	*DEC* 8400	*Convex* $SPP1000$	IBM^a $SP2$	SGI^b *PCh*	*Sun* *SS* 20
SOR	19.1	5.3	20.7	7.3	6.2	26.8
	(25.7)	(93)	(23.7)	(67.2)	(79.1)	(18.3)
MCSOR	3.3	12.1	52.1	8.5	9.5[c]	54.7
	(149)	(40.5)	(9.4)	(57.7)	(51.6)	(9.0)

[a] IBM SP2: IBM RS6000/590 66MHz wide node

[b] SGI PCh: SGI Power Challenge R8000 90MHz

[c] 1.83 (268) are the corresponding values for a 8 processor Power Challenge system

The current version of the program employs the 8th-order cross-like discretization stencil instead of the 6th-order one used by Laaksonen *et al.* (1)

and corresponding higher order numerical integration formulae. This, together with the more accurate boundary values at the (practical) infinity for the orbitals and the potentials allowed the grid density to ne halved while retaining the quality of the solution. Recoding the CPU intensive parts of the program, especially all differentiations and integrations, in the form of vector-vector and matrix-vector operations allowed them to be executed efficiently through calls to optimized library routines. Due to some modifications of the scf process the overall performance of the FD HF method using the SOR algorithm to solve linear equations could be increased by a factor of 10.

The original version of the FD HF program employed one grid of points of constant density to represent all orbitals and potentials. In the case of heavy systems where both tightly contracted atomic-like core orbitals and rather diffused, valence, orbitals are present this restriction has to be relaxed. Recently the multiple grids in ξ variable have been introduced which allow to further reduce the number of grid points (19).

Due to these developments of the FD HF method even moderate computer resources are sufficient to treat diatomic systems with up to 20-25 electrons routinely. Data from Table 1 can be used to estimate the CPU time needed to solve the FD HF equations for a given system. Typically, in every scf cycle, 10 (MC)SOR iterations are performed on each orbital and potential. For example, for the *AlF* molecule there are in all 57 Poisson equations to be solved in each scf iteration and this require about 60 seconds on a Sun SS20 workstation. Depending on the quality of the initial guess for the orbitals and the potentials and the accuracy of the solution 5–30 hundred scf cycles might be needed. The current version of the program will soon become available (20).

3. The calibration of basis sets

The majority of quantum-chemistry calculations have been carried out by employing the independent particle model in the framework of the HF method. In the most widely used approach molecular orbitals are expanded in predefined one-particle basis functions which results in recasting the integro-differential HF equations into their algebraic equivalents. In practice, however, the basis set used is never complete and very often far too limited to describe essential features of HF orbitals, for example, their behaviour in the vicinity of nuclei. That is why such calculations always suffer from the so called 'basis set truncation error'. This error is difficult to estimate and often leads to low credibility of the results.

Over the last three decades one has witnessed the extensive usage of the algebraic HF method accompanied by the continuous efforts to develop

basis sets appropriate for the description of various molecules and their properties. Difficulties in controlling the basis set truncation error (e.g. the presence of the basis set superposition effect) and dependence of the calculated properties on the basis sets quality mean that in principle *ab initio* calculations performed within the algebraic HF approach assume in fact a *quasi-empirical* character where basis set truncation errors are treated as a part of the model employed (21).

One way to estimate the quality of a basis set is to compare the total HF energy yielded by the algebraic HF method with the corresponding HF limit value for the system provided that this value is known. In the case of diatomic molecules the necessary data can be supplied by the FD HF method. For example, the FD HF method has been used to assess quality and calibrate sequences of *even-tempered* basis sets for systems such as N_2, CO, BF, NO^+, CS (22–25) and recently AlF and GaF (19). It has been shown that it is possible to construct basis sets which bring the discrepancies between finite basis set and finite difference HF results down to a couple of μHartree (Table 2). In the case of the GaF molecule the basis set consisted of 901 primitive spherical gaussian functions: $48s24p24d24f$ on the Ga centre, $30s15p15d15f$ on the F one and $27s12p14d15f$ functions at the bond centre.

Work is under way to calibrate basis sets for the InF and TlF molecules to the same level of accuracy in order to study the effects of parity and time reversal non-conservation in the latter (26,27) and to show that the FD HF method can be applied to such systems.

Table 2
Comparison of finite difference (E_{FD}) with finite basis set (E_{FB}) Hartree-Fock total energies for several diatomic molecules. All energies are in Hartree.

Molecule	E_{FB}	E_{FD}
N_2^a	−108.993 823 4	−108.993 825 7
CO^a	−112.790 904 5	−112.790 907 3
BF^b	−124.168 761 2	−124.168 779 2
NO^{+a}	−128.977 737 5	−128.977 740 7
AlF^b	−341.488 369 5	−341.488 385 5
CS^c	−435.362 417 7	−435.362 419 8
GaF^b	−2022.836 862 3	−2022.836 858 8

[a] D. Moncrieff, J. Kobus and S. Wilson, J. Phys. B: At. Mol. Opt. Phys. **2**, 4555 (1995)

[b] J. Kobus, D. Moncrieff and S. Wilson, Mol. Phys. **86**, 1315 (1995)

[c] J. Kobus, D. Moncrieff and S. Wilson, J. Phys. B: At. Mol. Opt. **27**, 2867 (1994)

There have been continuous attempts to develop schemes to circumvent the limitations imposed by the finite basis sets, e.g. the counterpoise method of Boys and Bernardi and its variants (28,29) or the complete basis set approach (30). It seems that the availibility of exact solutions of the Hartree-Fock equations for diatomic molecules could be of help in devising such methods by allowing the dependence of the basis set truncation and superposition errors on internuclear separation to be monitored (16).

4. Full CI with numerical orbitals

Exact solutions of the HF model provided by the FD HF method, are not that interesting from the physical point of view since correlation effects are missing. However, the exact FD HF orbitals of a diatomic system can be used to generate a set of numerical virtual orbitals in order to perform configuration interaction calculations. Table 3 contains the results of the full CI calculations for the beryllium atom (treated as a diatiomic system with zero charge at the other centre) and the helium dimer (for both systems the calculations were performed assuming $C_{\infty v}$ symmetry). The lowest virtual orbitals of σ, π and δ symmetry were chosen to maximize the correlation energy of the corresponding systems. For example, the bare-nuclei dimer systems He_2^{3+}, B_2^{9+} and Ne_2^{19+} had to be used to produce the best lowest virtual orbitals for the helium dimer. Then, after generating the other virtual orbitals, the corresponding molecular integral file was formed and the full CI calculations were performed using the CI program of Duch and Karwowski (31).

Table 3
Total energy (E_{total}) and full CI correlation energy (E_{corr}) for the beryllium atom and the helium dimer (R_e = 5.6 bohr) obtained with the numerical molecular basis sets. All energies are in Hartree.

	E_{total}	E_{corr}	$E_{corr}/E_{corr}^{exact}$ (%)
$Be: 5\sigma\ 3\pi\ 2\delta$	−14.647 12	−0.074 10	78.9
$exact^a$	−14.666 90	−0.093 87	100.0
$Be: 5\sigma\ 3\pi\ 2\delta$			
$1\sigma\ frozen$	−14.615 87	−0.042 85	91.6
$exact^a$	−14.619 82	−0.046 79	100.0
$He_2: 10\sigma\ 7\pi\ 4\delta$	−5.790 20	−0.066 98	79.6
$exact^b$	−5.807 36	−0.084 14	100.0

[a] C. Bunge, Phys. Rev. **A14**, 1965 (1976)

[b] J. A. Montgomery Jr., G. A. Petersson and N. Matsunaga, Chem. Phys. Lett. **155**, 413 (1989)

This approach is not very convenient when the potential energy curve has to be determined since for each internuclear separation the numerical basis set has to be constructed afresh. However, it could be of use for the study of weakly interacting systems for which basis set truncation errors make the algebraic approach too difficult to use.

5. One-electron diatomic states

The above demonstrated possibility of obtaining numerical virtual orbitals indicate that the FD HF method can also be used as a solver of the Schrödinger equation for a one-electron diatomic system with an arbitrary potential. Thus, the scheme could be of interest to those who try to construct exchange-correlation potential functions or deal with local-scaling transformations within the functional density theory (32,33).

Table 4
Camparison of FD energies (in Hartree) for the GaF^{39+} one-electron system (R = 3.353 bohr, $n_\nu \times n_\mu$ = 253 × 277, R_∞ = 45.9 bohr) with the exact values from Power's program (OEDM). Orbitals are labeled with nlm triplet where n, l and m are principal, orbital and magnetic quantum numbers, respectively.

nlm	$OEDM$	FD
100	−483.184 165 0	−483.184 165 0
210	−122.888 205 9	−122.888 208 5
200	−122.733 220 2	−122.733 273 7
320	−56.325 432 3	−56.325 343 3
310	−56.064 747 4	−56.064 742 8
300	−55.857 809 1	−55.857 817 7
430	−49.748 077 7	−49.748 077 7
540	−33.278 686 5	−33.278 686 5
420	−32.852 093 1	−32.852 093 0
211	−122.807 726 8	−122.807 726 8
321	−56.186 870 4	−65.186 870 2
311	−55.955 787 7	−55.955 787 7
431	−33.044 405 1	−33.044 405 1
322	−56.064 605 7	−56.064 605 7
432	−32.851 020 6	−32.851 020 5
422	−32.549 061 3	−32.549 061 3

As an example, in Table 4, eigenvalues of several σ, π and δ states of the GaF^{39+} system were calculated and compared with the corresponding values obtained from Power's quantum chemistry program exchange (QCPE) program which generates eigenvalues for bare-nuclei one-electron diatomic systems (34,35).

It is well known that for heavy atoms the effect of the finite nucleus charge distribution has to be taken into account (among other effects) in order to describe the electronic structure of the system correctly (see e.g. (36,37)). As a preliminary step in the search for the effect of the finite nuclei on the properties of molecules the potential energy curve of the Th_2^{179+} has been calculated for point-like and finite nuclei models (Table 5). For finite nuclei the Fermi charge distribution with the standard value of the "skin thickness" parameter was adopted ($t = 2.30$ fm) (38,39).

Table 5
Total (E_{pn}^{total}) and electronic energy curve of Th_2^{179+} with the point-like (E_{pn}) and finite (E_{fn}) nuclei charge distributions (38). The total energy is the sum of the electronic energy and Z_{Th}^2/R term. All energies are in Hartree.

R	E_{pn}^{total}	E_{pn}	$E_{fn} - E_{pn}$	Δ^a
0.005	1605 681.768 022	−14 318.231 978	2.994 712 421	2.494 260
0.01	797 838.809 046	−12 161.190 954	1.528 884 307	1.028 432
2/90	355 568.662 863	−8 931.337 137	0.658 730 772	0.158 278
1.0	3 959.999 722	−4 140.000 278	0.500 447 475	−0.000 005
2.0	−45.000 017	−4 095.000 017	0.500 452 353	0.000 000
∞	−4 050.000 000	−4 050.000 000	0.500 452 358	0.000 000

[a] difference between $E_{fn} - E_{pn}$ values and the corresponding values of nuclear volume effect for the separated system

In the case of the Th^{89+} atom the 2-dimensional FD HF scheme is capable of reproducing 1-dimensional FD $GRASP^2$ results to within μHartree accuracy (38,40). Thus one can infer that for the system studied the molecular volume effect is nonexistent at the μHartree level for internuclear distances ranging from the infinity down to 1 bohr. The effect begins to be seen at smaller, non-chemical, internuclear distances when both the nuclei are in the region of non-zero values of 1 σ electron density. When dealing with such internuclear distances one has to take into account the effect of overlapping charge distributions of the nuclei. Thus, when calculating the total energy of the system, the nuclear repulsion energy should be correctly taken into account with the assumption of point-like nuclear charges lifted.

In a many-electron molecular system the effect of finite nuclei should result in increasing its total energy. Whether the binding energy and the bond length are also changed should be further investigated.

6. Future developments

Any realistic description of molecules containing heavy atoms has to take into account relativistic effects (13, 41). Attempts to use the algebraic approach to solve the Dirac-Hartree-Fock (DHF) equations are now well advanced (42–45). The difficulties encountered are much greater than in the nonrelativistic case since the basis sets used have to be larger and have to fulfil the kinetic balance criterion to guarantee the proper description of the large and small components of the molecular orbitals (46–49).

For the same reasons as in the nonrelativistic case the availability of a numerical solver of the DHF equations for molecules would be very much desired. One possible way to proceed would be to deal with the DHF method cast in the form of the second-order equations instead of the system of first-order coupled equations and try to solve them by means of techniques used in the FD HF approach. The FD scheme was used by Laaksonen and Grant (50) and Sundholm (51) to solve the Dirac equation. Sundholm used the similar approach to perform Dirac-Hartree-Fock-Slater calculations for LiH, Li_2, BH and CH^+ systems (52,53).

Let us consider a closed shell atom. Following Grant's notation (37) we can write the corresponding DHF equations in the form

$$-(\frac{Z}{r}+\epsilon_{\alpha\alpha})P_\alpha - c(\frac{d}{dr}-\frac{\kappa_\alpha}{r})Q_\alpha + \sum_\beta \frac{U(\alpha,\beta;r)}{r}P_\beta = 0 \qquad (1)$$

$$c(\frac{d}{dr}+\frac{\kappa_\alpha}{r})P_\alpha - (2c^2+\epsilon_{\alpha\alpha}+\frac{Z}{r}-\frac{U(\alpha,\alpha;r)}{r})Q_\alpha + \sum_{\beta\neq\alpha}\frac{U(\alpha,\beta;r)}{r}Q_\beta = 0. \qquad (2)$$

Because of the nonlocality of the exchange potential (the terms $U(\alpha,\beta,r)$, $\alpha \neq \beta$) Eq. (2) cannot be used to eliminate the small component from Eq. (1) exactly. In the QR approaches the local exchange approximation is used in Eq. (2) and only the second-order equation for the large component is retained. However, if the nonlocal potential is written as the sum of its local and nonlocal parts then the small component can be expressed as

$$Q_\alpha = \frac{1}{2c^2}B_\alpha\left[c(\frac{d}{dr}+\frac{\kappa_\alpha}{r})P_\alpha + \sum_{\beta\neq\alpha}\frac{U(\alpha,\beta;r)}{r}Q_\beta\right]. \qquad (3)$$

with $B_\alpha^{-1} = 1 + (\epsilon_{\alpha\alpha} - V_\alpha)/2c^2$ and $V_\alpha = -(Z - U(\alpha,\alpha;r))/r$. Now we can readily eliminate the small component Q_α from Eq. (1) to obtain an equation for the large component P_α only. After some algebra the equation reads

$$\left[-\frac{1}{2}\left(\frac{d^2}{dr^2} - \frac{\kappa_\alpha(\kappa_\alpha+1)}{r^2}\right) + V_\alpha - \epsilon_{\alpha\alpha} - \frac{1}{2c^2}(\epsilon_{\alpha\alpha} - V_\alpha)^2 - \frac{1}{4c^2}B_\alpha\frac{dV_\alpha}{dr}\left(\frac{d}{dr} + \frac{\kappa_\alpha}{r}\right)\right] P_\alpha + B_\alpha^{-1}V_{\alpha\beta}^P + \frac{1}{2c}\left(\frac{\kappa_\alpha}{r} - \frac{1}{2c^2}B_\alpha\frac{dV_\alpha}{dr}\right)V_{\alpha\beta}^Q - \frac{1}{2c}\frac{dV_{\alpha\beta}^Q}{dr} = 0 \quad (4)$$

where

$$V_{\alpha\beta}^P = \sum_{\beta\neq\alpha}\frac{1}{r}U(\alpha,\beta;r)P_\beta \qquad V_{\alpha\beta}^Q = \sum_{\beta\neq\alpha}\frac{1}{r}U(\alpha,\beta;r)Q_\beta.$$

This is the exact second-order equation for the large component of the DHF α orbital which together with Eq. (3) could be used in the second-order formulation of the DHF method for atoms. It is believed that the corresponding equations for diatomic molecules in the prolate spheroidal coordinates can be solved by the same technique as the one used in the FD HF method.

Work is under way to extend the formulation of the FD HF method from diatomic molecules to the linear polyatomic ones. Following Becke (54) the idea is to divide, say, a linear triatomic molecule into two overlapping "diatomic regions". The solution of the orbital and potential equations for the whole molecule would be obtained by solving the HF equations for the two "diatomic" subsystems alternatively, until self-consistency is achieved.

7. Summary

An overview of the development of the finite difference Hartree-Fock method for diatomic molecules has been presented. Given the power of the currently available workstations the exact solutions of the HF equations for systems containing 20-25 electrons can be obtained routinely. The approach has been successfully used to calibrate *even-tempered* gaussian basis sets; the discrepancies between the finite difference and the finite basis set results for a number of diatomic molecules (including a 40-electron system GaF) could be narrowed to a couple of μHartree.

It has been shown that the finite difference HF orbitals can be augmented with the virtual ones to form numerical basis sets for the full configuration interaction calculations. In the case of the beryllium and the

helium dimer the small basis sets (up to 20 functions) yielded 80% of the total correlation energy.

The finite difference HF scheme can also be used to solve the Schrödinger equation of a one-electron diatomic system with an arbitrary potential. Thus the approach can be applied, for example, to the construction of exchange–correlation potentials employed by the density functional methods. The eigenvalues of several GaF^{39+} states have been reported and the Th_2^{179+} system has been used to search for the influence of the finite charge distribution on the potential energy curve. It has been also indicated that the machinery of the finite difference HF method could be used to find exact solutions of the Dirac-Hartree-Fock equations based on a second-order Dirac equation.

8. Acknowledgements

The work on the FD HF method, which was started at the Max-Planck-Institut für Astrophysik in Garching (Germany) and carried out over many years, would not be possibile without the financial support of the Alexander von Humboldt Stiftung and the Max-Planck-Geselschaft. The interest in the project, encouragement and hospitality of Geerd H. F. Diercksen are gratefully acknowledged. Recently support received from the the European Science Fundation programme *Relativistic Effects In Heavy Element Chemistry and Physics* and from Polish State Committee for Scientific Research (contract 8 T11F 011 10) are also acknowledged.

References

(1) L. Laaksonen, P. Pyykkö and D. Sundholm, Comp. Phys. Rep. **4,** 313 (1986).

(2) P. Pyykkö, in: *Numerical Determination of the Electronic Structure of Atoms, Diatomic and Polyatomic Molecules*, eds. M.Defranceschi and J.Delhalle, NATO ASI Series, Series C: Mathematical and Physical Sciences, Vol.271, Kluwer Academic Publishers, Dordrecht, 1989, p. 161.

(3) E.A. McCullough Jr., Comput. Phys. Rep. **4,** 265 (1986).

(4) L. Adamowicz and R.J. Bartlett, J. Chem. Phys. **84,** 4988 (1986).

(5) K. W. Richman, Z.-G. Shi and E. A. McCullough, Jr., Chem. Phys. Lett. **141,** 186 (1987).

(6) L. Adamowicz, J. Chem. Phys. **89,** 313 (1988).

(7) D. Heinemann, D. Kolb and B. Fricke, Chem. Phys. Lett. **137,** 180 (1987).

(8) D. Heinemann, B. Fricke and D. Kolb, Phys. Rev. **A 38,** 4994 (1988).

(9) D. Heinemann, A. Rosén and B. Fricke, Physica Scripta **42,** 692 (1990).

(10) D. Sundholm, J. Olsen, P-Ake Malmqvist and B.O. Roos, in *Numerical Determination of the Electronic Structure of Atoms, Diatomic and Polyatomic Molecules*, edited by M. Defranceschi and J. Delhalle, NATO ASI Series C271 (1989). p. 329.

(11) D. Sundholm and J. Olsen, in *Proc. 13th. IMACS World Congress on Computation and Applied Mathematics*, edited by R. Vichnevetsky and J.J.H. Miller, Criterion, Dublin, 1991, p. 861.

(12) R. R. Cowan and D. C. Griffin, J. Opt. Soc. Am. **66,** 1010 (1976).

(13) P. Pyykkö, Adv. Quantum Chem. **11,** 353 (1978).

(14) J. Karwowski and J. Kobus, Int.J.Quantum Chem. **30,** 809 (1986).

(15) J. Kobus and W. Jaskólski, J. Phys. B: At. Molec. Phys. **20,** 4949 (1987).

(16) J. Kobus, Chem. Phys. Lett. **202,** 7 (1993).

(17) J. Kobus, Comp. Phys. Commun. **78,** 247 (1994).

(18) K. Davstad, J. Comp. Phys. **99,** 33 (1992).

(19) J. Kobus, D. Moncrieff and S. Wilson, Mol. Phys. **86,** 1315 (1995).

(20) J. Kobus, L. Laaksonen, D. Sundholm, Comput. Phys. Commun., to be submitted.

(21) S. Huzinaga, Comput. Phys. Rep. **2,** 279 (1985).

(22) D. Moncrieff and S. Wilson, J. Phys. B: At. Mol. Opt. Phys. **27,** 1 (1994).

(23) J. Kobus, D. Moncrieff and S. Wilson, J. Phys. B: At. Mol. Opt. Phys. **27,** 2867 (1994).

(24) J. Kobus, D. Moncrieff and S. Wilson, J. Phys. B: At. Mol. Opt. Phys. **27,** 5139 (1994).

(25) D. Moncrieff, J. Kobus and S. Wilson, J. Phys. B: At. Mol. Opt. Phys. **2,** 4555 (1995).

(26) P. V. Convey and P. G. H. Sanders, J. Phys. B: Atom. Mol. Phys. **16**, 3727 (1983).

(27) S. Wilson, D. Moncrieff and J. Kobus, European Science Fundation Workshop on Parity Non–Conservation, Oxford, 7-10 April, 1994, Rutherford Appleton Laboratory Report RAL–94–082.

(28) S. F. Boys and F. Bernardi, Mol. Phys. **19**, 553 (1970).

(29) M. Gutowski, F. B. van Duijneveldt, G. Chałasiński and L. Piela, Mol. Phys. **61**, 233 (1987).

(30) G. A. Petersson, A. Bennett, T. G. Tensfeldt, M. A. Al-Laham, A. Shirley and J. Mantzaris, J. Chem. Phys. **89**, 2192 (1988).

(31) W. Duch and J. Karwowski, Comput. Phys. Reports **2**, 94 (1985).

(32) E. K. U. Gross and S. Kurth, in: *Relativistic and Electron Correlation Effects in Molecules and Solids*, ed. G. L. Malli, NATO ASI Series, Plenum, 1993, p. 367.

(33) E. V. Ludeña, R. Lopez-Boada, J. Maldonado, T. Koga and E. S. Kryachko, Phys. Rev. **A 48**, 1937 (1993).

(34) J. D. Power, Philos. Trans. R. Soc. London Ser. **A 274**, 663 (1973).

(35) J. D. Power, One electron diatomic molecules, QCPE program No. 233.

(36) I. P. Grant, Adv. Phys. **19**, 747 (1970).

(37) I. P. Grant, in: *Methods in Computational Chemistry*, ed. S. Wilson, vol. 2, Plenum Press, 1988, p. 1.

(38) J. Kobus, D. Moncrieff and S. Wilson, in preparation.

(39) F. A. Parpia and A. K. Mohanty, Phys. Rev. **A 46**, 3735 (1992).

(40) K. G. Dyall, I. P. Grant, C. T. Johnson, F. A. Parpia and E. P. Plummer, Comp. Phys. Commun. **55**, 425 (1989).

(41) P. Pyykkö, Chem. Rev. **88**, 563 (1988).

(42) G. L. Malli and N. C. Pyper, Proc. R. Soc. Lond. **A 407**, 377 (1986).

(43) O. Matsuoka, J. Chem. Phys. **97**, 2271 (1992).

(44) W. C. Nieuwpoort, P. J. C. Aerts and L. Visscher, in: *Relativistic and Electron Correlation Effects in Molecules and Solids*, ed. G. L. Malli, NATO ASI Series, Plenum, 1993, p. 59.

(45) K. G. Dyall, in: *Relativistic and Electron Correlation Effects in Molecules and Solids*, ed. G. L. Malli, NATO ASI Series, Plenum, 1993, p. 17.

(46) I. P. Grant and H. M. Quiney, Adv. At. Mol. Phys. **23,** 37 (1988).

(47) Y. Ishikawa, H. Sekino and R. C. Binning Jr., Chem. Phys. Lett. **165,** 237 (1990).

(48) K. G. Dyall and K. Fægri Jr., Chem. Phys. Lett. **174,** 25 (1990).

(49) O. Visser, L. Visscher, P. J. C. Aerts and W. C. Nieuwpoort, Theor. Chim. Acta **81,** 405 (1992).

(50) L. Laaaksonen and I. P. Grant, Chem. Phys. Lett. **109,** 485 (1984).

(51) D. Sundholm, Chem. Phys. Lett. **223,** 469 (1994).

(52) D. Sundholm, P. Pyykkö, Physica Scripta **36,** 400 (1987).

(53) D. Sundholm, Chem. Phys. Lett. **149,** 251 (1988).

(54) A. D. Becke, J. Chem. Phys. **88,** 2547 (1988).

Perturbation Theory for Low-Spin Open-Shell States [1]

Xiangzhu Li and Josef Paldus[2]

Department of Applied Mathematics, University of Waterloo, Waterloo, Ontario N2L 3G1, Canada

Abstract

Finite order perturbation theory (PT) for low–spin open–shell singlet states is formulated in terms of spin–free unitary group approach (UGA). Both Møller-Plesset and Epstein-Nesbet partitionings of the Hamiltonian are considered. The method is tested on low lying excited states of CH_2, NH_2^+ and H_2O using various basis sets.

[1] ***This paper is dedicated to Prof. Dr. G.H.F. Diercksen – a long time colleague and friend – at the occasion of his 60th birthday***

[2] **Also at: Department of Chemistry and Guelph–Waterloo Center for Graduate Work in Chemistry–Waterloo Campus, University of Waterloo, Waterloo, Ontario N2L 3G1, Canada.**

ADVANCES IN QUANTUM CHEMISTRY, VOLUME 28

0065-3276/97 $25.00

1. Introduction

The past decade witnessed a rapid development and widespread use of various post–Hartree-Fock methods that account for both dynamical and nondynamical many–electron correlation effects. The most prominent of these are based on configuration interaction (CI), many–body perturbation theory (MBPT) or coupled cluster (CC) approaches, and employ a single Slater determinant as a reference [single reference (SR) methods]. For ground states of closed shell (CS) systems near their equilibrium geometries the spin restricted Hartree–Fock (RHF) solution usually represents such a suitable reference configuration, while the open shell (OS) states generally require a multi–reference (MR) approach. However, for high spin (HS) OS states the demanding MR MBPT or CC methods are usually avoided by using a spin unresticted (UHF) reference of the DODS (different orbitals for different spins) type. Although the resulting theories are not properly spin adapted, they often provide very good results, at least for the total energy based properties. Unfortunately, when the spin contamination is appreciable, the UHF based PT series converge slowly and yield unsatisfactory results (1–4). Moreover, these methods cannot be used for the low spin OS states, which will be the focus of this paper.

The low spin OS states, in particular the open–shell singlet (OSS) states, play a very important role not only in molecular spectroscopy but also in various chemical or photochemical processes. Until recently, the only viable alternative to describe such states at the correlated level was the ROHF reference based CI or CI–related spin–adapted PT (4–6). In the framework of CC theory, the OSS states have been handled using MRCC methods of either valence universal (VU) or state universal (SU) types (7, 8) (the latter leading to the so–called two–determinant (TD) CCSD method (9)) or using the equation–of–motion (EOM) CC approaches (10). In a number of these approaches, the full spin adaptation is not easy to achieve. We have shown how such states may be effectively handled using the recently formulated unitary group based CC theory (11–13). Nonetheless, all these approaches are computationally rather demanding and cannot be easily applied to large molecular systems.

It is well known that for CS and HS OS systems the widely employed second order MBPT [often referred to as the Møller-Plesset PT (MP2) when a RHF or UHF operator is used as the unperturbed Hamiltonian (14)] provides computationally the cheapest, yet reasonably reliable, results. Surprisingly enough, no such method exists for the low spin OSS state mentioned above, as far as we know. This is likely due to the fact that the zero order wave function describing these states involves two Slater determinants and thus cannot be handled by the conventional MBPT relying on the spin orbital formalism. At the same time, in the MR theory

at the spin orbital level, one has to consider simultaneously both the OSS and HS triplet states, and a proper implementation requires a nontrivial spin adaptation. Yet, a SR description of OSS states is easily achieved when we employ a spin–free formalism, as represented for example by the unitary group approach (UGA) (15–19). in which case the OSS state reference function is represented by a single spin–free spatial configuration. In particular, we employ the Clifford algebra UGA (CAUGA) for this purpose (20–23).

It is the aim of this paper to develop a UGA based finite order PT for low spin OSS states. Such an approach will parallel the existing UGA based CC theory for these states (11–13, 24–26), which may be interpreted as an infinite order MBPT involving a certain restricted class of diagrams, but will be computationally much less demanding and thus applicable to much larger systems. Although the finite order MBPT is less versatile than the corresponding CC theory, it can certainly provide useful results for a number of "well–behaved" systems. The experience gained with this approach will also prove helpful in formulating the perturbation procedure accounting for the contribution of connected triples in UGA based CCSD method.

2. Basic formalism

Consider an eigenvalue problem for the time– and spin–independent Hamiltonian H,

$$H = H_0 + V, \tag{1}$$

assuming the spectral resolution of the unperturbed operator H_0 to be known. The perturbed problem for H can be formulated in powers of V. Note that the partitioning of H into H_0 and V is not unique.

In the UGA formalism, the exact electronic Hamiltonian H takes the form

$$H = \sum_{\mu,\nu} h^{\mu}_{\nu} E^{\mu}_{\nu} + \tfrac{1}{2} \sum_{\mu,\nu,\lambda,\kappa} (\mu\nu|\lambda\kappa)(E^{\mu}_{\nu} E^{\lambda}_{\kappa} - \delta^{\lambda}_{\nu} E^{\mu}_{\kappa}), \tag{2}$$

where h^{μ}_{ν} designates the one–electron component of H involving both the kinetic energy and the potential energy in the field of clamped nuclear framework, and E^{μ}_{ν} is the generator of the orbital unitary group $\mathrm{U}(n)$, n being the number of orbitals defining our model. For the two–electron integrals $(\mu\nu|\lambda\kappa)$ we employ Mulliken's notation. As the generic orbital labels we employ the lower case letters of the Greek alphabet $\mu, \nu, \cdots$. For general OS systems, these orbitals are further partitioned into the core $(a, b, c, \cdots)$, active or valence (i, j), and virtual or excited $(r, s, t, \cdots)$ orbitals which are, respectively, doubly occupied, singly occupied, and unoccupied in the reference configuration characterizing the unperturbed state of interest. For the

OSS states considered here, the zero order SCF (or ROHF) wave function Φ_0 in the standard spin orbital representation involves two Slater determinants, i.e.

$$\Phi_0 = (|(\text{core})i\alpha j\beta| - |(\text{core})i\beta j\alpha|)/\sqrt{2}, \tag{3}$$

where "(core)" stands for the singlet part consisting of doubly occupied core orbitals. In the CAUGA spin free formalism this wave function is represented by a single spatial configuration, which can be symbolically represented as follows

$$|\Phi_0\rangle = |\ (\text{core})\ \boxed{i}\boxed{j}\ \rangle\ . \tag{4}$$

Consequently, within the spin free N–electron Hilbert space, the MBPT for OSS states can be formulated as a SR theory with the spin free reference $|\Phi_0\rangle$, Eq.4, and the UGA representation of the perturbed and unperturbed Hamiltonians. The resulting theory has formally the same appearance as the spin orbital based MBPT theories for CS or HS OS cases.

To represent the perturbed wave functions we consider an excited state manifold $\{|\Phi_I\rangle\}_{I\neq 0}$, which together with $|\Phi_0\rangle$ spans the N–electron space considered, and which consists of eigenstates of H_0, i.e.

$$H_0|\Phi_0\rangle = E_0|\Phi_0\rangle, \qquad H_0|\Phi_I\rangle = E_I|\Phi_I\rangle. \tag{5}$$

Then the first order wave function is determined by the excited states that form the first order interacting space, i.e., by the states that have non-vanishing matrix elements of the perturbation V with the reference state, namely $\langle\Phi_0|V|\Phi_I\rangle$. Since we shall restrict ourselves in this paper to at most third order energy contributions, the higher than the first order wave functions will not be needed (recall Wigner's $2n+1$ rule). For subsequent derivations it is convenient to represent the required excited configurations $|\Phi_I\rangle$ in terms of suitable excitation operators G_I, producing the desired spin free (and thus spin adapted) excited configurations when acting on the reference state $|\Phi_0\rangle$, i.e.

$$|\Phi_I\rangle = G_I|\Phi_0\rangle. \tag{6}$$

For the OSS states, the set of excitation operators $\{G_I\}$ that generate the full singly and doubly (SD) excited manifold were given in Ref. (13), Eqs. 59–70. The subset of excitation operators generating the first order interacting space and thus the first order wave function $|\Psi^{(1)}\rangle$,

$$|\Psi^{(1)}\rangle = |\Phi_0\rangle + \sum_I a_I^{(1)}|\Phi_I\rangle = |\Phi_0\rangle + \sum_I a_I^{(1)}G_I|\Phi_0\rangle, \tag{7}$$

is obtained from the full SD set by deleting the operators ${}^2G^{rs}_{aa}$, ${}^2G^{rr}_{ab}$ and ${}^mG^{rs}_{ab}(m=3,4,5)$. Defining the relative energies of excited configurations

with respect to the reference by

$$\Delta_I = E_I - E_0, \tag{8}$$

we can express the coefficients $a_I^{(1)}$ defining the first order wave function $|\Psi^{(1)}\rangle$, Eq. 7, as

$$a_I^{(1)} = -V_{I0}/\Delta_I, \tag{9}$$

where

$$V_{I0} = \langle\Phi_I|V|\Phi_0\rangle = \langle\Phi_0|G_I^\dagger V|\Phi_0\rangle = V_{0I}, \tag{10}$$

assuming the interaction matrix elements, Eq.10, to be real. The first through third order energies are then given by

$$E^{(1)} = V_0 = \langle\Phi_0|V|\Phi_0\rangle, \tag{11}$$

$$E^{(2)} = \sum_I a_I^{(1)} V_{0I} = -\sum_I |V_{I0}|^2/\Delta_I, \tag{12}$$

$$E^{(3)} = \sum_I a_I^{(1)} w_I, \tag{13}$$

where

$$w_I = \sum_J a_J^{(1)} \bar{V}_{IJ}, \qquad \bar{V}_{IJ} = \langle\Phi_I|V - V_0|\Phi_J\rangle. \tag{14}$$

Clearly, independently of the partitioning scheme employed, the sum of the zero and first order energies gives always the reference state energy $\mathcal{E}_0$,

$$\mathcal{E}_0 \equiv \langle\Phi_0|H|\Phi_0\rangle = E_0 + V_0. \tag{15}$$

In the following, we consider two basic types of partitioning due to Møller–Plesset (27) (MP) and Epstein–Nesbet (28) (EN). The resulting PT expansions will be based on a single spin–free spatial configuration and will be formulated using the techniques that characterize CAUGA based CC theories. We shall thus refer to the resulting formalism as the UGA based MP and EN perturbation theories in order to distinguish them from the standard ones that are based on a generally spin nonadapted single Slater determinant reference.

3. Møller–Plesset UGA based PT

For the MP MBPT we choose for the unperturbed Hamiltonian H_0 the following diagonal one–body operator

$$H_0 = \sum_\mu F_\mu^\mu E_\mu^\mu, \tag{16}$$

with the diagonal Fock matrix elements defined as follows

$$\left.\begin{aligned} F_a^a &\equiv \varepsilon_a = f_a^a + \tfrac{1}{2}(ai|ai) + \tfrac{1}{2}(aj|aj), \\ F_i^i &\equiv \varepsilon_i = f_i^i + 2(ij|ij), \\ F_j^j &\equiv \varepsilon_j = f_j^j + 2(ij|ij), \\ F_r^r &\equiv f_r^r, \end{aligned}\right\} \tag{17}$$

where

$$f_\nu^\mu = h_\nu^\mu + \sum_a [2(aa|\mu\nu) - (a\mu|a\nu)] + \sum_i [(ii|\mu\nu) - (i\mu|i\nu)], \tag{18}$$

with the sums extending over all occupied (core and active) orbitals. For the core and active orbitals, the above given Fock matrix elements F_μ^μ are equal to the corresponding orbital energies ε_μ (see (29)), while this is not the case for the virtual orbitals. Clearly, there is arbitrariness in the choice of F_r^r matrix elements which would be worthwhile to explore in greater detail. The nonvanishing off-diagonal Fock operator matrix elements are included in the perturbation operator V.

Since H_0 contains only weight generators, the energy differences Δ_I, Eq. 8, are given by the corresponding differences of diagonal matrix elements F_μ^μ. Thus, for singly ($\Phi_I = \Phi_\mu^\nu$) and doubly ($\Phi_I = \Phi_{\mu\mu'}^{\nu\nu'}$) excited configurations we have

$$\Delta_I \equiv \Delta(\Phi_\mu^\nu) = F_\nu^\nu - F_\mu^\mu, \tag{19}$$

$$\Delta_I \equiv \Delta(\Phi_{\mu\mu'}^{\nu\nu'}) = F_\nu^\nu + F_{\nu'}^{\nu'} - F_\mu^\mu - F_{\mu'}^{\mu'}. \tag{20}$$

The required numerators for the second order energy are then given by

$$V_{I0} = \langle \Phi_I | V | \Phi_0 \rangle = \langle \Phi_I | H | \Phi_0 \rangle = \langle \Phi_0 | G_I^\dagger H | \Phi_0 \rangle, \tag{21}$$

which are identical with the absolute terms in CC equations (see Eq. 11 of (13)). The explicit expressions for V_{I0} for the first order interacting space configurations Φ_I are given in Table 1, together with appropriate ranges for the summation labels which must be accounted for when evaluating the second order energy. For example, the contribution of ${}^1\Phi_{ab}^{ri}$ type configurations to the MP2 energy is given by the expression

$$\sum_{a \le b, r, i} \frac{[(ar|bi) + (ai|br)]^2}{2(1+\delta_{ab})(F_r^r + F_i^i - F_a^a - F_b^b)}, \tag{22}$$

where the sums over $a \leq b$, r and i extend, respectively, over all core, virtual and active (i.e., over i and j in the case of the OSS considered) orbitals. The total MP2 energy is then given by the sum of contributions from all types of SD excitations listed in Table 1.

Table 1
Nonvanishing matrix elements V_{I0}, Eq. 10, for the MP2 and EN2 MBPTs. We define $\bar{i} = j$ and $\bar{j} = i$.

Φ_I	range	V_{I0}
Φ_a^i	a, i	$f_a^i + (ai\|ii) - (a\bar{i}\|i\bar{i})$
Φ_i^r	r, i	$f_i^r + 2(i\bar{i}\|\bar{i}r)$
${}^1\Phi_a^r$	a, r	$\sqrt{2} f_a^r + 2^{-1/2}\,[(ai\|ir) + (aj\|jr)]$
${}^2\Phi_a^r$	a, r	$\sqrt{3/2}\,[(ai\|ir) - (aj\|jr)]$
Φ_{ij}^{rs}	$r \leq s$	$(1+\delta_{rs})^{-1/2}\,[(ir\|js) + (is\|jr)]$
Φ_{ab}^{ij}	$a \leq b$	$(1+\delta_{ab})^{-1/2}\,[(ai\|bj) + (aj\|bi)]$
$\Phi_{ai}^{r\bar{i}}$	a, r, i	$2(ar\|i\bar{i}) - (a\bar{i}\|ir)$
${}^1\Phi_{ab}^{ri}$	$a \leq b, r, i$	$[2(1+\delta_{ab})]^{-1/2}\,[(ar\|bi) + (ai\|br)]$
${}^2\Phi_{ab}^{ri}$	$a < b, r, i$	$\sqrt{3/2}\,[(ar\|bi) - (ai\|br)]$
${}^1\Phi_{ai}^{rs}$	$a, r \leq s, i$	$[2(1+\delta_{rs})]^{-1/2}\,[(ar\|is) + (as\|ir)]$
${}^2\Phi_{ai}^{rs}$	$a, r < s, i$	$\sqrt{3/2}\,[(ar\|is) - (as\|ir)]$
${}^1\Phi_{ab}^{rs}$	$a \leq b, r \leq s$	$[(1+\delta_{ab})(1+\delta_{rs})]^{-1/2}\,[(ar\|bs) + (as\|br)]$
${}^2\Phi_{ab}^{rs}$	$a < b, r < s$	$\sqrt{3}[(ar\|bs) - (as\|br)]$

To evaluate the third order (MP3) energy, Eqs. 13 and 14, we also need matrix elements $\bar{V}_{IJ}$ between the SD excited states, namely

$$\bar{V}_{II} = H_{II} - \mathcal{E}_0 - \Delta_I = (H_N)_{II} - \Delta_I, \tag{23}$$

$$\bar{V}_{IJ} = H_{IJ} = (H_N)_{IJ}, \qquad (I \neq J) \tag{24}$$

where $(H_N)_{IJ}$ are standard, normal product form CI matrix elements,

$$(H_N)_{IJ} = \langle \Phi_I | H_N | \Phi_J \rangle = \langle \Phi_0 | G_I^\dagger H_N G_J | \Phi_0 \rangle, \tag{25}$$

$$H_N = H - \langle \Phi_0 | H | \Phi_0 \rangle = H - \mathcal{E}_0. \tag{26}$$

The excitation operators G_I being defined in terms of U(n) generators (cf. Eqs. 59–70 of (13)), these matrix elements may be evaluated as reference state mean values of multiple U(n) generator products using the same technique and codes that we developed when implementing the UGA CC method (13).

4. Epstein–Nesbet UGA based PT

In the case of the EN MBPT it is the diagonal part of H that we choose as an unperturbed Hamiltonian H_0. Thus, we set

$$H_0 = \sum_{I(\neq 0)} H_{II}|\Phi_I\rangle\langle\Phi_I|, \tag{27}$$

$$V = \sum_{I\neq J} H_{IJ}|\Phi_I\rangle\langle\Phi_J|, \tag{28}$$

where $H_{IJ} = \langle\Phi_I|H|\Phi_J\rangle$. The coefficients $a_I^{(1)}$ defining the first order wave function $|\Psi^{(1)}\rangle$, Eq. 7, are now given by

$$a_I^{(1)} = -V_{I0}/(\bar{H}_0)_{II}, \tag{29}$$

with

$$\bar{H}_0 = H_0 - E_0 = H_0 - \langle\Phi_0|H|\Phi_0\rangle. \tag{30}$$

Since the entire diagonal part of H is taken as H_0, the first order energy vanishes (i.e., $V_0 = 0$) and $\mathcal{E}_0 = E_0 = \langle\Phi_0|H|\Phi_0\rangle$. The second and third order EN energies are then given by

$$E^{(2)} = -\sum_I V_{I0}^2/(\bar{H}_0)_{II}, \tag{31}$$

$$E^{(3)} = \sum_I a_I^{(1)} w_I, \tag{32}$$

where

$$w_I = \sum_{J(\neq I)} a_J^{(1)} \bar{V}_{IJ}. \tag{33}$$

In calculating the EN2 energy $E^{(2)}$, Eq. 31, the V_{I0} matrix elements defining the numerators are identical with those of the MP theory (cf. Table 1), while the denominators become

$$(\bar{H}_0)_{II} = \langle\Phi_I|H_0|\Phi_I\rangle - E_0 = \langle\Phi_I|H|\Phi_I\rangle - E_0 = H_{II} - E_0. \tag{34}$$

We can again use the same technique as in the UGA CC method to derive explicit form of these matrix elements, and we list them in Table 2 for the relevant first order interacting space configurations $|\Phi_I\rangle = G_I|\Phi_0\rangle$. When evaluating the third order (EN3) energy $E^{(3)}$, Eqs. 32 and 33, we can employ the same expressions for off–diagonal $\bar{V}_{IJ}$'s as in the MP case (cf. Eq. 23), namely

$$\bar{V}_{IJ} = H_{IJ}, \qquad (I \neq J) \tag{35}$$

Table 2
EN MBPT denominators, Eq. 34. [a]

Φ_I	$(\bar{H}_0)_{II}$
Φ_a^i	$D_a^i - (aa\|ii) - (a\bar{i}\|a\bar{i}) + (ii\|ii) + 2(a\bar{i}\|a\bar{i}) - (i\bar{i}\|i\bar{i})$
Φ_i^r	$D_i^r - (ii\|rr) + (ir\|ir) + 2(\bar{i}r\|\bar{i}r) - 2(i\bar{i}\|i\bar{i})$
${}^1\Phi_a^r$	$D_a^r + [C_{rr} - B_{aa}]/2 + 2(ar\|ar) - (aa\|rr)$
${}^2\Phi_a^r$	$D_a^r + [B_{aa} + 3C_{rr}]/2 - 2(i\bar{i}\|i\bar{i}) - (aa\|rr)$
Φ_{ij}^{rs}	$D_{ij}^{rs} - (ii\|rr) - (ii\|ss) - (jj\|rr) - (jj\|ss) + C_{rs} + (ii\|jj) - 3(i\bar{i}\|i\bar{i})$ $+(rr\|ss) + (1-\delta_{rs})(rs\|rs)$
Φ_{ab}^{ij}	$D_{ab}^{ij} - (aa\|ii) - (bb\|ii) - (aa\|jj) - (bb\|jj) + (ii\|ii) + (jj\|jj)$ $+(ii\|jj) - (ij\|ij) + (aa\|bb) + (1-\delta_{ab})(ab\|ab)$
$\Phi_{ai}^{r\bar{i}}$	$D_{ai}^{r\bar{i}} + (aa\|ii) - (aa\|\bar{i}\bar{i}) - (ai\|ai) + (rr\|\bar{i}\bar{i}) - (rr\|ii) + (ri\|ri)$ $+2(ar\|ar) - (aa\|rr) + (\bar{i}\bar{i}\|\bar{i}\bar{i}) - (ii\|\bar{i}\bar{i}) - (i\bar{i}\|i\bar{i})$
Φ_{aa}^{ri}	$D_{aa}^{ri} + (aa\|aa) - 2(aa\|rr) - 2(aa\|ii) + (ii\|ii) + (rr\|ii) + 2(\bar{i}r\|\bar{i}r)$ $+(ar\|ar) - (i\bar{i}\|i\bar{i}) - (a\bar{i}\|a\bar{i})$
${}^1\Phi_{ab}^{ri}$	$D_{ab}^{ri} + (aa\|bb) + (ab\|ab) - (aa\|rr) - (bb\|rr) - (aa\|ii) - (bb\|ii)$ $+(ii\|ii) + (rr\|ii) + [A_{ab,rr} - (a\bar{i}\|a\bar{i}) - (b\bar{i}\|b\bar{i})]/2 + 2(\bar{i}r\|\bar{i}r) - (i\bar{i}\|i\bar{i})$
${}^2\Phi_{ab}^{ri}$	$D_{ab}^{ri} + (aa\|bb) - (ab\|ab) - (aa\|rr) - (bb\|rr) - (aa\|ii) - (bb\|ii)$ $+(ii\|ii) + (rr\|ii) + [3A_{ab,rr} + (a\bar{i}\|a\bar{i}) + (b\bar{i}\|b\bar{i})]/2 - (i\bar{i}\|i\bar{i})$
Φ_{ai}^{rr}	$D_{ai}^{rr} - 2(aa\|rr) + (ar\|ar) - 2(rr\|ii) + 2(ri\|ri) + (aa\|ii) - (ai\|ai)$ $+(rr\|rr) + (a\bar{i}\|a\bar{i}) + (r\bar{i}\|r\bar{i}) - 2(i\bar{i}\|i\bar{i})$
${}^1\Phi_{ai}^{rs}$	$D_{ai}^{rs} + (rr\|ss) + (rs\|rs) + [-A_{aa,rs} + (\bar{i}r\|\bar{i}r) + (\bar{i}s\|\bar{i}s)]/2 + (a\bar{i}\|a\bar{i})$ $-2(i\bar{i}\|i\bar{i}) - (rr\|ii) - (ss\|ii) + (ri\|ri) + (si\|si) + (aa\|ii) - (ai\|ai)$
${}^2\Phi_{ai}^{rs}$	$D_{ai}^{rs} + (rr\|ss) - (rs\|rs) + [A_{aa,rs} + 3(\bar{i}r\|\bar{i}r) + 3(\bar{i}s\|\bar{i}s)]/2 - (a\bar{i}\|a\bar{i})$ $-2(i\bar{i}\|i\bar{i}) - (rr\|ii) - (ss\|ii) + (ri\|ri) + (si\|si) + (aa\|ii) - (ai\|ai)$
Φ_{aa}^{rr}	$D_{aa}^{rr} + (aa\|aa) + (rr\|rr) - 4(aa\|rr) + 2(ar\|ar) - B_{aa} + C_{rr}$
Φ_{ab}^{rr}	$D_{ab}^{rr} + (rr\|rr) + (aa\|bb) + (ab\|ab) - 2(aa\|rr) - 2(bb\|rr) + A_{ab,rr}$ $+C_{rr} - B_{ab}/2$
Φ_{aa}^{rs}	$D_{aa}^{rs} + (aa\|aa) + (rr\|ss) + (rs\|rs) - 2(aa\|rr) - 2(aa\|ss) + A_{aa,rs}$ $-B_{aa} + C_{rs}/2$
${}^1\Phi_{ab}^{rs}$	$D_{ab}^{rs} + (aa\|bb) + (ab\|ab) + (rr\|ss) + (rs\|rs) - (A_{ab,rs} + B_{ab} - C_{rs})/2$
${}^2\Phi_{ab}^{rs}$	$D_{ab}^{rs} + (aa\|bb) - (ab\|ab) + (rr\|ss) - (rs\|rs) + (A_{ab,rs} - B_{ab} + C_{rs})/2$

[a] We define $D_{\mu\nu\ldots}^{\omega\tau\ldots} = [f_\omega^\omega + f_\tau^\tau + \ldots] - [f_\mu^\mu + f_\nu^\nu + \ldots]$,
$A_{ab,rs} = [(1+\delta_{ab})(1+\delta_{rs})]^{-1}\,[(ar|ar) + (as|as) + (br|br) + (bs|bs)]$,
$B_{ab} = (1+\delta_{ab})^{-1}\,[(ai|ai) + (aj|aj) + (bi|bi) + (bj|bj)]$,
$C_{rs} = (1+\delta_{rs})^{-1}\,[(ir|ir) + (is|is) + (jr|jr) + (js|js)]$.

while the diagonal elements vanish in the EN case,

$$\bar{V}_{II} = V_{II} = 0. \tag{36}$$

Before proceeding with actual applications, let us briefly point out the distinction between the MP and EN partitionings. The main difference is, clearly, in the values taken by $\bar{V}_{II}$. In the EN theory, the whole diagonal part of H is included in H_0, so that $\bar{V}_{II}$ identically vanish, while in the MP formalism, only the diagonal part of H that is included in the orbital energy differences Δ_I, Eqs. 19 and 20, is incorporated into H_0, the remaining diagonal part $\bar{V}_{II}^{(\mathrm{MP})}$, Eq. 24, being accounted for as a perturbation V, so that $(\bar{H}_0)_{II} = \Delta_I + \bar{V}_{II}^{(\mathrm{MP})}$. Using Taylor expansion, we can write the EN2 energy as a series

$$-\sum_I \frac{V_{0I}^2}{(\bar{H}_0)_{II}} = -\sum_I \frac{V_{0I}^2}{\Delta_I} + \sum_I \frac{V_{0I}^2 \bar{V}_{II}^{(\mathrm{MP})}}{\Delta_I^2} - \sum_I \frac{V_{0I}^2 (\bar{V}_{II}^{(\mathrm{MP})})^2}{\Delta_I^3} + \cdots, \tag{37}$$

indicating that the $\bar{V}_{II}^{(\mathrm{MP})}$ term, forming a part of the EN denominators, appears in higher order terms of the MP theory. Clearly, both theories will give the same result in the infinite order limit provided they converge, but they have a rather different behavior in the low orders of the theory.

5. Applications

To examine the performance of the above outlined PT's, we consider a few low-lying states of CH_2, NH_2^+ and H_2O.

We first examine the $^1B_1$ state of CH_2 and NH_2^+, and use double zeta (DZ) [$4s2p/2s$] and DZ plus polarization (DZP) [$4s2p1d/2s1p$] basis sets, as well as the reference configuration and geometries described in detail in (13). Also, throughout this paper, we use Cartesian Gaussians for the d and f orbitals, and the GAMESS package (30) for the ROHF and various CI calculations. All electrons are correlated when employing the DZ basis, while only valence electrons are correlated when using the DZP basis.

In Table 3, the MP2, MP3, EN2 and EN3 energies for the lowest $^1B_1$ state of CH_2 and NH_2^+ are compared with the SCF (ROHF), UGA-CC [at both linear and quadratic levels of the first interacting space (is) approximation, referred to as L-CCSD(is) and CCSD(is), respectively], and various CI [including full CI (FCI)] results, considering both DZ and DZP basis sets. (For full SD space CCSD results and other limited CI results, see Table 2 of (13)). These results indicate that MP2 underestimates the exact correlation energy by about 12–15%, yielding 84.8 and 88.5% of the correlation energy for the $^1B_1$ state of CH_2 and NH_2^+, respectively, with

Table 3
CC, CI and various 2nd- and 3rd-order perturbation energies[a] for the lowest $^1B_1$ states of CH_2 and NH_2^+, obtained with DZ and DZP basis sets. The percentage of the exact correlation energy is given in parentheses for each method.

Method	CH_2		NH_2^+	
	$^1B_1$/DZ	$^1B_1$/DZP	$^1B_1$/DZ	$^1B_1$/DZP
SCF	0.842 053	0.860 850	0.118 736	0.140 248
	(0.0)	(0.0)	(0.0)	(0.0)
MP2	0.912 807	0.970 152	0.191 040	0.260 771
	(84.8)	(88.8)	(88.5)	(91.8)
MP3	0.922 361	0.981 226	0.197 953	0.269 377
	(96.3)	(97.8)	(96.9)	(98.3)
EN2	0.930 775	0.995 950	0.206 647	0.284 145
	(106.4)	(109.7)	(107.6)	(109.6)
EN3	0.922 593	0.980 711	0.197 193	0.268 108
	(96.6)	(97.4)	(96.0)	(97.4)
L-CCSD(is)	0.926 152	0.985 148	0.200 816	0.272 507
	(100.8)	(101.0)	(100.5)	(100.7)
CCSD(is)	0.925 034	0.982 216	0.200 031	0.269 895
	(99.5)	(98.6)	(99.5)	(98.7)
CISD(is)	0.922 612	0.978 699	0.198 221	0.266 813
	(96.6)	(95.7)	(97.3)	(96.4)
$CISDTQ^+$	0.925 424	0.983 916	0.200 422	0.271 540
	(100.0)	(100.0)	(100.0)	(100.0)
FCI	0.925 457	0.983 970	0.200 448	0.271 581
	(100.0)	(100.0)	(100.0)	(100.0)

[a] The energies are in hartree and are reported as $-(E+38)$ for CH_2, and $-(E+55)$ for NH_2^+, respectively.

the DZ basis, and a similar result for the DZP basis. This behavior of underestimating the exact energy parallels that of the standard MP2 method when applied to CS systems. In contrast, EN2 overestimates the exact energy by about 5–6 millihartree (mhartree) with the DZ basis, and 12–13 mhartree with DZP. This translates into about 106–110% of the exact correlation energy. This overestimate by EN2 is similar to that by the linear CCSD method (L–CCSD).

The third order contribution improves the result for both MP and EN schemes. Thus, in the MP case, $E^{(3)}$ is small and negative, while the EN value is positive. Both MP3 and EN3 results thus recover 96–98% of the exact correlation energy. As noted at the close of the preceding

section, both MP and EN schemes will eventually converge to the same exact result. Remarkably enough, we find already the third order energies to be close to one another as well as to the computationally much more demanding CISD(is) result. Not surprisingly, the UGA based CCSD(is) gives the best result, representing a higher level of the theory.

Consider, next, the lowest states of $^1B_1$, $^1A_2$ and $^1B_2$ symmetry of the water molecule. These may be characterized by monoexcitations $1b_1(\pi) \rightarrow 4a_1$, $1b_1(\pi) \rightarrow 2b_2$ and $3a_1(n) \rightarrow 2b_2$, respectively. In all calculations for H_2O we correlate all the electrons. We first employ a DZ $[4s2p/2s]$ contraction (31) of the Huzinaga's primitive $(9s5p/4s)$ basis, for which FCI benchmark results are available (32, 33). We use the same geometries as do these benchmarks (see (32)). A comparison of our results for both total and vertical excitation energies with those obtained by other methods is summarized in Table 4. In order to calculate excitation energies, we also include the $^1A_1$ CS ground state (note that the EN partitioning for CS states also employs the entire diagonal part of H as H_0). We again find a similar behavior for the three OSS states of H_2O as in the case of CH_2 and NH_2^+: the MP2 and EN2 energies underestimate and overestimate true correlation energies, respectively, while the third order contributions invariably improve the second order results.

Turning our attention to vertical excitation energies, we first note that the SCF values are 0.7–0.8 eV too low. At the MP2 level, the excitation energies are rather well reproduced, the errors being 0.065, 0.047 and 0.089 eV for $^1B_1$, $^1A_2$ and $^1B_2$ states, respectively. At the MP3 level, these errors become, respectively, −0.06, −0.06 and −0.019 eV. Thus, the absolute errors of the MP2 and MP3 transition energies are roughly the same, MP2 values being slightly too high and MP3 ones slightly too low. The EN excitation energies are less satisfactory, the errors being about 0.5 eV at the second order and −0.3 eV at the third order levels. This inferior performance may be ascribed to the imbalance between the CS and OSS EN theories, since the former produces significantly poorer results for the individual energy levels than the latter one. Indeed, the OSS EN2 and EN3 energies are 11–14 mhartree below and 8–9 mhartree above the FCI values, respectively, while the corresponding CS energies for the $^1A_1$ state are 30 and 20 mhartree below and above the FCI energy (cf. Table 4). Thus, the CS errors, although in the same direction, are about twice as large as the OSS ones.

Having examined the performance of UGA based MP and EN MBPT schemes for a smaller DZ basis, where the comparison with the exact FCI results is possible, we can be reasonably confident that the MP2 and 3 methods, similarly as CCSD, will reproduce experimental results assuming that we employ a sufficiently large basis set. We have thus carried out a series of calculations at the MP2, MP3 and CCSD levels with different basis sets approaching the atomic natural orbital (ANO) basis set of (34). First, we

added polarization functions to our DZ set obtaining a DZP [4*s*2*p*1*d*/2*s*1*p*] basis set (see (35) for details). We then considered a sequence of ANO basis sets, i.e., [4*s*2*p*/2*s*], [4*s*2*p*1*d*/2*s*1*p*], [4*s*3*p*2*d*/3*s*2*p*] and [4*s*3*p*2*d*1*f*/3*s*2*p*1*d*] obtained by deleting the functions from the [6*s*5*p*3*d*2*f*/4*s*3*p*2*d*] ANO basis of (34). For these five ANO basis sets, we used the experimental geometry for H_2O ground state (i.e., $r_{O-H} = 1.81117$ a.u. and $\angle HOH = 104.44°$).

Table 4
Comparison of total and vertical excitation energies for the ground and singlet excited states of water obtained via various CI, CC, and 2nd- and 3rd-order PTs, using a DZ basis set (see the text).

Method	$^1A_1$	$^1B_1$	$^1A_2$	$^1B_2$
		$E_{tot}(a.u.)$		
SCF	−76.009 838	−75.715 210	−75.639 491	−75.551 826
MP2	−76.149 315	−75.827 365	−75.750 151	−75.658 554
MP3	−76.150 707	−75.833 337	−75.755 965	−75.663 936
EN2	−76.188 516	−75.852 310	−75.774 508	−75.681 760
EN3	−76.137 991	−75.830 287	−75.752 881	−75.661 381
CCSD(is)[a]	−76.156 076	−75.836 450	−75.759 166	−75.667 914
CISD(is)	−76.150 015	−75.833 300	−75.756 138	−75.665 054
CISDTQ	−76.157 603	−75.837 949	−75.760 920	−75.670 264
FCI/LCI[b]	−76.157 866	−75.838 288	−75.761 050	−75.670 379
		Vertical excitation energies (eV)		
SCF		8.017	10.078	12.463
MP2		8.761	10.862	13.354
MP3		8.636	10.741	13.246
EN2		9.148	11.266	13.790
EN3		8.373	10.479	12.969
CCSD(is)[a]		8.697	10.800	13.284
CISD(is)		8.618	10.718	13.196
CISDTQ		8.698	10.794	13.261
FCI/LCI[b]		8.696	10.798	13.265

[a] The standard SR CCSD for the ground $^1A_1$ state, UGA based OSS CCSD for other OSS excited states.

[b] FCI result for $^1A_1$ (32), $^1B_1$ and $^1A_2$ state (33), and very "large CI" (LCI) (which is in fact a CI SDTQQ, i.e. all up to and including quintuple excitations) for the $^1B_2$ state. We did not use the FCI result for the $^1B_2$ given in (33), −75.670141 a.u., which must involve a misprint since it is higher than the CI SDTQQ result generated by GAMESS.

The results of these calculations are compared with the available experimental data (36, 37) in Table 5.

We first observe that we do not get automatically better results by simply adding polarization functions (d orbitals on O and p orbitals on H). For the $^1B_1$ state, whose vertical excitation energy is well established to be around 7.4 eV (36, 37), the DZP result ($\sim$ 9.1 eV) at the MP3 and CCSD levels is about 0.4 eV further away from the experiment than the DZ result ($\sim$ 8.7 eV). It is thus important to employ more appropriate basis set in order to reach basis set converged results. We thus employ the ANO basis sets, resulting from correlated atomic calculations, first advocated by Almlöf and Taylor (38), which are known to efficiently account for molecular correlation effects.

As the results in Table 5 indicate, the SCF vertical excitation energies converge to about 6.5 eV for $^1B_1$, 8.1 eV for $^1A_2$ and 10.4 eV for $^1B_2$ states when fairly large basis sets (including d and f functions) are employed. For the $^1B_1$ and $^1A_2$ states, these are about 1 eV short of the experimental values. This is consistent with our DZ results in which case the SCF excitation energies were about 0.7–0.8 eV below the FCI ones. Examining the MP2, MP3 and SS CCSD excitation energies, we find that they follow a general pattern MP3 < CCSD < MP2. This again conforms with the above described DZ results, where we found the CCSD energies to be most reliable, while the MP2 and MP3 excitation energies slightly overestimated and underestimated the FCI values, respectively. It should also be noted that the difference between the SS CCSD and MP3 results never exceeds 0.05 eV.

Concerning the suitability of different basis sets and the related convergence of the computed excitation energies, we find an essential difference between the DZP and ANO type basis sets, while we observe only marginal changes within the ANO basis set sequence when adding d, f and p, d functions to the O and H atoms, respectively. For the largest $[4s3p2d1f/3s2p1d]$ ANO basis set employed, we find a good agreement of the MP3 and SS CCSD results with the experiment. A particularly remarkable feature is a relatively stable behaviour of the computed excitation energies when using ANO basis sets. This phenomenon is most remarkable for the Rydberg $^1B_1$ state. Deleting f and d functions from the O and H atoms, respectively, the $^1B_1 \leftarrow {}^1A_1$ excitation energies at the MP3 and CCSD levels change by only 0.1 eV. Even the differences between the results employing the largest $[4s3p2d1f/3s2p1d]$ and the smallest $[4s2p/2s]$ ANO basis sets do not exceed 0.1 eV. Thus, already the $[4s2p/2s]$ ANO basis, which contains no polarization functions, gives a rather good agreement with the experiment. Assuming this pattern to hold in general, we should be able to compute reasonably accurate excitation energies for a rather large system using such severely truncated ANO basis sets, at least for the low lying excited states.

Table 5
Experimental and theoretical vertical excitation energies (VEEs) of H_2O obtained with various basis sets and SCF, PT and CC theories[a]. The total energies are reported as $-(E+75)$.

	$E_{tot}(a.u.)$				VEE (eV)		
	$^1A_1$	$^1B_1$	$^1A_2$	$^1B_2$	$^1B_1$	$^1A_2$	$^1B_2$
DZP[4*s*2*p*1*d*/2*s*1*p*]							
SCF	1.046 512	0.735 392	0.662 851	0.556 241	8.47	10.44	13.34
MP2	1.263 201	0.927 189	0.853 377	0.745 012	9.14	11.15	14.10
MP3	1.269 578	0.937 032	0.862 737	0.754 398	9.05	11.07	14.02
CCSD	1.272 334	0.938 055	0.863 929	0.756 436	9.10	11.11	14.04
ANO[4*s*2*p*/2*s*]							
SCF	1.004 227	0.754 549	0.666 864	0.579 082	6.79	9.18	11.57
MP2	1.134 627	0.850 079	0.763 485	0.671 187	7.74	10.10	12.61
MP3	1.131 817	0.854 505	0.767 034	0.674 360	7.55	9.93	12.45
CCSD	1.138 226	0.858 272	0.770 470	0.678 055	7.62	10.01	12.52
ANO[4*s*2*p*1*d*/2*s*1*p*]							
SCF	1.058 149	0.809 542	0.719 787	0.623 803	6.76	9.21	11.82
MP2	1.274 833	0.986 546	0.899 068	0.801 315	7.84	10.23	12.89
MP3	1.278 078	0.996 501	0.908 012	0.809 837	7.66	10.07	12.74
CCSD	1.281 172	0.998 362	0.909 671	0.811 894	7.70	10.11	12.77
ANO[4*s*3*p*2*d*/3*s*2*p*]							
SCF	1.064 175	0.827 449	0.766 912	0.680 133	6.44	8.09	10.45
MP2	1.309 910	1.029 277	0.963 321	0.876 170	7.64	9.43	11.80
MP3	1.312 208	1.039 827	0.974 879	0.887 020	7.41	9.18	11.57
CCSD	1.315 468	1.041 540	0.976 853	0.889 152	7.45	9.21	11.60
ANO[4*s*3*p*2*d*1*f*/3*s*2*p*1*d*]							
SCF	1.066 391	0.829 063	0.768 848	0.683 842	6.46	8.10	10.41
MP2	1.346 648	1.062 417	0.996 242	0.910 720	7.73	9.54	11.86
MP3	1.349 866	1.073 854	1.008 859	0.922 656	7.51	9.28	11.62
CCSD	1.352 079	1.074 855	1.010 220	0.924 179	7.54	9.30	11.64
Exp.					7.49[b]	9.1[c]	
					7.4[c]		

[a] The standard MP*n* and SR CCSD for the ground $^1A_1$ state, UGA based MP*n* and OSS CCSD for the excited states.
[b] From (37).
[c] From (36).

6. Conclusions

This paper describes a simple finite order PT for low spin OSS states using the spin-free ROHF wave function as a reference. Relying on the UGA formalism the method retains the features of a SR theory. Both MP and EN partitionings of the Hamiltonian are considered. Similarly as with the CS and HS OS perturbation theories, we find the MP partitioning to give better results than the EN one. The focus of the paper is on the OSS states and the calculations are carried out at the second and third order levels. The capabilities of this approach are illustrated on the low lying OSS excited states of CH_2, NH_2^+ and H_2O. An extension of the theory to the MP4 level and to the HS OS states will be given elsewhere.

The results for H_2O, where the well established experimental data are available, clearly indicate the superiority of the ANO type basis sets, even when severely truncated, particularly for low lying Rydberg states. This finding is of a considerable practical value enabling a meaningful study of low lying excited states for larger systems using the low order finite PT and relatively small ANO basis sets. Nonetheless, we must emphasize that the states examined in this study are "well behaved", and we cannot expect the same quality of results for "difficult" quasidegenerate states. Clearly, in such cases we have to rely on the higher level CC methods, and in severe cases of quasidegeneracy the MR treatment may be unavoidable.

7. Acknowledgements

We very much appreciate the invitation to contribute to these proceedings. Continued support by the Natural Sciences and Engineering Research Council of Canada (J.P.) is gratefully acknowledged.

References

(1) A. T. Amos and G. G. Hall, Proc. Roy. Soc. (London) **A263**, 483 (1961).

(2) N. C. Handy, P. J. Knowles, and K. Somasundram, Theor. Chim. Acta **68**, 87 (1985).

(3) P. Čársky and I. Hubač, Theor. Chim. Acta **80**, 407 (1991).

(4) C. Murray and E. R. Davidson, Int. J. Quantum Chem. **43**, 755 (1992).

(5) I. Hubač and P. Čársky, Phys. Rev. A **22**, 2392 (1980).

(6) C. Murray and E. R. Davidson, Chem. Phys. Letters **187**, 451 (1991).

(7) J. Paldus, in: *Methods in Computational Molecular Physics*, eds. S. Wilson and G. H. F. Diercksen, NATO ASI Series, Series B: Physics, Vol. 293 (Plenum Press, New York, 1992) pp. 99–194.

(8) J. Paldus, in: *Relativistic and Electron Correlation Effects in Molecules and Solids*, ed. G. L. Malli, NATO ASI Series, Series B: Physics, Vol. 318 (Plenum Press, New York, 1994) pp. 207–282.

(9) A. Balková and R. J. Bartlett, Chem. Phys. Lett. **193**, 364 (1992).

(10) R. J. Bartlett, in: *Modern Electronic Structure Theory*, Part I, ed. D. R. Yarkony (World Scientific, Singapore, 1995) pp. 1047–1131.

(11) J. Paldus and X. Li, in: *Symmetries in Science VI: From the Rotation Group to Quantum Algebras*, ed. B. Gruber (Plenum Press, New York, 1993) pp. 573–592.

(12) X. Li and J. Paldus, Intern. J. Quantum Chem., Symp. **27**, 269 (1993).

(13) X. Li and J. Paldus, J. Chem. Phys. **101**, 8812 (1994).

(14) J. Paldus, in: *Atomic, Molecular and Optical Physics Reference Book*, Sec. II, *Mathematical Methods*, Chap. 5, *Perturbation Theory*, ed. G. W. F. Drake (American Institute of Physics, New York, 1996) pp. 76-87.

(15) J. Paldus, in: *Atomic, Molecular and Optical Physics Reference Book*, Sec. II, *Mathematical Methods*, Chap. 4, *Dynamical Groups*, ed. G. W. F. Drake (American Institute of Physics, New York, 1996) pp. 65-75.

(16) J. Paldus, J. Chem. Phys. **61**, 5321 (1974).

(17) J. Paldus, in: *Theoretical Chemistry: Advances and Perspectives*, Vol. 2, eds. H. Eyring and D. J. Henderson (Academic Press, New York, 1976) pp. 131–290.

(18) J. Paldus, in: *Mathematical Frontiers in Computational Chemical Physics*, ed. D. G. Truhlar (Springer Verlag, Berlin, 1988) pp. 262–299; in: *Contemporary Mathematics*, Vol. 160, eds. N. Kamran and P. J. Olver (American Mathematical Society, Providence, RI, 1994) pp. 209–236.

(19) F. A. Matsen and R. Pauncz, *The Unitary Group in Quantum Chemistry* (Elsevier, Amsterdam, 1986), Sec. 4.4.2.

(20) J. Paldus and C. R. Sarma, J. Chem. Phys. **83**, 5135 (1985).

(21) J. Paldus, M. J. Gao and J. Q. Chen, Phys. Rev. A **35**, 3197 (1987).

(22) J. Paldus, S. Rettrup and C. R. Sarma, J. Mol. Struct. (Theochem) **199**, 85 (1989).

(23) X. Li and J. Paldus, Int. J. Quantum Chem. **41**, 117 (1992).

(24) J. Paldus and B. Jeziorski, Theor. Chim. Acta **73**, 81 (1988).

(25) X. Li and Q. Zhang, Int. J. Quantum Chem. **36**, 599 (1989).

(26) B. Jeziorski, J. Paldus and P. Jankowski, Int. J. Quantum Chem. **56**, 129 (1995).

(27) C. Møller and M. S. Plesset, Phys. Rev. **46**, 618 (1934).

(28) P. S. Epstein, Phys. Rev. **28**, 695 (1926); R. K. Nesbet, Proc. Roy. Soc. (London) **A250**, 312 (1955).

(29) F. W. Bobrowicz and W. A. Goddard III, in: *Methods of Electronic Structure Theory*, ed. H. F. Schaefer III (Plenum Press, New York, 1977) pp. 79–127.

(30) GAMESS, M. W. Schmidt, K. K. Baldridge, J. A. Boatz, S. T. Elbert, M. S. Gordon, J. H. Jensen, S. Koseki, N. Matsunaga, K. A. Nguyen, S. J. Su, T. L. Windus, togetehr with M. Dupuis, and J. A. Montgomery, J. Comput. Chem. **14**, 1347 (1993).

(31) T. H. Dunning, J. Chem. Phys. **53**, 2823 (1970).

(32) P. Saxe, H. F. Schaefer III and N. C. Handy, Chem. Phys. Lett. **79**, 202 (1981); R. J. Harrison and N. C. Handy, Chem. Phys. Lett. **95**, 386 (1983).

(33) K. Hirao, Chem. Phys. Lett. **201**, 59 (1993).

(34) P. O. Widmark, P. A. Malmqvist and B. O. Roos, Theor. Chim. Acta **77**, 291 (1990).

(35) C. W. Bauschlicher and P. R. Taylor, J. Chem. Phys. **85**, 2779 (1986).

(36) D. Yeager, V. McKoy and S. A. Segal, J. Chem. Phys. **61**, 755 (1974).

(37) K. Watanabe and M. Zelikoff, J. Opt. Soc. Amer. **43**, 753 (1953).

(38) J. Almlöf and P. R. Taylor, J. Chem. Phys. **86**, 4070 (1987).

The Contracted Schrödinger Equation: Some Results

C. Valdemoro, L. M. Tel*, E. Pérez-Romero*

Instituto de Matemáticas y Física Fundamental
Consejo Superior de Investigaciones Científicas
Serrano 123. Madrid. 28006 Spain
*Dpto. de Química Física, Universidad de Salamanca
Salamanca. 37008 Spain

Abstract

The Contracted Schrödinger Equation is studied here in a spin-orbital representation coupled with the $\hat{S}^2$ eigenvalue equation as an auxiliary condition. A set of new algorithms for approximating RDM's in terms of the lower order ones are reported here. These new features improve significantly the method.

ADVANCES IN QUANTUM CHEMISTRY, VOLUME 28

0065-3276/97 $25.00

1. Introduction

The development of the Reduced Density Matrices (RDM) theory started more than fifty years ago (1, 2). It is not our aim here, to review this important theme on which excellent books and reviews have been written (3, 4, 5) since our interest is concentrated here on a very particular aspect of this vast field: to study the different problems arising when one attempts to solve iteratively the Contracted Schrödinger equation (CSE). This equation was first reported in an integro-differential form by Nakatsuji (6) and Cohen and Frishberg (7) who called it Density Equation (DE). The initial interest raised by the DE when it was obtained in 1976 faded away because this equation is indeterminate. The indeterminacy is caused by the fact that, after the integration has been carried out over N-q electron variables, the DE still depends not only on the q-RDM but also on the (q+1)- and (q+2)-RDM's. Later on, one of us, by applying the matrix Contracting Mapping (CM) (8, 9) to the matrix representation of the Schrödinger equation obtained a contracted form of this equation which was essentially identical to the DE although its matrix form renders it more easy to handle. In order, not only to distinguish the matrix representation of the equation from its integro-differential form, but mainly because it clearly indicates its origin and the way it is obtained, we continue to refer to it as Contracted Shrödinger Equation which was how we called it originally.

The possibility to decouple the CSE arose when a systematic way to approximate high order RDM's in terms of the lower order ones was found (10, 11, 12). Thus the iterative solution of the CSE was proposed by Colmenero and Valdemoro (11), who later on obtained the first results with this method (13).

Recently, Nakatsuji and Yasuda have proposed an alternative way to approximate the higher order RDM's in terms of the lower order ones (14) proceeding then, like us, to solve the DE iteratively.

In (13) the CSE was represented in a spin-free basis and a spin-adaptation was subsequently applied. However this kind of spin adaptation proved to be very costly, therefore we decided to take explicitly into account the spin by using spin-orbitals for the one-electron basis (15), to apply transformations of the basis only at some delicate stages and finally to combine the CSE with the contracted $\hat{S}^2$ eigen-value equation. To report these latter developments is the object of this paper.

The theoretical aspects concerning the equations themselves are developed in the following section. Then, in section three, we describe the algorithms for approximating higher order RDM's in terms of the lower order ones in a spin-orbital representation. Some new algorithms for approximating the 3-RDM that permit to avoid storing the 4-RDM are also reported in this section. The structure of the computational code is summarized in

section four. In the fifth section the results obtained for the BeH_2 molecule are discussed.

2. Theoretical outline

2.1. The Contracted Schrödinger Equation

The element $\{\Lambda, \Omega\}$ of the matrix representation of the Schrödinger equation for an N-electron system in the eigenstate $\mathcal{L}$ is

$$E_{\mathcal{L}} \ \mathcal{D}^{\mathcal{L}\mathcal{L}}_{\Lambda,\Omega} = (\ \mathcal{H} \ \mathcal{D}^{\mathcal{L}\mathcal{L}})_{\Lambda,\Omega} \tag{1}$$

where E is the energy of the eigen-state $\mathcal{L}$, the symbol $\mathcal{H}$ represents the Hamiltonian matrix and

$$\mathcal{D}^{\mathcal{L}\mathcal{L}}_{\Lambda,\Omega} = < \Omega|\mathcal{L} >< \mathcal{L}|\Lambda > \tag{2}$$

is the $\{\Lambda, \Omega\}$ element of the Density Matrix (DM).

The spin-orbital representation of the $C.M.$ is :

$${}^2D^{\mathcal{L}\mathcal{L}}_{i_\sigma j_{\sigma'}, k_\sigma \ell_{\sigma'}} = \sum_{\Lambda,\Omega} {}^2D^{\Lambda,\Omega}_{i_\sigma j_{\sigma'}, k_\sigma \ell_{\sigma'}} \ \mathcal{D}^{\mathcal{L}\mathcal{L}}_{\Lambda,\Omega} \tag{3}$$

where

$${}^2D^{\mathcal{L}\mathcal{L}}_{i_\sigma j_{\sigma'}, k_\sigma \ell_{\sigma'}} = < \mathcal{L}| \ b^\dagger_{i_\sigma} \ b^\dagger_{j_{\sigma'}} b_{\ell_{\sigma'}} b_{k_\sigma}|\mathcal{L} > \tag{4}$$

is the second order Reduced Density Matrix $(2 - RDM)$. Here, the letters i, j, k, ℓ and σ, σ' represent the orbitals and the spin-functions respectively. In Eq. 4 the indices are chosen in a given order, i.e.: $i_\sigma < j_{\sigma'}$ and $k_\sigma < \ell_{\sigma'}$. When, alternatively, the indices are allowed to take all the possible values, a factor $\frac{1}{2!}$ must multiply the r.h.s. of Eq. 4. The definitions for higher order RDM's are the natural generalization of Eq. 4. In what follows the explicit reference to eigenstate $\mathcal{L}$ is omitted and two kinds of simplified notations for RDM's are used indistinctly according to convenience:

$$D^{\alpha\beta}_{ij,kl} = D_{i\bar{j},k\bar{l}} = < \mathcal{L}| \ b^\dagger_i \ b^\dagger_{\bar{j}} b_{\bar{l}} b_k|\mathcal{L} > \tag{5}$$

where the bar over the indices indicates that the spin function is beta.

When applying the CM to both sides of Eq. 1 one obtains

$$E_{\mathcal{L}} \ {}^2D^{\mathcal{L}\mathcal{L}}_{i_\sigma j_{\sigma'}, k_\sigma \ell_{\sigma'}} = < \mathcal{L}|\hat{H} \ b^\dagger_{i_\sigma} \ b^\dagger_{j_{\sigma'}} \ b_{\ell_{\sigma'}} \ b_{k_\sigma}|\mathcal{L} > \tag{6}$$

where $\hat{H}$ is the the N-electron Hamiltonian:

$$H = \left\{ \begin{array}{l} \sum_{r<s;k<\ell} {}^0H^{\alpha\alpha}_{rs;k\ell} \ b^\dagger_{r\alpha} b^\dagger_{s\alpha} b_{\ell\alpha} b_{k\alpha} \\ + \sum_{uv;mn} {}^0H^{\alpha\beta}_{uv;mn} \ b^\dagger_{u\alpha} b^\dagger_{v\beta} b_{n\beta} b_{m\alpha} \\ + \sum_{r<s;k<\ell} {}^0H^{\beta\beta}_{rs;k\ell} \ b^\dagger_{r\beta} b^\dagger_{s\beta} b_{\ell\beta} b_{k\beta} \end{array} \right\} \tag{7}$$

the three ${}^0H^{\sigma\sigma'}$ matrices appearing in Eq. 7 are:

$$\begin{aligned} {}^0H^{\alpha\alpha}_{rs;k\ell} &= {}^0H_{rs;k\ell} - {}^0H_{rs;\ell k} \\ {}^0H^{\alpha\beta}_{uv;mn} &= {}^0H_{uv;m\bar{n}} \\ {}^0H^{\beta\beta}_{rs;k\ell} &= {}^0H_{\bar{r}\bar{s};\bar{k}\bar{\ell}} - {}^0H_{\bar{r}\bar{s};\bar{\ell}\bar{k}} \end{aligned} \tag{8}$$

$${}^0H_{i_\sigma j_{\sigma'};p_\sigma q_{\sigma'}} = \frac{1}{N-1}\left(\varepsilon^{\sigma}_{ip}\delta_{jq} + \varepsilon^{\sigma'}_{jq}\delta_{ip}\right) + < ij|pq >$$

where the symbol ε represents the one-electron integral matrix whereas $< rs|k\ell >$ is the two-electron repulsion integral in the Condon and Shortley notation.

Transforming into normal form Eq. 6 one obtains the CSE. In this representation it splits into the three following coupled equations (summations over all posible values of common indices are implicit with the restrictions $r < s$ and $k < \ell$):

$$E\ D^{\alpha\alpha}_{ij;pq} \underset{(i<j;p<q)}{=} \left\{ \begin{array}{l} D^{\alpha\alpha}_{ij;rs}\ {}^0H^{\alpha\alpha}_{rs;pq} \\ - D^{\alpha\alpha\alpha}_{ijm;qrs}\ {}^0H^{\alpha\alpha}_{rs;pm} + D^{\alpha\alpha\alpha}_{ijm;prs}\ {}^0H^{\alpha\alpha}_{rs;qm} \\ + D^{\alpha\alpha\beta}_{ijm;puv}\ {}^0H^{\alpha\beta}_{uv;qm} - D^{\alpha\alpha\beta}_{ijm;quv}\ {}^0H^{\alpha\beta}_{uv;pm} \\ + D^{\alpha\alpha\alpha\alpha}_{ijk\ell;pqrs}\ {}^0H^{\alpha\alpha}_{rs;k\ell} + D^{\alpha\alpha\beta\beta}_{ijk\ell;pqrs}\ {}^0H^{\beta\beta}_{rs;k\ell} \\ + D^{\alpha\alpha\alpha\beta}_{ijmn;pquv}\ {}^0H^{\alpha\beta}_{uv;mn} \end{array} \right\} \tag{9}$$

$$E\ D^{\alpha\beta}_{ij;pq} = \left\{ \begin{array}{l} D^{\alpha\beta}_{ij;uv}\ {}^0H^{\alpha\beta}_{uv;pq} \\ - D^{\alpha\alpha\beta}_{mij;rsq}\ {}^0H^{\alpha\alpha}_{rs;pm} + D^{\alpha\beta\beta}_{ijm;prs}\ {}^0H^{\beta\beta}_{rs;qm} \\ - D^{\alpha\alpha\beta}_{mij;puv}\ {}^0H^{\alpha\beta}_{uv;mq} - D^{\alpha\beta\beta}_{ijn;uvq}\ {}^0H^{\alpha\beta}_{uv;pn} \\ + D^{\alpha\alpha\alpha\beta}_{k\ell ij;rspq}\ {}^0H^{\alpha\alpha}_{rs;k\ell} + D^{\alpha\beta\beta\beta}_{ijk\ell;pqrs}\ {}^0H^{\beta\beta}_{rs;k\ell} \\ + D^{\alpha\alpha\beta\beta}_{imjn;puqv}\ {}^0H^{\alpha\beta}_{uv;mn} \end{array} \right\} \tag{10}$$

The relation for $M_s = -1$ follows directly from Eq. 9 by exchanging the spin functions. (The symmetric form of Eq. 6 generates another set of equivalent equations.)

The unknowns in these three equations are not only the Energy and the 2-RDM but also the higher order matrices - the 3-RDM and the 4-RDM. This, as has been mentioned, is what causes the indeterminacy of these equations. In spite of this drawback an approximate solution may be obtained (12, 13) by estimating the 3- and 4-RDM from an initial 1- and 2-RDM, replacing them into the equation and continue iterating until consistency. As can be observed, these three equations are coupled since the same high order RDM appears in more than one equation which, as will be discussed later on, renders necessary their simultaneous solution.

2.2. The Contracted Spin-eigen-equation

The application of this iterative method in a spin-free representation provided very good results for the Beryllium atom and some of its isoelectronic ions. However, one of the questions arising from this study was the need to introduce as many auxiliary conditions as possible in order to reduce to the outmost the indeterminacy of the CSE. The most obvious conditions to be imposed derive from the eigen-value equations of operators – other than the Hamiltonian – corresponding to constants of motion of the system and in our case that involving the $\hat{S}^2$ operator seemed most indicated.

The spin operator

$$\begin{aligned} \hat{S}^2 &= -\sum_{r,s} b_r^\dagger\, b_{\bar{s}}^\dagger b_{\bar{r}} b_s + \sum_r \left(\frac{b_r^\dagger b_r - b_{\bar{r}}^\dagger b_{\bar{r}}}{2}\right)^2 + \sum_r \frac{(b_r^\dagger b_r + b_{\bar{r}}^\dagger b_{\bar{r}})}{2} \\ &= -\hat{T} + \left(\frac{\hat{N}_\alpha - \hat{N}_\beta}{2}\right)^2 + \frac{\hat{N}}{2} \end{aligned} \tag{11}$$

when acting on an eigenstate of the system gives rise to an eigenvalue equation and this can be exploited in order to get the complementary condition

$$< \mathcal{L}|\, \hat{S}^2\, b_i^\dagger\, b_j^\dagger b_l b_k |\mathcal{L}> = S(S+1)\ < \mathcal{L}|\, b_i^\dagger\, b_j^\dagger b_l b_k |\mathcal{L}> \tag{12}$$

By replacing Eq. 11 into Eq. 12 and transforming the different strings of operators appearing in the l.h.s. into their normal form one gets the three following equations

$$D^{\alpha\alpha}_{pq;sr} = C\left(\sum_i(-D^{\alpha\alpha\beta}_{iqp;sri} + D^{\alpha\alpha\beta}_{ipq;sri}) - \sum_{ij} D^{\alpha\alpha\alpha\beta}_{pqij;srji}\right) \tag{13}$$

$$D^{\alpha\beta}_{pq;sr} = C\left(-D^{\alpha\beta}_{qp;sr} + \sum_i(-D^{\alpha\alpha\beta}_{pqi;sir} + D^{\alpha\beta\beta}_{ipq;sri}) - \sum_{ij} D^{\alpha\alpha\beta\beta}_{ipjq;sjri}\right) \tag{14}$$

where

$$C = \frac{1}{\frac{N}{2} + \frac{(N_\alpha - N_\beta)^2}{4} - S(S+1)} \tag{15}$$

and again the relation for $M_S = -1$ is analogous to the $\alpha\alpha$ one.

In order to ensure that these auxiliary conditions are satisfied when solving the set of coupled CSE's, we replace the $D^{\alpha\alpha}$ matrix element appearing in the first term of Eq. 9, by the expression given for this element by Eq. 13 and similarly for the other spin-equations. This is a trivial operation to perform leading however to a set of rather cumbersome expressions for the final equations which for the sake of brevity are omitted here.

3. *RDM*'s Approximations

The manner in which the approximating algorithms for the high order spin-free *RDM*'s were generated was described in detail in (11, 12). By using a similar reasoning we approximate the algorithms for determining the high order *RDM*'s in a spin-orbital representation. The whole procedure is very similar to the spin-free one and we will only recall here the general idea.

When one takes the expectation value of the conmutator/anticonmutator of a string of p annihilating operators and a string of p creator operators one obtains a series of terms involving products of Krönecker deltas and of $q-1$, $q-2$,...,1-*RDM*'s elements.

By replacing the Krönecker deltas by their value in terms of the expectation values of the lower order similar expressions, a new expression is obtained from which all the mixed products of elements of *holes RDM's* and of *RDM*'s may be eliminated without difficulty. As a result, one obtains a relation which can be summarized as:

$$\begin{array}{c} {}^{p}\bar{D}_{i_1,i_2,..,i_p;j_1,j_2,..,j_p} \\ \pm \\ {}^{p}D_{i_1,i_2,..,i_p;j_1,j_2,..,j_p} \end{array} = \begin{array}{c} f\left\{({}^{(p-1)}\bar{D},..,{}^{1}\bar{D})_{i_1,i_2,..,i_p;j_1,j_2,..,j_p}\right\} \\ \pm \\ f\left\{({}^{(p-1)}D,..,{}^{1}D)_{i_1,i_2,..,i_p;j_1,j_2,..,j_p}\right\} \end{array}$$

where the symmetry of the matrices has been used and the symbol $\bar{D}$ represents the *holes RDM*, i.e.

$$ {}^{2}\bar{D}_{ij,kl} = < \mathcal{L}|\ b_j\ b_i b_k^{\dagger} b_{\ell}^{\dagger}|\mathcal{L} > \tag{16}$$

This result is exact and from it the following equalities can be deduced:

$$ {}^{p}\bar{D}_{i_1,...,i_p;j_1,...,j_p} = f\left\{({}^{(p-1)}\bar{D},\ldots,{}^{1}\bar{D})_{i_1,...,i_p;j_1,...,j_p}\right\} + \bar{\Delta}_{i_1,...,i_p;j_1,...,j_p} $$

$$ {}^{p}D_{i_1,...,i_p;j_1,...,j_p} = f\left\{({}^{(p-1)}D,\ldots,{}^{1}D)_{i_1,...,i_p;j_1,...,j_p}\right\} + \Delta_{i_1,...,i_p;j_1,...,j_p} $$

where

$$ \bar{\Delta}_{i_1,i_2,..,i_p;j_1,j_2,..,j_p} = \mp\, \Delta_{i_1,i_2,..,i_p;j_1,j_2,..,j_p} $$

Our working hypothesis is that all Δ have small values and may be taken into account through a renormalization procedure which will be described in detail later on.

Recently, Nakasutji and Yasuda (14) have proposed a different approximation procedure for the high order *RDM*'s. It is based on a conjecture, that by analogy with the Green function expansion a similar perturbative expansion can be set for the *RDM*'s. In spite of some theoretical reservations which may be raised, the overall approach seems attractive and we are looking forward to see a more detailed work by these authors.

In the practice our approximating methods for high order RDM's approach differ from theirs on the way in which the Δ term is evaluated. They infer it from a Green's function diagram and we correct this error through a renormalization procedure which is described in some detail later on.

3.1. The 3-RDM algorithm

In the more general case where the six orbitals involved have the same spin one has:

$$
\begin{aligned}
&3!\,{}^3D_{i,j,k;\,p,q,r} \approx \\
&-2\, d_{i;\,p}\, d_{j;\,q}\, d_{k;\,r} \\
&+2\,(d_{i;\,p}\, d_{j;\,r}\, d_{k;\,q} + d_{i;\,r}\, d_{j;\,q}\, d_{k;\,p} + d_{i;\,q}\, d_{j;\,p}\, d_{k;\,r}) \\
&-2\,(d_{i;\,r}\, d_{j;\,p}\, d_{k;\,q} + d_{i;\,q}\, d_{j;\,r}\, d_{k;\,p}) \\
&+2!\,(d_{i;\,p}\, {}^2D_{j,k;\,q,r} + d_{j;\,q}\, {}^2D_{i,k;\,p,r} + d_{k;\,r}\, {}^2D_{i,j;\,p,q}) \\
&-2!\,(d_{k;\,q}\, {}^2D_{i,j;\,p,r} + d_{j;\,r}\, {}^2D_{i,k;\,p,q} + d_{i;\,q}\, {}^2D_{j,k;\,p,r} + d_{j;\,p}\, {}^2D_{i,k;\,q,r}) \\
&+2!\,(d_{i;\,r}\, {}^2D_{j,k;\,p,q} + d_{k;\,p}\, {}^2D_{i,j;\,q,r})
\end{aligned}
$$

where the letter d stands for the 1-RDM. Here no ordering of the indices has been imposed, hence the 2! and 3! factors. The structure of this relation can be appreciated easily in the diagrammatic form:

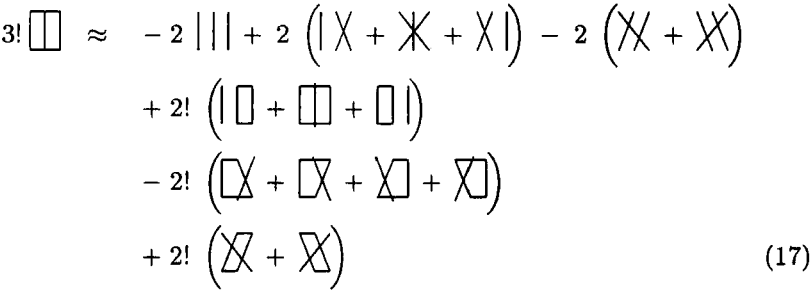

(17)

The graphs appearing in Eq. 17 have a similar meaning to that of the spin-free ones, except that no sum over spin variables is implied. As was the case in the spin-free representation, the classes and the operations of the Symmetric Group classify the terms appearing in the relation.

In order to obtain the algorithms for the cases $D^{\alpha\alpha\beta}$ and $D^{\alpha\beta\beta}$ one removes from the previous expressions those graphs which are forbidden because there is no coincidence between the spin of the creators and that of the corresponding annihilators.

Equivalent expressions for approximating the 4-RDM in terms of the lower order RDM's can be obtained in a similar way.

3.2. Renormalization of the *RDM*'s

As has been mentioned, the algorithms described in the previous section provide good approximations which, however, need a posterior renormalization in order to correct as closely as possible their error which manifests itself not only when the total contraction is applied in order to get the matrix trace but also when partial contractions are performed.

Thus, the relation for approximating the 3-*RDM* does not exactly coincide with the contraction of the 4-*RDM* into the three electron space. The way to correct this lack of consitency is to calculate the 4-*RDM*, renormalize it, and then contract it in order to get the 3- and the 2-*RDM*'s that will be replaced into the CSE. This is how the first calculations were performed (13). This procedure will be called *A* in order to distinguish it from a more economic alternative which will described in the next paragraph.

There are many possibilities for renormalizing these matrices which may be classified into three main cathegories:

1. The procedure described in (10), where the corresponding *holes* matrix is used.
2. The procedure where only the matrix diagonal undergoes the corrections.
3. The procedure where the operations involve the *RDM* eigenvalues which is far more expensive than the others and therefore, at present, is only used for renormalizing the 1-*RDM*.

In the spin-representation the two, three and four electron functions of the basis are simple products of fermion operators. Therefore, the upper limit of their occupation number **is one**. This upper bound value has also been adopted for the elements in a spin-adapted basis of representation. We know also that the diagonal elements must be **positive**. Finally, we know the value not only of the trace but also of the partial traces of the spin-adapted matrices (18, 19, 20).

Irrespectively of the linear form of the basis, when either procedure 2 or procedure 3 is applied the renormalization process has the following basic steps:

- Checking whether there are negative diagonal elements (or eigenvalues). When this is the case, the negative elements are replaced by zero.
- All the diagonal elements (or eigenvalues) are multiplied by the coefficient:

$$X = \frac{\sum_i D_{i,i}^{exact}}{\sum_i D_{i,i}^{approximated}} \tag{18}$$

- Those diagonal elements which - after the previous operation - have become larger than **one** are put equal to **one**.
- Let us suppose that there are three elements which have now the upper bound value, then the value of X is modified as:

$$X = \frac{\sum_i D_{i,i}^{exact} - 3}{\sum_i' D_{i,i}^{approximated}} \tag{19}$$

  where the *prime* on the sum means that only those elements whose value is different from one are summed up.
- If more diagonal elements larger than one appear, the procedure restarts.

For the 3-RDM the correction which originated from a comparison of the approximated 3-RDM and the FCI one in the case of the Be atom (13) is also applied now before the renormalization step starts. It should be noted that although in the four-electron systems calculation (13) the renormalization was practically not needed, in the study of other systems this step of the approximating procedure is important.

There are many other possibilities for performing the renormalization of the RDM's, and in principle we do not think that at this stage of development of the method there are sufficient grounds to decide whether this procedure or Nakatsuji's et al. for approximating the Δ term is the *best* one.

3.3. Avoiding the storage of the 4-RDM

The most expensive parts of this method are the calculation of the numerous 4-RDM elements and the storing of this large matrix. This difficulty is overcome here by calculating only once – at each iteration – each 4-RDM element and entering it at all the places where it is needed. Because of the imperfect consistency mentioned earlier between the 3-RDM directly determined and that obtained by contraction of the 4-RDM this strategy is not trivial to apply. What solved the problem is a set of algorithms which simulate that the contraction has been performed. These algorithms are employed for calculating the off-diagonal elements of the 3-RDM. The diagonal elements must be obtained by contraction of the 4-RDM diagonal after renormalization. For the sake of brevity, these algorithms are not reported here, since they are quite cumbersome [1] . An interesting feature of these algorithms is that many of the terms are not simple products of elements of lower order matrices.

[1] These algorithms are available upon request.

Let us recall that if the 4-RDM were N- and S- representable the $D^{\alpha\alpha\alpha}$ could be obtained in three apparently different manners all three yielding the same result. Thus, the $D^{\alpha\alpha\alpha}$ can be obtained in the three alternative following ways:

$$\begin{aligned} D^{\alpha\alpha\alpha}_{ijk;\ell qs} &= \tfrac{4}{N_\alpha - 3} \sum_r D^{\alpha\alpha\alpha\alpha}_{ijkr;\ell qsr} \\ D^{\alpha\alpha\alpha}_{ijk;\ell qs} &= \tfrac{4}{N_\beta} \sum_r D^{\alpha\alpha\alpha\beta}_{ijkr;\ell qsr} \\ D^{\alpha\alpha\alpha}_{ijk;\ell qs} &= \tfrac{4}{N-3} \sum_r \left(D^{\alpha\alpha\alpha\alpha}_{ijkr;\ell qsr} + D^{\alpha\alpha\alpha\beta}_{ijkr;\ell qsr} \right) \end{aligned} \tag{20}$$

Since, our RDM's are not perfectly N- and S- representable each of these formulae gives slightly different results. Consequently, in our approach we have always used the more symmetric one. This implies that eight different contractions have to be evaluated.

4. Computational details

In a similar way as in (13) the procedure is iterative. The main differences with the spin-free approach are:

1. There are now three coupled equations which must be solved simultaneously.

2. Each 4-RDM element is calculated and entered at all the places that it appears into the equation. Prior to this operation, the diagonal elements of the $4-RDM$ are collected in a vector which is renormalized by following the procedure described above and stored.

3. The 3-RDM is built by making use of the contraction simulating algorithms for the off-diagonal elements and by explicitly contracting the 4-RDM diagonal obtained in the previous step.

4. The 2-RDM is obtained by contraction of the 3-RDM. After including in the CSE the spin conditions, Eqs. 13, 14 and the $\beta\beta$ corresponding one, the ${}^2D^{\alpha\beta}$ is the only 2-RDM still appearing in the equation.

5. Once the three CSE blocks are built they are symmetrized.

6. The trace of each block is divided by that corresponding, respectively, to $-\ {}^2D^{\alpha\alpha}$, ${}^2D^{\alpha\beta}$ or ${}^2D^{\beta\beta}$ $-$ (15). Each one of these values, or their average gives a new estimate of the energy.

7. Each block is divided by the energy and the new 2-RDM is obtained. The renormalization applied here is that described in (10).

8. The 1-RDM is obtained by contraction and its eigen-values are renormalized.

9. The 3-RDM is calculated and the partial traces for the spin-adapted blocks are used in the renormalization of its diagonal.

The programm structure just described speeds up the calculation and significantly reduces the computer capacity requirement with respect to the previous approach. At the moment, we are working on a procedure where the only matrices to be stored are the 1- and 2-RDM's which should greatly improve the applicability of the method.

5. Results and General Discussion

At the Sanibel Symposium of 1994 we presented the results obtained for the BeH_2 molecule by using the CSE method in a spin-orbital representation but without a spin-adaptation. These results while showing that the method could be applied succesfully to systems of more than four electrons motivated the research which has been reported in the previous sections.

Although other small molecules have been already calculated with our method, we think that, the results obtained for the BeH_2 molecule, in the linear geometry, describe in a compact way the general performance of the new developments. The first verification carried out was to see that the same result was obtained by following paths A and B, that is, to contract explicitly the 4-RDM or to use the simulating new algorithms. Once this important point was settled two calculations were carried out. In the first calculation – thereafter refered to as a – we used a minimal basis set with Slater exponents on the Beryllium atom and 1.1 on the Hydrogen atoms. The molecular basis was formed by the *average natural orbitals* which diagonalize the Spin-adapted Reduced Hamiltonian (8, 16). In the second calculation – thereafter refered to as b – we use the same basis as in (17) and the molecular orbitals are Hartree Fock ones.

The energy results obtained in these calculations are reported in Figure 1. The analysis of this figure, as well as other quantities results can be summarized as follows:

- The accumulation of errors, which is clearly apparent when analysing the results at each iteration, together with the high non linearity of the problem continue to cause the instabilities in the last iterations leading to a final divergence. At this respect, it is interesting to note that the onset of instabilities has been delayed by making equal to zero at the main steps of the calculation those quantities whose absolute value was less that 10^{-17}. These kind of instabilities is not in our opinion an important drawback since there are many techniques –

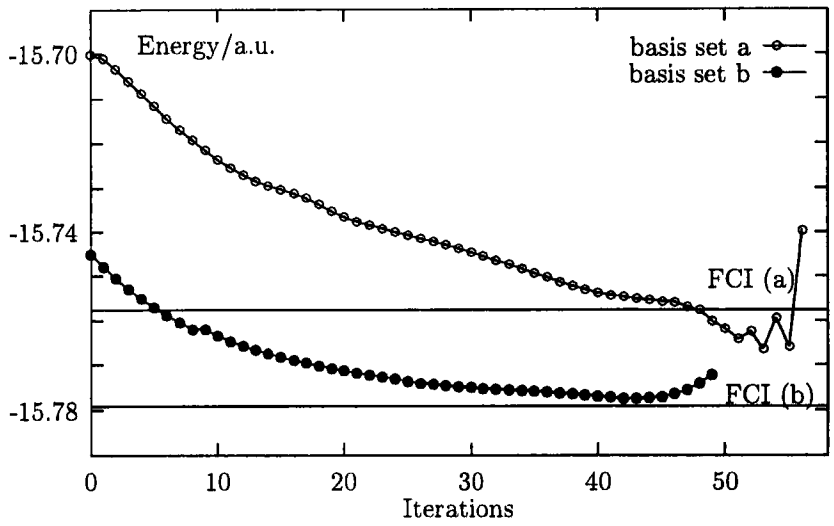

Figure 1: Iteration Curve of Energy.

similar to those developed for ensuring convergence in the Hartree Fock method – available to handle this difficulty.

- The energy value at the onset of instabilities, is, we think, very satisfactory when compared with the Full Configurations Interaction one (FCI).

- During the iterative process, all fluctuations which – without the improvements introduced in this version of the code – rendered necessary the use of a damping technique are not any longer needed since the convergence is smooth until the final steps.

- The fluctuation of the expectation value of the $\hat{S}^2$ operator around the zero value is now of the order of 10^{-16} .

- The ensemble N-representability (21) of the 1-RDM is satisfied up to 10^{-4}.

- The α-block of the 1-RDM obtained by contraction from the $D^{\alpha\beta}$ matrix and from the $D^{\alpha\alpha}$ coincided up to the 4th decimal. This consistency criterium is highly restrictive, therefore this result can be considered very good.

From all these results several conclusions, theoretical as well as technical, can be drawn.

The cleaning of all the matrices by making equal to zero all quantities which in absolute value are smaller than 10^{-17} (in double precision) must be rendered more systematic. In this way we expect the accumulation of errors to diminish noticeably. The introduction of the Newton method as well as Aitken's extrapolation and other standard techniques to speed up convergency may be suitable in future application. However, before having recourse to these standard convergence techniques, we hope to find other more fundamental basic conditions – such as the spin equation which smoothed the oscillations away – in order to attain a complete control of the process. The most important question which remains open is the way in which the renormalizations of the p-*RDM*'s is performed. Another possible improvement is to extend the spin-adaptation to the renormalization of the 4-*RDM* in order to make a thorough use of the partial traces of the different symmetries.

6. Acknowledgments

It is a great pleasure to dedicate this work to Prof. Geerd H. Diercksen on the ocasion of his 60^{th} birthday. The authors also acknowledge the partial financial support of the Dirección General de Investigación Científica y Técnica del Ministerio de Educación y Ciencia under project PB93-0112.

References

(1) K. Husimi, Proc. Phys. Soc. Japan **22** 264 (1940).

(2) P. O. Löwdin, Phys. Rev. **97** 1474 (1955).

(3) E. R. Davidson,*Reduced Density Matrices in Quantum Chemistry* (Academic Press, Inc, (London), Ltd., (1976))

(4) A. J. Coleman *Density Matrices and Density Functionals* Proceedings of the A.J. Coleman Symposium, Kingston, Ontario, 1985 (R. Erdahl and V. Smith ,Reidel, Dordrecht, 1987)

(5) P. O. Löwdin in *Density Matrices and Density Functionals*, Proceedings of the A.J. Coleman Symposium, Kingston, Ontario, 1985 (R. Erdahl and V. Smith, Reidel, Dordrecht, 1987), p.1.

(6) H. Nakasutji, Phys. Rev. A **14** 41 (1976).

(7) L. Cohen and C. Frishberg, Phys. Rev. A **13** 927 (1976).

(8) C. Valdemoro, Phys. Rev.A **31** 2114 (1985).

(9) C. Valdemoro in *Density Matrices and Density Functionals*, Proceedings of the A.J. Coleman Symposium, Kingston, Ontario, 1985 (R. Erdahl and V. Smith Reidel, Dordrecht, 1987), p.275.

(10) C. Valdemoro, Phys. Rev. A **45** 4462 (1992).

(11) F. Colmenero, C. Perez del Valle, C. Valdemoro, Phys. Rev. A **47** 971 (1993).

(12) F. Colmenero, C. Valdemoro, Phys. Rev. A **47** 979 (1993).

(13) F. Colmenero and C. Valdemoro, Int. J. Quantum Chem., **51** 369 (1994)

(14) H. Nakatsutji, K. Yasuda, Phys. Rev. Let. **76** 1039 (1996).

(15) C. Valdemoro, oral communication at the *34*, Sanibel Symposium (1994)(unpublished)

(16) P.Viciano, J. Planelles, J. Math. Chem. **16** 149 (1994)

(17) G. D. Purvis III, R. Shepard, F. B. Brown, R. J. Bartlett, Int. J. Quantum Chem. **23** 835 (1983)

(18) R. McWeeny, Y. Mizuno, Proc. Roy. Soc., London **A259** 554 (1961)

(19) W. Kutzelnigg Zeit. für Naturforschg 18a 1058 (1963)

(20) E. Pérez-Romero, L. M. Tel, C. Valdemoro, Int. J. Quantum Chem. **xx** xxx (1996)

(21) A. J. Coleman, Rev. Mod. Phys. **35** 668 (1963).

Distributed Gaussian Basis Sets: Some Recent Results and Prospects

S. Wilson
Rutherford Appleton Laboratory, Chilton, Oxfordshire OX11 0QX, England

D. Moncrieff
Supercomputer Computations Research Institute, Florida State University, Tallahassee, Florida 32306, U.S.A.

Abstract

Systematic implementation of finite basis set expansion techniques using Gaussian functions has acquired increasing importance in recent years in both non-relativistic and relativistic molecular electronic structure theory as the controlled reduction of basis set truncation errors is seen as a primary objective in a wide range of applications of quantum chemical methods. A promising development is the distributed Gaussian basis set in which both the exponents and distribution of the Gaussian basis functions in space are generated in a systematic fashion. Some results obtained recently by using distributed Gaussian basis sets are surveyed and future prospects are considered.

Contents

ADVANCES IN QUANTUM CHEMISTRY, VOLUME 28

0065-3276/97 $25.00

1. Introduction

Because of the lack of any suitable coordinate system with which to simplify the treatment of arbitrary polyatomic molecules, the use of expansions in terms of analytic basis sets has emerged as perhaps the most powerful element of contemporary computational quantum chemistry. The systematic implementation of finite basis set expansions in both non-relativistic and relativistic molecular electronic structure calculations has acquired increasing importance in recent years as the controlled reduction of basis set truncation errors is seen as a primary objective in a wide range of applications of quantum chemical methods. The development of the algebraic approximation continues to demand attention as increasingly powerful computing machines facilitate the use of basis sets of ever larger size. The matrix formulation associated with the use of finite basis set expansions supports a representation of the spectrum which is required for correlation treatments and for going beyond the "no virtual pair" approximation in relativistic studies.

Gaussian functions are appropriate functions for electronic structure calculations not only because of the widely recognized fact that they lead to molecular integrals which can be evaluated efficiently and accurately but also because such functions do not introduce a cusp into the approximation for the wave function at a physically inappropriate point when off-nuclei functions are employed. Furthermore, Gaussian functions are suitable for the description of wave functions in the vicinity of nuclei once the point nucleus model is abandoned in favour of a more realistic finite nucleus model.

Although the first proposals(1) (2) to use Gaussian basis functions in molecular electronic structure calculations were made in the late 1940s and early 1950s, in a recent historical review Shavitt(3) records how the first applications *"met with very limited success because they used rather small numbers of Gaussians, and little additional work was reported in the fifties"* but then *"interest in Gaussian basis sets and exploration of variants and extensions increased substantially in the early sixties"*. In 1960, Nesbet(4) identified two approaches to the design of molecular basis sets:

> *i)* addition of atom-centred polarization functions to the atomic basis sets
>
> *ii)* addition of off-centre functions of the same symmetry as the atomic Hartree-Fock basis set.

Approach *i)* forms the foundation of the majority of current 'mainstream' practice (see the review by Shavitt(3) for an overview). However, continued advances in computing machines and algorithms for their effective exploitation, such as, for example, the 'direct' self-consistent field algorithms(5),

which avoid the storage of the two-electron integrals over the basis functions, have enabled calculations using in excess of 10^3 functions to be carried out on a workstation and calculations using basis sets of a size approaching 10^4 to be seriously contemplated. It is, therefore, timely to reconsider approaches *i)* and *ii)* in the light of these developments. We note that these approaches are not mutually exclusive in that hybrid prescriptions for molecular basis set design can be adopted. Amongst the proposals considered in the sixties, Gaussian bond functions(6)-(8), Gaussian lobes functions(9)-(19) and floating spherical Gaussian functions(20)-(25) should be mentioned.

It is the choice of basis functions in which the description of the quasiparticles are developed which ultimately determines the accuracy of a particular calculation. No resummation of higher order diagrammatic terms will compensate for an inadequate choice of basis set.

2. Basis Sets for Atoms

For atoms the exhaustive optimization of a small number of exponents, which was a practice necessitated by computer limitations in the sixties, has been largely replaced by systematically generated sequences of basis sets with which, for example, the Hartree-Fock limit can be approached with almost machine accuracy. For example, even-tempered basis sets in which exponents are generated according to the formula

$$\zeta_k = \alpha_N \beta_N^k, \quad k = 1, 2, ..., N$$

can be systematically extended to a complete set by using the recursions (26) (27)

$$\ln \beta_N = \left[\frac{N}{N-1}\right]^b \ln \beta_{N-1}$$

and

$$\alpha_N = \left[\frac{\beta_N - 1}{\beta_{N-1} - 1}\right]^a \alpha_{N-1}$$

where N is the number of basis functions. The use of systematic sequences of even-tempered basis sets in matrix Dirac-Hartree-Fock calculations is illustrated in Table 1 where finite basis set calculations for the ground state of the argon atom are compared with the results of a relativistic finite difference calculation(28). In this Table ΔE_{mDHF} denotes the energy decrease observed on increasing N by one.

Table 1
The use of systematic sequences of even-tempered basis sets in matrix Dirac-Hartree-Fock calculations for the argon atom ground state.

N	$-E_{mDHF}$	ΔE_{mDHF}
9	528.64394819	
10	528.68336415	39415.96
11	528.68431173	947.58
12	528.68428973	−22.00
13	528.68443068	140.95
14	528.68443246	1.72
15	528.68444856	16.10
16	528.68444990	1.34
17	528.68445050	0.60
finite difference	528.68445077	

3. Distributed Gaussian Basis Sets

For molecules one can, in principle, make an expansion in terms of a set of Gaussian functions centred on any arbitrary point since the functions form a complete set; indeed they form an overcomplete set. In practice, such an approach is found to be poorly convergent even for systems consisting of one heavy atom, which is taken as the expansion centre, bonded to off-centre hydrogen atoms, and has now been largely abandoned.

By far the most widely used type of basis set can be regarded as a particular type of distributed basis set. In the **L**inear **C**ombination of **A**tomic **O**rbitals approach the global basis set is built from basis subsets centred on each of the component atoms in the system; that is

$$S_{LCAO} = \sum_i \oplus S_{atom,i}$$

Most work on the design of molecular basis sets has concentrated on the development of atom-centred polarization sets which can be added to atomic basis sets to describe the molecular environment.

It should be emphasised, however, that there is no unique solution to the problem of designing molecular basis sets. The idea of using bond functions in molecular structure calculations is an old one(6). The molecular basis set is then written

$$S_{LCAO+bond\ centre} = \sum_i \oplus S_{atom,i} \oplus \sum_{i>j} \oplus S_{bond,ij}$$

Indeed, a number of authors have advocated the use of basis functions located at the bond centre in both self-consistent fields and in calculations

taking account of correlation effects(29)-(60). Such functions were introduced to provide the same effects as the addition of a set of polarization functions but at a considerably lower cost. Davidson and Feller(48) point out that *For first-row diatomics the introduction of a single (s,p) set at the centre of the bond provides* 90% *of the energy lowering obtained with a single set of d functions at the nuclear centres.*

Off-atom functions effectively introduce linear combinations of higher harmonics centred on the atom. Partial wave expansions of an off-centre Gaussian function have been discussed, for example, by Christoffersen *et al*(61) and by Kaufmann and Baumeister(62).

4. Independent Particle Models

4.1 One-electron diatomic molecules

The present authors(63) (64) asked "Can the ground state of the simplest of molecules, the hydrogen molecular ion, be described to sub-μhartree accuracy using a basis set of s-type Gaussian-type functions?" The exact ground state energy of the hydrogen molecule ion for a nuclear separation of 2.0 bohr is -1.1026342214 hartree. A calculation using an extensive set of atom-centred s-type Gaussian functions

$$S_H \oplus S_H$$

gave an energy of -1.090950562 hartree, which is in error by $11,683$ μhartree. Adding an extensive set of bond centre functions, resulting in a basis set which can be written

$$S_H \oplus S_H \oplus S_{H|H}$$

gave an energy of -1.102442554 hartree thereby reducing the error to 191.7 μhartree, whilst adding sets of s-type Gaussian functions centred on points on the line passing through the nuclei designated

$$S_H \oplus S_H \oplus S_{H|H} \oplus S_{|HH} \oplus S_{HH|}$$

gave a total energy of -1.102632641 hartree. Finally, using an electric field variant basis set in place of each of the atom-centred sets

$$S_{H\rightarrow} \oplus S_{H\leftarrow} \oplus S_{H|H} \oplus S_{|HH} \oplus S_{HH|}$$

gave an energy of -1.102633861 hartree, which is in error by ~ 0.3 μhartree.

Another distributed Gaussian basis set is the Gaussian Cell model of Haines *et al*(65) in which Gaussian s-type functions with a single common

exponent are arranged on a regular cubic lattice. The nuclei are taken to coincide with lattice points.

$$S_{Gaussian\ Cell\ Model} = \left(\sum_{p} \oplus S_1^{(\lambda_p)} \right)$$

Extending this lattice to the $11 \times 11 \times 11$ case (that is 1331 basis functions), Ralston and Wilson(66) reported an energy of -1.094929 hartree for the hydrogen molecular ion with a nuclear separation of 2.0 bohr; an error of 7705 μhartree. These authors considered an extension of the Gaussian Cell model, which they termed a molecular lattice basis set, since the lattice basis set is required to describe only 'molecular' effects, being supplemented by atomic basis sets of high precision. This basis set is written

$$S_{Molecular\ Lattice\ Basis\ Set} = \left(\sum_{p \in \{L'\}} \oplus S_1^{(\lambda_p)} \right) \oplus \left(\sum_{q \in \{A\}} \oplus S_{N_{atom}}^{(\lambda_q)} \right)$$

where $\{L'\}$ denotes the lattice points which are not associated with nuclei whilst $\{A\}$ denotes those which are. This extension of the Gaussian Cell model represents a considerable improvement giving a total energy of -1.102597 hartree for an $11 \times 11 \times 11$ lattice; an error of 27 μhartree. A further extension, the molecular lattice even-tempered basis set was introduced(67)

$$S_{Molecular\ Lattice\ Even\text{-}tempered\ Basis\ Set} = \left(\sum_{p \in \{L'\}} \oplus S_{N_{lattice}}^{(\lambda_p)} \right) \oplus \left(\sum_{q \in \{A\}} \oplus S_{N_{atom}}^{(\lambda_q)} \right)$$

in which atomic basis sets are located on the nuclei and lattice basis sets on each lattice point. The results displayed in Table 2 demonstrate that this approach is capable of approaching a sub-μhartree level of accuracy.

An application of the molecular cubic lattice of systematically constructed distributed basis sets to the linear H_3^{2+} system, for which finite element results are available(68), has also been described(69).

A review of the application of distributed Gaussian basis sets to one-electron molecules has recently been given by one of us(70).

Table 2
Convergence of the ground state energy of the hydrogen molecular ion using a systematic sequence of distributed even-tempered Gaussian basis sets.

N	$E_{H_2^+}/Hartree$	N	$E_{H_2^+}/Hartree$
1	+0.111257	11	−1.102428
2	−0.920270	12	−1.102512
3	−1.054177	13	−1.102560
4	−1.083943	14	−1.102588
5	−1.094463	15	−1.102605
6	−1.098597	16	−1.102616
7	−1.100551	17	−1.102622
8	−1.101516	18	−1.102626
9	−1.102014	19	−1.102629
10	−1.102281	20	−1.102631
		Exact	−1.102634

4.2 Diatomic molecules

For many-electron diatomic molecules the electronic structure problem is usually attacked in two distinct stages: the approximation of the solutions of the Hartree-Fock equations and then the determination of correlation corrections.

For diatomic molecules finite difference solutions to the Hartree-Fock equations are available for ground states. For example, the Hartree-Fock energy for the nitrogen molecule with a nuclear separation of 2.068 bohr has been reported by Kobus(71) as −108.9938257 hartree.

The present authors(72) explored the use of basis subsets containing functions of just s and p symmetry, the symmetries required to describe the Hartree-Fock ground state of the nitrogen atom, distributed along the line passing through the nuclei, which are placed at $\left(0, 0, \pm\frac{1}{2}R\right)$. Nearly saturated atom centred basis sets resulted in an energy of −108.91072760 hartree, which is in error by 83098.1 μhartree. Adding bond centre functions of nearly saturated sets of s and p symmetry reduced this error to 4386.5 μhartree. A further reduction of the error to 660 μhartree was achieved by adding nearly saturated sets of s and p functions centred on points $\left(0, 0, \pm\left[\frac{1}{2} + \nu\right] R\right)$, $\nu > 0$. Finally, centring s and p functions on points on the line segment joining the nuclei to the bond centre gave a total Hartree-Fock energy of −108.9937768 hartree thereby reducing the error to 48.9 μhartree. Thus, it has been shown that the Hartree-Fock ground state of the nitrogen molecule can be described quite accurately using a basis set of s and p functions distributed along the line passing through the

nuclei. Furthermore, the largest basis set was employed in a second order many-body perturbation theory study in which it was shown to recover in excess of 77% of an estimate of the exact second-order energy.

Using a hybrid approach which admits higher harmonics on the nuclear centres but also including bond centre functions, the present authors(73) (74) demonstrated that an accuracy approaching the 1 μhartree level could be achieved in Hartree-Fock calculations for the nitrogen molecule. This work has been extended and, in a collaboration with Kobus(75)-(77) (see also the article by Kobus in this volume(78)), a detailed comparison of finite difference and finite basis set calculations for a range of diatomic systems has been reported. Some results for systems isoelectronic with the nitrogen molecule are collected in Table 3. In this Table, δ denotes the difference between the Hartree-Fock energies for a given molecule in μhartree.

Table 3
Comparison of finite difference Hartree-Fock total energies for some fourteen electron diatomic molecules with matrix Hartree-Fock energies obtained by using a universal basis set.[a]

Molecule	$E_{f.d.}$	$E_{u.b.s.}$	δ
N_2	−108.9938257	−108.9938234	−2.3
CO	−112.7909073	−112.7909045	−2.8
BF	−124.1687792	−124.1687612	−18
NO^+	−128.9777407	−128.9777375	−3.2
CN^-	−92.3489506	−92.348837	−114

[a] All energies are in hartree. Internuclear separations are taken from Moncrieff and Wilson(79)

4.3 Polyatomic molecules

An application of the molecular cubic lattice of systematically constructed distributed basis sets to the one-electron linear H_3^{2+} system, for which finite element results are available, has been described(69).

For many-electron systems the CO_2 has been taken as a prototype(80). Using a basis set containing higher harmonics on the nuclear centres, together with bond centred functions originally developed for N_2 and later applied to CO as a universal basis set, a molecular basis set was developed for CO_2 which may be designated

$$S_O \oplus S_C \oplus S'_O \oplus S_{CO} \oplus S'_{CO}$$

Some care was required in the control of computational linear dependence, which was achieved by deleted diffuse, bond centre functions. It is suggested that a total Hartree-Fock energy of an accuracy comparable with that obtained for the CO molecule was thereby achieved.

Recent work has concentrated on the application of distributed Gaussian basis sets to non-linear polyatomic molecules taking H_2O as a prototype(81). Some preliminary results for the Hartree-Fock ground state energy are collected in Table 4. The basis sets employed on each centre are nearly saturated. A:ν denotes a basis set containing functions of symmetries ν centred on the nucleus A; AB:ν denotes a basis set centred on the mid point of the line from AB. ΔE_{mHF} denotes the difference between the energy obtained by using the basis set indicated and that obtained with the isotropic set O:sp;H:s. The basis set designated O:sp;H:sp;OH:sp;HH:sp containing only functions of s and p symmetry lies 1183 μhartree below that obtained with the set containing atom centred functions of d symmetry.

Table 4
Some matrix Hartree-Fock calculations for the water ground state using distributed Gaussian basis sets.

	E_{mHF}	ΔE_{mHF}
O:sp;H:s	−76.0264878	−
O:sp;H:s;OH:s	−76.0460721	19584.3
O:sp;H:s;OH:s;HH:s	−76.0541377	27649.9
O:sp;H:sp	−76.0564372	29949.4
O:sp;H:sp;OH:sp	−76.0669971	40509.3
O:sp;H:sp;OH:sp;HH:sp	−76.0670547	40566.9
O:spd;H:sp	−76.0658714	39383.6

5. Electron Correlation Effects

Solution of the matrix equations associated with an independent particle model gives rise to a representation of the spectrum which is an essential ingredient of any correlation treatment. Finite order many-order perturbation theory(82) forms the basis of a method for treating correlation effects which remains tractable even when the large basis sets required to achieve high accuracy are employed. Second-order many-body perturbation theory is a particularly simple and effective approach especially when a 'direct' implementation is employed. The total correlation energy is written

$$E_{correlation} = E_2 + R_2$$

where, for the approach to be useful, the remainder term must be small: $R_2 < \epsilon$.

Using the distributed Gaussian basis set designated $2nsnpndnf : 2nsnpndnf\ bc$ with $n = 15$ gives a matrix Hartree-Fock energy $E_{mHF} = -108.9938245$ hartree and a second order correlation energy component $E_2 = -0.5201846$ hartree(83). Including higher harmonics in both the atom centred and the bond centred basis subsets to give a molecular basis set designated $2nsnpndnfngnh : 2nsnpndnfngnh$ with $n = 10$ gives a matrix Hartree-Fock energy $E_{mHF} = -108.9937920$ hartree and a second order correlation energy component of $E_2 = -0.5304337$ hartree(83). The addition of bond centre functions did not improve the calculated correlation energy estimates as much as the Hartree-Fock energies(83). An extrapolated second-order energy component to estimate the effects of higher harmonics gave $E_2 = -0.5354$ hartree, a result which differs by just 0.7 mhartree from the value reported by Klopper(84) from second order perturbation theory calculations which include an *ad hoc* factor depending linearly on the interelectronic distance in the sum-over-states perturbation expansion at a slightly different nuclear separation ($2.07bohr$).

The results of the distributed basis set study of the second-order correlation energy for the nitrogen molecule(83) is compared with the second-order correlation energies obtained by employing other recently reported basis sets for this system in Figure 1.

The results of some preliminary calculations of the second order correlation energy component for the water molecule, a prototype non-linear polyatomic system, are displayed in Table 5. ΔE_2 is again the difference between the correlation energy estimate obtained with a given basis set and that obtained with the O:*sp*;H:*s* set. It can be seen that, whereas the O:*sp*;H:*sp*;OH:*sp*;HH:*sp* set gave a lower energy than the O:*spd*;H:*sp* set in matrix Hartree-Fock calculations, the situation is reversed for the correlation energy studies.

Table 5
Some second order correlation energy components for the water molecule ground state using distributed Gaussian basis sets.

	E_2	ΔE_2
O:*sp*;H:*s*	−0.1954759	–
O:*sp*;H:*s*;OH:*s*	−0.2099508	14474.9
O:*sp*;H:*s*;OH:*s*;HH:*s*	−0.2239499	28474.0
O:*sp*;H:*sp*	−0.2267254	31249.5
O:*sp*;H:*sp*;OH:*sp*	−0.2881889	92713.0
O:*sp*;H:*sp*;OH:*sp*;HH:*sp*	−0.2967608	101284.9
O:*spd*;H:*sp*	−0.3132383	117762.4

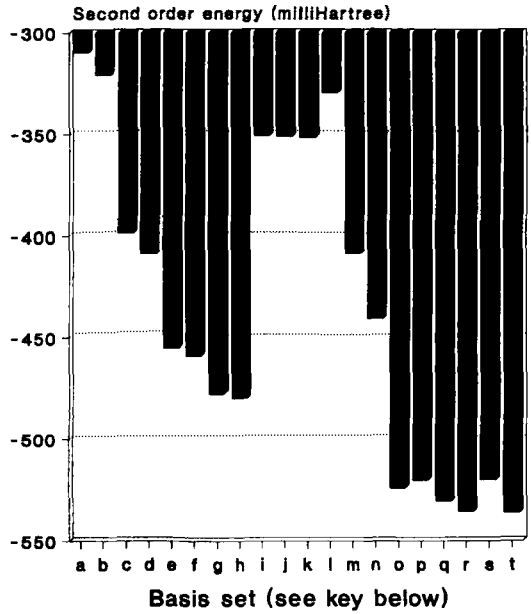

Figure 1: Second order components of the correlation energy determined from a variety of basis sets

[a] correlation consistent-polarized Valence Double Zeta basis set due to Dunning(85)

[b] augmented correlation consistent-polarized Valence Double Zeta basis set due to Dunning *et al*(85) (86)

[c] correlation consistent-polarized Valence Triple Zeta basis set due to Dunning(85)

[d] augmented correlation consistent-polarized Valence Triple Zeta basis set due to Dunning *et al*(85) (86)

[e] correlation consistent-polarized Valence Quadruple Zeta basis set due to Dunning (85)

[f] augmented correlation consistent-polarized Valence Quadruple Zeta basis set due to Dunning *et al*(85) (86)

[g] correlation consistent-polarized Valence Quintuple Zeta basis set due to Dunning(85)

[h] augmented correlation consistent-polarized Valence Quintuple Zeta basis set due to Dunning *et al*(85) (86)

[i] Basis set due to Partridge(87)

[j] Basis set due to Partridge(87)

[k] Basis set due to Partridge(87)

[l] augmented Double Zeta Atomic Natural Orbital basis set due to Widmark *et al*(88) (89)

[m] augmented Triple Zeta Atomic Natural Orbital basis set due to Widmark *et al*(88) (89)

[n] Atomic Natural Orbital basis set due to Almlof and Taylor(90)

[o] correlation consistent-polarized Core Valence Quintuple Zeta basis set due to Dunning *et al*(91) [Energy reported by Wilson and Moncrieff(92)]

[p] Moncrieff and Wilson(83) $2nsnpndnf$: $2nsnpndnf\ bc$ basis set with $n = 15$

[q] Moncrieff and Wilson(83) $2nsnpndnfngnh$: $2nsnpndnfngnh\ bc$ basis set with $n = 10$

[r] Moncrieff and Wilson extrapolated value(83)

[s] MP2 calculation due to Klopper(84)

[t] MP2-R12 calculation due to Klopper(84)

In Table 6, the present calculations for the water ground state are compared with previous work.

Table 6
Comparison of matrix Hartree-Fock and second-order correlation calculations using distributed Gaussian basis sets for the water ground state with some previous work.

Basis set	E_{mHF}	E_2
O:*sp*;H:*sp*;OH:*sp*;HH:*sp*[a]	−76.0670547	−0.29676
O:*spd*;H:*sp*[a]	−76.0658714	−0.3132383
aug-cc-pVTZ[b]	−76.0606	−0.2684
7s8p6d1f/4s2p1d[c]	−76.067361	−0.31563
28s18p8d3f/11s7p2d[d]	−76.06742	−0.3437545

[a] Present work

[b] Feller (1992)(93)

[c] Chakravorty and Davidson (1993)(94)

[d] Clementi, Corongui and Stradella (1991)(95)

6. Summary and Prospects

Some recently obtained results using distributed Gaussian basis sets in both matrix Hartree-Fock and second-order correlation treatments have been described and the utility of this approach has been established.

Work is in hand in a number of areas, including: *(i)* high precision electron correlation studies of N_2-like systems using a distributed universal Gaussian basis set; *(ii)* special consideration of such basis sets for molecular negative ions, using CN^- as a prototype; *(iii)* high precision electron correlation studies of the ground state of the water molecule considered as a prototype non-linear polyatomic molecule; *(iv)* virtual elimination of basis set superposition effects in studies of van der Waals interactions, thereby avoiding the use of counterpoise corrections; *(v)* visualization of basis set deficiencies by means of detailed comparison with the results of finite difference calculations; *(vi)* high precision valence bond studies using distributed Gaussian basis sets; *(vii)* studies of diatomic systems containing heavier atoms and detailed comparison with finite difference studies; *(viii)* use of distributed Gaussian basis sets in relativistic electronic structure studies; *(ix)* systematic integral approximation schemes; *(x)* effective exploitation of parallel processing techniques in integral evaluation, self-consistent field and low order correlation treatments. Progress will be reported in due course.

It is our pleasure to dedicate this paper to Professor G.H.F. Diercksen on the occasion of his sixtieth birthday.

7. Acknowledgement

One of us (DM) acknowledges the support of the US Department of Energy through contract no. DE-FC05-85ER2500000 and US Department of Energy Chemical Science Contract no. DE-FG05-95ER-14523.

References

(1) R. McWeeny, *Dissertation, University of Oxford* (1948)

(2) S.F. Boys, *Proc. Roy. Soc. London* **A200**, 542 (1950)

(3) I. Shavitt, Israel J. Chem. **33**, 357 (1993)

(4) R.K. Nesbet, Rev. Mod. Phys. **32**, 272 (1960)

(5) J. Almlöf, K. Faegri and K. Korsell, J. Comput. Chem. **3**, 385 (1982)

(6) H. Preuss, Z. Naturforsch. **19a**, 1335 (1964)

(7) H. Preuss, Z. Naturforsch. **20a**, 17 (1965)

(8) H. Preuss, Z. Naturforsch. **20a**, 21 (1965)

(9) G.H.F. Diercksen and H. Preuss, Z. Naturforsch. **20a**, 863 (1966)

(10) H. Preuss and G.H.F. Diercksen, Intern. J. Quantum Chem. **1**, 349 (1967)

(11) H. Preuss and G.H.F. Diercksen, Intern. J. Quantum Chem. **1**, 361 (1967)

(12) H. Preuss and G.H.F. Diercksen, Intern. J. Quantum Chem. **1**, 369 (1967)

(13) H. Preuss and G.H.F. Diercksen, Intern. J. Quantum Chem. **1**, 605 (1967)

(14) H. Preuss and G.H.F. Diercksen, Intern. J. Quantum Chem. **1**, 631 (1967)

(15) H. Preuss and G.H.F. Diercksen, Intern. J. Quantum Chem. **1**, 641 (1967)

(16) G.H.F. Diercksen and H. Preuss, Intern. J. Quantum Chem. **1**, 357 (1967)

(17) G.H.F. Diercksen and H. Preuss, Intern. J. Quantum Chem. **1**, 365 (1967)

(18) G.H.F. Diercksen and H. Preuss, Intern. J. Quantum Chem. **1**, 637 (1967)

(19) R. Janoschek, G.H.F. Diercksen and H. Preuss, Intern. J. Quantum Chem. **1**, 373 (1967)

(20) A.A. Frost, B.H. Prentice, III and R.A. Rouse, J. Am. Chem. Soc. **89**, 3064 (1967)

(21) A.A. Frost, J. Chem. Phys. **47**, 3707 (1967)

(22) A.A. Frost, J. Chem. Phys. **47**, 3714 (1967)

(23) A.A. Frost, J. Phys. Chem. **72**, 1289 (1968)

(24) A.A. Frost and R.A. Rouse, J. Am. Chem. Soc. **90**, 1965 (1968)

(25) B. Ford, G.G. Hall and J.C. Packer, Intern. J. Quantum Chem. **4**, 533 (1970)

(26) M.W. Schmidt and K. Ruedenberg, J. Chem. Phys. **71**, 3951 (1979)

(27) S. Wilson, Theoret. chim. Acta **57**, 53 (1980)

(28) H.M. Quiney, I.P. Grant and S. Wilson, *Many-Body Methods in Quantum Chemistry*, edited by U. Kaldor, Lecture Notes in Chemistry **52**, 307 (Springer-Verlag, Berlin, 1989)

(29) S. Rothenberg and H.F. Schaefer III, J. Chem. Phys. **54**, 2765 (1971)

(30) G. Hirsch, P.J. Bruna, S.D. Peyerimhoff and R.J. Buenker, Chem. Phys. Letts. **52**, 442 (1977)

(31) W. Butscher, S. Shih, R.J. Buenker and S.D. Peyerimhoff, Chem. Phys. Lett. **52**, 457 (1977)

(32) D. Neisius and G. Verhaegen, Chem. Phys. Lett. **66**, 358 (1979)

(33) L. Lawlor, K. Vasudevan and F. Grein, Chem. Phys. Lett. **75**, 79 (1980)

(34) C.W. Bauschlicher Jr., Chem. Phys. Lett. **74**, 277 (1980)

(35) P. Čársky and M. Urban *Ab initio Calculations. Methods and Applications in Chemistry*, Lecture Notes in Chemistry **16** (Springer-Verlag, Berlin, 1980)

(36) J.S. Wright and R.J. Williams, J. Chem. Phys. **78**, 5264 (1983)

(37) J.S. Wright and R.J. Williams, J. Chem. Phys. **79**, 2893 (1983)

(38) J.S. Wright and R.J. Buenker, Chem. Phys. Lett. **106**, 570 (1984)

(39) J.S. Wright and R.J. Buenker, J. Chem. Phys. **83**, 4059 (1985)

(40) J.S. Wright and E.J. Kruus, J. Chem. Phys. **85**, 7251 (1986)

(41) J.S. Wright and V.J. Barclay, J. Chem. Phys. **86**, 3054 (1987)

(42) J.S. Wright, V.J. Barclay and R.J. Buenker, Chem. Phys. **115**, 23 (1987)

(43) J.S. Wright and V.J. Barclay, Chem. Phys. **121**, 381 (1988)

(44) V.J. Barclay and J.S. Wright, J. Comput. Chem. **12**, 690 (1991)

(45) J.S. Wright and V.J. Barclay, J. Comput. Chem. **12**, 697 (1991)

(46) P. Mach and O. Kysel, J. Comput. Chem. **6**, 312 (1985)

(47) C.W. Bauschlicher Jr., Chem. Phys. Lett. **122,** 572 (1985)

(48) E.R. Davidson and D. Feller, Chem. Rev. **86**, 681 (1986)

(49) J.M.L. Martin, J.P. Francois and R.J. Gijbels, J. Comput. Chem. **10**, 152 (1989)

(50) J.M.L. Martin, J.P. Francois and R.J. Gijbels, J. Comput. Chem. **10**, 346 (1989)

(51) J.M.L. Martin, J.P. Francois and R.J. Gijbels, J. Comput. Chem. **10**, 875 (1989)

(52) J.M.L. Martin, J.P. Francois and R.J. Gijbels, Theoret. chim. Acta **76**, 195 (1989)

(53) F.-M. Tao and Y.K. Pan, Chem. Phys. Lett. **194**, 162 (1992)

(54) F.-M. Tao and Y.K. Pan, J. Chem. Phys. **97**, 4989 (1992)

(55) F.-M. Tao, J. Chem. Phys. **98**, 2481 (1993)

(56) F.-M. Tao, J. Chem. Phys. **98**, 3049 (1993)

(57) F.-M. Tao and W. Klemperer, J. Chem. Phys. **99**, 5976 (1993)

(58) H.-C. Chang, F.-M. Tao, W. Klemperer, C. Healey and J.M. Hutson, J. Chem. Phys. **99**, 9337 (1993)

(59) F.-M. Tao, J. Chem. Phys. **100**, 3645 (1994)

(60) F.-M. Tao and Y.K. Pan, Molecular Physics **81**, 507 (1994)

(61) R.E. Christoffersen, D. Spangler, GG. Hall and G.M. Maggiora, J. Amer. Chem. Soc. **95**, 8526 (1973)

(62) K. Kaufmann and W. Baumeister, J. Phys. B: At. Mol. Opt. Phys. **22**, 1 (1989)

(63) S. Wilson and D. Moncrieff, Molecular Physics **80**, 461 (1993)

(64) D. Moncrieff and S. Wilson, Molecular Physics **82**, 523 (1994)

(65) L. Haines, J.N. Murrell, B.J. Ralston and D.J. Woodnutt, J. Chem. Soc. Faraday Transactions II **70**, 1794 (1974)

(66) B. Ralston and S. Wilson, J. Molec. Struct. THEOCHEM **341**, 115 (1995)

(67) S. Wilson, J. Molec. Struct. THEOCHEM **357**, 37 (1995)

(68) S. Hackel, D. Heinemann, D. Kolb and B. Fricke, Chem. Phys. Lett. **206**, 91 (1993)

(69) S. Wilson, Intern. J. Quantum Chem. *(in press)*

(70) S. Wilson, in *New Methods in Quantum Theory*, Proceedings of the NATO Advanced Research Workshop, Halkidiki, Greece, May 1995, edited by C.A. Tsipis, V.S. Popov, D.R. Herschbach and J.S. Avery, Kluwer, Dordrecht (1996)

(71) J. Kobus, Chem. Phys. Lett. **202**, 7 (1993)

(72) D. Moncrieff and S. Wilson, Molecular Physics **85**, 103 (1995)

(73) D. Moncrieff and S. Wilson, Chem. Phys. Lett. **209**, 423 (1993)

(74) D. Moncrieff and S. Wilson, J. Phys. B: At. Mol. Opt. Phys. **26**, 1605 (1993)

(75) J. Kobus, D. Moncrieff and S. Wilson, J. Phys. B: At. Mol. Opt. Phys. **27**, 2867 (1994)

(76) J. Kobus, D. Moncrieff and S. Wilson, J. Phys. B: At. Mol. Opt. Phys. **27**, 5139 (1994)

(77) J. Kobus, D. Moncrieff and S. Wilson, Molec. Phys. **86**, 1315 (1995)

(78) J. Kobus, Adv. Quantum Chem (this volume)

(79) D. Moncrieff and S. Wilson, J. Phys. B: At. Mol. Opt. Phys. **27**, 1 (1994)

(80) D. Moncrieff and S. Wilson, J. Phys. B: At. Mol. Opt. Phys. (1995)

(81) S. Wilson and D. Moncrieff, *On the accuracy of the algebraic approximation in molecular electronic structure calculations. VI. Matrix Hartree-Fock and Many-Body Perturbation Theory Calculations for the Ground State of the Water Molecule*, preprint

(82) S. Wilson, *Electron correlation in molecules*, Clarendon Press, Oxford (1984)

(83) D. Moncrieff and S. Wilson, J. Phys. B: At. Mol. Opt. Phys. *(accepted for publication)*

(84) W. Klopper, J. Chem. Phys. **102**, 6168 (1995)

(85) T.H. Dunning Jr., J. Chem. Phys. **90**, 1007 (1989)

(86) R.A. Kendall, T.H. Dunning Jr., and R.J. Harrison, J. Chem. Phys. **96**, 6769 (1992)

(87) H. Partridge, J. Chem. Phys. **90**, 1043 (1989)

(88) P.O. Widmark, P.A. Malmqvist and B.O. Roos, Theoret. chim. Acta. **77**, 291 (1990)

(89) P.O. Widmark, B.J. Persson and B.O. Roos, Theoret. chim. Acta. **79**, 419 (1991)

(90) J. Almlöf and P.R. Taylor, J. Chem. Phys. **86**, 4070 (1987)

(91) D.E. Woon and T.H. Dunning Jr., J. Chem. Phys. **103**, 4572 (1995)

(92) S. Wilson and D. Moncrieff, *A note on large correlation consistent Gaussian basis sets*, preprint

(93) D. Feller, J. Chem. Phys, **96**, 6104 (1992)

(94) S.J. Chakravorty and E.R. Davidson, J. Phys. Chem. **97**, 6374 (1993)

(95) E. Clementi, G. Corongui and O.G. Stradella, Modern Techniques in Computational Chemistry, MOTECC-91, pp. 295-380 (ESCOM Science Publishers, Leiden 1991)

The Nuclear Motion Problem in Molecular Physics

B. T. Sutcliffe[1]

Department of Chemistry, University of York
Heslington, York YO1 5DD, England

Abstract

Modern highly accurate electronic structure calculations are undertaken with a view to elucidating molecular structure. For this to be possible the relationship of nuclear motion to electronic structure must be specified. An outline of how this specification might be made and some of the problems encountered in making it are discussed.

[1] btsl@york.ac.uk

ADVANCES IN QUANTUM CHEMISTRY, VOLUME 28

0065-3276/97 $25.00

1. Introduction

The idea that the proper way to treat molecules in quantum mechanics is to try to separate the electronic and nuclear motions as far as possible, dates from the very earliest days of the subject. The genesis of the idea is usually attributed to Born and Oppenheimer (1), but it is an idea that was in the air at the time, for the earliest papers in which the idea is used, predate the publication of their paper. The physical picture that informs the attempted separation is one well known and widely used even in classical mechanics, namely division of the problem into a set of rapidly moving particles, here electrons and a much more slowly moving set, here the nuclei. Experience is that it is wise to try and separate such incommensurate motions both to calculate efficiently and to get a useful physical picture.

The object of the separation in the molecular case is to get an electronic motion problem in which the nuclear positions can be treated as parameters and whose solutions can be used to solve the nuclear motion problem. The insights arising from classical chemistry seem to predicate that, for lowish energies, the nuclear motion function should be strongly peaked at a nuclear geometry that corresponds to the traditional molecular geometry. A function of this kind would allow a good account of the electronic structure of a molecule to be given in terms of a single choice for the nuclear geometry, If such a function were possible, it would support the classical chemical picture of an isolated molecule that retains a reasonably well specified shape while performing small vibrations and undergoing essentially rigid rotations. Carl Eckart (2) was among the first to discuss how this picture might be supported but he did so in a context that assumed the separation of electronic and nuclear motions. In his approach, the electrons are regarded simply as providing a potential. This potential is invariant under all uniform translations and rigid rotations of the nuclei that form the molecule. It is usually referred to as a potential energy surface (strictly, *hyper*-surface) and the nuclei are said to move on this surface. Eckart actually treats the nuclear motions by classical rather than quantum mechanics but it is his approach and developments from it that have dominated the interpretation of molecular spectra since 1936.

Schrödinger's Hamiltonian describing the molecule as a system of N charged particles in a coordinate frame fixed in the laboratory is

$$\hat{H}(\mathbf{x}) = -\frac{\hbar^2}{2}\sum_{i=1}^{N} m_i^{-1}\nabla^2(\mathbf{x}_i) + \frac{e^2}{8\pi\epsilon_o}\sum_{i,j=1}^{N}{}' \frac{Z_i Z_j}{x_{ij}} \tag{1}$$

where the separation between particles is defined by

$$x_{ij}^2 = \sum_{\alpha}(x_{\alpha j} - x_{\alpha i})^2 \tag{2}$$

It is convenient to regard $\mathbf{x}_i$ as a column matrix of three Cartesian components $x_{\alpha i}$, $\alpha = x, y, z$ and to regard $\mathbf{x}_i$ collectively as the 3 by N matrix $\mathbf{x}$. Each of the particles has mass m_i and charge $Z_i e$. The charge-numbers Z_i are positive for a nucleus and minus one for an electron. In a neutral system the charge-numbers sum to zero.

To distinguish between electrons and nuclei, the variables are split up into two sets, one set consisting of L variables, $\mathbf{x}_i^e$, describing the electrons and the other set of H variables, $\mathbf{x}_i^n$, describing the nuclei and $N = L + H$. When it is necessary to emphasise this split, (1) will be denoted $\hat{H}(\mathbf{x}^n, \mathbf{x}^e)$.

If the full problem has eigenstates that are square-integrable so that

$$\hat{H}(\mathbf{x}^n, \mathbf{x}^e)\psi(\mathbf{x}^n, \mathbf{x}^e) = E\psi(\mathbf{x}^n, \mathbf{x}^e) \tag{3}$$

then, as Hunter showed (3), an eigenstate can be written rigorously as a product of the required form

$$\psi(\mathbf{x}^n, \mathbf{x}^e) = \Phi(\mathbf{x}^n)\phi(\mathbf{x}^n, \mathbf{x}^e)$$

The function, $\Phi(\mathbf{x}^n)$ is determined as a solution of an effective nuclear motion equation, obtained from the full equation (3) by multiplying from the left by $\phi^*(\mathbf{x}^n, \mathbf{x}^e)$ and integrating over all $\mathbf{x}_i^e$. The difficulty with this approach is that it seems not to be possible to specify the required electronic function $\phi(\mathbf{x}^n, \mathbf{x}^e)$ except in terms of the full exact solution. But if that solution were known then it is at least arguable that one would not be interested anyway in separating electronic from nuclear motions. However it is possible to guess a plausible electronic function, to form up the required nuclear motion problem and to use its solutions to improve the electronic function and so on, until a satisfactory solution is obtained. Traditionally a good guess for the electronic wave function is supposed to be provided by a solution of the clamped nuclei electronic Hamiltonian. One way in which a guess might be improved is to extend the the single product form to a sum of products form using more of the spectrum of the clamped nuclei Hamiltonian. Thus the wave function for the full problem is written as

$$\Psi(\mathbf{x}) = \sum_p \Phi_p(\mathbf{x}^n)\psi_p(\mathbf{x}^n, \mathbf{x}^e) \tag{4}$$

where $\psi_p(\mathbf{x}^n, \mathbf{x}^e)$ is the p-th clamped nuclei solution.

This is essentially the approach advocated by Born in the early nineteen-fifties which is given in appendix VIII in the book by Born and Huang (4). This approach to the problem of separation, we shall call the *standard* approach.

But it is not possible to use the Hunter approach or the standard approach to approximate it, because the Hamiltonian (1) is invariant under

uniform translations in the frame fixed in the laboratory. This means that the centre of molecular mass moves through space like a free particle and the states of a free particle are not quantised and eigenfunctions are not square integrable. The centre of mass motion must therefore be separated out to disentangle any bound states from the continuum and this must be done in such a way as to lead to a translationally invariant form for the potential energy surface if the Eckart approach is to be maintained.

The molecular Hamiltonian is invariant under all orthogonal transformations (rotation-reflections) of the particle variables in the frame fixed in the laboratory. The usual potential energy surface is similarly invariant so it is sensible to separate as far as possible the orientational motions of the system from its purely internal motions because it is in terms of the internal motions that the potential energy surface is expressed. The internal motions comprise dilations, contractions and deformations of a specified configuration of particle variables so that the potential energy surface is a function of the molecular geometry only.

The Hamiltonian is also invariant under the permutation of the variable sets of all identical particles and it is natural to require, if possible, that the potential energy surface is invariant under permutations of the variable sets of the identical nuclei. But in any case it is essential that the permutational properties of the various parts of the decoupled wavefunction be well specified in order that they are properly symmetric or antisymmetric, according to particle type, when spin variables are included.

These observations seem perfectly harmless but to achieve the objectives expressed by them causes some very unpleasant complications.

2. The Schrödinger equation for bound molecular states

Making no notational distinction between electrons and nuclei, the laboratory-fixed form of the Schrödinger Hamiltonian describing the molecule as a system of N particles is

$$\hat{H}(\mathbf{x}) = -\frac{\hbar^2}{2}\sum_{i=1}^{N} m_i^{-1}\nabla^2(\mathbf{x}_i) + \frac{e^2}{8\pi\epsilon_o}{\sum_{i,j=1}^{N}}' \frac{Z_i Z_j}{x_{ij}} \tag{5}$$

where the separation between particles is defined by

$$x_{ij}^2 = \sum_{\alpha}(x_{\alpha j} - x_{\alpha i})^2 \tag{6}$$

with the α - sum running over x y and z. Otherwise, the notation is standard. This will be taken as the full molecule Hamiltonian.

It is easy to remove the centre-of-mass motion from the full molecule Hamiltonian. All that it needs is a coordinate transformation symbolised by

$$(\mathbf{t}\ \mathbf{X}_T) = \mathbf{x}\ \mathbf{V} \tag{7}$$

In (7) $\mathbf{t}$ is a 3 by $N-1$ matrix and $\mathbf{X}_T$ is a 3 by 1 matrix. $\mathbf{V}$ is an N by N matrix which, from the structure of the left hand side of (7), has a special last column whose elements are

$$V_{iN} = {M_T}^{-1} m_i, \qquad M_T = \sum_{i=1}^{N} m_i \tag{8}$$

so that $\mathbf{X}_T$ is the standard centre-of-mass coordinate. The coordinates $\mathbf{t}_j, j = 1, 2, ...N-1$ are to be translationally invariant, so it is required on each of the remaining columns of $\mathbf{V}$ that

$$\sum_{i=1}^{N} V_{ij} = 0, \qquad j = 1, 2, ...N-1 \tag{9}$$

and it is easy to see that (9) forces $\mathbf{t}_j \to \mathbf{t}_j$ as $\mathbf{x}_i \to \mathbf{x}_i + \mathbf{a}$, all i.

Dropping the centre of mass part, the Hamiltonian (5) in the new coordinates becomes

$$\hat{H}(\mathbf{t}) = -\frac{\hbar^2}{2} \sum_{i,j=1}^{N-1} \mu_{ij}^{-1} \vec{\nabla}(\mathbf{t}_i).\vec{\nabla}(\mathbf{t}_j) + \frac{e^2}{8\pi\epsilon_o} {\sum_{i,j=1}^{N}}' \frac{Z_i Z_j}{f_{ij}(\mathbf{t})}. \tag{10}$$

Here

$$\mu_{ij}^{-1} = \sum_{k=1}^{N} {m_k}^{-1} V_{ki} V_{kj} \qquad i, j = 1, 2, ...N-1 \tag{11}$$

and f_{ij} is just x_{ij} as given by (6) but expressed as a function of the $\mathbf{t}_i$. Thus

$$f_{ij}(\mathbf{t}) = (\sum_{\alpha} (\sum_{k=1}^{N-1} ((\mathbf{V}^{-1})_{kj} - (\mathbf{V}^{-1})_{ki}) t_{\alpha k})^2)^{1/2} \tag{12}$$

In (10) the $\vec{\nabla}(\mathbf{t}_i)$ are the usual grad operators expressed in the Cartesian components of $\mathbf{t}_i$ and the first term represents the centre-of-mass kinetic energy and the eigenfunctions of this, the *translation-free* Hamiltonian are denoted $\Psi(\mathbf{t})$.

For an expansion like (4) to be valid as a solution to the problem specified by $\hat{H}(\mathbf{t})$ and hence for the idea of a potential energy surface to be well-founded, the translation-free Hamiltonian must have bound-states. But

whether or not it has, is rather problematic. The whole matter is discussed rather carefully in (5), (6), and (7) and it is at least plausible that it can have bound states. Indeed it was this form of the Hamiltonian (in the special case of a diatomic system) that Born and Oppenheimer actually considered.

It is apparent why the separation of translation is problematic for the identification of electrons and nuclei. In the translation-free Hamiltonian the inverse effective mass matrix μ^{-1} and the form of the potential functions f_{ij} depend intimately on the choice of $\mathbf{V}$ and the choice of this is essentially arbitrary. In particular it should be observed that because there are only $N-1$ translation-free variables they cannot, except in the most conventional of senses, be thought of as particle coordinates and that the non-diagonal nature of μ^{-1} and the peculiar form of the f_{ij} also militate against any simple particle interpretation of the translation-free Hamiltonian. It is thus not an entirely straightforward matter to identify electrons and nuclei once this separation has been made.

Because the spectrum of the translation-free Hamiltonian is independent of the choice of $\mathbf{V}$, the way in which it is chosen is immaterial if it is possible to construct exact solutions. But since it is always necessary in practice to use an approximation scheme, it is rational to choose a $\mathbf{V}$ that is adapted to the scheme. Here the aim is to design the approximate wave functions so as to decouple electronic and nuclear motions as far as possible. Ideally, the electronic part of the approximate wave function should consist of solutions of an electronic Hamiltonian which is as much like the clamped nuclei Hamiltonian as possible and whose eigenvalues can be identified with electronic energies as functions of the nuclear coordinates. The nuclear part of the approximation should, again ideally, consist of solutions to a problem composed of the nuclear motion kinetic energy operator expressed entirely in terms of coordinates that arise from the laboratory-fixed nuclear coordinates alone together with a potential that consists of a sum of the electronic energy and the nuclear repulsion potential. If this can be achieved, then the potential energy function is identified and nuclear motion and electronic structure can be related.

The details of how this can be done are presented in some earlier work, (5), (6) and (7) and the results can be summarised as yielding a new translation-free Hamiltonian expressed in terms of a set of $H-1$ coordinates $\mathbf{t}_i^n$ that depend only on the original nuclear coordinates and L coordinates $\mathbf{t}_i^e$ that are the original electronic coordinates referred to the centre of nuclear mass.

It is always possible to make a transformation of the translation-free coordinates such that the rotational motion can be expressed in terms of three orientation variables, with the remaining motions expressed in terms of variables (usually called internal coordinates) which are invariant un-

der all orthogonal transformations of the translation-free coordinates. To construct the body-fixed system it is supposed that the three orientation variables are specified by means of an orthogonal matrix $\mathbf{C}$, parameterised by the three Euler angles $\phi_m, m = 1,2,3$ as orientation variables. In the present case it will be required that the the matrix $\mathbf{C}$ is specified entirely in terms of the H translation-free nuclear variables and so there will be just $3H-6$ internal variables for the nuclei. It should be noted that for $H = 2$ only two orientation variables are required and that this is a rather special case (the diatomic molecule) and it will be excluded from all subsequent discussion.

Thus the translation-free nuclear Cartesian coordinates $\mathbf{t}^n$ can be thought of as being related to a body-fixed set $\mathbf{z}^n$ by

$$\mathbf{t}^n = \mathbf{C}\mathbf{z}^n \tag{13}$$

The body-fixed electronic variables can now be defined in terms of the transformation defined above by

$$\mathbf{z}_i = \mathbf{C}^T\mathbf{t}_i^e \qquad\qquad i = 1,2,....L \tag{14}$$

where there is no explicit superscript on the electronic body-fixed variables. The above equations *define* the body-fixed variables and thus *any* orthogonal transformation of the $\mathbf{t}^n$ (including the inversion) leaves them, by definition, invariant. However not all the $3H-3$ components of the $\mathbf{z}_i^n$ are independent for there must be three relations between them. What this means is that the components of $\mathbf{z}_i^n$ must be writable in terms of $3H-6$ independent internal coordinates $q_i, i = 1,2....3H-6$. Of course it is possible that some of the q_i are some of the components of the $\mathbf{z}_i^n$ but generally speaking the q_i will be expressible in terms of scalar products of the $\mathbf{t}_i^n$ (and equally of the $\mathbf{z}_i^n$) since scalar products are the most general constructions that are invariant under orthogonal transformations of their constituent vectors.

The transformation of the translation-free kinetic energy operator into body-fixed form yields

$$\hat{K}(\mathbf{z}) + \hat{K}(\mathbf{q},\mathbf{z}) + \hat{K}(\phi,\mathbf{q},\mathbf{z}) \tag{15}$$

The first term in (15) is simply the electronic kinetic energy operator

$$\hat{K}(\mathbf{z}) = -\frac{\hbar^2}{2\mu}\sum_{i=1}^{L}\nabla^2(\mathbf{z}_i) - \frac{\hbar^2}{2\mu'}{\sum_{i,j=1}^{L}}'\vec{\nabla}(\mathbf{z}_i).\vec{\nabla}(\mathbf{z}_j) \tag{16}$$

while

$$\hat{K}(\mathbf{q},\mathbf{z}) = -\frac{\hbar^2}{2}\Big(\sum_{k,l=1}^{3H-6} G_{kl}\frac{\partial^2}{\partial q_k \partial q_l} + \sum_{k=1}^{3H-6}\tau_k\frac{\partial}{\partial q_k}\Big) + \frac{\hbar^2}{2}\Big(\sum_{\alpha\beta} M_{\alpha\beta}\hat{l}_\alpha\hat{l}_\beta + \sum_\alpha \lambda_\alpha \hat{l}_\alpha\Big) \tag{17}$$

and

$$\hat{K}(\phi, \mathbf{q}, \mathbf{z}) = \frac{1}{2}(\sum_{\alpha\beta} M_{\alpha\beta}\hat{L}_\alpha\hat{L}_\beta + \hbar\sum_\alpha(\lambda_\alpha + 2(\mathbf{M}\hat{\mathbf{l}})_\alpha)\hat{L}_\alpha) \tag{18}$$

with $\hat{\mathbf{l}}$ as a 3 by 1 column matrix of Cartesian components

$$\hat{\mathbf{l}} = \frac{1}{i}\sum_{i=1}^{L}\hat{\mathbf{z}}_i\frac{\partial}{\partial \mathbf{z}_i} \tag{19}$$

The potential energy operator has the form

$$V(\mathbf{q}, \mathbf{z}) = V^e(\mathbf{z}) + V^n(\mathbf{q}) - V^{ne}(\mathbf{q}, \mathbf{z}) \tag{20}$$

where the electronic repulsion expressed in terms of the $\mathbf{z}_i$, takes the usual form. The angular parts of the problem are contained entirely in the angular momentum operators $\hat{L}_\alpha$ which in this formulation obey the standard commutation relations. The angular eigenfunctions are written as usual, $|JMk>$. All the other terms in the Hamiltonian depend on the internal and electronic variables alone.

The matrix $\mathbf{M}$ is an inverse generalised inertia tensor while $\mathbf{G}$ is is an inverse metric matrix. The operator λ_α is associated with the Coriolis coupling and so no coordinate system can be found in which it will vanish. The operator τ_k is dependent on internal coordinate choice and it is possible to choose a coordinate system in which this term vanishes.

The eigenfunction $\Psi(\mathbf{t})$ can be written as an eigenfunction of the body-fixed Hamiltonian in the form

$$\Psi(\mathbf{t}) \rightarrow \Psi^{J,M}(\phi, \mathbf{q}, \mathbf{z}) = \sum_{k=-J}^{+J}\Phi_k^J(\mathbf{q}, \mathbf{z})|JMk> \tag{21}$$

where the internal coordinate function on the right hand side cannot depend on M because, in the absence of a field, the energy of the system does not depend on M.

It is thus possible to eliminate the angular motion from the problem and to write down an effective body-fixed Hamiltonian within any (J, M, k) rotational manifold, that depends only on the internal coordinates. The transformation from the laboratory-fixed to the translation-free frame is linear and so its jacobian is simply a constant that can be ignored and since the transformation from the $\mathbf{t}_i^e$ to the $\mathbf{z}_i$ is essentially a constant orthogonal one, it has a unit jacobian. The transformation from the translation-free nuclear coordinates to the body-fixed ones is, however, non-linear and has a jacobian $|\mathbf{J}|^{-1}$ where $\mathbf{J}$ is the matrix constructed from the nuclear first derivative terms.

It can be shown (8) that the non-linearity of the body-fixing transformation is a topological consequence of any transformation that allows rotational motion to be separated. Furthermore it can be shown that there is always some configuration of the particles that causes the jacobian to vanish. Clearly where the jacobian vanishes, the transformation is undefined. This failure manifests itself in the Hamiltonian by the presence of terms which diverge unless, acting on the wavefunction, they vanish. This can occur either by cancellation or by the wavefunction itself being vanishingly small in the divergent region. These and related matters are discussed in more detail in (9).

It should be stressed that the origin of these divergences is not physical. They arise simply as a consequence of coordinate choice. However a particular choice can obviously preclude the description of a possible physical state of a system. Thus suppose that a triatomic is described in the Eckart approach with the equilibrium geometry specified as bent. In this case the jacobian vanishes when the internal coordinates correspond to a linear geometry. The problem then becomes ill-conditioned for states with large amplitude bending motions. Of course such large amplitude bending states are physically reasonable, it is just that they cannot be described in this formulation.

The important point to be made is that a body-fixing transformation cannot be globally valid. It has only local validity and so one one can at best get only a local Hamiltonian which is valid in a particular domain. However general topological considerations (8) again show that it is always possible to construct a sequence of body-fixing transformations which have common ranges of validity sufficient for passage from one to another to cover the whole space.

To remove the rotational motion it is convenient to write (15) as

$$\hat{K}_I(\mathbf{q},\mathbf{z}) + \hat{K}_R(\phi,\mathbf{q},\mathbf{z}) \tag{22}$$

where the first term, $\hat{K}_I$, consists of the first two terms in (15). The matrix elements with respect to the angular functions of the operators that depend only on the q_k and the $\mathbf{z}_i$ are quite trivial. Thus

$$< J'M'k' \mid \hat{K}_I + V \mid JMk >= \delta_{J'J}\delta_{M'M}\delta_{k'k}(\hat{K}_I + V) \tag{23}$$

In what follows explicit allowance for the diagonal requirement on J and M will be assumed and the indices suppressed to save writing. Similarly the fact that the integration implied is over the angles only will be left implicit.

To deal with the second term in (22) is much more complicated and since it is not required here, it will not be considered further. Details can

be found in (6). For the present it can be imagined that only states with $J = 0$ are being discussed.

Thus within any rotational manifold it is the eigensolutions of the effective Hamilton given by (23) which are invariant to orthogonal transformations and it these functions that will be used to consider the separation of electronic and nuclear motion.

3. Separating electronic and nuclear motions.

Returning to (21), it is seen that the form of the standard expansion that applies to the internal motion part of the problem, is expressed in terms of a sum of products

$$\Phi^J_{kp}(\mathbf{q})\psi_p(\mathbf{q},\mathbf{z}) \tag{24}$$

where p labels the electronic state and the sum is over p. The function $\psi_p(\mathbf{q},\mathbf{z})$ is assumed known, just as $|JMk>$ is assumed known and the effective nuclear motion Hamiltonian is obtained in terms of matrix elements of the effective internal motion Hamiltonian between the $\psi_p(\mathbf{q},\mathbf{z})$ with respect to the variables $\mathbf{z}$, just as the effective internal motion Hamiltonian itself is expressed in terms of matrix elements of the full body-fixed Hamiltonian between the $|JMk>$ with respect to the $\boldsymbol{\phi}$. The effective nuclear motion Hamiltonian then contains the electronic state labels p as parameters, in much the same way that the full effective Hamiltonian for internal motion contains the angular momentum labels k. Of course the analogy between the two derivations is simply a formal one. There is no underlying symmetry structure in the effective nuclear problem and neither is the sum over p of definite extent as is the sum over k. In the original formulation of the standard approach it was stipulated that the set of known functions, $\psi_p(\mathbf{q},\mathbf{z})$, were to be looked on as exact solutions of a problem like

$$(\hat{K}(\mathbf{z}) + V^e(\mathbf{z}) - V^{ne}(\mathbf{q},\mathbf{z}))\psi_p(\mathbf{q},\mathbf{z}) = E_p(\mathbf{q})\psi_p(\mathbf{q},\mathbf{z})$$

that is

$$\hat{H}^{elec}(\mathbf{q},\mathbf{z})\psi_p(\mathbf{q},\mathbf{z}) = E_p(\mathbf{q})\psi_p(\mathbf{q},\mathbf{z}) \tag{25}$$

Because in this equation there are no terms which involve derivatives with respect to the q_k, there is no development with respect to $\mathbf{q}$ in $E_p(\mathbf{q})$ or $\psi_p(\mathbf{q},\mathbf{z})$. Thus the $\mathbf{q}$ act here simply as parameters that can be chosen at will.

In fact it is not absolutely essential for what follows to require the ψ_p to be eigenfunctions of $\hat{H}^{elec}$. A reasonably concise and useful form can be obtained simply by requiring that

$$\int \psi^*_{p'}(\mathbf{q},\mathbf{z})\psi_p(\mathbf{q},\mathbf{z})d\mathbf{z} \equiv < \psi_{p'}|\psi_p >_{\mathbf{z}} = \delta_{p'p} \tag{26}$$

and, using the above abbreviation to denote integration over all **z** only

$$< \psi_{p'} | \hat{H}^{elec} | \psi_p >_{\mathbf{z}} = \delta_{p'p} E_p(\mathbf{q}) \tag{27}$$

The requirements (26) and (27) can be met in a simple and practical way by requiring the ψ_p to be solutions of a linear variation problem with matrix elements determined by integration over the **z** alone, for each and every value assigned to **q**.

The effective nuclear motion Hamiltonian, depending only on the **q**, is expressed in terms of matrix elements of the Hamiltonian just as before, between pairs of functions like (21) but with internal coordinate parts like (24) integrated over the **z** as well as the angular factors. Doing this yields an equation rather like (23) but with coupling between different electronic states, labelled by p. The term analogous to (23) become

$$< JMk'p' \mid \hat{K}_I + V \mid JMkp >_{\mathbf{z}} \quad =$$

$$\delta_{p'p}\delta_{k'k}(\hat{K}_H + E_p(\mathbf{q}) + V^n(\mathbf{q})) + \delta_{k'k}\gamma_{p'p}(\mathbf{q}) \tag{28}$$

where the designation of the angular integration variables has been left implicit as before, as have the diagonal requirement on J and M. The term $\hat{K}_H$ consists of the first group of terms from (17), namely the nuclear kinetic energy terms. The last term in (28) is given by:

$$\gamma_{p'p}(\mathbf{q}) = \frac{\hbar^2}{2}\left(\sum_{\alpha\beta} < \psi_{p'} | \hat{l}_\alpha \hat{l}_\beta | \psi_p >_{\mathbf{z}} M_{\alpha\beta} + \sum_{\alpha} < \psi_{p'} | \hat{l}_\alpha | \psi_p >_{\mathbf{z}} \lambda_\alpha \right.$$

$$- \sum_{k,l=1}^{3H-6} G_{kl}(< \psi_{p'} | \frac{\partial^2}{\partial q_k \partial q_l} | \psi_p >_{\mathbf{z}} + < \psi_{p'} | \frac{\partial}{\partial q_k} | \psi_p >_{\mathbf{z}} \frac{\partial}{\partial q_l} + < \psi_{p'} | \frac{\partial}{\partial q_l} | \psi_p >_{\mathbf{z}} \frac{\partial}{\partial q_k})$$

$$\left. + \sum_{k=1}^{3H-6} (\frac{2}{i} < \psi_{p'} | (\mathbf{W}\hat{\mathbf{l}})_k \frac{\partial}{\partial q_k} | \psi_p >_{\mathbf{z}} - \tau_k < \psi_{p'} | \frac{\partial}{\partial q_k} | \psi_p >_{\mathbf{z}}) \right) \tag{29}$$

If the last term in (28) is ignored, then what is left seems to be the right sort of nuclear motion Hamiltonian for present purposes. The function $E_p(\mathbf{q}) + V^n(\mathbf{q})$ is clearly a potential in the nuclear variables and the kinetic energy operator depends only on the nuclear variables too. It is not quite true that (25) is actually the clamped nuclei Hamiltonian but it is shown in (7) that the correspondence is very close.

4. The Relationship of nuclear motion to electronic structure

The nuclear motion problem specified by the first term in (28) will be well-defined provided that the potential energy function is an analytic function of the internal coordinates everywhere that the product approximation, (24), to the solution is well-defined. To ensure that the product is well-defined, the functions $\Phi^J_{kp}(\mathbf{q})$ for the body-fixed coordinate system, must be chosen so as to make a vanishing contribution when the jacobian vanishes, because electronic functions alone will not generally vanish there. Thus, somewhat paradoxical though it might seem, it is formally possible to generate non-existent states in this approach unless a very careful watch is kept on the behaviour or the nuclear motion functions. Any scheme of body fixing must have regions in which the definitions fail because the jacobian vanishes. However as internal coordinates for the problem can always be written in terms of scalar products of a set of translationally invariant coordinates, the internal coordinates remain well defined even when a particular scheme of body fixing fails. In principle one may move from one embedding scheme to another keeping a single set of internal coordinates. It is therefore sufficient to assume this condition and to concentrate on identifying the molecule in terms of internal coordinates. For this purpose in this approach, we must assume that there are real systems in which the coupling term $\gamma_{p'p}(\mathbf{q})$ is properly defined and small, so that (28) can be sensibly treated as an operator diagonal in the electronic state label; if it is supposed that the $\psi_p(\mathbf{q}, \mathbf{z})$ are eigenfunctions of the electronic Hamiltonian (25) then it is easy to show that the first derivative terms in (29) can be written as

$$< \psi_{p'} | \frac{\partial}{\partial q_k} | \psi_p >_{\mathbf{z}} = (E_{p'}(\mathbf{q}) - E_p(\mathbf{q}))^{-1} < \psi_{p'} | \frac{\partial V^{ne}}{\partial q_k} | \psi_p >_{\mathbf{z}} \qquad (30)$$

In so far as this is a valid approach it is seen that the coupling term must be divergent whenever the two electronic energy hypersurfaces touch or intersect unless the integral on the right hand side of (30) vanishes strongly.

There is no reason to believe that the electronic wave function is generally such as to cause the right side of (30) to vanish nor is there reason to believe that the electronic wave function itself will vanish either here or where the jacobian vanishes. The electronic functions alone will not generally vanish because they contain internal coordinates (and hence the nuclear conformations) simply as parameters and these coordinates are definable independently of the embedding choice.

The electronic function enters the full problem only as part of a product function such as (24): it is sufficient then that the matrix elements of the full Hamiltonian between such products not diverge. To ensure this condition

the functions $\Phi^J_{kp}(\mathbf{q})$ for the particular coordinate system fixed in the body must be chosen to force any potentially divergent matrix element to vanish. Whether this is possible is clearly contingent - it must be checked in any concrete case. For present purposes it will be assumed that it is possible at least in some cases. In such cases the diagonal term from (29) may be incorporated into the potential terms in (28) and this equation solved as an uncoupled equation. If it has bound state solutions then they are prime candidates for recognition as molecules.

For the nuclear motion problem to be well-posed the potential must be an analytic function of internal coordinates. Schmelzer and Murrell investigated this question in an attempt to determine internal coordinates invariant under permutations of identical particles (10) and further work was done by Collins and Parsons (11). It is instructive to consider the question somewhat indirectly. The set of internuclear distances forms a proper set of internal coordinates and in the general case of a system with H nuclei, there are $H(H-1)/2$ of these of which only $3H-6$ can be independent. When there are either just three or just four nuclei then there are the same number of inter-nuclear distances as there are independent coordinates. In this case the inter-nuclear distances can be used as internal coordinates. However when there are five or more nuclei, the number of inter-nuclear distances exceeds the number of independent internal coordinates, that is they form a redundant set. If they are to be used, an independent subset of them must be chosen. But it is easy to see that it is possible to construct two (or more) distinct figures for the nuclear geometry in which all the chosen independent inter-nuclear distances are the same. (An example in the case of five nuclei is given in the paper by Collins and Parsons cited above, (11).) Thus in such cases the potential energy function cannot be an analytic function of the internal coordinates. It would be comforting to be able to connect this failure in analyticity with the singular regions of the jacobian, but the possibility of such a connection seems unlikely since the singular regions of the jacobian can be placed at will, simply by choosing different embeddings.

Now this observation does not, of itself, show that for systems containing five or more nuclei, it is impossible to find a set of internal coordinates in which the potential energy is an analytic function, but it does make it clear that if there is such a set, it will have to be sought rather carefully.

To put any such search in context it is necessary to consider the behaviour of both the internal coordinates and the Euler angles under the permutation of of identical nuclei. The permutation of electrons yields the standard representation, which need not be further considered.

It can be shown (7) that, if $\mathbf{H}$ is the representation of a permutation in

the space of the $\mathbf{t}^n$ then under a nuclear permutation

$$\mathbf{z}^n \rightarrow \mathbf{U}^T \mathbf{z}^n \mathbf{H}^{-1} \tag{31}$$

while

$$\mathbf{C} \rightarrow \mathbf{CU} \tag{32}$$

where $\mathbf{U}$ is an orthogonal matrix whose elements are, at most, functions of the internal coordinates. Notice that while the effect of the permutation on q_k can at most produce a function of the q_k, the effect of the permutation on ϕ_m can produce a function of both the ϕ_m and the q_k. Rather delicate arguments (5), (7) can be used to show that the change induced in the general symmetric-top function under $\mathcal{P}$ is

$$|JMk> \rightarrow \sum_{n=-J}^{+J} |JMn> \mathcal{D}^J_{nk}(\mathbf{U}) \tag{33}$$

In this equation $\mathcal{D}^J(\mathbf{U})$ is the matrix made up from the elements of $\mathbf{U}$ in exactly the same way that $\mathcal{D}^J$ is made up from the elements of $\mathbf{C}$. A precise account of how this is to be done is given in Section 6.19 of (12). Should it turn out that $\mathbf{U}$ is a constant matrix then $\mathcal{D}^J(\mathbf{U})$ is a constant matrix and (33) simply represents a linear combination. If $\mathbf{U}$ is a unit matrix then $|JMk>$ is invariant. It should be noted here that this coupling of rotations by the permutations can mean that certain rotational states are not allowed by the Pauli principle and this is important in assigning statistical weights to rotational states.

It is rather difficult to say anything precise about the change induced in the q_k under the permutation for it has no general form. The best that can be said is that a permutation of nuclei induces a general function change

$$\Phi^J_k(\mathbf{q}, \mathbf{z}) \rightarrow \Phi'^J_k(\mathbf{q}, \mathbf{z}) \tag{34}$$

where the precise nature of the function change depends on the permutation, the chosen form of the internal coordinates and on the chosen functional form.

The results of a permutation will clearly be very difficult to handle for not only will $\mathbf{U}$ be difficult to determine, but one must be found for each distinct permutation of the identical nuclei and in a problem of any size there will be a very large number of such permutations. Similarly there will be one new internal motion function for each permutation. Only if the results of the all permutations result in simple changes of variable will the problem be tractable.

The embedding in the Eckart approach is generally invariant only under the subset of permutations of the identical nuclei which correspond to point

group operations on the equilibrium geometry figure. This is because the nuclei are identified in a clamped nucleus calculation and thus the permutational symmetry of the problem is generally broken. This point seems first to have been noted in print by Berry, (13) and is discussed in (14) and (15)). Thus it is clear that in the Eckart approach unless attention is confined only the broken symmetry solutions, the standard view of the separation of rotational and vibrational motion must break down. These matters are discussed a little more in (6) and (16).

Why typical broken symmetry solutions to the clamped nuclei problem turn out to be so effective in practice has been a vexing puzzle since the very beginning of molecular quantum mechanics. It has occasioned an enormous amount of work, particularly since the publication in 1963 of a paper (17) by H. C. Longuet-Higgins in which permutations were divided into *feasible* and *un-feasible* types and in which it was argued that it was necessary to consider only the (often rather small) set of feasible permutations in a given problem.

The idea of un-feasibility rests on the notion that the permutation is a real motion of particles in the potential computed from a clamped nucleus calculation. If between the typical geometry and the permuted geometry there is a high potential barrier, then the permutation is un-feasible. The idea that a permutation is a real motion of particles is an incongruous one, from a mathematical point of view, as is the idea of un-feasibility, outside the single product approximation for the wave function and hence a single uncoupled potential function.

5. Conclusions

It seems that there are still difficulties in the way of specifying precisely how nuclear motions are related to electronic structure and, at present, it is not clear that the relationship can be determined with any confidence.

References

(1) M. Born and J. R. Oppenheimer: *Ann.der Phys.* **84**, 457-484 (1927).

(2) C. Eckart: *Phys. Rev.* **47**, 552-558 (1935).

(3) G. Hunter: *Int. J. Quant. Chem.***9**, 237-242 (1975).

(4) M. Born and K. Huang: *Dynamical Theory of Crystal Lattices* , Oxford U.P., 1955, Appendix 8.

(5) B. T. Sutcliffe: *J. Chem. Soc., Faraday Transactions*, **89**, 2321-2335 (1993).

(6) B. T. Sutcliffe: in *Conceptual Trends in Quantum Chemistry*, Eds E. S. Kryachko and J. L. Calais, Kluwer Academic, Dordrecht, pp 53-85 (1994).

(7) B. T. Sutcliffe: *Journ. molec. struct (Theochem)* **34**, 217-235 (1995).

(8) B. Schutz: *Geometrical methods of mathematical physics*, C. U. P., Cambridge (1980).

(9) B. T. Sutcliffe: in *Theoretical models of chemical bonding* , Pt. 1 ed. Z Maksić, Springer-Verlag Berlin, pp 1-28 (1990).

(10) A. Schmelzer and J. N. Murrell: *Int J. Quant. Chem* **28**, 287-295 (1985).

(11) M. A. Collins and D. F. Parsons: *J. Chem. Phys.* **99**, 6756-672 (1993).

(12) L. C. Biedenharn and J. C. Louck: *Angular Momentum in Quantum Physics* , Addison- Wesley, Reading, Mass. (1982).

(13) R. S. Berry: *Rev. Mod. Phys.* **32**, 447-454 (1960).

(14) G. Ezra: *Symmetry properties of molecules* , Lecture Notes in Chemistry **28**, Springer-Verlag, Berlin (1982).

(15) J. D. Louck and H. W. Galbraith: *Rev. Mod. Phys.* **48**, 69-106 (1976).

(16) B. T. Sutcliffe: in *Methods in Computational Chemistry* Vol. 4, ed. S. Wilson, Plenum Press, New York and London pp 33-89 (1991).

(17) H. C. Longuet-Higgins: *Molec. Phys.* **6**, 445-460 (1963).

Combining Quantum Chemistry and Molecular Simulation

Florian Müller-Plathe

Laboratorium für Physikalische Chemie
Eidgenössische Technische Hochschule Zürich
CH-8092 Zürich, Switzerland

Abstract

Recently, semiempirical molecular-orbital methods have been combined with force-field-based molecular-dynamics techniques into hybrid schemes: The "interesting" part of the system is described by quantum chemistry, while the surroundings are treated by a classical force field. These hybrid schemes allow calculation of the energy and gradients fast enough for molecular dynamics simulations of hundreds of picoseconds (10^5 time steps) duration to be feasible. This provides sufficient sampling for the calculation of many statistical-mechanical properties. A short synopsis is given of work carried out at ETH Zürich on conformational equilibria in solution, reactions in solution and enzyme reactions.

ADVANCES IN QUANTUM CHEMISTRY, VOLUME 28

0065-3276/97 $25.00

1. Introduction

Modern quantum-chemical methods can, in principle, provide all properties of molecular systems. The achievable accuracy for a desired property of a given molecule is limited only by the available computational resources. In practice, this leads to restrictions on the size of the system: From a handful of atoms for highly correlated methods to a few hundred atoms for direct Hartree-Fock (HF), density-functional (DFT) or semiempirical methods. For these systems, one can usually afford the few evaluations of the energy and its first one or two derivatives needed for optimisation of the molecular geometry. However, neither the affordable system size nor, in particular, the affordable number of configurations is sufficient to evaluate statistical-mechanical properties of such systems with any level of confidence. This makes quantum chemistry a useful tool for every molecular property that is sufficiently determined (i) at vacuum boundary conditions and (ii) at zero Kelvin. However, all effects from finite temperature, interactions with a condensed-phase environment, time-dependence and entropy are not accounted for.

Molecular simulation and especially molecular dynamics (MD), on the other hand, is very effective at describing thermodynamic (e.g. density, heat of vaporisation, excess free energy), structural (solution structure, radial distribution functions), dynamic (diffusion coefficient, viscosity) and dielectric properties of condensed phases. However, MD has in the past relied upon empirical potential energy functions (force fields) to describe the physics and chemistry of the system under study. Modern force fields are well parametrised for standard compounds, e.g. liquids, organics and biomolecules. In fact, most force fields will provide more accurate structural and energetic information than all but the most expensive quantum-chemical treatments. However, force fields have serious limitations when it comes to describing properties and processes that explicitly involve the electronic degrees of freedom. Hence, the following classes of problems cannot be studied:

(i) Chemical reactions. Force fields can in fact be parametrised to describe the making and breaking of chemical bonds. However, one first has to know the potential energy curve along a breakable bond before it can be modelled by a suitable function (no predictive power). Secondly, one has to specify which bonds can be formed or destroyed, whereas ideally one would like the system to decide which chemistry takes place in a simulation, since it might be different from the simulator's preconceived ideas.

(ii) Electronically excited states. Again, it would be possible to derive parameters for the interaction of a molecule in its first excited state with a solvent, if there only were data to parametrise against.

(iii) Transition metals. With their numerous oxidation states and varying

coordination numbers they are a pain for force fields and most applications have used ad-hoc patches rather than systematically derived parameters.

In recent years, there have been many attempts to combine the best of both worlds. Continuum solvent models (reaction field and variations thereof) are very popular now in quantum chemistry but they do not solve all problems, since the environment is treated in a static mean-field approximation. The Car-Parrinello method has found its way into chemistry and it is probably the most rigorous of the methods presently feasible. However, its computational cost allows only the study of systems of a few dozen atoms for periods of a few dozen picoseconds. Semiempirical cluster calculations on chromophores in solvent structures obtained from classical Monte Carlo calculations are discussed in the contribution of Coutinho and Canuto in this volume. In the present article, we describe our attempts with so-called hybrid or quantum-mechanical/molecular-mechanical (QM/MM) methods. These concentrate on the part of the system which is of primary interest (the reactants or the electronically excited solute, say) and treat it by semiempirical quantum chemistry. The rest of the system (solvent, surface, outer part of enzyme) is described by a classical force field. With this, we hope to incorporate the essential influence of the in itself uninteresting environment on the dynamics of the primary system. The approach lacks the rigour of the Car-Parrinello scheme but it allows us to surround a primary system of up to a few dozen atoms by an environment of several ten thousand atoms and run the whole system for several hundred thousand time steps which is equivalent to several hundred picoseconds.

2. Hybrid method

The hybrid scheme used by us has been described in detail (1). Therefore, only a short summary is given here. The system is divided into a primary (QM) part treated quantum-chemically and the environment treated by a force field (MM part). For the QM part, a semi-empirical calculation is carried out. We have used the MOPAC program (2) for this task and have, consequently, employed all NDDO methods (MNDO, AM1, PM3) in the course of our work. The interactions among atoms of the MM part are described entirely by a classical force field. They are evaluated using the GROMOS87 program (3), and the GROMOS force field or close variations of it were used in our work.

The interactions between the QM part and the MM part are treated by a combination of quantum-chemical and force-field contributions. If the system can be separated into a QM solute and an MM solvent, the partitioning of interactions arises naturally: The electrons of the QM part feel the electric field of the partial charges of the solvent molecules which enter the one-electron Hamiltonian as additional point charges. The dispersion attraction and the short-range repulsion are modelled by a Lennard-Jones 6-12 potential. If, on the other

hand, a molecule extends over the QM/MM boundary, parts of it are described quantum-chemically and parts by the force field, and there are chemical bonds crossing the boundary. On the QM side, the dangling bonds are saturated by hydrogen atoms. The interaction across the boundary is then described by force field terms (bond stretching, bond angle bending and dihedral angle deformation). The partial charges of the first three atoms on the MM side (fewer than 4 chemical bonds away from the last QM atom) do not enter the QM Hamiltonian.

In this way, forces on all atoms are calculated which may come from quantum chemistry, the force field or both. These forces are used by the leap-frog integrator of the GROMOS MD program to propagate the atoms to the configuration at the next time step. The length of a time step is 0.5 fs, so this is repeated many times to generate a trajectory of suitable length for analysis. Additional techniques of molecular simulation such as umbrella sampling for the calculation of potentials of mean force are used as needed.

3. The conformations of dimethoxy ethane in aqueous solution

Conformational equilibria of the dimethoxy ethane molecule (ethylene glycol dimethyl ether, glyme) have puzzled researchers for quite a while. This molecule has three rotatable dihedral angles involving heavy atoms only, which can assume *trans* (180°), *gauche*$^+$ or *gauche*$^-$ (±60°) conformations, giving rise to ten different molecular conformers. Of these, the all-*trans* (*ttt*), *trans-gauche-trans* (*tgt*) and the *trans-gauche*$^+$-*gauche*$^-$ (*tgg*$^-$) have the lowest energies. While all quantum chemical calculations in vacuum unanimously have found *ttt* to be the minimum, all experimental measurements in condensed phases (crystal, melt, solution) found mainly *tgt*. It could be shown that this effect is due to the different boundary conditions (vacuum vs. condensed phase) and that it could be reproduced by a simple self-consistent reaction-field treatment (4) which just assumed a polarisable dielectric continuum around the glyme molecule. The shift in relative stability is caused by the large difference of the dipole moments of *ttt* (zero by symmetry) and *tgt* (1.4 D).

However, the reaction field treatment cannot account for the third low-energy conformer (*tgg*$^-$). This is within 0.1 kJ/mol of *ttt* in the gas phase as found by ab initio calculations, the stabilisation being ascribed to an intramolecular weak hydrogen bond between a methyl hydrogen and an ether oxygen at the other end of the molecule. Because of the large dipole moment (1.7 D), reaction-field treatments predict this conformer to be by far the most stable in solution (5), completely at odds with experiment where this conformer is never observed. On the other hand, the presence or absence of this conformer has serious

implications in the physics of poly(ethylene oxide) and polymer electrolytes derived from it (6). We have addressed this problem with a hybrid calculation which described the glyme solute by MNDO and the aqueous environment by the SPC water model (1). The MD calculation confirmed not only the experimental finding (nearly complete absence of the *tgg*$^-$ conformer) but also provided the explanation: Water molecules compete very effectively with the intermolecular methyl group for positions near the ether oxygens, since they are much better hydrogen donors.

3.2. An S_N2 reaction at nitrogen

We have studied the symmetric reaction

$$Cl^- + NH_2Cl \rightarrow NH_2Cl + Cl^-$$

in dimethyl ether (DME) solution at 248 K (7). First, the above reaction was studied in vacuum using both semiempirical and ab initio methods, after which it was decided that the PM3 method reproduced best the transition state energy found by MBPT2/6-311+G**. It was subsequently used in a hybrid scheme to treat the reactants, whereas a rigid model was developed for DME within the framework of the GROMOS force field. Umbrella sampling was used to calculate the free energy along the reaction path. The calculation yielded a number of important results on the modification of this reaction as one goes from the gas phase into solution. Firstly, there is a considerable screening of the reactants at large distances. Secondly, the energy of the encounter complex (Cl^- hydrogen-bonded to one of the hydrogens of chloro amine) with respect to infinite separation changes from -18.9 kcal/mol to -12.5 kcal/mol due to the better solvation of the separated reactants. Thirdly, the transition barrier is raised from 6.4 kcal/mol to 15.0 kcal/mol, for the same reason. Fourth, comparison of Mulliken populations qualitatively shows an increased charge separation in the encounter complex as well as in the transition state.

3.3. The mechanism of HIV protease

This enzyme hydrolyses proteins and plays an important role in the replication of the human immune deficiency virus. It belongs to the family of aspartic proteases. It catalyses the reaction

$$R1\text{-}NH\text{-}CO\text{-}R2 + H_2O \rightarrow R1\text{-}NH_2 + HOOC\text{-}R2$$

where R1 and R2 denote the rest of the protein chain. HIV protease achieves catalysis by a combined acid-base mechanism. There are two aspartic acid residues in the active site, only one of which is protonated. At the time of the reaction, the protein is firmly bound in the active site as is the water molecule which is to be split ("lytic water"). The role of the unprotonated aspartate is

clear from X-ray crystallography: It removes a proton from the lytic water so the latter can attack the carbonyl carbon in an activated form, often described as a quasi-free OH^-. The protonated aspartic acid transfers its proton either to the nitrogen (to form a better leaving group) or to the carbonyl oxygen (to activate the carbonyl group and facilitate the water attack). From the available experimental information alone, it cannot be decided which of the two mechanisms prevails, basically because X-ray crystallography cannot determine which of the two aspartic acids initially carries the proton. Moreover, it is not clear in how far the mechanism of the nucleophilic water attack and the two proton transfers is step-wise or concerted.

We have used the hybrid method to study both possible variants of the enzyme mechanism (8). A part of the substrate peptide, the lytic water molecule and relevant parts of the two aspartic acids are described by the PM3 method, after we had determined that this method reproduces best ab initio (MBPT2/6-31G**) energetics of the uncatalysed, acid-catalysed and base-catalysed hydrolysis of formamide in vacuum. The calculations clearly favoured one mechanism over the other (carbonyl oxygen is protonated, not nitrogen). Moreover, the proton transfers and the nucleophilic attack appear to be concerted. We used umbrella sampling to drive the oxygen of the lytic water towards the carbonyl carbon, and, within a few picoseconds of the oxygen going over the transition state, the proton transfers took place spontaneously.

4. Prospects and loose ends

This synopsis summarises three applications of the hybrid method, two of which actually involve chemical reactions. The combination of a semiempirical kernel and a force-field environment has been very successful in these application and has yielded information that could – at present – be obtained by other means (experimental or computational) only with considerable difficulty or not at all. One has to realise, though, that in practice there is a window of usefulness of the method: If the energy differences are large enough the energetics will be mainly determined by vacuum values, i.e. environment effects will be negligible. If, on the other hand, the energy differences are small compared to the intrinsic inaccuracies of semiempirical method and force field the results cannot be trusted.

However, the method also has more serious problems. They mainly arise from the often limited accuracy of the semiempirical schemes. For the time being, one is forced to compromise between accuracy of the quantum-chemistry part and the convergence of statistical-mechanical quantities which is determined mainly by the number of time steps sampled. Our calculations are biased toward longer simulation times and better statistical sampling. As a minimum safety measure, we have always calculated the system or a truncated version of it in

vacuum both by ab initio methods (usually MBPT2 and polarised bases) and the semiempirical schemes at our disposal. This calibration helps to answer three vital questions:

(i) Does a semiempirical scheme make any sense for the system under study? Often, none of the semiempirical methods is able to describe, say, a reaction correctly. For example, originally we had planned to study the reaction of fluoride with fluoro amine (Section 3.2) for which there were ab initio data in the literature. This had to be given up when the ab initio transition state structures were not reproduced. Similarly, our first choice of protein was a thioredoxin (Section 3.3). Here, the semiempirical estimates of the transition state energy were too far off to be useful.

(ii) Which of the semiempirical schemes works best (or least badly) for the system under study? For example, only MNDO did distinguish between the *ttt* and *tgt* conformers of glyme (Section 3.1). Neither AM1 nor PM3 gave a barrier between these states.

(iii) What are the residual errors? For example, the *ttt-tgt* barrier in glyme is 5 kJ/mol by MNDO and 12 kJ/mol by ab initio (Section 3.1). This means that calculated transition rates would be too high, whereas the equilibrium concentrations are still correct.

As long as it is not feasible to use more accurate quantum-chemical schemes (probably ab initio or DFT) inside the hybrid method, we believe it is mandatory to carry out test calculations before embarking on hybrid MD calculations. Otherwise, one's results can easily be wrong quantitatively as well as qualitatively.

References

(1) H. Liu, F. Müller-Plathe and W.F. van Gunsteren, J. Chem. Phys. **102**, 1722 (1995).
(2) J.J.P. Stewart, Comput.-Aided Mol. Design **4**, 1 (1990).
(3) W. Scott and W.F. van Gunsteren, in: E. Clementi and G. Corongiu (Eds.) *Methods and Techniques in Computational Chemistry METECC-95* (STEF, Cagliari, 1995).
(4) F. Müller-Plathe and W.F. van Gunsteren, Macromolecules **27**, 6040 (1994).
(5) F. Müller-Plathe, Braz. J. Phys. **24**, 965 (1994).
(6) F. Müller-Plathe, H. Liu and W.F. van Gunsteren, Comput. Polym. Sci. **5**, 89 (1995).
(7) H. Liu, F. Müller-Plathe and W.F. van Gunsteren, Chem. Eur. J. **2**, 191 (1996).
(8) H. Liu, F. Müller-Plathe and W.F. van Gunsteren, J. Mol. Biol. (submitted).

Solvent Effects from a Sequential Monte Carlo - Quantum Mechanical Approach

Kaline Coutinho and Sylvio Canuto

Instituto de Física,
Universidade de São Paulo, CP 66318
05389-970 São Paulo, SP, Brazil

Abstract

An approach based on the sequential use of Monte Carlo simulation and Quantum Mechanics is suggested for the treatment of solvent effects with special attention to solvatochromic shifts. The basic idea is to treat the solute, the solvent and its interaction by quantum mechanics. This is a totally discrete model that avoids the use of a dielectric continuum. Statistical analysis is used to obtain uncorrelated structures. The radial distribution function is used to determine the solvation shells. Quantum mechanical calculations are then performed in supermolecular structures and the spectral shifts are obtained using ensemble average. Attention is also given to the case of specific hydrogen bond between the solute and solvent.

ADVANCES IN QUANTUM CHEMISTRY, VOLUME 28

0065-3276/97 $25.00

1. Introduction

Solvent effects is one of the most important topics in theoretical chemistry. This is of course not without a reason as most experimental measurements are made in solution and several chemical reactions do not occur in gas phase(1). The general study of solvation effects has been the subject of some important review articles(2, 3). In particular, the study of solvent effects in molecular absorption spectroscopy in the visible/UV region has its own motivation and complexities(4). In this case the solvation involves also the excited states of the system. The difference in solvation energy between the ground and excited states leads to a shift of the absorption band as compared to the same transition in the gas phase. This is usually referred to as solvatochromic shift. If the ground state stabilizes more in the solvent than the excited state the shift is towards the blue region of the spectrum; the so-called hypsochromic shift. If, on the other hand, the excited state stabilizes more, the shift is toward the red long wavelength of the spectrum and one has the bathochromic shift. For instance, the $n - \pi^*$ absorption transition of acetone in water is well characterized to suffer a hypsochromic shift of about 1600cm^{-1}(5). On the other hand, the first $\pi - \pi^*$ transition of benzene, $^1B_{2u}(\pi - \pi^*)$ band, suffers bathochromic shifts of about 310cm^{-1} in cyclohexane and 140cm^{-1} in water(6). Interest in these solvatochromic shifts due to the difference in the solvation energies of the ground initial and excited final states of the chromophore leads to an analysis of the complex intermolecular forces between the solute and solvent molecules. This intermolecular solute-solvent interaction may conveniently be treated by perturbation theory assuming that there is no overlap of the wave functions of the solute and the solvent. Explicit and useful equations were obtained using second-order(3). Bayliss has earlier used classical analysis to relate spectral shifts to the index of refraction under the assumption that the solvent influences the shift by a dielectric constant(7). More recently, the idea of a solute enclosed by a cavity and interacting with the solvent as a polarizable dielectric continuum has been extended to a form convenient for actual calculations(8).

These approaches date back to the classical papers by Onsager(9) and Kirkwood(10). A self-consistent reaction field (SCRF) was developed and applied to several solvent effects with reasonable success(8, 11). However, it seems to become clear that these models where the solute and the solvent are represented by separated non-overlapping wave functions are too crude in some cases(12). Studies of solvent effects involving the interaction of the solute with a proton donor solvent (the so-called protic solvents) for instance usually leads to hydrogen bonds and therefore neglecting the overlap of the electron densities between the two subsystem is very difficult to justify. A similar difficulty is obtained for those absorptions where electron is trans-

ferred from the solute to the solvent or vice-versa(13). Furthermore, these models neglect entirely possible exchange effects between the solute and the solvent. An attempt to overcome these above mentioned difficulties is to explicitly include in the quantum mechanical considerations not only the bare solute (chromophore) but also a few solvent molecules(14). Although this supermolecular approach (though "supermolecule" really means a solute and one or two solvent molecules) addresses to the important short-range effects of the solute-solvent interaction it still misses the point that in a real (liquid) solution there is not one but a great number of supermolecular structures equally probable. Also, this approach very often depends on the number of solvent molecules included. In this direction some sort of ensemble average has to be performed.

More recently computer simulation methods are becoming a general tool for treating liquid systems. Thus the idea of generating liquid structures of one solute surrounded by solvent molecules is a natural one. However for these large, real supermolecular systems, consisting of hundreds of molecules, a complete quantum mechanical calculation is largely impractical. This is complicated even further because as the liquid has many structures (geometrical arrangements of atoms and molecules) equally possible and some sort of ensemble average has to be performed a very large number of quantum mechanical calculations is implied. Monte Carlo and/or Molecular Dynamics simulations have been used to obtain solvatochromic shifts but have treated the solute quantum mechanically and the solvent system is approximated by classical potentials(15, 16). In some cases good results for solvatochromic shifts were obtained compared to experiment but it is clear that the solvent being treated by classical charges can not describe the induction-polarization effects completely. In particular, the London dispersion forces involving the induced moments of the solute and solvent are not considered. However, dispersion forces are ubiquitous and contribute to a red shift(17). In some cases the dispersion effects are entirely responsible for the (red) shift.

In this paper we address to these important issues. We essentially use a sequential Monte Carlo Simulation - Quantum Mechanical approach to obtain solute-solvent interactions and solvatochromic shifts. First the Monte Carlo simulation is performed in the solute-solvent liquid. During the simulation molecular structures are obtained and separated. These structures are used after in the quantum mechanical calculation. As a MC simulation involves several thousands of steps for averaging of the thermodynamic properties, and now also of the transition energies, a specific procedure for reducing the total number of structures needed for the quantum calculation is of great need. We shall show that this is indeed possible using the concept of time correlation and statistical efficiency. Therefore instead of performing a quantum mechanical calculation on every structure generated by the

Monte Carlo simulation this is performed only on some few uncorrelated structures without compromising the final average result. This procedure is analyzed in greater detail in a separate contribution(18). Another interesting point is that the MC simulation can also be used to suggest the local molecular arrangement between the solute and solvent and this information can also input the quantum mechanical analysis of the specific short range interaction, such as hydrogen bonds. These aspect will be illustrated by the interesting problem of the $n-\pi^*$ absorption blue shift of acetone in water that has attracted considerable attention recently(16, 19, 20). Finally, as each structure obtained by the simulation contains hundreds of solvent molecules, a quantum mechanical treatment of the solvent requires a judicious reduction of the total number of solvent molecules included. We therefore analyze the results for the radial distribution function that defines the solvation shells. All molecules within a certain shell are explicitly included.

This paper is divided as follows: we first discuss the MC procedure and introduce the analysis of time correlation function for simulation of solute-solvent structures. Next we give results for the radial distribution function and consider the case of protic and aprotic solvents. The quantum mechanical analysis is made next. The paper is closed with a summary of the most important achievements and a few suggestions derived from our ongoing research.

2. Monte Carlo Simulation

2.1. General Description

Our Monte Carlo (MC) simulation uses the Metropolis sampling technique and periodic boundary conditions with image method in a cubic box(21). The NVT ensemble is favored when our interest is in solvent effects as in this paper. A total of 344 molecules are included in the simulation with one solute molecule and 343 solvent molecules. The volume of the cube is determined by the density of the solvent and in all cases used here the temperature is $T = 298K$. The molecules are rigid in the equilibrium structure and the intermolecular interaction is the Lennard-Jones potential plus the Coulombic term

$$U_{ab} = \sum_{i}^{\text{on } a} \sum_{j}^{\text{on } b} 4\varepsilon_{ij} \left[\left(\frac{\sigma_{ij}}{r_{ij}} \right)^{12} - \left(\frac{\sigma_{ij}}{r_{ij}} \right)^{6} \right] + \frac{q_i q_j e^2}{4\pi\epsilon_0 r_{ij}} \qquad (1)$$

where $\sum^a$ is the sum over the atoms of molecule a, $\sum^b$ is the sum over the atoms of molecule b, $\varepsilon_{ij} = \sqrt{\varepsilon_i \varepsilon_j}$, $\sigma_{ij} = \sqrt{\sigma_i \sigma_j}$ and σ_i, ε_i and q_i are

the parameters of the atom i. The potential parameters for the systems studied here are well characterized in the literature(22).

The initial configuration of the liquid is generated randomly considering the position and orientation of each molecule. A new configuration, or one MC step is generated after **all** molecules sequentially attempt to translate in all cartesian directions and also attempt to rotate around a randomly chosen axis. Acceptance of each move is governed by the Metropolis sampling technique. The maximum displacement of the molecules is self adjusted after 50 MC steps to give an acceptance rate around 50%. The full simulation involves a thermalization stage between 2000 and 5000 MC steps that is followed by the average stage of around 30000 MC steps. Thermodynamic properties and pairwise radial distribution functions are then obtained.

The average value of the energy in the MC simulation, is given as the average over a chain of size l of instantaneous values:

$$\langle E \rangle_l = \frac{1}{l} \sum_i^l E_i \tag{2}$$

A full quantum mechanical calculation of the energy of a supermolecular system, composed of 344 molecules, over $\sim$ 30000 MC steps is of course not possible. The alternative we suggest here is to perform quantum mechanical calculations after the simulation but using only a few selected number of solvent molecules and a selected number of MC structures. The number of solvent molecules included in the calculation is obtained from the analysis of the pairwise radial distribution function, using all molecules surrounding the solute up to a certain solvation shell. This number is still large enough to preclude sophisticated *ab initio* calculations but lies well within the range of semiempirical methods. As to the number l of necessary MC structures for ensemble average we shall show that it can be reduced dramatically over the entire number of MC steps without modifying the calculated average energy. This is done by calculating the time correlation function or the statistical inefficiency of the energy as described next.

2.2. The Time Correlation Function

The time correlation function for the energy, over a chain of size l is defined as

$$C(t) = \frac{\langle E_i E_{i+t} \rangle_{l-t} - \langle E_i \rangle_{l-t} \langle E_{i+t} \rangle_{l-t}}{\langle E^2 \rangle_l - \langle E \rangle_l^2} \tag{3}$$

where "time" t is measured in units of MC steps.

The correlation time $\mathcal{T}$ is obtained from

$$\mathcal{T} = \int_0^\infty C(t) dt \tag{4}$$

For Markovian processes it can be shown(23) that

$$C(t) = e^{-t/\mathcal{T}} \tag{5}$$

Therefore calculating $C(t)$ from eq.(3) and fitting to an exponential function as eq.(5) will give $\mathcal{T}$ for the simulation. Configurations obtained between MC steps smaller than $\mathcal{T}$ are so highly correlated to one another that gives no new statistical information. Here we consider that configurations, or molecular structures, obtained after $2\mathcal{T}$ MC steps are uncorrelated. The correlation time of the energy is therefore an important parameter in selecting and reducing the number of configurations to be used in the quantum mechanical calculations. Using correlated structures is a waste that does not contribute to the average. In practical uses made by us, it became clear that in real situations of solute-solvent systems $\mathcal{T}$ is reasonably large. This is of great advantage in reducing the number of QM calculations by a factor of $2\mathcal{T}$. However to obtain this $\mathcal{T}$ a very long over our usual MC simulation has to be performed hindering somewhat the total gain. It is thus of interest to have an alternative and more efficient procedure for obtaining the time correlation parameter $\mathcal{T}$. This can be accomplished with the so-called statistical inefficiency.

2.3. The Statistical Inefficiency

To calculate the statistical inefficiency s, a chain of size l is divided in n_b parts of size l_b, $l = n_b l_b$. s is then defined as(24)

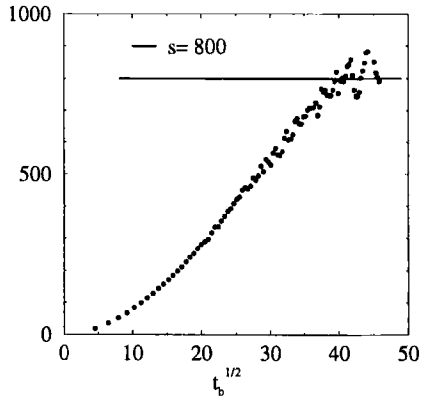

Figure 1: **Statistical inefficiency from a MC simulation of acetone in water**

$$s = \lim_{l_b \to \infty} \frac{l_b \langle \delta E^2 \rangle_b}{\langle \delta E^2 \rangle} \tag{6}$$

where $\langle \delta E^2 \rangle_b$ is the fluctuation of the energy over the parts

$$\langle \delta E^2 \rangle_b = \frac{1}{n_b} \sum_{b=1}^{n_b} (\langle E \rangle_b - \langle E \rangle_l)^2 \tag{7}$$

where $\langle E \rangle_b$ is the average of the energy in part b. For a Markovian process, the correlation time $\mathcal{T}$ and the statistical inefficiency are related by $s \approx 2\mathcal{T}$.

Figure 1 shows the statistical inefficiency obtained after a conventional MC simulation of one acetone molecule surrounded by 343 waters. This is a typical figure for the statistical inefficiency $s(24)$. Performing an ensemble average of the solvatochromic shift over all structures generated by the MC simulation is indeed a great waste as in fact only one after around each 800 MC steps is relevant. This dramatic reduction in the number of quantum mechanical calculations needed can be favorably used.

It is interesting to mention that the statistical inefficiency is obtained only after performing the simulation and therefore it is of little practical use until the simulation is halted. However, for our applications in solvent effects it shows that within a given accuracy determined only by the total number of MC steps there is a great saving of the total calculation if only uncorrelated structures are used in the subsequent quantum mechanical calculations. For the case of the acetone-water calculations only 40 uncorrelated structures are used for the ensemble average of the calculated quantum mechanical results, instead of the total number of 32000.

3. Sequential Monte Carlo - Quantum Mechanical Analysis

3.1. Long Range Effects

The molecular structure of liquids are best analyzed using the concept of the radial distribution function (RDF). This is of particularly important use in solute-solvent structures as it defines the solvation shells around the solute molecule(24).

We consider next the MC simulation of benzene in cyclohexane and benzene in water. The RDF's of both systems are shown in figure 2. Benzene in cyclohexane is an interesting system involving the interaction of two non-polar systems. As the electron densities of the two subsystems do not strongly interact this would be an adequate system for the application of cavity models and SCRF. However, the experimentally observed red shift of 310cm^{-1} for the lowest $^1B_{2u}(\pi - \pi^*)$ absorption of benzene(6) can be attributed to dispersion effects as none of the subsystems, solute benzene or

solvent cyclohexane, has a permanent dipole moment, and higher moments have only a minor effect. Analysis of our calculated RDF shown in figure 2a suggests the inclusion of all cyclohexane molecules within a C(carbon atom of benzene)-C(carbon atom of cyclohexane) distance of $7.9\mathring{A}$ that defines the first peak of the RDF. The integration of this peak defines the coordination number that corresponds to 11 cyclohexane molecules. The calculated statistical inefficiency of the benzene-cyclohexane system is

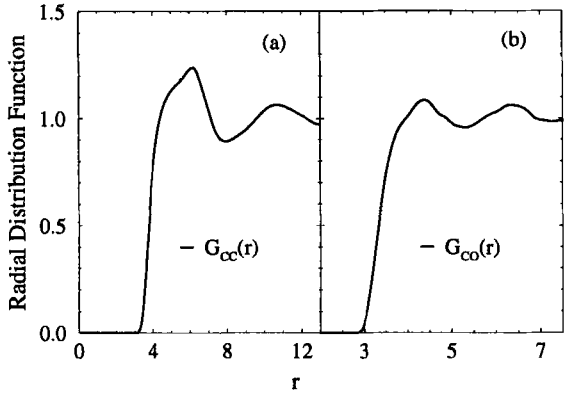

Figure 2: **RDF of C of benzene and (a) C of cyclohexane and (b) O of water obtained from a MC simulation of benzene in cyclohexane and of benzene in water using 343 solvent molecules at 298K**

$s = 550$. Therefore based on these results, we selected for the quantum mechanical calculations a total of 40 MC supermolecular structures separated by 500 MC steps and each supermolecule being composed of the benzene chromophore and the 11 nearest cyclohexane molecules ordered by center-of-masses distances. Figure 3 shows examples of the local environment around the benzene chromophore. To facilitate the illustration only two selected structures with only 5 solvent molecules are shown. These structures are similar to the usual configurations of benzene clusters(25).

A similar analysis is made for the case of benzene in water. This interesting system is considered stimulated by nice experimental results for the spectral shifts obtained by Bayliss and Hulme(6). Possible hydrophobic effects are not identified nor discussed by Bayliss but it is under current investigation in our group.

Figure 2b shows the C(carbon of benzene)-O(oxygen of water) RDF. Again, the first peak defines the solvation shell of interest. Integration of this peak until the distance of $5.3\mathring{A}$ suggests the first solvation shell to be composed of 18 water molecules. Based on these results we have selected for

the quantum calculations a total of 40 MC structures separated by 800 MC steps with each supermolecule being composed of the benzene chromophore and the 18 nearest water molecules ordered by center-of-masses distances. Figure 4 shows the local environment around the benzene chromophore us-

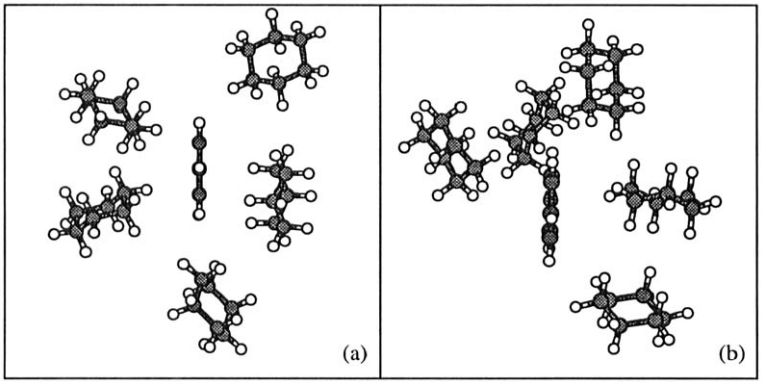

Figure 3: **Examples of two structure obtained by the MC simulation of benzene in cyclohexane. The benzene is shown in the center of the figure. A cyclohexane is seen at the right of the benzene in the (a) parallel and (b) perpendicular orientations.**

ing only one selected MC structure for illustration. Figure 4 also shows, for this structure, how the calculated energy shifts of the first $\pi - \pi^*$ transition of benzene vary with the number of solvent water molecules included in the quantum calculation. For this illustration, we used the semiempirical ZINDO program(26).

A similar behavior is obtained for all MC structures but only one result is shown to avoid excessive congestion in the figure. For this case of benzene in water the calculated energy shift stabilizes when the number of solvent water molecules reaches 18, that corresponds to the first solvation shell, obtained here by integration of the first peak of the RDF.

The final ensemble averaged results for the red shift of the first $\pi - \pi^*$ band of benzene in cyclohexane and water are 200cm^{-1} and 120cm^{-1}, respectively, in good agreement with the corresponding experimental results of 310cm^{-1} and 140cm^{-1}(6). These averaged results are found to be stable with respect to the number of MC structures included.

3.2. Short Range Specific Effects

A most interesting system to analyze is acetone in water. Similar to the case of formaldehyde the lone pair of the oxygen forms a hydrogen bond

with the water. Opposite to the case of formaldehyde, however, the blue shift of the $n - \pi^*$ transitions is well characterized(5). An important issue is the relative influence of the specific hydrogen bond in the final effect.

The RDF of acetone in water is shown in figure 5a. In fact only the O(oxygen of the carbonyl)-H(hydrogen of water) distribution is shown. The first peak (with maximum in $r = 1.80\AA$) corresponds to the hydrogen bond

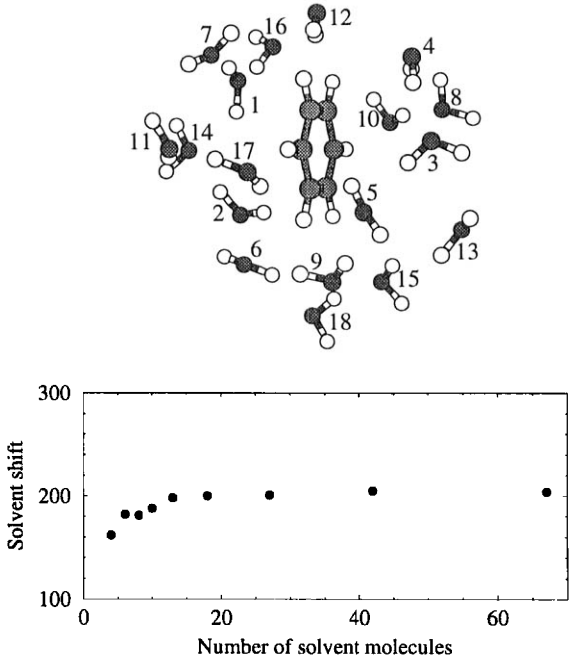

Figure 4: **Example of one structure obtained by the MC simulation of one benzene surrounded by 343 water molecules. The calculated energy (red) shift of the $^1B_{2u}(\pi - \pi^*)$ transition is shown as a function of the number of molecules included in the quantum calculation. The energy shift is given in cm^{-1}.**

that is of interest here. Figure 5b-5d shows the type of arrangements for these bonds that are obtained as a result of the MC simulation. Only those structures with a single hydrogen bond is shown. The structure 5b has also been obtained in formaldehyde(27) and 5c is similar to the *ab initio* structure of formaldehyde obtained by Taylor(19) and others(28). For such weak bonds it is not possible to energetically distinguish between structures 5c and 5d and they should be considered equivalent.

ZINDO calculations of the $n - \pi^*$ shift of acetone in water using one acetone molecule surrounded by up to thirty water molecules were first performed(29). The 40 MC structures separated by 800 MC steps ($s = 800$) were used in the quantum mechanical calculations to obtain the ensemble average. The results obtained for the spectral shift were always lower than the experimental value. Similar results were obtained using *ab initio*

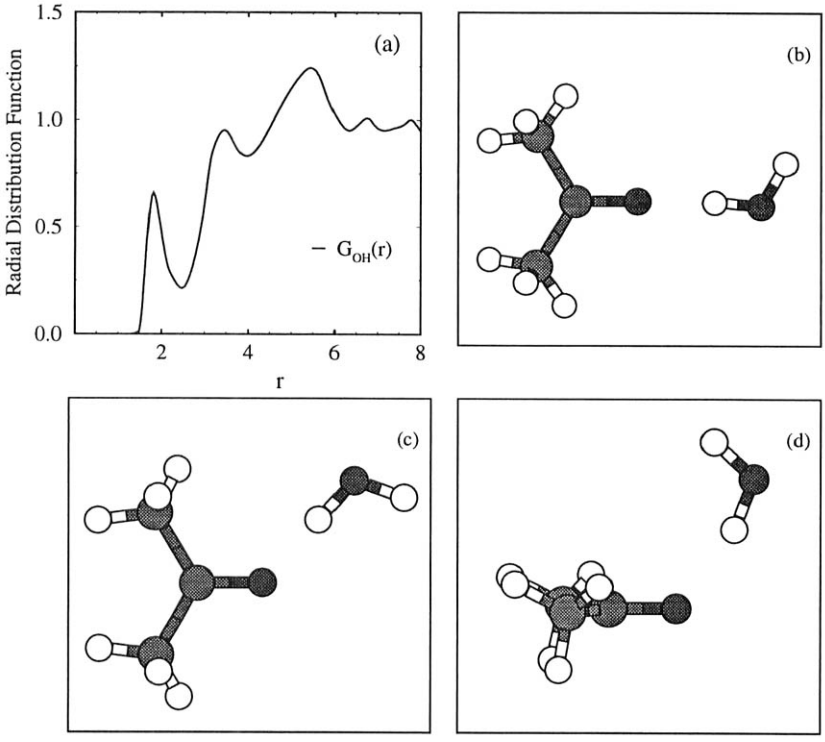

Figure 5: **RDF of *O* of acetone and *H* of water (a) and examples of MC structures showing hydrogen bonds between acetone and the first nearest neighbor water molecule (b,c,d) obtained in the MC simulation of one acetone surrounded by 343 water molecules at 298K.**

CIS calculations with a minimal basis set. Substituting the solvent water molecules by classical point charges led to results for the calculated shift that were very similar to those obtained by Gao(16). We have found however a great dependence of the results with those MC structures showing a hydrogen bond and this can not be described by treating the solvent as

classical charges.

We now perform an *ab initio* investigation of the $n - \pi^*$ blue shift of acetone in water. Using structures 4b and 4c of the MC simulation as input a full geometry optimization of these two structures were performed using several theoretical models and basis sets. All results suggest that structure 4c is the most stable. At the second order MBPT(2) with a 3-21G basis set it is found that the structure 5c is more stable than the structure 5b by about 6 kcal/mole. The optimized hydrogen bond distance $O \cdots H$ distance is 1.89$\AA$. With the same basis but at the SCF level this distance increases to 1.95$\AA$. Overall, improving the basis set at the SCF level of calculation increases this distance whereas inclusion of the correlation effects decreases it. For these reasons we now favor the geometries obtained at the SCF/3-21G level. For isolated acetone this SCF/3-21G calculation gives the best result for the geometry as compared to experiment, among all models we have considered.

Table 1
Calculated binding energies of the ground state of acetone in water, using geometries optimized at the SCF/3-21G levels. All energies are given in kcal/mole.

Theoretical Model	Binding Energy
SCF	11.2
$MBPT(2)$	12.9
$MBPT(3)$	12.3
$DQ - MBPT(4)$	12.2
$SDQ - MBPT(4)$	12.4
$MBPT(4)$	12.8
$CCSD$	12.4
$CCSD(T)$	12.6

Table 1 gives the calculated binding energy of acetone-water obtained as the difference between the energy of the composite system (acetone-water) and the energy of the two separate parts. These results suggest that correlation effects are not of great importance. In fact, we have found(30) that basis sets influence the calculated binding energies but at a fixed geometry and a fixed basis set the single-point results are not much influenced by correlation results. If one consider an stabilization energy of the ground state of the acetone in water of about 10 kcal/mole than the excited state is implied to stabilize by about 5.5 kcal/mole to give a difference of 4.5 kcal/mole in stabilization energies as suggested by the observed blue shift of 1560cm^{-1}. This difference in stabilization energies for the ground and excited states of acetone in water is in reasonable agreement with the result

that could be inferred by the difference in dipole moments of acetone in the ground and excited states. With all theoretical models considered, from SCF to CCSD(T), the stabilization energy of the ground state of acetone in water is larger than the shift of the $n-\pi^*$ transition thus suggesting also a stabilization of the excited state of this transition(31).

Table 2
Calculated energies of $n-\pi^*$ transition of pure and solvated acetone. All energies are in cm^{-1}.

	CIS/3-21G	Experimental(5)
Acetone	39227	36200
Acetone-Water	40966	37760
Spectral Shift	1739	1560

Table 2 finally gives the calculated $n-\pi^*$ transition of isolated acetone and acetone-water using the *ab initio* optimized SCF/3-21G geometries. This calculated blue shift of $1740cm^{-1}$ is in a fairly good agreement with the experimental result of $1560cm^{-1}$. Considering that the CIS calculations of one acetone bound to one water molecule, as we consider here do not include dispersion effects and that dispersion effects are negative(17) this calculated blue shift should overestimate the observed value as it in fact does. Before concluding let us address to the important question of the role of the influence of the short range specific effects compared to the total observed shift. We therefore want to consider a calculation of the blue shift of the $n-\pi^*$ transition of acetone in water as the number of water molecules increases. Clearly, it is a difficult problem to fully optimize the geometry of the supermolecule composed of one acetone and several water molecules at the *ab initio* level, even if one restricts to the SCF model with small basis set. Therefore, we shall again use the MC structures discussed previously. Figure 6 shows one MC structure consisting of one acetone and seven water molecules. The upper part of the figure shows the structure and it orders the water molecules according to the $O\cdots H$ distance. The bottom part shows the calculated blue shift of the $n-\pi^*$ transition as the number of solvent molecules is increased according to the numbering given in the upper part. This figure 6 seems to suggest that at this level of calculation the first water molecule is responsible for most of the shift and that including more water molecules has only a small influence. This emphasizes the importance of the proper treatment of the local specific interaction of the hydrogen bond between the solute and the solvent.

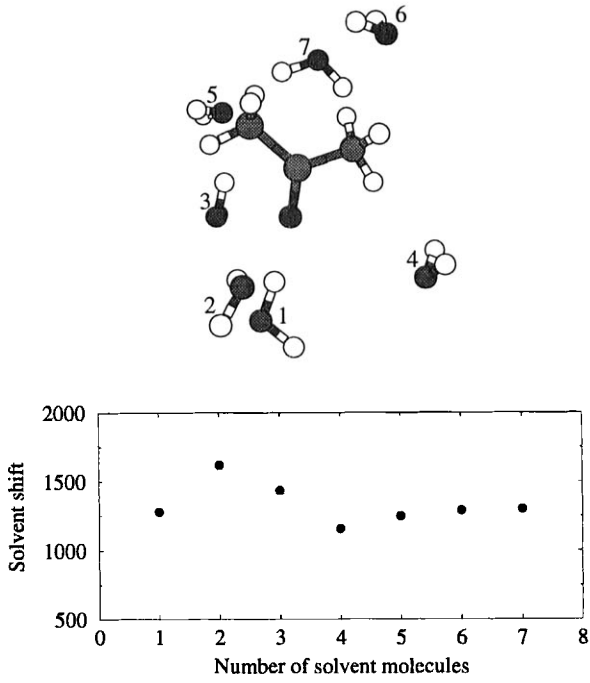

Figure 6: **Example of one structure obtained by MC simulation of one acetone surrounded by 343 water molecules. The calculated energy shift is shown as function of the number of molecules included in the quantum calculation. The energy is given in cm^{-1}.**

4. Summary

The study of solvatochromic shifts is of great importance and has received enormous theoretical attention in recent years. Progress has been achieved in the use of the self-consistent reaction field and cavity models. These advances have also shown several limitations. It is thus of great interest to have alternative procedures to calculate solvent effects. In this respect the use of Monte Carlo/Molecular Dynamics simulations has been growing. In this paper we suggest a procedure to allow a full quantum mechanical calculation of the solute-solvent system. The basic idea is to treat the solute, the solvent and its interaction by quantum mechanics. First a Monte Carlo simulation is performed to characterize the liquid structure. These structures are then used in the quantum mechanical calculation. As a liquid has not one but a great number of structures equally possible within a

given temperature ensemble average should be performed. Using the calculated statistical inefficiency and time correlation function the number of structures needed is greatly reduced. This makes it possible to perform only a few quantum mechanical calculations without affecting the final average value of the energy shift. In our present approach the size of the supermolecule used is limited up to first solvation shell and the number of solvent molecules is obtained by integration of the radial distribution function. This usually gives a number of solvent molecules that precludes sophisticated *ab initio* calculations but it is well within the range of applicability of most semiempirical models. If more sophisticated calculations are demanded the structures obtained by the Monte Carlo simulation could still be used. In our applications these classical structures were successfully used both in the case of long range intermolecular effects and in the case of short range specific interactions. Further progress along these lines is underway in our group with some emphasis on hydrogen-bonded solute-solvent systems. In these cases the simulations can proceed by utilizing the solute-solvent hydrogen bonded as the chromophore and the classical Monte Carlo structures for the outer solvation shells thus completely avoiding the use of a dielectric continuum, if one so desires.

5. Acknowledgments

This work is dedicated to Prof. Geerd H. F. Diercksen on the occasion of his 60th birthday.

We thank Prof. M. C. Zerner for continuous discussions of solvent effects in spectroscopy.

This work is supported by CNPq and FAPESP.

References

(1) C. Reichardt, *Solvent Effects in Organic Chemistry*, Verlag Chemie, Weinheim, New York, 1979.
C. Reichardt, *Chem. Rev.* **94,** 2319 (1994).
E. S. Amis and J. F. Hinton, *Solvent Effects on Chemical Phenomena*, Vol 1, Academic Press, New York, 1973.

(2) J. Tomasi and M. Persico, *Chem. Rev.* **94,** 2027 (1994).
C. J. Cramer and D. G. Truhlar, in *Reviews in Computational Chemistry*, eds. D. B. Boyd and K. B. Lipkowitz, Vol 6, VCH, New York, 1995.

(3) S. Basu, *Adv. Quantum Chem.* **1,** 145 (1964).
A. T. Amos and B. L. Burrows, *Adv. Quantum Chem* **7,** 289 (1973).

(4) H. Suzuki, *Electronic Absorption Spectra of Organic Molecules*, Academic Press, New York, 1967.
M. F. Nicol, *Solvent Effects on Electronic Spectra*, *App. Spectr. Rev.* **8**, 183 (1974).
N. S. Bayliss and E. G. McRae, *J. Phys. Chem* **58**, 1002 (1954).
E. G. McRae, *J. Phys. Chem.* **61**, 562 (1957).
N. Mataga and T. Kubota, *Molecular Interactions and Electronic Spectra*, Dekker, New York, 1970.

(5) N. S. Bayliss and E. G. McRae, *J. Phys. Chem* **58**, 1006 (1954).

(6) N. S. Bayliss and L. Hulme, *Australian J. Chem.* **6**, 257 (1953).

(7) N. S. Bayliss, *J. Chem. Phys.* **18**, 292 (1950).

(8) O. Tapia and O. Goscinski, *Molec. Phys.* **29**, 1653 (1975).
J. L. Rivail and D. Rinaldi, *Chem. Phys.* **18**, 233 (1976).
K. V. Mikkelsen, H Ågren and H. J. A. Jensen, *J. Chem. Phys.* **89**, 3086 (1988).
M. M. Karelson and M. C. Zerner, *J. Phys. Chem.* **96**, 6949 (1992).

(9) L. Onsager, *J. Am. Chem. Soc.* **58**, 1486 (1936).

(10) J. G. Kirkwood, *J. Chem. Phys.* **2**, 351 (1934).
J. G. Kirkwood and F. H. Westheimer, *J. Chem. Phys.* **6**, 506 (1938).
C. J. F. Bottcher, *Theory of Electric Polarization*, Elsevier, Amsterdam, 1973.

(11) J. Wu and M. C. Zerner, *J. Chem. Phys.* **100**, 7487 (1994).
H. Ågren, C. M. Llanos and K. V. Mikkelsen, *Chem. Phys.* **115**, 43 (1987).

(12) P. Th. van Duijnen and A. H. De Vries, *Int. J. Quantum Chem. Symp.* **29**, 523 (1995).
D. M. Chipman, *J. Chem. Phys.* **104**, 3276 (1996).

(13) M. J. Blandamer and M. F. Fox, *Chem. Rev.* **70**, 59 (1970).
R. A. Marcus, *J. Chem Phys.* **24**, 966 (1956).
R. A. Marcus and N. Sutin, *Biochem. Biophys. Acta* **811**, 265 (1985).

(14) P. Claverie, J. P. Daudey, J. Langlet, B. Pullman, D. Piazzola and M. J. Huron, *J. Phys. Chem.* **82**, 405 (1978).

(15) J. T. Blair, K. Krogh-Jespersen and R. M. Levy, *J. Am. Chem Soc.* **111**, 6948 (1989).
J. Gao and X. Xia, *Science* **258**, 631 (1992).

(16) J. Gao, *J. Am. Chem. Soc.* **116,** 9324 (1994).

(17) W. Liptay, in *Modern Quantum Chemistry*, ed. O. Sinanoglu, Part II, p. 173, Academic Press, New York, 1966.

(18) K. Coutinho, M. J. de Oliveira and S. Canuto, in preparation.

(19) P. Taylor, *J. Am. Chem. Soc.* **104,** 5248 (1982).

(20) P. Th. van Duijnen, private communication.

(21) K. Coutinho and S. Canuto, *DICE*, a general Monte Carlo program for liquid simulation, Univ. São Paulo, 1994.

(22) W. L. Jorgensen, J. D. Madura and C. J. Swenson, *J. Am. Chem Soc.* **106,** 6638 (1984).
W. L. Jorgensen, J. Chadrasekhar and J. D. Madura, *J. Chem. Phys.* **79,** 926 (1983).
W. L. Jorgensen, J. M. Briggs and M. L. Contreras, *J. Phys. Chem.* **94,** 1683 (1984).

(23) C. Chatfield, *The Analysis of Time Series. An Introduction*, 3nd edn. Chapman and Hall, 1984.

(24) M. P. Allen and D. J. Tildesley, *Computer Simulation of Liquids*, Oxford Science Publ., Oxford, 1987.

(25) G. Karlström, P. Linse, A. Wallqvist and B. Jönsson, *J. Am. Chem. Soc.* **105,** 3777 (1983).
P. Hobza, H. L. Selzle and E. W. Schlag, *Chem. Rev.* **94,** 1767 (1994).
Z. Q. li, K. Ohno, Y. Kawazoe, M. Mikami and Y. Masuda, *Comp. Mat. Science* **4,** 241 (1995).

(26) J. Ridley and M. C. Zerner, *Theor. Chim. Acta* **32,** 111 (1973).

(27) J. T. Blair, J. D. Westbrook, R. M. Levy and K. Krogh-Jespersen, *Chem. Phys. Letter* **154,** 531 (1989).

(28) S. Iwata and K. Morokuma, *Chem. Phys. Letter* **19,** 94 (1973).
J. E. Del Bene, *J. Am. Chem. Soc.* **95,** 6517 (1973).

(29) K. Coutinho, S. Canuto, and M. C. Zerner, in progress.

(30) K. Coutinho and S. Canuto, in preparation.

(31) P. Haberfield, *J. Am. Chem. Soc.* **96,** 6526 (1974).
P. Haberfield, M. S. Lux and D. Rosen, *J. Am. Chem. Soc.* **99,** 6828 (1977).

Energy Deposition of Swift Alphas in Neon: An Electron Nuclear Dynamics Study

John R. Sabin

Department of Physics
University of Florida
Gainesville, Florida 32611 U.S.A.

Abstract

The time dependent variational principle is used to study energy deposition by swift ions in material targets. One important aspect of this process is charge exchange between the projectile and the target in single collisions. Preliminary results are reported for the model system $He^{2+} \rightarrow Ne$.

ADVANCES IN QUANTUM CHEMISTRY, VOLUME 28

0065-3276/97 $25.00

1. Introduction

The problem of energy deposited by a swift ion in a target medium has been, from the early days of the field to the present, burdened with a thick layer of classical modeling. From the time of the first quantal treatment of Bohr (1, 2) and the first Born approximation of Bethe (3, 4), the models used are classical in conception, but with an ever increasing quantal component. In the case of the Bethe Theory (3, 4), which is the *de facto* standard theory for use in the interpretation of experimental data, the linear energy loss or stopping power is generally written in terms of the stopping cross section, $S(v)$, which depends on projectile velocity v and the number density of the scattering centers, n:

$$-\frac{dE}{dx} = nS(v) \tag{1}$$

The stopping cross section is related to the stopping number $L(v)$ by

$$S(v) = \frac{4\pi Z_1^2 Z_2}{mv^2} L(v) \tag{2}$$

where Z_1 is the fixed (*vide infra*) projectile charge and Z_2 is the number of electrons associated with each scattering center. The stopping number, $L(v)$, is frequently written as a Born series (5) in the projectile charge

$$L(v) = \left[\ln \frac{2mv^2}{I} - \frac{C.}{Z_2}\right] + \sum_{i=1} Z_1^i L_i(v) \tag{3}$$

where the first term is the Bethe (first Born) term and the following terms are higher order terms in the Born series. Except at small v, the higher Born terms (6) are generally ignored. In the conventional view of the Bethe formulation, all of the energy transfer is from projectile kinetic energy to target electronic energy. The quantum mechanics in the problem is hidden in the single material parameter I, the mean excitation energy

$$\ln I = \frac{\int \frac{\partial f}{\partial E} E \ln E dE}{\int \frac{\partial f}{\partial E} E \, dE} \tag{4}$$

which is the first excitation energy weighted moment of the dipole oscillator strength distribution of the system, and measures the ease with which the electronic structure of the target can accept energy.

In fact, this is not the only place that quantum mechanics enters the problem. The charge state of the projectile, which is a dynamic quantity varying over the allowed ion charge states as a function of velocity, as the projectile traverses the target, is also quantum mechanically determined. Although most treatments

consider an incoming particle beam to be of unique, fixed charge, capture and loss of electrons by the projectile during target penetration cause precipitant changes in the stopping power at each encounter. A proper treatment of the stopping, especially for heavier projectiles with many possible charge states, obviously requires that these dynamic charge changing effects be taken into account.

Perhaps the simplest way to account for projectile charge states is to invoke the Bohr criterion (7, 8) which assumes simply that the charge state of the projectile is quickly equilibrated and that all electrons with orbital velocity less than the projectile velocity are stripped off. Even such a simple criterion is difficult to employ operationally, however, as a fast, multiply charged, heavy projectile depositing a reasonable fraction of its energy in a target would be expected to gain several electrons stepwise as it slows down. However, if some *average* degree of ionization could be established for projectiles, then an *effective* projectile charge for the stopping process could be defined, and the traditional stopping theory of Bethe (3, 4) could be maintained. As the idea of effective charge and subsequent retention of the Bethe theory of stopping is appealing, many effective charge theories have been developed (9, 10), both for gaseous and solid targets. Perhaps the most utilized scheme is that of Brandt and Kitagawa (14), which is also based on the Thomas-Fermi atomic model. It is, however, only one of many (15).

A statistical treatment of stopping and straggling which includes the possibility of charge changing events and is capable of dealing with any number of projectile states has been proposed by Sigmund (13), and has been implemented by Närmann (20, 21). Again, the theory needs transfer rates (capture and loss cross sections) as input, but given reasonable values, which must be taken from either experiment or other theory, it performs well.

Another approach is to consider only projectiles at velocities such that they remain completely stripped. This effectively restricts the investigation to protons, if energies as low as a few hundred keV/amu are to be considered. Over the past several years, we have been interested in molecular targets, and have taken this approach. In particular, we have collaborated with Geerd Diercksen (22, 23) using the MUNICH (24) system of programs to calculate dipole oscillator strength distributions, and thus mean excitation energies *via* a discrete version of Eq. (4). It is desirable, however, to calculate energy deposition directly, avoiding, as much as possible, assumptions which limit the physics. In this case, one would obtain the stopping by calculating the energy transfer ($T(b)$) directly for a series of trajectories at various impact parameters, and integrating

$$\frac{dE}{dx} = 2\pi n Z_2 \int_0^\infty b\ T(b)\ db \tag{5}$$

To accomplish this, one would like a theory which avoids both reliance on outside data, theoretical or experimental, and disparate approximations in different projectile velocity regimes. Neither the above methods nor any of the numerous other methods not mentioned offer this possibility. What is needed is a time dependent dynamical method that considers the dynamics of all the nuclei and electrons, both projectile and target, in the system, and allows for unrestricted charge and energy transfer between them. Within the binary encounter approximation, this means that the projectile is allowed to encounter target atoms or molecules serially, changing velocity and charge state at each collision. A method which accomplishes this is Electron Nuclear Dynamics, or END method of Deumens and Öhrn (25, 26), which is reviewed briefly in the next section. In Section 3, we discuss results for some particular trajectories with implications for stopping and charge exchange in the prototype system of alpha particles on neon gas.

2. Theory

2.1. General Considerations

In this development, we compute the coupled dynamics of the nuclei and electrons involved in each collision using the END formalism, which employs the time-dependent variational principle (TDVP) (27) to determine a set of dynamical equations that approximate the time-dependent Schrödinger equation for the simultaneous dynamics of electrons and atomic nuclei.

The END approach differs in general outlook and technical details from those that employ potential energy surfaces. Such approaches use the traditional notion that the difference of the mass of even the lightest nucleus and that of an electron is so great that the electron dynamics effectively takes place in the field of fixed nuclei. This introduces the theoretical concepts of an electronic Hamiltonian, stationary electronic states, and associated potential energy surfaces to be determined for discrete nuclear arrangements. Interpolation schemes are necessary for their determination at intermediate geometries. Except for possibly thermal processes, reactive collisions do not take place on a single potential energy surface. Several surfaces and associated nonadiabatic coupling terms are needed to provide an adequate description. The evolving physical state of a reactive process can be expressed in terms of stationary electronic states, but then these states play the role of a basis. Since the determination of stationary electronic states, their potential surfaces, and relevant coupling terms is difficult and costly, one may ask whether there is a more direct way and a simpler basis that would work just as well or better.

The END theory answers this question by treating the simultaneous dynamics of electrons and nuclei and thereby avoiding the use of potential energy surfaces and stationary electronic states. The END formalism, even in its sim-

plest approximation, offers a general dynamical approach in the sense that it can, in principle, treat any number and rearrangement of nuclei and electrons (for bound states or scattering problems).

Finally, END uses a laboratory frame of Cartesian coordinates, thus avoiding transformations to internal coordinates. This provides great simplifications and generality and is possible since the formalism guarantees strict adherence to fundamental conservation laws (28). For instance, the conservation of total momentum makes it possible to eliminate the overall translational motion at any time point in the evolution. It should also be noted that there is no restriction in principle on the complexity of either the target or the projectile, and that all accessible product channels, including breakup of cluster or molecular projectiles and targets, can be reached.

The evolving state obtained from integration of the END equations is projected on a suitable final state at a time where product species are well separated. This permits direct calculation of transition probabilities. A distribution of initial conditions must be chosen sufficient to make possible the integration over impact parameters and orientation angles to obtain relevant cross sections (26).

In order to make the END formalism practical, some approximations must be made in the representation of the wavefunctions of the electrons and nuclei. The particulars are outlined in the next section. In the simple model employed in this work, we choose to represent the electronic wavefunction by a group theoretical coherent states parametrization of a single determinant (SD). The nuclear wave function is formulated in terms of a frozen Gaussian wave packet (FGWP) and the limit of a narrow width is taken. This latter approximation corresponds to the classical limit for describing the nuclei. The coherent state representation of a single determinant leads to the so-called Thouless parametrization (29). For the description of the nuclear wavefunction, a quantum description has also been worked out (26, 30), but is yet to be implemented.

2.2. Summary of Formalism

The most important component of the scheme presented in this paper is the END formalism, as it is this that describes the interactions during individual collisions. As the full details of the method, including detailed derivation and interpretation of the END equations, have been published elsewhere (25, 26, 28, 31), we only summarize the salient points here.

The simplest level of the END approach employs a single spin unrestricted determinant

$$|z\rangle = det\{\chi_i(x_j)\} \tag{6}$$

for the electrons and treats the nuclei as classical particles. The determinantal wavefunction is built from so called dynamical spin orbitals

$$\chi_i = \phi_i + \sum_{j=N+1}^{K} \phi_j z_{ji}, \quad i = 1, 2, \cdots, N \tag{7}$$

which are expressed in terms of a basis of atomic spin orbitals $\{\phi_i\}$ of rank K centered on the participating atomic nuclei. The particular form of parametrization of $|z\rangle$ with complex coefficients z_{ji} is due to Thouless (29) and is example of a so called generalized coherent state (32). These coefficients are assumed to be functions of the time parameter t, as are the nuclear position coordinates $\vec{R}_k$ and momenta $\vec{P}_k$.

As is well-known, the time-dependent variational principle (TDVP) applied to the quantum mechanical action, when fully general variations in state vector space are possible, yields the time-dependent Schrödinger equation. However, when the variations take place in a limited space determined by the choice of an approximate form of wavefunction the result is a set of coupled first-order differential equations that govern the time-evolution of the wavefunction parameters (27).

This formulation of the problem treats simultaneously the dynamics of electrons and nuclei with all the nonadiabatic coupling terms and without the use of the stationary electronic states and the associated potential energy curves. It has been applied with considerable success to ion-atom and ion-molecule collisions involving light elements (25, 26, 28, 31).

Application of the TDVP then yields the dynamical equations in matrix form as

$$\begin{pmatrix} iC & 0 & iC_R & 0 \\ 0 & -iC^* & -iC_R^* & 0 \\ iC_R^\dagger & -iC_R^T & C_{RR} & -I \\ 0 & 0 & I & 0 \end{pmatrix} \begin{pmatrix} \dot{z} \\ \dot{z}^* \\ \dot{R} \\ \dot{P} \end{pmatrix} = \begin{pmatrix} \partial E/\partial z^* \\ \partial E/\partial z \\ \partial E/\partial R \\ \partial E/\partial P \end{pmatrix}, \tag{8}$$

where E is the total energy and the dot above a symbol means differentiation with respect to the time parameter. The nonadiabatic coupling terms between the electron and nuclear dynamics are expressed in terms of the elements of the dynamical metric on the left. In particular

$$C = \frac{\partial^2 \ln S(z^*, R, z, R')}{\partial z^* \partial z}\Big|_{R'=R}, \tag{9}$$

$$C_R = \frac{\partial^2 \ln S(z^*, R, z, R')}{\partial z^* \partial R'}\Big|_{R'=R}, \tag{10}$$

and

$$C_{RR} = -2\mathrm{Im}\frac{\partial^2 \ln S(z^*, R, z, R')}{\partial R \partial R'}\Big|_{R'=R} \tag{11}$$

are defined in terms of the overlap of the determinantal states of two different nuclear configurations

$$S(z^*, R, z, R') = \det\{(I^\bullet \quad z^\dagger)\Delta\begin{pmatrix} I^\bullet \\ z \end{pmatrix}\}. \tag{12}$$

Here $I^\bullet$ is the $N \times N$ unit matrix and Δ the metric of the atomic spin orbital basis, which depends on the nuclear coordinates. In somewhat more detail one can write

$$C\dot{z} + \sum_l C_{\vec{R}_l}\dot{\vec{R}}_l = -\frac{i\partial E}{\partial z^*}$$

$$\dot{P}_k + 2\,\mathrm{Im}\, C_{\vec{R}_k}\dot{z} - \sum_l C_{\vec{R}_k \vec{R}_l}\dot{\vec{R}}_l = -\nabla_{\vec{R}_k} E \tag{13}$$

$$\dot{\vec{R}}_l = \frac{\vec{P}_l}{M_l}$$

where M_l is a nuclear mass. The coupling of the electronic dynamical variables z and z^* with the nuclear position coordinates and momenta can be seen clearly, and the purely classical equation of motion for the nuclear positions can be discerned.

2.3. Details of the Calculation

We consider swift (~10 keV) alpha particles impinging on Ne gas (*e.g.* at STP) as our test case. As the average distance between Ne atoms is large (~60 a.u.) compared to the radius of interaction between the projectile and target in such a case, we may employ the binary encounter approximation without problem. This study, then, will consider the dynamics of the interaction of He^{2+} ions incident on Ne.

The calculations are carried out using a "supermolecule" description of the system, that is, a single determinantal wavefunction is used to describe the system as a whole. As the calculation is exploratory, a small basis was employed. For He, a (2s,1p) 6–31G** uncontracted Gaussian basis (33) was used, while for Ne a (7s,4p) → [3s,2p] contracted basis (34) was used. The basis functions are centered on the moving nuclei, and electron translation factors are not employed. The nuclei are described by Gaussian wavepackets in the narrow width limit, corresponding to classical nuclei, but retaining non-Born-Oppenheimer coupling between electrons and nuclei.

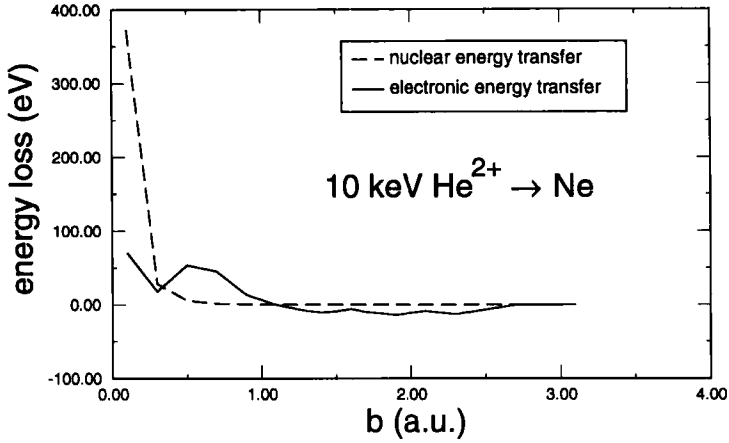

Figure 1: Nuclear and electronic energy loss of 10 keV He^{2+} as a function of impact parameter

3. Results

In a previous publication (35), we considered the energetics of the collision of 10 keV He^{q+} on Ne, and determined that the highest probability charge state was q=2+ (P=0.74). Here, we consider He^{2+}/Ne collision in somewhat more detail.

In Fig. 1, the total energy loss and the portions deposited into nuclear and electronic modes is presented. Not unexpectedly, collisions at small impact parameter ($b < 0.1$) are dominated by nuclear stopping; kinetic energy transferred to the Ne nucleus. At larger impact parameters, the nuclear stopping goes rapidly to zero, and the energy is transferred primarily to the Ne electrons. As the ionization cross section is very small under these conditions, the energy is mostly used in excitation of the electrons. Looking at the energy transfer at a particular impact parameter, *e.g.* $b = 0.7$ a.u. (Fig. 2), it is clear that, again, nuclear stopping is important only at the lowest projectile energies, while the bulk of the energy transfer over the whole energy range is due to electronic excitation. The structure in the electronic energy transfer should also be noted. There is some structure at low energy suggesting a resonance. At ~35 keV there is a region where essentially no energy transfer takes place. This is understood in terms of lack of the proper orbital and energy overlap between projectile and target in this region.

Figs. 3 and 4 display the scattering angles for the projectile and target atoms as a function of impact parameter at 10 keV. As expected, the projectile scattering angle is large only for small impact parameters. Thus, for a He^{2+} particle beam in gaseous Ne at STP, the average scattering angle will be very small. Even though there will be occasional events with large scattering angle,

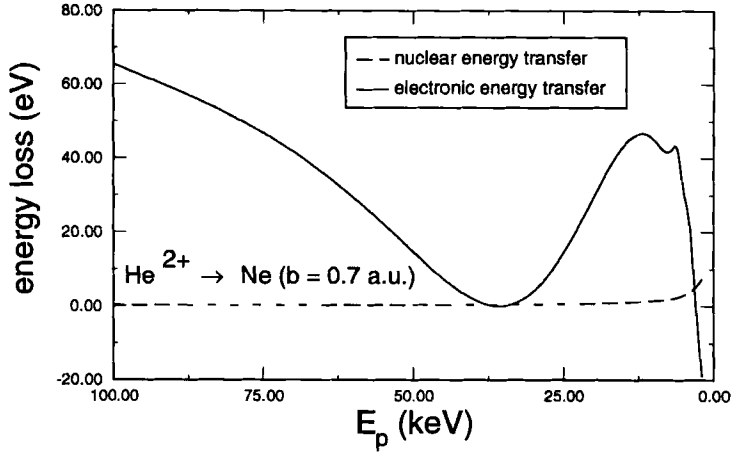

Figure 2: Nuclear and electronic energy loss of He^{2+} at b = 0.7 a.u. as a function of projectile energy

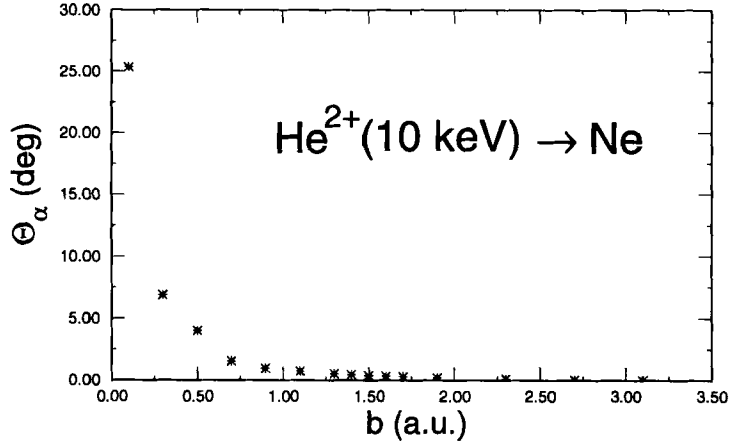

Figure 3: Scattering angle for 10 keV He^{2+} → Ne as a function of impact parameter: He^{2+}

the approximation of straight line trajectories can be used without problem. In the classical case and for a straight line trajectory, there can be no longitudinal (in the direction of the incoming projectile trajectory) momentum transferred to the target as the impulse from the approaching and exiting projectile are equal and opposite. This is also nearly the case here, with recoil angles being only a few degrees from the expected classical value of 90°. Although the recoil is forward for small impact parameters and backward for larger ones, the recoil energy is exceedingly small (see Fig. 1), making a simple explanation of the

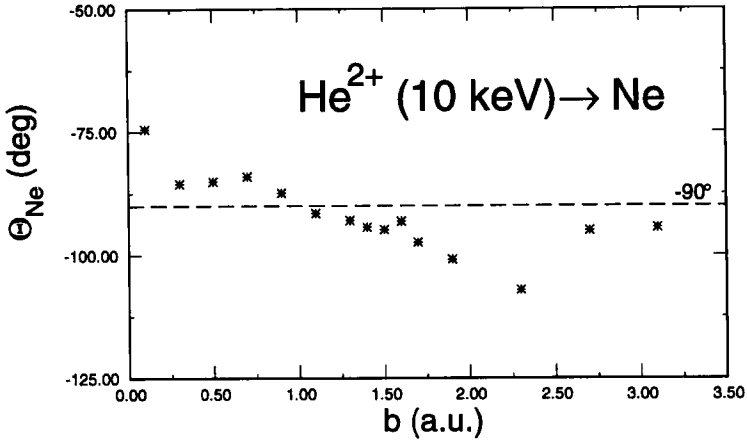

Figure 4: Scattering angle for 10 keV He^{2+} → Ne as a function of impact parameter: Ne

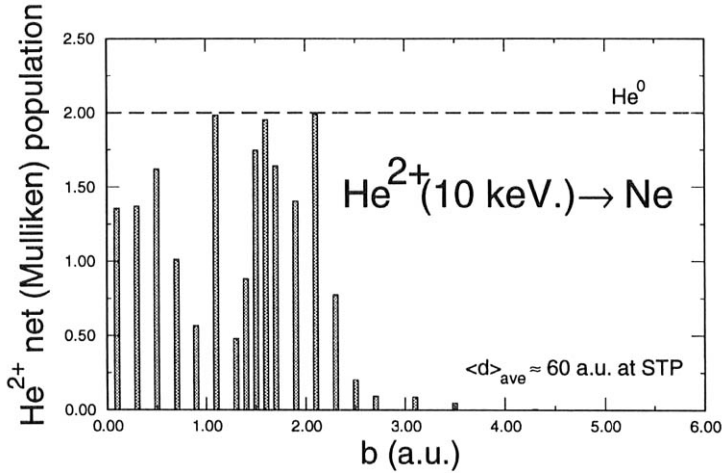

Figure 5: Final net Mulliken population of 10 keV He^{2+} projectile after collision with Ne, as a function of impact parameter

nonlinear, quantum mechanical interaction difficult. In general terms, the recoil angle will depend on two factors: 1) the details of charge exchange, leading to coulomb repulsion, and 2) the charge induced dipole interaction while the alpha particle is fully stripped. That the problem is complicated can be seen from the net Mulliken population of the projectile as a function of impact parameter (Fig. 5). It is only at low impact parameter that the projectile picks up electrons, leaving a charged target nucleus.

4. Summary

The Electron Nuclear Dynamics scheme utilized here starts from the time dependent Schrödinger equation rather than the Born series. Thus it allows the description of energy loss by a swift particle in a material target completely, including all Born terms as well as charge changing. It is noted that both projectile energy and impact parameter are important parameters for description of the energy deposition. However, for most cases, charge and energy exchange takes place only for small impact parameter collisions. Similarly, deviations of the projectile from a straight line trajectory occur only at small impact parameter, and thus with small probability.

Stopping powers will be obtained as a function of projectile velocity *via* Eq. 5.

Acknowledgments

It has been a great pleasure to work together with Geerd Diercksen over the years, and his friendship and lively discussions are gratefully acknowledged. The author is grateful to Mauricio Netto-Coutinho and Dr. Erik Deumens for helpful discussions. The work was supported in part by a grant from the Army Research Office (DAA H04-95–1–0326).

References

(1) N. Bohr, Philos. Mag. **25**, 10 (1913).

(2) N. Bohr, Philos. Mag. **30**, 581 (1915).

(3) H. Bethe, Ann. Phys. (Leipzig) **5**, 325 (1930).

(4) H. Bethe, Z. Physik **76**, 293 (1932).

(5) J. Lindhard, Nucl. Instrum. and Meth. **132**, 1 (1976).

(6) J. R. Sabin and J. Oddershede, Nucl. Instrum. and Meth. **B64**, 678 (1992).

(7) N. Bohr, Phys. Rev. **58**, 654 (1940).

(8) N. Bohr, Phys. Rev. **59**, 270 (1941).

(9) H.-D. Betz, Rev. Mod. Phys. **44**, 465 (1972).

(10) See refs. 11, 12 and 13 for short but more current reviews and references to the previous literature on the subject.

(11) J. F. Ziegler, J. P. Biersack, and U. Littmark, *The Stopping and Range of Ions in Solids*, volume 1 of *The Stopping and Ranges of Ions in Matter*, Pergamon, 1985.

(12) P. M. Echenique, F. Flores, and R. H. Ritchie, Solid State Phys. **43**, 229 (1990).

(13) P. Sigmund, Nucl. Instrum. and Meth. **B69**, 113 (1992).

(14) W. Brandt and M. Kitagawa, Phys. Rev. B **25**, 5631 (1982).

(15) *Cf. e.g.* refs. 16 - 19.

(16) V. S. Nikolaev and I. S. Dmitriev, Phys. Lett. **28a**, 277 (1968).

(17) K. Shima, T. Ishihara, and T. Mikumo, Nucl. Instrum. and Meth. **200**, 605 (1982).

(18) P. M. Echenique, R. M. Nieminen, J. C. Ashley, and R. H. Ritchie, Phys. Rev. A **33**, 897 (1986).

(19) Q. Yang, Phys. Rev. A **49**, 1089 (1994).

(20) A. Närmann and P. Sigmund, Phys. Rev. A **49**, 4709 (1994).

(21) A. Närmann, Phys. Rev. A **51**, 548 (1994).

(22) J. R. Sabin, J. Oddershede, and G. H. F. Diercksen, Phys. Rev. A **42**, 1302 (1990).

(23) G. H. F. Diercksen, J. Oddershede, I. Paidarova, and J. R. Sabin, Int. J. Quantum Chem. **39**, 755 (1991).

(24) G. H. F. Diercksen and W. P. Kraemer, MUNICH reference manual, Technical report, Max-Planck-Institute for Astrophysics, Munich, Germany, 1981.

(25) Y. Öhrn et al., Time-evolution of electrons and nuclei in molecular systems, in *Time Dependent Molecular Dynamics*, edited by J. Broeckhove and L. Lathouwers, page 272, Plenum, New York, 1992.

(26) E. Deumens, A. C. Diz, H. Taylor, and Y. Öhrn, J. Chem. Phys. **96**, 6820 (1992).

(27) P. Kramer and M. Saraceno, *Geometry of the Time-Dependent Variational Principle in Quantum Mechanics*, Springer Verlag, New York, 1981.

(28) E. Deumens, A. C. Diz, R. Longo, and Y. Öhrn, Rev. Mod. Phys. **66**, 917 (1994).

(29) D. J. Thouless, Nucl. Phys. **21**, 225 (1960).

(30) A. Diz, E. Deumens, and Y. Öhrn, Chem. Phys. Lett. **166**, 203 (1990).

(31) A. C. Diz, *Electron Nuclear Dynamics: A Theoretical Treatment Using Coherent States and the Time-Dependent Variational Principle*, PhD thesis, University of Florida, Gainesville, Florida, 1992.

(32) J. R. Klauder and B.-S. Skagerstam, *Coherent States, Applications in Physics and Mathematical Physics*, World Scientific, Singapore, 1985.

(33) M. J. Frisch et al., *Gaussian 88*, Gaussian Inc., PA, 1988.

(34) A. Schäfer, H. Horn, and R. Alrichs, J. Chem. Phys. **97**, 2571 (1992).

(35) A. C. Diz, Y. Öhrn, and J. R. Sabin, Nucl. Instrum. and Meth. **B96**, 633 (1995).

Theoretical Modeling of Spectra and Collisional Processes of Weakly Interacting Complexes

Robert Moszynski[1], Tino G.A. Heijmen[2], Paul E.S. Wormer[3], and Ad van der Avoird[4]

Department of Chemistry, University of Warsaw
ul. Pasteura 1, 02-093 Warsaw, Poland
and
Institute of Theoretical Chemistry, NSR Center,
University of Nijmegen, Toernooiveld,
6525 ED, Nijmegen, The Netherlands

Abstract

The present status of symmetry-adapted perturbation theory applied to intermolecular potentials and interaction-induced properties is presented, and illustrated by means of applications to the calculations of the collision-induced Raman spectra, rovibrational spectra of weakly bound dimers, and second (pressure and dielectric) virial coefficients.

[1] rmoszyns@chem.uw.edu.pl, [2] tino@theochem.kun.nl, [3] pwormer@theochem.kun.nl, [4] avda@theochem.kun.nl

ADVANCES IN QUANTUM CHEMISTRY, VOLUME 28

0065-3276/97 $25.00

1. Introduction

Over the last decades, there has been an increasing interest in theoretical (1, 2) and experimental (3) studies of weakly interacting complexes, the so-called van der Waals molecules. One of the reasons for this interest is that the spectra of these complexes depend very sensitively on the intermolecular potentials and other properties, such as interaction-induced dipole moments and polarizabilities, the knowledge of which is crucial for understanding the behavior of molecular bulk species.

Weakly bound complexes display unusual structural and dynamical properties resulting from the shape of their intermolecular potential energy surfaces. They show large amplitude internal motions, and do not conform to the dynamics and selection rules based on the harmonic oscillator/rigid rotor models (4). Consequently, conventional models used in the analysis of the spectroscopic data fail, and the knowledge of the full intermolecular potential and dipole/polarizability surfaces is essential to determine the assignments of the observed transitions.

The interaction-induced dipole moments and polarizabilities are also responsible for a wide range of dielectric, refractive, and optical properties of gases and fluids (5, 6). In pioneering studies Crawford *et al.* (7) and Chisholm and Welsh (8) have shown that during a collision of a helium atom with a hydrogen molecule the complex becomes temporarily infrared-active because of its relative translational motions, so that absorption and emission bands can be observed. Later, Levine and Birnbaum (9) predicted that all Raman spectra of gases should have a component caused by collision-induced changes in the polarizabilities, and it was first demonstrated by McTague and Birnbaum (10, 11) that colliding argon atoms undergo transitions between translational states when interacting with photons.

Despite the growing body of experimental work on bound state and collision-induced absorption and light scattering in weakly interacting complexes, not many full *ab initio* studies have been reported thus far. This is due, in part, to the enormous difficulty of obtaining an accurate *ab initio* description of the van der Waals bonding.

Recently, a new theoretical method of calculating potential energy and dipole/polarizability surfaces for van der Waals molecules based on symmetry-adapted perturbation theory (SAPT) of intermolecular forces (12)–(15) has been developed (16)–(24). In this method, referred to as many-body symmetry-adapted perturbation theory, all physically important contributions to the potential and the interaction-induced properties, such as *electrostatics, exchange, induction*, and *dispersion* are identified and computed separately. By making a perturbation expansion in the intermolecular interaction as well as in the intramolecular electronic correlation, it is possible to sum the correlation contributions to the different physical

effects only as far as necessary. The SAPT approach does not use the multipole expansion (24)–(29), so all charge penetration (damping) effects are automatically included. Since these various contributions show a different dependence on the intermolecular distance R, they can be fitted separately, with physically interpretable parameters.

In the present paper we review recent advances in the symmetry-adapted perturbation theory calculations of interaction potentials and interaction-induced properties. We will give a brief description of the theoretical methods needed on the route from the intermolecular potential and properties to rovibrational spectra and collision-induced Raman spectra. We also discuss applications of the interaction potentials and interaction-induced polarizabilities to compute (thermodynamic and dielectric) second virial coefficients. Finally, we illustrate these theoretical approaches on several examples from our own work.

2. Ab Initio Potential Energy Surfaces

The concept of an intermolecular potential appears in the Born-Oppenheimer approximation. The energy of interaction between molecules A and B is defined as,

$$E_{int} = E_{AB} - (E_A + E_B), \tag{1}$$

where E_A, E_B, and E_{AB} are the exact ground-state energies of the monomers A and B, and of the dimer AB, and it is assumed that the internal coordinates of the monomers used in the calculations of E_A and E_B are the same as within the dimer AB.

Modern *ab initio* techniques used to calculate the interaction energy can be classified as *supermolecular* and *perturbational*. In a *supermolecule* approach the exact energies in Eq. (1) are replaced by approximations $\tilde{E}_{AB}$, $\tilde{E}_A$, and $\tilde{E}_B$ obtained from any of the available methods of solving the clamped-nuclei Schrödinger equation. The main drawback of this approach is that it does not permit an analysis of the interaction energy in terms of distinct, physically meaningful components, and it is not *a priori* obvious which contributions are neglected and which are included in a given supermolecular approach.

By contrast, the symmetry-adapted perturbation theory (1) defines the interaction energy directly, as the sum of polarization and exchange contributions,

$$E_{int} = E_{pol}^{(1)} + E_{exch}^{(1)} + E_{pol}^{(2)} + E_{exch}^{(2)} + \cdots , \tag{2}$$

where $E_{pol}^{(1)}$ is the classical electrostatic (Coulomb) energy calculated with full account of the penetration (overlap) of the charge distributions of the

monomers, $E_{pol}^{(2)}$ is the sum of the nonexpanded classical induction and quantum-mechanical dispersion energies,

$$E_{pol}^{(2)} = E_{ind}^{(2)} + E_{disp}^{(2)}, \tag{3}$$

and $E_{exch}^{(n)}$, n=1,2, are the exchange components, which can be physically interpreted as an effect of the resonance tunneling of electrons between the interacting systems. The second-order exchange energy is also split into an induction and a dispersion part,

$$E_{exch}^{(2)} = E_{exch-ind}^{(2)} + E_{exch-disp}^{(2)}. \tag{4}$$

The exchange-induction energy $E_{exch-ind}^{(2)}$ and the exchange-dispersion energy $E_{exch-disp}^{(2)}$ can be viewed as a result of the coupling of the electron exchange with the induction and dispersion interactions.

Since the symmetry-adapted perturbation theory provides the basis for the understanding of weak intermolecular interactions, it is useful to discuss the convergence properties of the SAPT expansion. High-order calculations performed for model one-electron (H_2^+) (30), two-electron (H_2) (14, 15), and four-electron (He_2 and He–H_2) (31) systems show that the SAPT series converges rapidly. In fact, already the second-order calculation reproduces the exact variational interaction energies with errors smaller than 4%. Several recent applications strongly indicate that this optimistic result holds for larger systems as well.

In practical applications of the SAPT approach to interactions of many-electron systems, one has to use the many-body version of SAPT, which includes order-by-order the intramonomer correlation effects. The many-body SAPT is based on the partitioning of the total Hamiltonian as $H = F+V+W$, where the zeroth-order operator $F = F_A + F_B$ is the sum of the Fock operators for the monomers A and B. The intermolecular interaction operator $V = H - H_A - H_B$ is the difference between the Hamiltonians of interacting and noninteracting systems, and the intramonomer correlation operator $W = W_A + W_B$ is the sum of the Møller-Plesset fluctuation potentials of the monomers: $W_X = H_X - F_X$, $X = A$ or B. The interaction operator V is taken in the non-expanded form, *i.e.*, it is not approximated by the multipole expansion. The interaction energy components of Eq. (1) are now given in the form of a double perturbation series,

$$E_{pol}^{(n)} = \sum_{l=0}^{\infty} E_{pol}^{(nl)} \qquad \text{and} \qquad E_{exch}^{(n)} = \sum_{l=0}^{\infty} E_{exch}^{(nl)}, \tag{5}$$

where the superscripts n and l denote the orders of perturbation in V and in W, respectively.

In practice, one has to truncate the expansions (5). Recent studies of the convergence of the many-body perturbation expansions of the electrostatic (18), exchange (19, 20), induction (21), and dispersion (22) energies led to the development of approximation schemes which can be used to compute these components with controlled accuracy. See Refs. (1, 23) for a detailed discussion of this point.

3. Ab Initio Interaction-Induced Properties

The interaction-induced dipole moment of a pair of molecules A and B is defined as the difference between the dipole moment of the complex AB and the sum of dipole moments of the noninteracting molecules A and B,

$$\Delta\mu_i = \mu_i^{AB} - (\mu_i^A + \mu_i^B), \tag{6}$$

where μ_i^{AB} is a Cartesian component of the dipole moment of the dimer AB, and μ_i^A and μ_i^B denote components of the dipole moments of the isolated molecules A and B. A similar definition holds for the interaction-induced polarizability of a pair of molecules A and B, *i.e.*,

$$\Delta\alpha_{ij} = \alpha_{ij}^{AB} - (\alpha_{ij}^A + \alpha_{ij}^B), \tag{7}$$

where α_{ij}^{AB} is a Cartesian component of the dimer polarizability tensor, and α_{ij}^A and α_{ij}^B denote components of the polarizability tensors of the isolated monomers A and B. By the use of the Hellmann-Feynman theorem Eqs. (6) and (7) can be conveniently rewritten as,

$$\Delta\mu_i = -\left(\frac{\partial E_{int}}{\partial F_i}\right)_{\boldsymbol{F}=\boldsymbol{0}}, \qquad \Delta\alpha_{ij} = -\left(\frac{\partial^2 E_{int}}{\partial F_i \partial F_j}\right)_{\boldsymbol{F}=\boldsymbol{0}}, \tag{8}$$

where E_{int} is the interaction energy for the dimer in the presence of a static, uniform electric field $\boldsymbol{F}$.

Equations (2) and (8) define the SAPT expansions of the interaction-induced dipole moment and polarizability,

$$\Delta\mu_i = \Delta\mu_{i,pol}^{(1)} + \Delta\mu_{i,exch}^{(1)} + \Delta\mu_{i,pol}^{(2)} + \Delta\mu_{i,exch}^{(2)} + \cdots, \tag{9}$$

$$\Delta\alpha_{ij} = \Delta\alpha_{ij,pol}^{(1)} + \Delta\alpha_{ij,exch}^{(1)} + \Delta\alpha_{ij,pol}^{(2)} + \Delta\alpha_{ij,exch}^{(2)} + \cdots, \tag{10}$$

where the superscripts again indicate the order in the intermolecular interaction V. Obviously an nth-order contribution to $\Delta\mu_i$ or $\Delta\alpha_{ij}$ is obtained by differentiating once or twice the corresponding energy contribution $E_{pol}^{(n)}$ or $E_{exch}^{(n)}$, calculated when the system is placed in a (small) external electric field $\boldsymbol{F}$.

As discussed in Ref. (24), Eq. (9) relates the interaction-induced part of the dipole moment of the complex AB to the distortion of the electron density associated with the electrostatic, exchange, induction, and dispersion interactions of the monomers in the external field. For instance, the first-order multipole-expanded polarization contribution $E_{pol}^{(1)}$ is due to the interactions of permanent multipole moments on A with moments induced on B by the external field $\boldsymbol{F}$, and vice versa. The terms linear in $\boldsymbol{F}$ give $\Delta\mu_{i,pol}^{(1)}$. The mechanism that yields the second-order induction dipole $\Delta\mu_{i,ind}^{(2)}$ is more complicated, and one can distinguish two principal categories. The first mechanism is the interaction of a permanent multipole on monomer A with a multipole on B induced by the nonlinear (second-order) effect of both a permanent multipole on A and the external field $\boldsymbol{F}$ (plus a contribution obtained by interchanging the roles of the monomers A and B). The second mechanism is the interaction of a multipole moment on A, induced by a permanent multipole on B, with a moment on B induced by the field $\boldsymbol{F}$, and vice versa. Again, the energy terms linear in $\boldsymbol{F}$ give the corresponding induced dipoles. Finally, the dispersion term $\Delta\mu_{i,disp}^{(2)}$ represents the intermonomer correlation contribution to the dipole moment of the dimer AB. The physical components to the interaction-induced polarizability can be classified analogously.

In practical applications of the SAPT approach to interaction-induced properties one has to use the many-body perturbation expansions discussed in the previous section. Thus, the physical contributions to $\Delta\mu_i$ or $\Delta\alpha_{ij}$ can be obtained by differentiating Eq. (5) once or twice.

Table 1
Comparison of the interaction-induced trace and anisotropy of the He_2 polarizability computed by SAPT with the FCI results (in 10^{-3} a.u.).

	$R = 3$ bohr		$R = 4$ bohr		$R = 5$ bohr		$R = 8$ bohr
	$\alpha(R)$	$\gamma(R)$	$\alpha(R)$	$\gamma(R)$	$\alpha(R)$	$\gamma(R)$	$\gamma(R)$
SAPT	−130.034	175.693	−34.037	110.519	−5.439	78.365	22.368
FCI	−133.327	171.826	−34.262	111.912	−5.343	79.766	22.738

Recently, the convergence of the many-body SAPT expansion for the interaction-induced dipole moment of He–H_2 (24) and the polarizability of He_2 (24, 32). has been checked by comparison with FCI results in the same basis set. The numerical results for the helium dimer are summarized in Table 1 where we consider the anisotropy γ and the trace α: $\gamma = \Delta\alpha_{zz} - \Delta\alpha_{xx}$ and $\alpha = (\Delta\alpha_{zz} + 2\Delta\alpha_{xx})/3$, in which the z-axis is the molecular axis. An inspection of Table 1 shows that for all distances considered in Ref. (32) the many-body SAPT expansion reproduces the FCI results to

within 3%. Similar results for the interaction-induced dipole moment of He–H_2 have been reported in Ref. (24). Hence, the convergence of the many-body SAPT series for the interaction-induced electrical properties appears to be satisfactory, at least for simple four-electron dimers.

4. Applications

A. Collision-Induced Light Scattering in Helium Gas

In collision-induced Raman experiments laser light of wavenumber ω_0 is scattered inelastically by the interacting atoms in the gas. The intensities of the depolarized and polarized scattered light are given by (33, 34),

$$D(\nu) = \frac{2}{15}\omega^3\omega_0 G(\nu), \qquad P(\nu) = \omega^3\omega_0 A(\nu), \tag{11}$$

where ν is the frequency shift, $\omega = \omega_0 - 2\pi\nu/c$, and c is the speed of light. The spectral functions $G(\nu)$ and $A(\nu)$ can be written as,

$$G(\nu) = \frac{2hc\lambda_B^3}{(2I+1)^2}\sum_{J,J'} g_J(2J+1)\int_0^\infty dE e^{-E/k_BT} b_{J'}^J |\langle E', J'|\gamma(R)|E, J\rangle|^2 \tag{12}$$

$$A(\nu) = \frac{2hc\lambda_B^3}{(2I+1)^2}\sum_{J} g_J(2J+1)\int_0^\infty dE e^{-E/k_BT} |\langle E', J|\alpha(R)|E, J\rangle|^2, \tag{13}$$

where $E' - E = h\nu$, $J' = J, J \pm 2$, h is the Planck constant, k_B is the Boltzmann constant, T denotes the temperature, $\lambda_B = (h^2/2\pi\mu k_B T)^{\frac{1}{2}}$ is the de Broglie wavelength, μ is the reduced mass of the collisional complex, and I and g_J designate the nuclear spin and nuclear spin statistical weight, respectively. The constants $b_{J'}^J$ are given by Eqs. (12)–(14) of Ref. (34) and the matrix elements of the trace and anisotropy of the polarizability appearing in Eqs. (12) and (13) are defined as,

$$\langle E', J'|X(R)|E, J\rangle = \int_0^\infty \psi^*_{E'J'}(R) X(R) \psi_{EJ}(R) dR, \tag{14}$$

where the scattering wave functions $\psi_{EJ}(R)$ are solutions of the radial Schrödinger equation describing the relative motion of the atoms in the potential $V(R)$, subject to the energy normalization condition.

The collision-induced light scattering in the helium gas has been subject of many experimental studies (35)–(42). Most of these measurements were done at high densities (35)–(37), so the reported Raman intensities were affected by three-body contributions, and pure pair spectra had to be separated out (37) by applying simplified models. Only the polarized

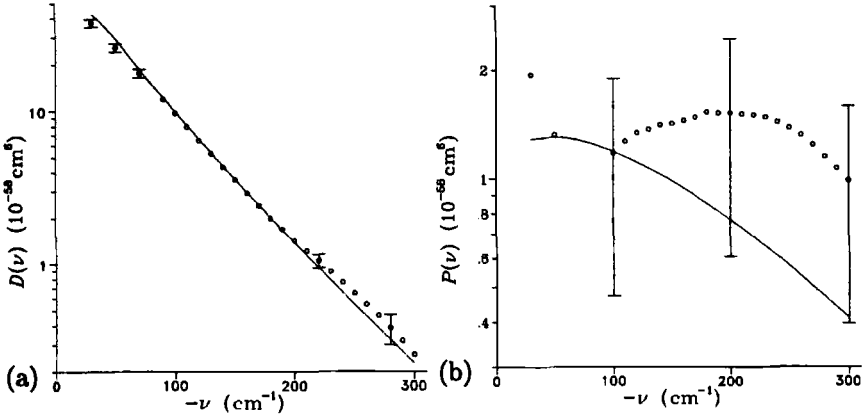

Figure 1
Comparison of the theoretical (solid lines) and experimental (circles and error bars) depolarized spectra (a), and polarized spectra (b), for the ^{4}He diatom.

and depolarized Raman spectra reported by Proffitt, Keto, and Frommhold (41, 42) were shown to be free from three-body contributions.

These experimental advances stimulated associated theoretical developments. In an extensive theoretical study Dacre and Frommhold (43) have checked the accuracy of the *ab initio* CISD (CISD stands for the Configuration Interaction method restricted to single and double substitutions) trace and anisotropy polarizabilities of He_2 (44) by exposing them to the test of computing the observed Raman intensities. While the depolarized spectra computed from Dacre's polarizability (44) showed good agreement with the experiment, the theoretical polarized spectrum was much less intense than the spectrum derived from the experiment (43).

The reasons for the less satisfactory agreement between the theoretical and experimental polarized Raman spectra may be both on the theoretical and on the experimental sides. The experimental polarized spectrum is obtained as the difference of two nearly equal signals excited with different beam polarizations (41, 42), and the accuracy of the polarized intensities deduced from the experiment is rather poor. On the other hand, the theoretical values of the interaction-induced trace may suffer from the size-inconsistency of the CISD method or from the basis set superposition error.

Recently, the SAPT approach has been applied (32) to compute the interaction-induced polarizability for the helium diatom. The computed polarizability invariants have been analytically fitted, and used in quantum-dynamical calculations of the binary collision-induced Raman spectra. The results of the dynamical calculations are summarized in Fig. 1.

An inspection of Fig. 1 shows that the agreement of the theoretical and

measured (42) depolarized Raman intensities is satisfactory. Most of the intensities agree within 3% or better. Only at very low and high frequency shifts this good agreement deteriorates somewhat. Still, the predicted intensities at high frequencies are within the experimental error bars. At very low frequencies the theoretical results are outside the experimental error bars, but these discrepancies are consistent with the estimated (combined) error of the SAPT and dynamical calculations.

The theoretical polarized Raman intensities agree with the experiment within the large ($\pm 50\% - 60\%$) experimental error bars over a wide range of the frequency shifts. Except for the low frequency region, the predicted polarized spectrum is much less intense. It is worth noting that our results for the depolarized and polarized Raman intensities are in good agreement with those generated from the CISD polarizability invariants (43). Both these observations suggest that the theoretical results are rather well converged, and that the error in the *ab initio* polarized intensities is considerably smaller than the experimental error of 50 to 60%. Hence, the improvement of the agreement between theory and experiment for these intensities should mainly come from the experimental side.

B. Second Dielectric Virial Coefficient of Helium Gas

It is well known that for atomic gases at low densities the Clausius-Mossotti function can be related to the atomic polarizability via the relation:

$$\frac{\epsilon - 1}{\epsilon + 2} = \frac{4\pi\alpha_0}{3}\rho, \tag{15}$$

where ϵ is the dielectric constant, α_0 is the atomic polarizability, and ρ denotes the gas number density. At higher pressures deviations from this relation are observed, and they can be attributed to intermolecular interactions. Buckingham and Pople (45) have shown that the leading correction to Eq. (15), quadratic in the gas density, is given by $B_\epsilon(T)\rho^2$, where the second dielectric virial coefficient $B_\epsilon(T)$ is related to the interatomic potential and interaction-induced polarizability trace by,

$$B_\epsilon(T) = \frac{2\pi}{3}\int_0^\infty \alpha(R)\exp(-V(R)/k_BT)R^2dR. \tag{16}$$

At very low temperatures Eq. (16) is no longer valid, and one has to use the exact quantum-statistical expression. The quantum equivalent of Eq. (16) has been recently developed in Ref. (46). Its derivation starts with the general relation between the second dielectric virial coefficient and the ordinary (pressure) second virial coefficient of an atomic gas in a uniform

electric field (46),

$$B_\epsilon(T) = -\frac{4\pi k_B T}{3}\left(\frac{\partial^2 B_2(T;F)}{\partial F^2}\right)_{F=0}, \tag{17}$$

where $B_2(T;F)$ denotes the ordinary (pressure) second virial coefficient for the gas in the electric field F. Using Eq. (17) and an expression for $B_2(T;F)$ in terms of the field-dependent Slater sum (47), one finds the following formula for $B_\epsilon(T)$,

$$\begin{aligned} B_\epsilon(T) &= \frac{2\pi\lambda_B^3}{3}\sum_{J=0}^{\infty}(2J+1)\left[1+\frac{(-1)^{J+2I}}{2I+1}\right] \\ &\times\Bigg[\sum_{n} e^{-E_{nJ}/k_BT}\langle n,J|\alpha(R)|n,J\rangle \\ &+\frac{2}{\pi}\int_0^\infty e^{-\hbar^2k^2/2\mu k_BT}\langle E,J|\alpha(R)|E,J\rangle dk\Bigg], \end{aligned} \tag{18}$$

where

$$\langle n,J|\alpha(R)|n,J\rangle \equiv \int_0^\infty \psi^*_{nJ}(R)\alpha(R)\psi_{nJ}(R)dR, \tag{19}$$

$|n,J\rangle = \psi_{nJ}(R)$ denote the bound-state eigenfunctions of the Schrödinger equation for the relative motion in the potential $V(R)$, with eigenvalues E_{nJ}, and $|E,J\rangle$ are the scattering states with energies $E = \hbar^2k^2/2\mu$ defined above.

Equation (17) can also be used to derive the semiclassical expansion of the second dielectric virial coefficient. Indeed, one may hope that at intermediate temperatures an expansion of $B_\epsilon(T)$ as a power series in $\hbar^2$ will give sufficiently accurate results, making full quantum-statistical calculations unnecessary. Thus, one can approximate $B_\epsilon(T)$ as,

$$B_\epsilon(T) = B_\epsilon^{(0)}(T) + B_\epsilon^{(1)}(T) + B_\epsilon^{(2)}(T), \tag{20}$$

where the classical term $B_\epsilon^{(0)}(T)$ is given by the r.h.s. of Eq. (16), while the quantum corrections of the order $\hbar^2$ and $\hbar^4$ (denoted by $B_\epsilon^{(1)}(T)$ and $B_\epsilon^{(2)}(T)$, respectively), can be written as (32),

$$\begin{aligned} B_\epsilon^{(1)}(T) = -\frac{\pi^2\hbar^2}{9\mu k_B^2T^2}\int_0^\infty &\exp(-V(R)/k_BT) \\ &\times\left[\frac{\alpha(R)}{k_BT}\left(\frac{dV}{dR}\right)^2 - 2\frac{dV}{dR}\frac{d\alpha}{dR}\right]R^2dR, \end{aligned} \tag{21}$$

$$B_\epsilon^{(2)}(T) = \frac{\pi^2\hbar^4}{180\mu^2k_B^3T^3}\int_0^\infty \exp(-V(R)/k_BT)\left[\frac{\alpha(R)}{k_BT}f(R)+g(R)\right]R^2dR, \tag{22}$$

Table 2
Second dielectric virial coefficient of ^{4}He (in cm^{6}mol^{-2}) as function of the temperature (in K).

T	$B_\epsilon^{(0)}(T)$	$B_\epsilon^{(1)}(T)$	$B_\epsilon^{(2)}(T)$	$B_\epsilon(T)^a$	$B_\epsilon(T)^b$
5	−0.0512	0.3040	−2.0226	−1.7699	−0.0081
7	−0.0298	0.1028	−0.4354	−0.3624	−0.0085
10	−0.0209	0.0403	−0.1088	−0.0894	−0.0093
20	−0.0170	0.0100	−0.0121	−0.0191	−0.0121
30	−0.0183	0.0054	−0.0041	−0.0171	−0.0152
40	−0.0203	0.0036	−0.0021	−0.0187	−0.0179
50	−0.0223	0.0028	−0.0012	−0.0208	−0.0204
75	−0.0274	0.0018	−0.0005	−0.0261	−0.0260
100	−0.0320	0.0013	−0.0003	−0.0309	−0.0309
150	−0.0401	0.0009	−0.0001	−0.0393	−0.0393
200	−0.0472	0.0007	−0.0001	−0.0466	−0.0466

[a] Semiclassical approximation through the second-order.
[b] Exact quantum-statistical calculation.

where the functions $f(R)$ and $g(R)$ are given by Eqs. (35)–(36) of Ref. (32).

Recently, a detailed study of the importance of the quantum effects and of the applicability of the semiclassical expansion has been reported (46). This study started from the *ab initio* SAPT trace polarizability (32) and it involved semiclassical and full quantum calculations of the second dielectric virial coefficient for the ^{4}He gas at various temperatures. Illustrative results of these calculations are presented in Table 2.

An inspection of Table 2 shows that the quantum effects are small for temperatures larger than 100 K, and $B_\epsilon(T)$ can be approximated by the classical expression with an error smaller than 2.5%. At lower temperatures the dielectric virial coefficient of ^{4}He starts to deviate from the classical value. Still, for $T \geq 50$ K the quantum effects can be efficiently accounted for by the sum of the first and second quantum corrections. Indeed, for $T = 50$, 75, and 100 K the series $B_\epsilon^{(0)}(T) + B_\epsilon^{(1)}(T) + B_\epsilon^{(2)}(T)$ reproduces the exact results with errors smaller than 2%. Only at temperatures below 50 K the semiclassical expansion of the second dielectric virial coefficient in powers of $\hbar^2$ starts to diverge, and full quantum calculations are needed.

The dielectric properties of helium gas are of great experimental interest, and it is not surprising that since the early 1960's increasingly accurate measurements (48)–(57) are reported in the literature. The comparison of the theoretical and experimental values of the second dielectric virial coefficient can serve as a further check of the accuracy of the *ab initio* trace polarizability. An example of such a comparison is shown on Fig. 2, where

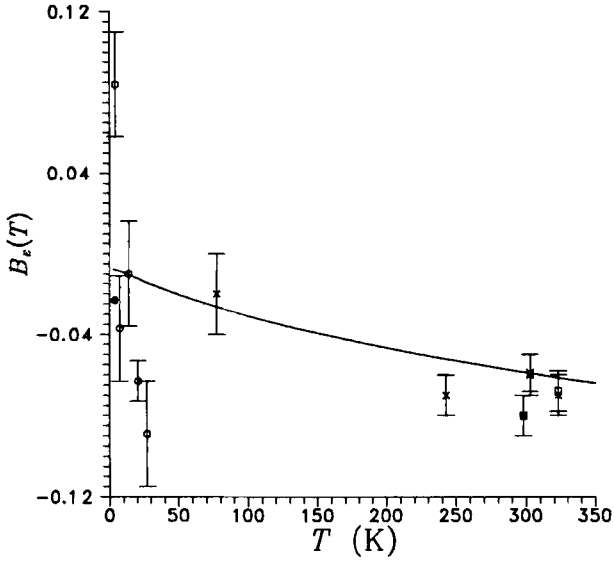

Figure 2
Comparison of the *ab initio* and experimental second dielectric virial coefficients of ^{4}He at various temperatures. The solid line represents the second dielectric virial coefficients generated from the *ab initio* polarizability trace of Ref. (32), and the empirical potential of Ref. (58). Crosses label the indirect measurements from Refs. (51, 55, 56, 57), open circles and squares the measurements from Refs. (54), and (49), respectively, and filled circles and squares represent experimental data from Refs. (50) and (52, 53).

the theoretical and experimental second dielectric virial coefficients for the ^{4}He gas at various temperatures are reported. The *ab initio* data have been generated (46) from the SAPT trace polarizability of He_2 (32).

At high temperatures the *ab initio* results agree well with the data from indirect measurements (51, 55, 56, 57). The only exception is the value at $T = 242.95$ K. Here the theoretical result is slightly outside the experimental error bars. The agreement with the results of direct measurements (49, 50, 52, 53, 54) is less satisfactory. The *ab initio* results agree very well with the old experimental data of Orcutt and Cole (49), and disagree with the data of Vidal and Lallemand (52, 53). Since the theoretical values agree with the majority of the high-temperature experimental data, and since the second dielectric virial coefficient changes very slowly with temperature, it is very likely that the results of direct measurements reported by Vidal and Lallemand (53) are contaminated by nonadditive three-body effects.

At low temperatures the situation is more complex. The *ab initio* result at 77.4 K agrees very well with the value from indirect measurements re-

ported by Huot and Bose (56). Other low temperature data were obtained from direct measurements (54) and show much scatter. At $T = 13.804$ K the *ab initio* value agrees with the measurement, while at $T = 7.198$ K the theoretical result is almost within the experimental error bars. At other temperatures the disagreement is quite substantial, and it is unlikely that the theoretical polarizability trace will change so drastically. Therefore, these data should probably be remeasured.

C. Rovibrational Spectra of Weakly Bound Complexes: He–CO and He–HF

Depending on the strength of the anisotropy in the interaction potential, nuclear motions in weakly bound van der Waals complexes are usually described using a set of coordinates related to a space-fixed or body-fixed frame (2). When the anisotropy of the potential in the region of the van der Waals minimum is relatively weak one can expect that the diatomic molecule in the complex should behave as a nearly free rotor, *i.e.*, that the space-fixed description is appropriate. As a consequence, the energy levels and infrared transitions can be approximately classified by the use of the case *a* coupling of Bratoz and Martin (59) (see Refs. (2, 60) for a review). Moreover, the intramolecular vibrations can, to a good approximation, be decoupled from the intermolecular modes due to their high frequency, and vibrationally averaged rotational constants b_v of the diatom can be used. Thus, we have the following Hamiltonian describing the nuclear motion,

$$H = -\frac{\hbar^2}{2\mu R}\frac{\partial^2}{\partial R^2}R + \frac{l^2}{2\mu R^2} + b_v j^2 + V, \tag{23}$$

where μ is the reduced mass of the dimer, j is the angular momentum of the diatom, and l denotes the angular momentum associated with the end-over-end rotation of the complex.

In the limit of vanishing anisotropy the quantum numbers j, which describes the rotation of the diatom in the dimer, and l, which corresponds to the rotation of the vector R are good quantum numbers. The total angular momentum $J = j + l$ is always conserved, due to the isotropy of space, but j and l are broken by the anisotropy in the potential. A degenerate (j, l)-level splits into sublevels $J = |j - l|, \ldots, j + l$ under the influence of the anisotropy. If these splittings are small, like in the Ar–H_2 (61) and He–C_2H_2 (62) cases, the states can still be labeled to a good approximation by j and l.

The wave function $\Psi^{JM}(R, \hat{R}, \hat{r})$ can be expanded in a basis of products of radial functions $\chi_n(R)$ and angular functions which are Clebsch-Gordan

coupled spherical harmonics,

$$[Y^j(\hat{r}) \otimes Y^l(\hat{R})]^J_M = \sum_{m_l,m_j} \langle jm_j; lm_l|JM\rangle\, Y^j_{m_j}(\hat{r})\, Y^l_{m_l}(\hat{R}), \qquad (24)$$

where Y^l_m denotes the normalized spherical harmonics, $\langle j_1 m_1; j_2 m_2|JM\rangle$ is the Clebsch-Gordan coefficient (63), $\hat{R}$ stands for the spherical polar angles of R with respect to a space-fixed frame and an analogous definition holds for $\hat{r}$. The angular basis functions have a well defined parity $p = (-1)^{j+l}$, so the full Hamiltonian, Eq. (23), is blocked in both p and J. Within each block various j and l are mixed through the potential.

The infrared transitions in the atom–diatom complexes will obey the following selection rules: $|\Delta p| = 1$, and $|\Delta J| = 1$ or 0. Additionally, if the energy levels can be labeled with the quantum numbers j and l, the selection rules $\Delta l = 0$ and $|\Delta j| = 1$ should hold approximately.

When the leading anisotropic term is large compared to the rotational constant of the complex, and small compared with the rotational constant of the free diatom, the energy levels and infrared transitions can be approximately classified using the case *b* coupling of Bratoz and Martin (59), *i.e.*, the diatom in the complex should behave as a hindered rotor. Choosing the *embedded* reference frame such that the vector R connecting the diatom center of mass with the atom defines the new z axis, the Hamiltonian describing the nuclear motion can be written as (64)–(66),

$$H = -\frac{\hbar^2}{2\mu R}\frac{\partial^2}{\partial R^2}R + \frac{J^2 + j^2 - 2j\cdot\overline{J}}{2\mu R^2} + b_v j^2 + V. \qquad (25)$$

Here, the operator j acts on the angular coordinates of the vector r in the body-fixed frame. Note, that the present coordinate system corresponds to the so-called "two-thirds body-fixed" system of Refs. (2, 66). Therefore, the angular momentum operator j and the pseudo angular momentum operator $\overline{J}$ *do not* commute, so the second term in Eq. (25) cannot be factorized.

The only rigorously conserved quantum numbers are, again, the total angular momentum J and the spectroscopic parity σ. [The spectroscopic parity σ is related to the conventional parity p by the relation $\sigma = p(-1)^J$.] The diatom rotational quantum number j, and the projection K of J (or j) onto the intermolecular axis, are only approximately conserved. This conservation is broken by off-diagonal Coriolis interaction. Since K is the projection of an angular momentum, states with $K = 0, \pm 1$, etc., are denoted as Σ, Π, etc.. In addition, levels with $\sigma = +1$ and $\sigma = -1$ will be designated by superscripts e and f, respectively. For $K = 0$ only e parity states exist. The case *b* coupling of Bratoz and Martin (59) gives a very simple classification of the rovibrational energy levels of the complex: each monomer rotational level j is split into $j + 1$ levels corresponding to any

$J \geq |K|$ with $K = 0, \pm 1, \pm 2, ..., \pm j$. The inclusion of the Coriolis interaction introduces further splitting of the states with $|K| \neq 0$ (the so-called l-doubling) into states with e and f parity labels.

The wave function describing the nuclear motion can be expanded in a basis of products of radial functions $\chi_n(R)$ and angular functions of the form,

$$[Y_K^j(\vartheta, \varphi)\mathcal{D}_{M,K}^{(J)*}(\alpha, \beta, 0) + \sigma Y_{-K}^j(\vartheta, \varphi)\mathcal{D}_{M,-K}^{(J)*}(\alpha, \beta, 0)], \qquad (26)$$

where (β, α) are polar angles of the $\boldsymbol{R}$ vector in the space-fixed coordinates, ϑ and φ are the spherical angles of the $\boldsymbol{r}$ vector in the body-fixed coordinates, and $\mathcal{D}_{M,K}^{(J)}(\alpha, \beta, \gamma)$ is an element of the Wigner rotation matrix (63). The angular basis functions have a well defined parity σ, so the full Hamiltonian, Eq. (25), is blocked in both σ and J. Within each block functions with different K are mixed through the off-diagonal Coriolis interaction.

The allowed dipole transitions between the states of the complex can be deduced from an analysis of the expression for the transition intensity, and it follows easily that the observed dipole transitions must obey the following rigorous selection rules: $|\Delta J| = 1$, $\Delta\sigma = 0$ or $\Delta J = 0$, $|\Delta\sigma| = 2$. Since the K quantum number is nearly conserved, an additional approximate selection rule should hold: $|\Delta K| = 0, 1$.

The wave functions for the initial and final states obtained by solving the Schrödinger equation with the Hamiltonian of Eq. (23) or (25) can be used to compute the infrared absorption intensities for the complex. The infrared absorption coefficient $\mathcal{I}(J'' \rightarrow J')$ for the transition $J'' \rightarrow J'$ is proportional to,

$$\frac{\exp(-E_{J''}/k_B T)}{Z(T)} (E_{J'} - E_{J''}) S(J'' \rightarrow J'), \qquad (27)$$

where E_J denotes the energy of the state labeled by J, $Z(T)$ is the partition function, the line strength is given by,

$$S(J'' \rightarrow J') = \sum_{M'', M', m} \left| \langle \Psi^{J'M'} | \mu_m | \Psi^{J''M''} \rangle \right|^2, \qquad (28)$$

and μ_m is the spherical component of the dipole moment of the dimer (for the far-infrared transitions) or the spherical component of the transition dipole (for the near-infrared transitions).

He–CO and He–HF complexes are very suitable systems to verify how well the theory that goes all the way from *ab initio* calculations of the intermolecular potentials to line positions and intensities can reproduce the experimentally observed spectra. For both systems high-resolution infrared spectra have been recorded (67, 68). In addition, for He–HF also the rotational predissociation line widths have been measured (68).

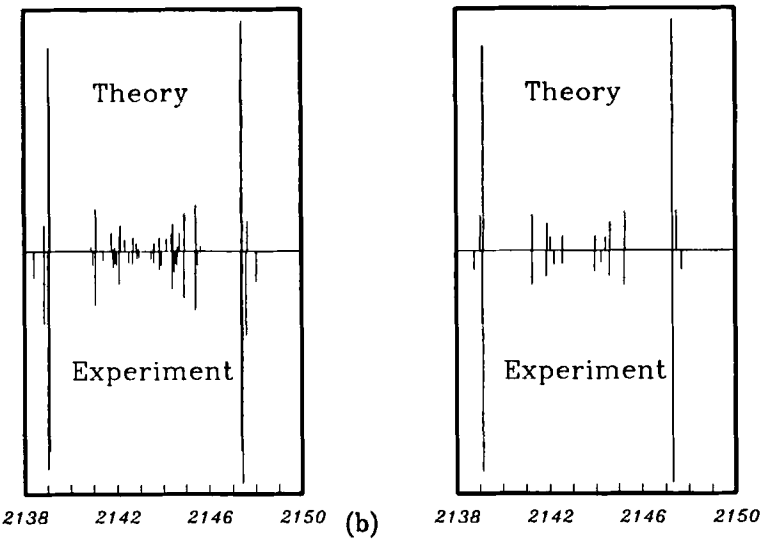

Figure 3
Comparison of theoretical and experimental infrared spectra of the ^{4}He–CO complex (a), and ^{3}He–CO (b) complex, accompanying the fundamental band of CO. The temperature is 50 K.

Recently, SAPT and dynamical calculations for the He–CO complex have been reported (69). Although the anisotropy of the interaction potential around the van der Waals minimum is not particularly weak, we followed Ref. (67) and described the nuclear dynamics in the space-fixed coordinates. The computed infrared spectra for the ^{4}He–CO and ^{3}He–CO complexes are presented in Fig. 3.

An inspection of Fig. 3 shows that the agreement of theoretical transition frequencies and intensities with the results of high-resolution measurements (67) is satisfactory. Most of the line positions agree within 0.1–0.2 cm^{-1} or better. The intensities are also accurately predicted by the *ab initio* potential. However, some transition frequencies are in error by ~ 0.5 cm^{-1}, suggesting that the anisotropy of the *ab initio* potential is not entirely correct. The reason for this small disagreement has been traced (69) to the neglect of higher-order contributions (in the intramonomer correlation) to the exchange-repulsion energy. Bound state calculations using a scaled potential (in which the contribution of the short-range energy to the second Legendre component was increased by 4.5%) gave a spectrum in much better agreement with the experiment. It is worth noting that this scaling is consistent with the estimated effect of the higher-order correlations on the first-order exchange energy.

A similar application has been recently reported for the He–HF system

(70, 71). Starting from the *ab initio* SAPT potential energy surface for this system (70) the authors of Ref. (71) performed converged variational calculations of the energy levels and transition frequencies in the near-infrared spectrum of He–HF accompanying the fundamental band of HF. Although the anisotropy of the interaction potential at the van der Waals minimum is not particularly strong, the body-fixed description of the nuclear motion was found to be the most appropriate. In Table 3 the computed transition frequencies are compared with the measured values (68).

Table 3
Near-infrared transitions in He–HF (in cm^{-1}) accompanying the fundamental band of HF.

transition	J''	J'	$\Delta E(J'' \to J')$ Ref. (71)	$\Delta E(J'' \to J')$ observed (68)	Δ^a
$\Sigma \to \Sigma^e$	0	1	3999.860	3999.953	−0.094
	1	2	4000.044	4000.137	−0.093
	2	3	4000.164	4000.251	−0.087
	3	4	4000.266	4000.345	−0.079
	4	5	4000.378	4000.449	−0.071
$\Sigma \to \Pi^e$	0	1	4003.102	4003.161	−0.059
	1	2	4004.402	4004.418	−0.016
	2	1	4000.806	4000.904	−0.098
	3	2	4000.655	4000.735	−0.080
	4	3	4000.583	4000.639	−0.056
$\Sigma \to \Pi^f$	1	1	4001.916	4002.005	−0.089
	2	2	4001.871	4001.952	−0.081
	3	3	4001.796	4001.859	−0.063
	4	4	4001.669	4001.680	−0.011

[a] Absolute error of the transition frequency computed from the *ab initio* potential (70).

The agreement of theoretical transition frequencies with the results of high-resolution measurements (68) is excellent. The *ab initio* potential energy surface predicts all infrared transitions with errors smaller than 0.1 cm^{-1}. In particular, the band origins of the computed and measured near-infrared spectra agree within 0.2% or better. It follows from the case *b* coupling of Bratoz and Martin (59) that the transition energies are mainly sensitive to even terms in the Legendre expansion of the potential. The results reported in Table 3 show that at least even terms in the SAPT potential are very accurate.

The correctness of the small odd terms has been checked by computing the rotational predissociation line widths. Rotational predissociation life-

times can be obtained from the Fermi golden rule expression (72) which shows that the mixing of states with $j = 0$ and $j = 1$ occurs mainly via the first Legendre component of the potential. In Ref. (71) the widths of the resonances that correspond to rotational predissociation were directly obtained from close-coupling calculations. In Table 4 the widths of the Σ^e and Π^e resonances calculated from the *ab initio* potential (70) are compared with the experimental results (68).

Table 4
Calculated widths (MHz) of the HeHF resonance states. The widths corresponding to the scaled potential are given in parentheses.

	J	Γ_J Ref. (71)	Γ_J observed (68)
Σ^e bend	1	7203 (3452)	3020 ± 500
	2	5731 (2673)	2830 ± 200
	3	4453 (2001)	1640 ± 150
	4	3280 (1397)	1260 ± 100
	5	2158 (848)	770 ± 100
Π^e bend	1	1080 (575)	530 ± 100
	2	1773 (928)	890 ± 150
	3	1930 (993)	1000 ± 400

The agreement here is less satisfactory: all computed widths are a factor of two larger than the measured line widths (68). This suggests that the small $P_1(\cos\vartheta)$ anisotropy of the potential is not correct. To confirm this assumption the widths of the Σ^e and Π^e resonances were recomputed using a potential in which the contribution of the short-range energy to this first Legendre component was scaled by 0.95. The resulting widths are given in parentheses. The agreement with the measured line widths is very good: almost all widths computed using the scaled potential agree with the experimental data within the experimental error bars. It should be noted that this 5% scaling of the short-range $P_1(\cos\vartheta)$ term introduces only a very small change in the interaction potential. In the repulsive region ($R = 5$ bohr and $\vartheta = 0°$) the scaled potential is $\approx 4\%$ smaller than the *ab initio* potential, while the depth of the van der Waals well is only 2% lower. This confirms that the overall anisotropy of the *ab initio* potential is correct. Small inaccuracies of the order of 2% may be due to basis set unsaturation of the exchange-repulsion contribution.

D. Excess Second Virial Coefficients for He–CO

Additional information about the accuracy of the theoretical interaction potentials can be obtained by comparison of the measured and computed

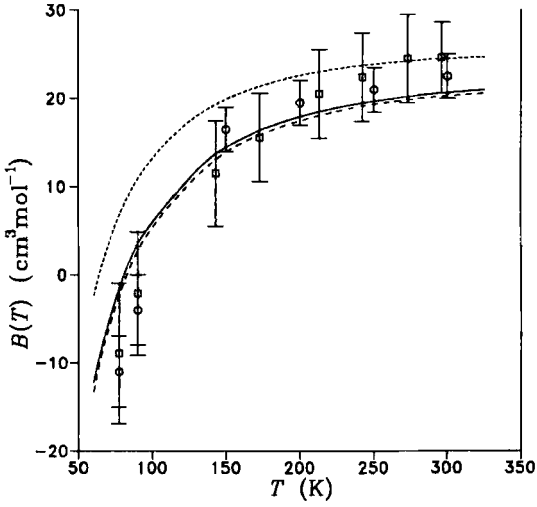

Figure 4
Comparison of the *ab initio* and experimental second virial coefficients. The solid and dashed lines represent second virial coefficients generated from the original and scaled *ab initio* potentials, respectively, while the dotted line shows the second virial coefficient calculated using the isotropic component of the *ab initio* potential. Circles and squares are experimental points from Refs. (74) and (73), respectively.

excess second virial coefficients. The *ab initio* potential energy surface for He–CO (69) has been checked by computing the second virial coefficient $B(T)$ over the temperature range in which it has been measured (73, 74). We used directly the formulas for atom-linear molecule derived by Pack (75). Specifically, we have computed the classical term, $B^{(0)}(T)$, and included the first quantum corrections due to relative translational motions, $B_R^{(1)}(T)$, to molecular rotations, $B_A^{(1)}(T)$, and to the Coriolis term, $B_C^{(1)}(T)$:

$$B(T) = B^{(0)}(T) + B_R^{(1)}(T) + B_A^{(1)}(T) + B_C^{(1)}(T). \tag{29}$$

The results of these calculations are presented in Fig. 4.

An inspection of Fig. 4 shows that the *ab initio* results agree well with the experimental data of Schramm and collaborators (73, 74). Only at the two lowest temperatures this good agreement deteriorates somewhat, and the present results are just outside the error bars of the new measurements (74), but within the (larger) error bars of the previous experimental data (73). However, at low temperatures the quantum corrections become rather significant, so higher corrections may be important. Especially, the second ($O(\hbar^4)$) radial correction may be nonnegligible. Also presented in Fig. 4 is the second virial coefficient computed using the scaled *ab initio* potential

(*cf.* previous section). This scaling has a negligible effect on the computed second virial coefficients. Finally, it is worth noting that the effect of the anisotropy in the potential is relatively important (see Fig. 4). Except for the high temperature region, the neglect of the anisotropic terms in the potential would lead to second virial coefficients outside the experimental error bars.

5. Summary and Conclusions

In this paper we have given a short overview of the application of symmetry-adapted perturbation theory to intermolecular potentials and interaction-induced properties, and of the methods going directly from these intermolecular properties to experimentally measurable quantities such as collision-induced Raman spectra, rovibrational spectra, and second (pressure and dielectric) virial coefficients. The results presented in this paper show that intermolecular potentials and dipole/polarizability surfaces obtained from *ab initio* SAPT calculations can be used to correctly describe the spectroscopic and dynamical processes involving weakly bound complexes.

Acknowledgements

This work was supported by the Netherlands Foundation of Chemical Research (SON), the Netherlands Organization for Scientific Research (NWO), and Polish Scientific Research Council (KBN), grant No. 3 T09A 072 09.

References

(1) B. Jeziorski, R. Moszynski, and K. Szalewicz, Chem. Rev. **94**, 1887 (1994).

(2) A. van der Avoird, P.E.S. Wormer, and R. Moszynski, Chem. Rev. **94**, 1931 (1994).

(3) Faraday Discuss. Chem. Soc. **97**, (1994).

(4) G. Herzberg, *Infrared and Raman Spectra of Polyatomic Molecules*, (Van Nostrand, New York, 1945).

(5) *Phenomena Induced by Intermolecular Interactions*, edited by G. Birnbaum, NATO ASI Series B, vol. 127, (Plenum, New York, 1985).

(6) *Collision- and Interaction-Induced Spectroscopy*, edited by G.C. Tabisz and M.N. Neuman, NATO ASI Series C, vol. 452, (Kluwer, Dordrecht, 1995).

(7) M.E. Crawford, H.L. Welsh, J. C. F. MacDonald, and J. L. Locke, Phys. Rev. **80**, 469 (1950).

(8) D.A. Chisholm and H.L. Welsh, Can. J. Phys. **32**, 291 (1954).

(9) H.B. Levine and G. Birnbaum, Phys. Rev. Lett. **20**, 439 (1968).

(10) J.P. McTague and G. Birnbaum, Phys. Rev. Lett. **21**, 661 (1968).

(11) J.P. McTague and G. Birnbaum, Phys. Rev. A **3**, 1376 (1971).

(12) B. Jeziorski and W. Kolos, Int. J. Quantum Chem. (Suppl. 1) **12**, 91 (1977).

(13) B. Jeziorski and W. Kolos, in *Molecular Interactions*, edited by H. Ratajczak and W.J. Orville-Thomas, (Wiley, New York, 1982), vol. 3, p. 1.

(14) T. Cwiok, B. Jeziorski, W. Kolos, R. Moszynski, and K. Szalewicz, J. Chem. Phys. **97**, 7555 (1992).

(15) T. Cwiok, B. Jeziorski, W. Kolos, R. Moszynski, and K. Szalewicz, J. Mol. Struct. (Theochem) **307**, 135 (1994).

(16) K. Szalewicz and B. Jeziorski, Mol. Phys. **38**, 191 (1979).

(17) S. Rybak, B. Jeziorski, and K. Szalewicz, J. Chem. Phys. **95**, 6576 (1991).

(18) R. Moszynski, B. Jeziorski, A. Ratkiewicz, and S. Rybak, J. Chem. Phys. **99**, 8856 (1993).

(19) R. Moszynski, B. Jeziorski, and K. Szalewicz, J. Chem. Phys. **100**, 1312 (1994).

(20) R. Moszynski, B. Jeziorski, S. Rybak, K. Szalewicz, and H.L. Williams, J. Chem. Phys. **100**, 5080 (1994).

(21) R. Moszynski, S.M. Cybulski, and G. Chalasinski, J. Chem. Phys. **100**, 4998 (1994).

(22) H.L. Williams, K. Szalewicz, R. Moszynski, and B. Jeziorski, J. Chem. Phys. **103**, 4586 (1995).

(23) B. Jeziorski, R. Moszynski, A. Ratkiewicz, S. Rybak, K. Szalewicz, and H.L. Williams "SAPT: A Program for Many-Body Symmetry-Adapted Perturbation Theory Calculations of Intermolecular Interactions", in *Methods and Techniques in Computational Chemistry: METECC-94, vol. B Medium Size Systems*, edited by E. Clementi, (STEF, Cagliari 1993), p. 79.

(24) T.G.A. Heijmen, R. Moszynski, P.E.S. Wormer, and A. van der Avoird, Mol. Phys. **00**, 0000 (1996).

(25) P. E. S. Wormer, F. Mulder, and A. van der Avoird, Int. J. Quantum Chem. **11**, 959 (1977).

(26) A. van der Avoird, P. E. S. Wormer, F. Mulder, and R. M. Berns, Top. Curr. Chem. **93**, 1 (1980).

(27) W. Rijks and P.E.S. Wormer, J. Chem. Phys. **88**, 5704 (1988).

(28) P.E.S. Wormer and H. Hettema, J. Chem. Phys. **97**, 5592 (1992).

(29) P.E.S. Wormer and H. Hettema, POLCOR package (Nijmegen 1992).

(30) B. Jeziorski, K. Szalewicz, and G. Chalasinski, Int. J. Quantum Chem. **14**, 271 (1978).

(31) T. Korona, B. Jeziorski, and R. Moszynski, Adv. Quantum Chem. – this issue.

(32) R. Moszynski, T.G.A. Heijmen, P.E.S. Wormer, and A. van der Avoird, J. Chem. Phys. **104**, 6997 (1996).

(33) A.T. Prengel and W.S. Gornall, Phys. Rev. A **13**, 253 (1976).

(34) L. Frommhold, K. Hong Hong, and M.H. Proffitt, Mol. Phys. **35**, 665 (1978).

(35) Y. Le Duff, Phys. Rev. A **20**, 48 (1979).

(36) F. Barocchi, P. Mazzinghi, and M. Zoppi, Phys. Rev. Lett. **41**, 1785 (1978).

(37) F. Barocchi, P. Mazzinghi, and M. Zoppi, in *Intermolecular Spectroscopy and Dynamical Properties of Dense Systems*, Proceedings of the International School 'Enrico Fermi', Course LXXV, edited by J. van Kranendonk, (North-Holland, Amsterdam, 1981), p. 263.

(38) M. Proffitt and L. Frommhold, Phys. Rev. Lett. **42**, 1473 (1979).

(39) L. Frommhold and M. Proffitt, J. Chem. Phys. **70**, 4803 (1979).

(40) M. Proffitt and L. Frommhold, J. Chem. Phys. **72**, 1377 (1980).

(41) M. Proffitt, J. W. Keto, and L. Frommhold, Phys. Rev. Lett. **45**, 1843 (1980).

(42) M. Proffitt, J. W. Keto, and L. Frommhold, Can. J. Phys. **59**, 1459 (1981).
(43) P.D. Dacre and L. Frommhold, J. Chem. Phys. **76**, 3447 (1982).
(44) P.D. Dacre, Mol. Phys. **45**, 17 (1982).
(45) A.D. Buckingham and J.A. Pople, Trans. Faraday Soc. **51**, 1029, 1079 (1955).
(46) R. Moszynski, T.G.A. Heijmen, and A. van der Avoird, Chem. Phys. Lett. **247**, 440 (1995).
(47) J. de Boer, Rept. Prog. Phys. **12**, 305 (1949).
(48) D.R. Johnston, G.J. Oudemans, and R.H. Cole, J. Chem. Phys. **33**, 1310 (1960).
(49) R.H. Orcutt and R.H. Cole, J. Chem. Phys. **46**, 697 (1967).
(50) E.C. Kerr and R.H. Sherman, J. Low Temp. Phys. **3**, 451 (1970).
(51) S. Kirouac and T.K. Bose, J. Chem. Phys. **64**, 1580 (1976).
(52) D. Vidal and M. Lallemand, J. Chem. Phys. **64**, 4293 (1976).
(53) M. Lallemand and D. Vidal, J. Chem. Phys. **66**, 4776 (1977).
(54) D. Gugan and G.W. Michel, Metrologia **16**, 149 (1980).
(55) H.J. Achtermann, G. Magnus, and T.K. Bose, J. Chem. Phys. **94**, 5669 (1991).
(56) J. Huot and T.K. Bose, J. Chem. Phys. **95**, 2683 (1991).
(57) H.J. Achtermann, J.G. Hong, G. Magnus, R.A. Aziz, and J. Slaman, J. Chem. Phys. **98**, 2308 (1993).
(58) R.A. Aziz, F.R. McCourt, abd C.C.K. Wong, Mol. Phys. **61**, 1487 (1987).
(59) S. Bratoz and M.L. Martin, J. Chem. Phys. **42**, 1051 (1965).
(60) J.M. Hutson, Adv. Mol. Vib. Collision Dyn. **1**, 1 (1991).
(61) R. Moszynski, B. Jeziorski, P.E.S. Wormer, and A. van der Avoird, Chem. Phys. Lett. **221**, 161 (1994).
(62) R. Moszynski, P.E.S. Wormer, and A. van der Avoird, J. Chem. Phys. **103**, 8385 (1995).
(63) D.M. Brink and G.R. Satchler, *Angular Momentum*, (Clarendon, Oxford, 1975).
(64) J. Tennyson and B.T. Sutcliffe, J. Chem. Phys. **77**, 4061 (1982).
(65) B.T. Sutcliffe and J. Tennyson, Mol. Phys. **58**, 1053 (1986).
(66) G. Brocks, A. van der Avoird, B.T. Sutcliffe, and J. Tennyson, Mol. Phys. **50**, 1025 (1983).
(67) C.E. Chuaqui, R.J. Le Roy, and A.R.W. McKellar, J. Chem. Phys. **101**, 39 (1994).
(68) C.M. Lovejoy and D.J. Nesbitt, J. Chem. Phys. **93**, 5387 (1990).
(69) R. Moszynski, T. Korona, P.E.S. Wormer, and A. van der Avoird, J. Chem. Phys. **103**, 321 (1995).
(70) R. Moszynski, P.E.S. Wormer, B. Jeziorski, and A. van der Avoird, J. Chem. Phys. **101**, 2811 (1994).
(71) R. Moszynski, B. Jeziorski, A. van der Avoird, and P.E.S. Wormer, J. Chem. Phys. **101**, 2825 (1994).
(72) S.C. Tucker and D.G. Truhlar, J. Chem. Phys. **86**, 6251 (1986).
(73) E. Elias, N. Hoang, J. Sommer, and B. Schramm, Ber. Bunsenges. Phys. Chem. **90**, 342 (1986).
(74) B. Schramm, unpublished results (1994).
(75) R.T. Pack, J. Chem. Phys. **78**, 7217 (1983).

Quantum Chemical Treatment of Molecules in Condensed Disordered Media

Mati Karelson
Department of Chemistry, University of Tartu, Tartu EE2400, Estonia

Abstract

A short overview of the quantum chemical and statistical physical methods of modelling the solvent effects in condensed disordered media is presented. In particular, the methods for the calculation of the electrostatic, dispersion and cavity formation contributions to the solvation energy of electroneutral solutes are considered. The calculated solvation free energies, proceeding from different geometrical shapes for the solute cavity are compared with the experimental data. The self-consistent reaction field theory has been used for a correct prediction of the tautomeric equilibrium constant of acetylacetone in different dielectric media,. Finally, solvent effects on the molecular geometry and charge distribution in condensed media are discussed.

Contents:

ADVANCES IN QUANTUM CHEMISTRY, VOLUME 28

0065-3276/97 $25.00

1. Introduction

The unprecedented progress in computer technology and in computer science has had a tremendous impact on computational molecular physics and chemistry. Methods, algorithms, and software for performing molecular structure calculations have been developed to predict molecular properties and processes with high accuracy [1-3]. Notably, almost all these methods are applicable only for the isolated molecules thus corresponding to the gas phase at low pressure and temperature. Most chemical processes, in particular biochemical reactions *in vivo* and *in vitro*, and industrial processes of great impact take place, however, in condensed (liquid) phase.

The physical properties and chemical reactivity of molecules may be and often are drastically changed by a surrounding medium. In many cases specific complexes are formed between the solvent and solute molecules whereas in other cases only the non-bonded intermolecular interactions are responsible for the solvational effects. By one definition, the environmental effects can be divided into two principally different types, i.e. to the static and dynamic effects. The former are caused by the coulombic, exchange, electronic polarization and correlation interactions between two or more molecular species at fixed (close) distances and relative orientation in space. The dynamic interactions are due to the orientational relaxation and atomic polarization effects, which can be accounted for rigorously only by using time-dependent quantum theory.

The static intermolecular interactions have been studied by two approaches, which are conventionally quoted as the *supermolecule* and *perturbation* approach, respectively. In the supermolecule approach [3-5], the interaction energy between two molecular species A and B is usually calculated as the difference between the energies of the system consisting these two species at their fixed relative orientation and distance (supermolecule), and of the isolated species at the infinite separation. The energies are usually calculated within the self-consistent field (SCF) theory or within one of the approximations including electron correlation effects, like the configuration interaction (CI) method, the many-body perturbation theory (MBPT), or the coupled-cluster (CC) approach. In studying intermolecular interactions, the "size-extensivity" [6,7] of the methods applied is of crucial importance. Furthermore, the interaction energies calculated using the supermolecule approach usually suffer from the basis set superposition error (BSSE) [7], a spurious energy improvement resulting from the use of truncated basis sets in the quantum calculation. This error is unavoidable in most cases except for very small systems [8]. The advantage of the perturbation theory is that the

interaction energy is calculated directly and not as a difference of large numbers. Also, it may be separated into components of well defined physical meaning. However, the supermolecule approach and all perturbation theories developed so far for studying weak intermolecular interactions are not directly applicable to condensed media because of considering only small number of liquid particles and thus neglecting the bulk solvation effects [8].

In principle, two alternative approaches for the approximate description of the bulk (dynamic) solvation effects in liquids and solutions have been developed. First, the molecular dynamics approach [9-11] is based on the computer simulation of a system of particles which interact by the known model potential and undergo the rotational and translational movement in the field caused by this interaction according to the classical (Newtonian) mechanics. By applying various boundary conditions and using step-by-step time evolution, the potential energy and forces are calculated for a large number of configurations. Time–averages of the free energy, internal energy and other thermodynamic and dynamic characteristics of the system are obtained from the resulting partition function. An alternative is the stochastic Monte Carlo method [12] which is based on the ergodic theorem and provides the ensemble averages calculated from randomly generated and weighed configurations. In spite of substantial progress made in the study of principal solvation interactions using molecular dynamics or Monte Carlo approach, the practical applicability of these methods to real solutions is still limited because of high computer time and resource requirements.

The second approach to the approximate description of the dynamic solvation effects is based on the semiempirical account for the time-dependent electrical polarization of the medium in the field of the solute molecule. In this case, the statistical averaging over the solute-solvent intermolecular distances and configurations is presumed before the solution of the Schrödinger equation for the solute and correspondingly, the solvent is described as a polarizable dielectric continuum. The respective electrostatic solvation energy of a solute molecule is given by the following equation[13]

$$E_{el} = \frac{1}{8\pi} \int_V \mathbf{E}_S \cdot \mathbf{E}_O (\varepsilon - 1) dV \qquad (1)$$

where $\mathbf{E}_0$ is the electrostatic field of the charges in the molecule *in vacuo* and $\mathbf{E}_S$ is the modified field in the presence of dielectric. The numerical integration over V presents a difficult mathematical task which can be simplified by the application of the Gauss divergence theorem. According to this theorem, the volume integral (1) is transformed into a surface integral over some boundary

$$E_{el} = \frac{\varepsilon - 1}{8\pi} \int_S \Phi_S \cdot \mathbf{E}_O \mathbf{n} dS \qquad (2)$$

where S is the boundary surface, **n** the unit outward normal vector on S and $grad\Phi_S = -\mathbf{E}_S$. Different representations of this integral, corresponding to different molecular shapes, have been applied to find electrostatic solvation energies of compounds in liquids [13-15]. According to the classical reaction field theory of Kirkwood and Onsager [16,17], the solute molecule is represented by a set of point charges fixed inside of sphere of radius a_0 and the electrostatic equation (2) is solved by applying the appropriate boundary conditions inside and outside the sphere. In the quantum chemical extension of this theory, the interaction energy is represented by the respective additional terms to the solute Hamiltonian which can be divided into nuclear-nuclear, nuclear-electron and electron-electron terms [18]. The self-consistent reaction field (SCRF) procedure [19,48] has been used in most cases to find the solutions of the respective Schrödinger equation for a solute molecule in a polarizable dielectric medium.

Simple spherical cavity model SCRF calculations, performed at *ab initio* [19-27] and semiempirical level [28-35] of quantum molecular theory have given important new information about the chemical and physical properties of compounds in solutions and liquids. First of all, the equilibrium molecular geometry of a polar molecule, calculated in the framework of the Born-Oppenheimer approximation, may significantly depend on the polarizable medium surrounding this molecule in the condensed phase (cf. [19, 29-34]). Also, the charge distribution and dipole and higher electrical moments of the solute molecule may be significantly altered by the solvent reaction field [29-39]. Numerous successful applications of the SCRF theory to the chemical reactivity are known [14]. For instance, the SCRF model gives a good description of prototropic tautomeric equilibria [22,23, 39-31]. The SCRF method has also been extended to the calculations of molecular spectra [24-26, 29-31], to the investigation of the interrelationship between the medium and intramolecular electronic effects [37,38, 41-45], to the calculation of hydrogen bonding energies [46] and reaction paths in liquids and solutions [47].

The use of the SCRF model in a quantum-chemical theory requires that the *shape* and the *size* of the solute cavity must be defined uniquely for any set of compounds. A number of approaches to estimate these molecular characteristics have been developed [14], but no non-empirical way of their calculation is known. Therefore, it is important to study the dependence of the calculated properties of molecules in condensed media on the size and shape of the molecular cavity applied in the theory.

2. Aqueous free energies of solvation of organic compounds.

First, it is of primary importance to study the dependence of the solvation free energy on the cavity size and shape applied in the calculations. Notably, it has recently been of substantial interest to different groups [69,70]. Conventionally, the solvation free energy, ΔG_S, can be divided into the following contributions

$$\Delta G_S = \Delta G_{el} + \Delta G_{disp} + \Delta G_{cav} + \Delta G_{HB} \quad (3)$$

where $\Delta G_{el} = E_{el}$ is the electrostatic interaction energy of the solute charge distribution with the reaction field it creates in the surrounding polarizable dielectric medium; $\Delta G_{disp} = E_{disp}$ is the dispersion interaction energy between the solute and adjacent solvent molecules, ΔG_{cav} is the free energy of the cavity formation in the solution and ΔG_{HB} is the solute-solvent hydrogen bonding energy. Notably, the first three terms in Equation (3) are directly related to the size and shape of the molecular cavity. The electrostatic and dispersion interaction energies can be calculated quantum chemically by solving the appropriate Schrödinger equations. The free energy of the cavity formation has essentially an entropic nature and, therefore, it should be calculated using the statistical mechanical approach. In the present application, two different cavity shapes (the spherical and ellipsoidal) were considered in the calculation of individual free energy contributions given in Equation (3).

The self-consistent reaction field method [19,48,49] can be used to calculate the electrostatic interaction energy, E_{el}, between the solute and its reaction field

$$E_{el} = E_{rf} - E_o, \quad (4)$$

where E_o and E_{rf} are the quantum chemically calculated total energies for the isolated solute molecule and for the solute molecule in the condensed dielectric medium, respectively. A full relaxation of the polarizable medium in the electrostatic field of the solute molecule was assumed in the present analysis (model B in Ref. [32]). In this case, E_{rf} is obtained directly as the solution of the respective SCRF Schrödinger equation

$$\left[\hat{\mathbf{H}}_o + \Gamma\langle\phi|\hat{\mu}|\phi\rangle\hat{\mu}\right]\psi = E_{rf}\psi \quad (5)$$

where $\hat{\mathbf{H}}_o$ is the Hamiltonian for the isolated molecule, $\hat{\mu}$ the dipole moment operator, $\langle\phi|\hat{\mu}|\phi\rangle$ the self-consistent reaction field expectation value of the solute dipole moment, and ψ the solute total wavefunction in the condensed medium. In the last equation, factor Γ describes the intensity of the reaction field response of the solvent. This factor depends both on the dielectric constant

of the solvent and the size and shape of the solute cavity. In the case of the simplest, spherical model for the solute cavity (SCa SCRF)

$$\Gamma = \frac{(1-\varepsilon)}{(2\varepsilon+1)a_o^3}, \tag{6}$$

where a_o is the cavity radius and ε - the dielectric constant of medium. In the case of the ellipsoidal cavity with principal axes a, b and c (ECa SCRF), Γ becomes a tensor [13,28]

$$\Gamma = \begin{pmatrix} \frac{3A_a(1-A_a)(\varepsilon-1)}{abc[\varepsilon+(1-\varepsilon)A_a]} & 0 & 0 \\ 0 & \frac{3A_b(1-A_b)(\varepsilon-1)}{abc[\varepsilon+(1-\varepsilon)A_b]} & 0 \\ 0 & 0 & \frac{3A_c(1-A_c)(\varepsilon-1)}{abc[\varepsilon+(1-\varepsilon)A_c]} \end{pmatrix} \tag{7}$$

where A_a, A_b and A_c are the standard ellipsoidal shape factor integrals.

In the present analysis, the dispersion energy was calculated using the quantum-mechanical method developed by Rösch and Zerner [50] on the basis of Abe's theory [51]. According to this method, the dispersion energy, E_{disp}, for a solute molecule in a spherical cavity is given as follows

$$E_{disp} = -\frac{2}{3}\frac{1}{a_S^3 a_M^3}\sum_{J\neq I}\sum_{K\neq O}\frac{\left(\mu_{IJ}^M\right)^2\left(\mu_{KO}^S\right)^2}{E_K^S - E_O^S + E_J^M - E_I^M} \tag{8}$$

where the superscript S refers to the solvent molecule and the superscript M to the solute molecule. Thus, μ_{IJ}^M and μ_{KO}^S are the transition dipoles between the respective states of the solute (I and J) and the solvent (K and O) molecules. In Eq. (8), E_K^S, E_O^S and E_J^M, E_I^M, denote the energies of the K-th and O-th state of the solvent and of the J-th and I-th state of the solute molecule, respectively. The a_S and a_M are the cavity radii for the solvent and solute molecules, respectively. In the case of an ellipsoidal cavity, the following equation was implemented for the calculation of the dispersion energy

$$E_{disp} = -\frac{2}{9}\left(\frac{1}{a^3 a_S^3}+\frac{1}{b^3 a_S^3}+\frac{1}{c^3 a_S^3}\right)\sum_{J\neq I}\sum_{K\neq O}\frac{\left(\mu_{IJ}^M\right)^2\left(\mu_{KO}^S\right)^2}{E_K^S - E_O^S + E_J^M - E_I^M} \tag{9}$$

where a, b and c are the principal axes of the ellipsoid.

The free energy of the cavity formation, ΔG_{cav}, was calculated proceeding from the scaled particle theory (SPT) [52,53]. According to this theory, the free energy of formation of a spherical cavity is given by the following formula

$$\Delta G_{cav} = RT\left\{1 - ln(1-y) + \left(\frac{3y}{1-y}\right)\frac{a_M}{a_S} + \left[\frac{3y}{1-y} + \frac{9}{2}\left(\frac{y}{1-y}\right)^2\right]\left(\frac{a_M}{a_S}\right)^2\right\} \quad (10)$$

where

$$y = \frac{4\pi\rho a_S^3}{3} \quad (11)$$

is the reduced number density of the solvent. In the last formulae, a_M and a_S denote the intrinsic radii of the solute and solvent molecules, respectively, and ρ is the number density of the solvent. In the case of the ellipsoidal cavity, the SPT cavity formation energy is given by the following equation [54]

$$\Delta G_{cav} = RT\left\{1 - ln(1-y) + \left(\frac{\alpha y}{1-y}\right)\frac{a}{a_S} + \left[\frac{\beta y}{1-y} + \gamma\left(\frac{y}{1-y}\right)^2\right]\left(\frac{a}{a_S}\right)^2\right\} \quad (12)$$

where α, β, and γ denote geometrical coefficients and a is the characteristic length of the ellipsoid (the major semi-axis).

A critical parameter in all individual terms of the solvation free energy is the cavity size. Different assumptions have been used to estimate its value either from the experimental mass densities of compounds or quantum-chemically calculated electron isodensity surfaces of molecules [55]. Notably, the general appearance of the dependence of different terms of the solvation free energy on the cavity radius is rather similar for different solutes (cf. Fig. 1. for methanol and acetonitrile).

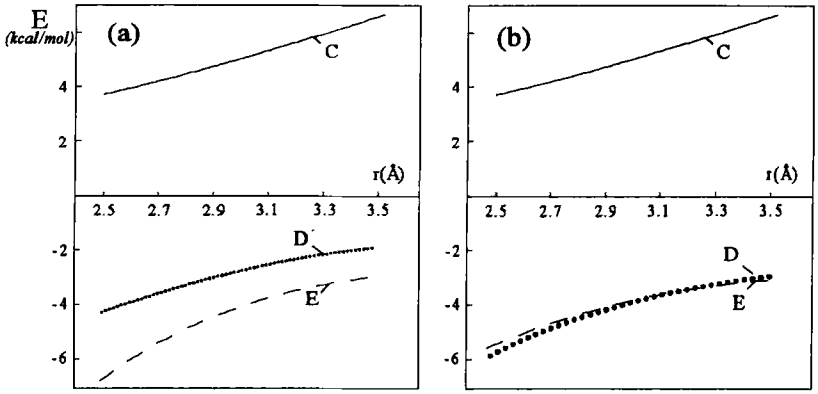

Figure 1. Dependence of the AM1 SCa SCRF Calculated Electrostatic Solvation Energies (E), INDO/1 SCa Calculated Dispersion Energies (D) and SPT Spherical Cavity Formation Free Energies (C) on the Cavity Radius for Methanol (a) and Acetonitrile (b).

Therefore, the best estimate of a solute cavity size can be found by minimizing the difference between the calculated and experimental solvation free energies at different cavity sizes. However, a common scheme for the calculation of the cavity size for different compounds is necessary in order to minimize the number of empirical parameters involved in the theory. For convex cavity shapes (sphere and ellipsoid), it is feasible to assume that the solute cavity is formed by adding the contributions from both the solute and solvent molecules. Such scheme allows to account for the dielectric saturation at the vicinity of the solute molecule and for the change of the cavity size in the solvents with molecules of different size. Thus, in the present study the radius of a spherical cavity was calculated as the sum of the intrinsic radius of the solute molecule , a_{OS}, and a constant additive term by solvent (water), a_W. In the case of the ellipsoidal cavity, the additive solvent term was added to each semi-axis of the intrinsic ellipsoid of the solute molecule.

The intrinsic volume of the solute molecule was calculated from the molar mass MW and density ρ of the respective pure compound as follows

$$V = \frac{\pi}{6}\frac{MW}{\rho N_A}, \tag{13}$$

where N_A is the Avogadro's number. This formula corresponds to a cubic or parallelepiped packing of the spherical or ellipsoidal cells in the pure liquid, respectively, with a single molecule in each cell.

The constant term of the solvent (water) molecule to the cavity size can be estimated using different independent data. For instance, the hydration energies of simple inorganic ions can be correctly predicted using the following modified Born equation

$$\Delta H^0_{hydr} = \frac{1-\varepsilon}{\varepsilon}\frac{Q^2}{r_C + a_w} \tag{14}$$

where Q is the ionic charge and r_C the crystallographic radius of a cation. An average value of the $a_w = 0.72 \pm 0.03$ Å was found from the experimental data on ΔH^0_{hydr} [56-59].

The calculated individual contributions to the total aqueous solvation free energies of 30 organic compounds are given in Table 1. The electrostatic (SCRF) contributions were calculated using semiempirical AM1 (Austin Model 1 [60,61]) method. The dispersion energies were calculated using INDO/1 parameterization [62] and AM1 optimized molecular geometries in solution. A comparison of different columns in Table 1 with the experimental solvation

free energies in aqueous solution ΔG(exp) reveals the absence of a correlation between ΔG(exp) and any individual contribution to the solvation energy.

Table 1.

AM1 SCRF Calculated Electrostatic Solvation Energies, E_{el}, INDO/1 Calculated Dispersion Energies, E_{disp}, SPT Cavity Formation Free Energies, ΔG_{cav}, and Experimental Solvation Free Energies, ΔG(exp) (*kcal/mol*), [63] of 30 Organic Compounds in Aqueous Solution.

Compound	E_{el} (SCa)	E_{el} (ECa)	E_{disp} (SCa)	E_{disp} (ECa)	ΔG_{cav} (SCa)	ΔG_{cav} (ECa)	ΔG (exp)
Methane	0.00	0.00	-2.75	-2.75	4.22	4.22	1.95
Ethane	0.00	0.00	-3.55	-3.40	4.95	4.96	1.81
n-Hexane	0.00	0.00	-4.99	-4.95	7.34	7.50	2.58
Cyclohexane	0.00	0.00	-5.30	-4.79	6.74	6.31	1.24
Ethene	0.00	0.00	-3.64	-3.55	4.81	4.84	1.30
Ethyne	0.00	0.00	-3.50	-3.95	4.53	4.60	-0.01
Propyne	-0.05	-0.01	-4.40	-4.99	5.11	5.19	-0.48
Benzene	0.00	0.00	-6.49	-6.52	6.18	6.35	-0.90
Methyl fluoride	-1.06	-0.95	-3.76	-3.70	4.28	4.24	-0.22
Methyl chloride	-0.91	-0.61	-4.29	-3.92	4.60	4.66	-0.56
Methyl bromide	-0.67	-0.51	-4.06	-3.78	5.10	5.11	-0.80
Methyl iodide	-0.53	-0.43	-4.13	-3.99	5.31	5.33	-0.90
Dimethyl ether	-0.78	-0.70	-3.56	-3.20	5.69	5.24	-1.92
Dimethyl sulphide	-0.61	-0.66	-4.39	-4.32	5.68	5.73	-1.56
Methanol	-0.92	-1.06	-3.34	-3.30	4.46	4.47	-5.07
Ethanol	-1.95	-1.98	-4.26	-3.80	5.02	5.03	-4.96
Glycol	-1.78	-3.06	-4.96	-4.44	5.08	5.11	-7.75
Ethanal	-2.23	-1.97	-4.34	-3.81	5.09	4.92	-3.55
Acetone	-2.27	-2.04	-4.86	-4.34	5.69	5.33	-3.81
Acetic acid	-1.08	-0.82	-4.92	-3.93	5.02	5.33	-6.78
Methyl formate	-0.66	-0.65	-4.16	-3.88	5.29	5.32	-2.81
Acetonitrile	-2.81	-1.89	-4.21	-3.71	4.94	4.85	-3.94
Pyridine	-0.92	-0.73	-6.78	-6.39	5.93	6.10	-4.75
Dimethyl amine	-0.69	-0.88	-4.48	-3.75	5.16	5.24	-4.33
Trifluoromethane	-0.97	-0.73	-5.05	-4.88	4.69	4.70	-0.59
Tetrafluoromethane	0.00	0.00	-6.76	-6.76	4.17	4.17	-2.32
Ethylene diamine	-1.39	-1.20	-5.13	-4.27	5.47	5.52	-9.88
Methyl amine	-0.88	-0.99	-3.67	-3.54	4.72	4.73	-5.07
Acetamide	-0.12	-0.09	-5.05	-4.45	5.20	5.23	-9.70
Methyl mercaptane	-1.87	-1.78	-3.95	-4.25	5.06	5.08	-1.26

The combination of the first three terms of Equation (3) for both cavity models does not also lead to a satisfactory correlation with the experimental data. However, the difference $\delta\Delta G = \Delta G(exp) - E_{el} - E_{disp} - \Delta G_{cav}$ correlates satisfactorily with the number of hydrogen bonding donor (#HBD) and hydrogen bonding acceptor (#HBA) sites in the solute molecule.

The following linear relationships were obtained

$$\delta\Delta G(SCa) = (-0.27 \pm 0.25) - (1.94 \pm 0.33)\#HBA - (1.37 \pm 0.25)\#HBD$$
$$R = 0.94; \quad s = 0.98$$
$$\delta\Delta G(ECa) = (-0.40 \pm 0.29) - (2.20 \pm 0.38)\#HBA - (1.33 \pm 0.28)\#HBD$$
$$R = 0.93; \quad s = 1.28$$

for the spherical and ellipsoidal cavity models, respectively. Notably, the regression coefficients for the hydrogen-bonding parameters are smaller than the energies of isolated hydrogen bonds. However, the formation of hydrogen bonds between the solute and water molecules in aqueous solutions is accompanied with a simultaneous breaking of the water-water hydrogen bonds. Therefore, those coefficients reflect an average difference between the energies of the solute-solvent and solvent-solvent hydrogen bonds.

The data presented above demonstrate that the total solvation free energy of organic compounds in aqueous solution can be calculated with some confidence using a minimum number of parameters (the dielectric constant and the solute cavity size contibution for the solvent) and provided that appropriate quantum chemical and statistical physical models are used for the description of the reaction field and dispersion interactions, and the cavity formation in solution.

3 Tautomeric equilibrium constants.

One of the most important applications of the quantum theory of molecules in condensed media is the prediction of their chemical reactivity. It is often necessary to predict the rate or equilibrium constant of a chemical reaction in different organic and inorganic media. However, in most cases the theoretical calculations have been limited to the aqueous solutions. Therefore, it would be important to study the applicability of the solvation theories in different dielectric media. An appropriate reaction for such study is the tautomeric equilibrium between acetylacetone (1) and its enol form (2)

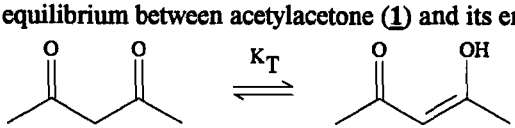

1 2 (15)

The experimental equilibrium constant of this reaction has been precisely measured using bromatometry and NMR spectroscopy [64] in the dioxane-water mixtures with a large variation of the dielectric constant of the medium, from pure dioxane ($\varepsilon = 2.209$) to water ($\varepsilon = 78.4$). It is obvious that the solute-solvent dispersion energy, the cavity formation free energy and the hydrogen bonding energy should be very similar for the two tautomeric forms. Therefore, the theoretical tautomeric equilibrium constant could be calculated from the following equation:

$$log K_T = \frac{\Delta G_T}{2.3RT} \approx \frac{E_{el}}{2.3RT} = \frac{\delta \Delta H}{2.3RT} \qquad (16)$$

where ΔG_T is the free energy of the tautomeric equilibrium and $\delta\Delta H$ is the difference in the calculated heats of formation of the tautomeric species participating in this equilibrium. An excellent agreement between the calculated and experimental $log K_T$ values in different media was obtained using self-consistent reaction field methods (cf. Table 2. and Figure 2.). Notably, the AM1 SCa SCRF and ECa SCRF results are practically identical.

Table 2.

AM1 SCa SCRF and ECa SCRF Calculated and Experimental $\log K_T$ of the Tautomeric Equilibrium (15) in Dioxane-Water Mixtures.

Dioxane (% by wt. in water)	ε	$\log K_T$ (SCa)	$\log K_T$ (ECa)	$\log K_T$ (exp)
0	78.4	-0.89	-0.85	-0.74
10	69.7	-0.66	-0.67	-0.66
20	61.0	-0.66	-0.63	-0.57
29	53.3	-0.61	-0.55	-0.50
39	44.5	-0.35	-0.32	-0.33
48	36.2	-0.26	-0.22	-0.22
58	28.3	0.12	-0.10	-0.10
67	21.2	0.14	0.12	0.06
78	10.8	0.22	0.20	0.16
87	7.6	0.27	0.29	0.33
100	2.209	0.55	0.61	0.67

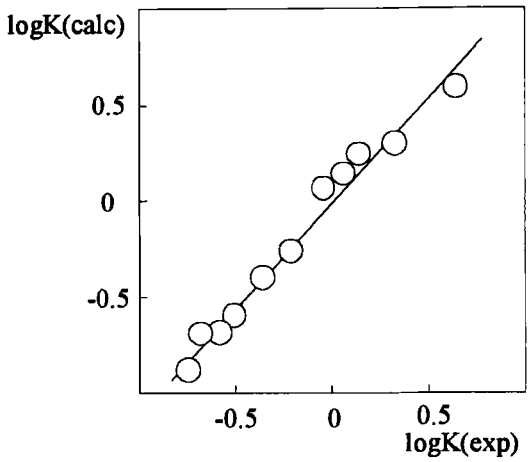

Figure 2. AM1 SCa SCRF Calculated *vs.* Experimental Tautomeric Equilibrium Constants logK for Acetylacetone in Different Dioxane/Water Mixtures.

4. Dipole moments and charge distribution.

In classical structural chemistry, the electronic structure of a molecule is assumed to be independent of the surrounding medium. The electrostatic solvation energy is correspondingly described as the interaction between the fixed charge distribution of the solute and the solvent. However, because of their close distance in condensed media, the intermolecular interactions can substantially affect the charge distribution of the molecules. As an example, the AM1 SCF and SCa SCRF calculated dipole moments of eight heterocyclic molecules, pyrrole (1), furan (2), pyrazole (3), isoxazole (4), 5(H)-3-pyrrolenone (5), 2(H)-3-furanone (6), 2(H)-3-pyrazolone (7), and 2(H)-3-isoxazolone (8), corresponding to the gas phase ($\varepsilon = 1$) and to the aqueous solution ($\varepsilon = 80$), are given in Table 3.

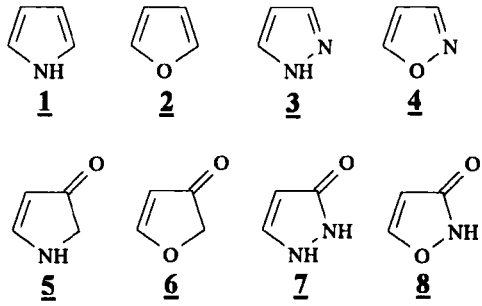

As a rule, the presence of a high dielectric constant medium leads to the rise of the dipole moment of the compound. However, the relative increase of the dipole moment varies substantially from one structure to another. For instance, the calculated dipole moment of 2(H)-3-pyrazolone (7) increases by 72% when transferred from the medium with $\varepsilon = 1$ to the medium with $\varepsilon = 80$, whereas the corresponding change in the dipole moment of pyrazole (3) is only 15%. Therefore, it is questionable to assume constant dipole moment values for a series of congeneric compounds in different dielectric media and derive correlations of the chemical reactivity or physical properties of such series of compounds with some fixed function of the dielectric constant of the solvent (a common approach in the linear free energy relationship studies of solvent effects, cf. [65-67]).

Table 3.

AM1 SCF and SCa SCRF Calculated Dipole Moments (*Debye*) of Some Heterocycles in Two Different Dielectric Media

ε	Molecule							
	1	2	3	4	5	6	7	8
1	1.95	0.49	2.11	1.85	3.81	2.41	3.81	3.43
80	2.30	0.57	2.43	2.04	6.32	3.03	6.57	4.14

Notably, the geometry of a molecule can be also substantially affected by a surrounding dielectric medium. For instance, the calculated carbonyl C–O bond length in 2(H)-3-pyrazolone (7) increases significantly in high dielectric constant medium (from 1.232 Å for the isolated molecule to 1.290Å for this molecule in a dielectric medium with $\varepsilon = 80$). This corresponds to a substantial increase of the weight of the polar resonance form in a high dielectric constant medium.

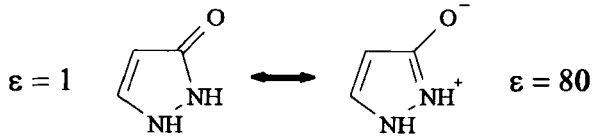

Correspondingly, the chemical reactivity of this compound is significantly altered in different dielectric media (e.g. gas phase and aqueous solution) [68].

5. Conclusions.

It is obvious that the surrounding environment can substantially affect both the chemical reactivity and physical properties of the chemical compounds dissolved in condensed media. However, the complexity of the solute-solvent interactions in condensed media requires the use of different physical models for the description of different interactions at quantum level. A combination of such models for the electrostatic, dispersion and hydrogen-bonding interactions together with the statistical physical treatment of the cavity formation free energy gives an insight to the relative importance of each of these interactions into the total solvation energy. Better quantitative and predictive results can be obtained in cases, when due to the nature of the phenomenon or process studied, the influence of one or more components of the solvation energy is negligible. Nonetheless, a general theory of solvation, applicable to any chemical structure and liquid, is still absent and leaves a challenging open field for the theoretical and physical chemists of next generations.

Acknowledgements.

We wish to thank Professor M.C. Zerner for valuable discussions. This work was supported by the Estonian Science Foundation Grant #230 and by the NSF Grant #CHE-93-12651.

References.

1. K.P. Lawley (Ed.), *Ab initio Methods in Quantum Chemistry*, Adv. Chem. Phys., vol. 58., 59., J. Wiley & Sons, Chichester, 1987.
2. W.J. Hehre, L. Radom, P.v.R. Schleyer, *Ab Initio Molecular Orbital Theory*, J. Wiley & Sons, New York, 1986.
3. E. Clementi and G. Corongiu, *Methods and Techniques in Computational Chemistry, METECC-95,* STEF, Cagliari, 1995.
4. E. Clementi, *Computational Aspects for Large Chemical Systems, Lecture Notes in Chemistry, vol 19.*, Springer-Verlag, Berlin, 1980.
5. S.Swaminathan, R.J Whitehead, E. Guth, and D.L. Beveridge, J. Am. Chem. Soc., **99**, 7817 (1976).
6. P. Čarsky and M. Urban, *Ab Initio Calculations*, Springer-Verlag, Berlin, 1980.
7. S.F. Boys and F. Bernardi, Mol. Phys., **19**, 553 (1970).

8. P. Arrighini, *Intermolecular Forces and Their Evaluation by Perturbation Theory, Lecture Notes in Chemistry, vol. 25*, Springer-Verlag, Berlin, 1981.
9. F.H. Stillinger, Adv. Chem. Phys., **31**, 1 (1975).
10. K. Heinzinger and P.C. Vogel, Z. Naturforsch., **29a**, 1164 (1974).
11. P.J. Rossky and M. Karplus, J. Am. Chem. Soc., **101**, 1913 (1979).
12. K. Binder (Ed.) *Monte Carlo Methods in Statistical Physics, Topics in Current Physics*, Springer-Verlag, vol. 7., Berlin, 1979.
13. C.J.F. Böttcher and P. Bordewijk, *Theory of Electric Polarization*, 2nd ed., vol. II, Elsevier Co, Amsterdam, 1978.
14. J. Tomasi, M. Persico,. Chem. Rev. **94**, 2027 (1994),.
15. R.J. Abraham, B.D. Hudson, M.W. Kermode, J.R. Mines, J. Chem. Soc. Farad. Trans. **84**, 1911 (1988).
16. J.G. Kirkwood, J. Chem. Phys., **2**, 351 (1934).
17. L. Onsager, J. Am. Chem. Soc., **58**, 1486 (1936).
18. J. Hylton, R.E. Christoffersen, and G.G. Hall, Chem. Phys. Lett., **26**, 501 (1974).
19. M.M. Karelson, Org. React. **17**, 357 (1980).
20. M.M. Karelson, Org. React., **17**, 366 (1980).
21. M.M. Karelson, Org. React., **20**, 132 (1983).
22. O.G. Parchment, I.H. Hillier, D.V.S. Green, N.A. Burton, J.O. Morley, and H.F. Schaefer, III, J. Chem. Soc. Perkin Trans. 2, 1681 (1992).
23. I.R. Gould, D.V.S. Green, P. Young, and I.H. Hillier, J. Org. Chem., **57**, 4434 (1992).
24. M.W. Wong, K.B. Wiberg, and M.J. Frisch, J. Am. Chem. Soc., **114**, 1645 (1992).
25. H. Ågren and K.V. Mikkelsen, J. Mol. Struct. (THEOCHEM), **80**, 425 (1991).
26. H. Ågren, S. Knuts, K.V. Mikkelsen, and H.J. Aa Jensen, Chem. Phys., **159**, 211 (1992).
27. K.V. Mikkelsen, P. Jorgensen and H.J. Aa Jensen, J. Chem. Phys., **100**, 6597 (1994).
28. M.M. Karelson, T. Tamm, A.R. Katritzky, S.J. Cato, and M.C. Zerner, Tetrahedron Comput. Methodol., **2**, 295 (1989).
29. M.M. Karelson, A.R. Katritzky, M. Szafran, and M.C. Zerner, J. Org. Chem., **61**, 6030 (1989).
30. M.M. Karelson, A.R. Katritzky, M. Szafran, and M.C. Zerner, J. Chem. Soc. Perkin Trans 2, 161 (1990).
31. A.R. Katritzky and M. Karelson, J. Am. Chem. Soc., **113**, 1561 (1991).
32. M. Karelson and M.C. Zerner, J. Phys. Chem., **92**, 6949 (1992).
33. M.M. Karelson, A.R. Katritzky, and M.C. Zerner, Int. J. Quant. Chem., **S20**, 521 (1986).

34. M.M. Karelson, T. Tamm, A.R. Katritzky, M. Szafran, and M.C.Zerner, Int. J. Quantum Chem., **37**, 1 (1990).
35. B.T. Thole and P.Th. van Duijnen, Theoret. Chim. Acta, **55**, 307 (1980).
36. R.R. Contreras and A.J. Aizman, Int. J. Quant. Chem., **S25**, 281 (1991).
37. T. Tamm and M. Karelson, Org. React., **26**, 211 (1989).
38. G.H.F. Diercksen, M. Karelson, T.Tamm and M.C. Zerner, Int. J. Quant. Chem., **S28**, 339 (1994).
39. S. Woodcock, D.V.S. Green, M.A. Vincent, I.H. Hillier, M.F. Guest, and P. Sherwood, J. Chem. Soc. Perkin Trans. 2, 2151 (1992).
40. M. Karelson and M.C. Zerner, J. Am. Chem. Soc., **112**, 9405 (1990).
41. M. Luhmer, M-L. Stien, and J. Reisse, Heterocycles, **37**, 1041 (1994).
42. R. Parrondo, P. Karafiloglou, R.R. Pappalardo, and E.Sanchez Marcos, J. Phys. Chem., **99**, 6461 (1995).
43. A. Broo, Chem. Phys., **169**, 135 (1993).
44. A. Broo, Chem. Phys., **169**, 151 (1993).
45. M. Karelson and A.R. Katritzky, ACH Models in Chemistry, **131**, 415 (1994).
46. P. Burk and M. Karelson, Proc. Acad. Sci. Est., Chem., **40**, 104 (1991).
47. U. Maran, T.A. Pakkanen, and M. Karelson, J. Chem. Soc. Perkin 2, 2445 (1994).
48. O Tapia and O. Goscinski, Mol. Phys. **29**, 1683 (1975).
49. J-L. Rivail and D. Rinaldi, Chem. Phys. **18**, 233 (1976).
50. N. Rösch and M.C. Zerner, J. Phys. Chem. **98**, 5817 (1994).
51. T. Abe, Y. Amako, T. Nishioka and H. Azumi, Bull. Chem. Soc. Jpn. **39**, 845 (1966).
52. H. Reiss, H.L. Frisch and J.L. Lebowitz, *J.* Chem. Phys. **31**, 369 (1959).
53. H. Reiss, Adv. Chem. Phys. **9**, 1 (1966).
54. R.M. Gibbons, Mol. Phys. **17**, 81 (1969).
55. *Gaussian 94, Revision B.1*, M.J. Frisch, G.W. Trucks, H.B. Schlegel, P.M. W. Gill, B.G. Johnson, M.A. Robb, J.R. Cheeseman, T. Keith, G.A. Petersson, J.A. Montgomery, K. Raghavachari, M.A. Al-Laham, V.G. Zakrzewski, J.V. Ortiz, J.B. Foresman, J. Cioslowski, B.B. Stefanov, A. Nanayakkara, M. Challacombe, C.Y. Peng, P.Y. Ayala, W. Chen, M.W. Wong, J.L. Andres, E.S. Replogle, R. Gomperts, R.L. Martin, D.J. Fox, J.S. Binkley, D.J. Defrees, J.Baker, J.P. Stewart, M. Head-Gordon, C. Gonzalez, and J.A. Pople, Gaussian, Inc., Pittsburgh PA, (1995).
56. R.W. Gurney, *Ions in Solution*, Dover Press, New York, 1962.
57. Y. Marcus, *Ion Solvation*, Wiley Interscience, Chichester, 1986.
58. G.A. Krestov, *Thermodynamics of Ion Solvation*, Ellis Horwood, New York, 1991.
59. R.C. Weast (Ed.) *Handbook of Chemistry and Physics*, 57th ed., CRC Press, Cleveland,1985.

60. M.J.S. Dewar, E.G. Zoebisch, E.F. Healy, and J.P. Stewart, J. Am. Chem. Soc., **107**, 3902 (1985).
61. J.J.P. Stewart, *MOPAC Program Package*, QCPE, No 455 (1989).
62. J. Ridley and M.C. Zerner, Theor. Chim. Acta, **32**, 111 (1973).
63. J. Hine and P.K. Mokerjee, J. Org. Chem., **40**, 292 (1975).
64. C.H. Lochmüller, T. Maldacker and M. Cefola, Anal. Chim. Acta **48**, 139 (1969).
65. C. Reichardt, *Solvents and Solvent Effects in Organic Chemistry,* 2nd ed., VCH, Weinheim, 1988.
66. J.J. Gajewski, J. Org. Chem. **57**, 5500 (1992).
67. M.H. Abraham, Theoret. Comput. Chem., **1**, 83 (1994).
68. A.R. Katritzky, *Handbook of Heterocyclic Chemistry,* Pergamon Press, London, 1985.
69. C. Cramer and D. Truhlar, in *Solvent Effects and Chemical Reactivity*, Ed. O. Tapia and J. Bertran, Kluwer, Dordrecht, 1995.
70. T. Tamm, K. Stavrev and M.C. Zerner, Int. J. Quant. Chem. Quant. Biol. Symp., **23**, (1996) in press.

Determining the Shapes of Molecular Electronic Bands from their Intensity Distribution Moments

Dorota Bielińska-Wąż and Jacek Karwowski

Instytut Fizyki, Uniwersytet Mikołaja Kopernika
ul. Grudziądzka 5/7, 87-100 Toruń, Poland

Abstract

Shapes of molecular electronic bands are studied using the methods of the statistical theory of spectra. It is demonstrated that while the Gram-Charlier and Edgeworth type expansions give a correct description of the molecular bands in the case of harmonic-oscillator-like potentials, they are inappropriate if departure from harmonicity is considerable. The cases considered include a set of analytically-solvable model potentials and the numerically exact potential of the hydrogen molecule.

ADVANCES IN QUANTUM CHEMISTRY, VOLUME 28

0065-3276/97 $25.00

1. Introduction

Statistical theories of spectra have been developed starting from several, rather diverse, motivations. Originally it was mainly applied in nuclear physics, where the unknown form of the interparticle interaction potentials stimulated the development of the so called *random matrix theory* (1 - 3). However already then it was noticed that very useful information about some global properties of spectra may be derived by applying the methods of statistical spectroscopy to systems for which the Hamiltonian matrix does not contain any randomness (1, 3). This gave a rise to the statistical theory of atomic spectra, developed into a powerful theoretical tool by the Bauches (4), Karazija (5) and others, to whose works references may be found in the papers quoted above. The most important advantage of this approach is a global description of the spectrum, in contrast to the level-by-level description of conventional methods. The methodology of statistical spectroscopy, in which the spectral density distribution moments appear as the basic quantities characterizing the spectrum, gives a relatively easy description of spectra consisting of very large numbers of transitions. In the case of atoms, it proved to be particularly useful for the interpretation of plasma emission and absorption spectra and for opacity calculations (4).

The methods of statistical spectroscopy are applicable where spectra consist of many lines and where the manifold of the quantum states involved may be described using a well defined finite-dimensional model space. Then the spectral density distribution moments are obtained as averages of powers of the pertinent Hamiltonian projected onto the model space. In the case of nuclei, the model space corresponds to a specific configuration of the nucleons. In the case of atoms - to a single or to several coupled electronic configurations. In the case of electronic transitions in molecules, the full configuration interaction space is the model space and only a very small fraction of the resulting states correspond to the molecular bound states. However the discrete spectrum of the electronic Hamiltonian in the model space may be used to simulate the molecular continuum and, consequently, used to describe the photoionization processes (6 - 11). In the case of vibronic molecular spectra, the manifold of the vibrational states associated with a given electronic state forms a space in which all (or at least many) states are physically meaningful. The first studies on statistical properties of vibrational spectra were published about a decade ago (12) and, since then, various aspects of this subject have been treated by many authors, as e.g. (13, 14).

In this paper we are concerned with determining the envelopes of the bands in vibronic spectra corresponding to transitions between two electronic states, from a knowledge of the intensity distribution moments. We develop here a method, formulated by Ivanov and Sovkov (15, 16) and,

independently, by the present authors (17 - 19), which may be considered as a modification of the approach used by Diercksen *et al.* to calculate the photoionization cross sections in molecules (6 - 11) and by the Bauches (4) to generate the envelopes of complex atomic spectra. In this method, first the moments of the transition energy distribution corresponding to the exact solutions of the pertinent quantum-mechanical model are evaluated and then, a smooth function for which the appropriate moments are equal to the "exact" ones is constructed. If p moments have been used in this procedure, then the smooth function gives us the p-moment approximation to the envelope of the spectrum.

The application of this method to systems described by one-dimensional potentials is particularly simple (15, 18). Therefore, in this paper, the feasibility and the accuaracy of the approach has been illustrated by considering transitions between states described by several exactly solvable one-dimensional models (20) and between $X\,^1\Sigma_g^+$ and $B\,^1\Sigma_u^+$ states of H_2 described by the numerically exact potentential energy curves (21). It results, that with a proper choice of the functional form of the envelope, already three-moment curves give a very accurate description of the band shape. For harmonic oscillators (22), the Gram-Charlier-type expansions (23) are very accurate. They are also rather good for the cases reasonably well approximated by harmonic-oscillator-type potentials (15, 18). However, if the departure from harmonicity is considerable, these kinds of expansions are inappropriate.

In the future development, the most important and interesting applications of this theory will be concerned with the molecular spectra obtained using potential energy surfaces derived from *ab initio* molecular structure calculations. The formal generalization of this approach to the cases of multidimensional potential hypersurfaces, is rather straightforward. However its implementation may be connected with some considerable computational effort, though much smaller than in the case of a detailed calculation of the spectrum.

This article is dedicated to Geerd Diercksen on his 60-th birthday. Apart of his works on the photoionization spectra of molecules (6 - 11), he has contributed to the development of the statistical theory of spectra publishing several studies on the application of the spectral density moments to checking correctness of the algorithms for construction of the operator matrices in the full CI spaces (24, 25) and a work on the dependence of the spectral density distributions upon the Hamiltonian (26). Some ideas of this paper have been developed in discussions with Geerd during visits of JK at the Molecular Astrophysics Group of the Max-Planck-Institut für Astrophysik in Garching and during a stay of DBW in this Group during summer 1993 as a TEMPUS student.

2. General Theory

Let $\mathcal{I}(E)$ be a function describing the intensity distribution of a molecular absorption or emission band associated with a given electronic transition. For simplicity we assume that the band has been normalized so that

$$\int_{-\infty}^{\infty} \mathcal{I}(E)dE = 1. \tag{1}$$

The q-th moment of this distribution is defined as (23, 4, 15, 18)

$$\mu_q[\mathcal{I}] = \int_{-\infty}^{\infty} \mathcal{I}(E)E^q \, dE. \tag{2}$$

According to the so called *principle of moments* (23), we expect that if we identify the lower moments of two distributions, we bring these distributions to approximate identity. Then, given p moments, one may approximate the corresponding (unknown) distribution by a trial function containing p adjustable parameters determined so that the lowest p moments calculated with this function are the same as the ones corresponding to the distribution. In this way one may determine a p-moment approximation $\mathcal{I}_p(E)$ to the distribution $\mathcal{I}(E)$. This kind of approach constitutes a base for numerous *methods of moments* known in many areas of physics and chemistry.

If the spectrum is discrete, the intensity distribution function may be represented as

$$\mathcal{I}(E) = \sum_n \mathcal{I}_n \, \delta(E - E_n), \tag{3}$$

where E_n is the transition energy and $\mathcal{I}_n$ is the intensity of the corresponding line. In this case Eq. (1) becomes

$$\sum_n \mathcal{I}_n = 1 \tag{4}$$

and Eq. (2) gives the following expression for the q-th intensity distribution moment

$$\mu_q[\mathcal{I}] = \sum_n \mathcal{I}_n \, (E_n)^q. \tag{5}$$

Let us assume that we are interested in the intensity distribution corresponding to transitions from the ground vibrational state $|v_0^i\rangle$ belonging to the initial electronic state $|\Psi_i\rangle$ to all vibrational states $|v_n^f\rangle$ associated with the final electronic state $|\Psi_f\rangle$. Then $\mathcal{I}_n$ is proportional to the corresponding transition probability and the proportionality factor may be determined from Eq. (4). In the dipole approximation,

$$\mathcal{I}_n = \frac{1}{w} |\langle v_0^i | \vec{\mathcal{M}}_i^f | v_n^f \rangle|^2, \tag{6}$$

where $\vec{\mathcal{M}}_i^f$ is the nuclear-coordinate-dependent electronic dipole transition moment and

$$w = \sum_n |\langle v_0^i|\vec{\mathcal{M}}_i^f|v_n^f\rangle|^2 = \langle v_0^i||\vec{\mathcal{M}}_i^f|^2|v_0^i\rangle. \tag{7}$$

The last equation is valid if the set $\{|v_n^f\rangle\}$ is complete. Assuming that

$$E_n = \mathcal{E}_n^f - \mathcal{E}_0^i = \langle v_n^f|\hat{H}_f - \mathcal{E}_0^i|v_n^f\rangle, \tag{8}$$

where $\hat{H}_f = \hat{T} + V_f$ is the nuclear motion Hamiltonian of the final electronic state and $\mathcal{E}$ stand for the energies of the appropriate states, after some manipulation (see (18) for details), one gets

$$\mu_q[\mathcal{I}] = \frac{1}{w}\langle v_0^i|\vec{\mathcal{M}}_i^f(\hat{H}_f - \mathcal{E}_0^i)^q\vec{\mathcal{M}}_i^f|v_0^i\rangle. \tag{9}$$

The last equation gives a recipe for an evaluation of the intensity distribution moments directly from the knowledge of $\hat{H}_f$, of the transition moment $\vec{\mathcal{M}}_i^f$ and of the initial state $|v_0^i\rangle$. Let us note that in order to evaluate the moments we do not need the wavefunctions of the final states, however we have to assume the closure relation, i.e. their effective completeness.

3. One-Dimensional Problems

In the one-dimensional cases, as e.g. in diatomic molecules, the vibrational wavefunctions of the initial (i) and of the final (f) states are eigenfunctions of the one-dimensional Schrödinger equation:

$$\left(-\frac{1}{2}\frac{d^2}{dQ^2} + V_t(Q) - \mathcal{E}_n^t\right)v_n^t(Q) = 0; \quad n = 0, 1, 2\ldots; \quad t = i, f. \tag{10}$$

For simplicity, the reduced mass of the particles and the Planck constant have been set equal to 1. Since $\vec{\mathcal{M}}_i^f$ is a function of Q, we can define

$$\tilde{V}_i(Q) = \frac{1}{2\tilde{v}_0^i}\frac{d^2\tilde{v}_0^i}{dQ^2} + \mathcal{E}_0^i \tag{11}$$

where $|\tilde{v}_0^i\rangle = |\vec{\mathcal{M}}_i^f||v_0^i\rangle$. Then, assuming $w = \langle\tilde{v}_0^i|\tilde{v}_0^i\rangle = 1$, we can rewrite Eq. (9) as

$$\mu_q[\mathcal{I}] = \langle\tilde{v}_0^i|[\tilde{H}(Q) + U]^q|\tilde{v}_0^i\rangle. \tag{12}$$

where $\tilde{H}(Q) = -\frac{1}{2}\frac{d^2}{dQ^2} + \tilde{V}_i(Q) - \mathcal{E}_0^i$ and $U = V_f(Q) - \tilde{V}_i(Q)$. With this definition of $\tilde{H}$ we have

$$\tilde{H}|\tilde{v}_0^i\rangle = 0. \tag{13}$$

Usually the potentials are given as numerical functions of the nuclear coordinates and all integrations have to be performed numerically. Though in the one-dimensional case the integration itself is quite trivial (the functions $\tilde{v}_0^i(Q)$ are nodeless), the evaluation of high-order derivatives may cause a considerable loss of the accuracy. Therefore it is essential that the moments are expressed so that they contain derivatives of the lowest possible order. In particular,the first four moments may be expressed as follows:

$$\begin{aligned}
\mu_1 &= \langle\tilde{v}_0^i|U|\tilde{v}_0^i\rangle, \\
\mu_2 &= \langle\tilde{v}_0^i|U^2|\tilde{v}_0^i\rangle, \\
\mu_3 &= \langle\tilde{v}_0^i|U^3|\tilde{v}_0^i\rangle + \frac{1}{2}\langle\tilde{v}_0^i|(U')^2|\tilde{v}_0^i\rangle, \\
\mu_4 &= \langle\tilde{v}_0^i|U^4|\tilde{v}_0^i\rangle + \frac{1}{4}\langle\tilde{v}_0^i|(U'')^2|\tilde{v}_0^i\rangle + 2\langle\tilde{v}_0^i|U(U')^2|\tilde{v}_0^i\rangle \\
&\quad + \langle(\tilde{v}_0^i)'|(U')^2|(\tilde{v}_0^i)'\rangle + \langle\tilde{v}_0^i|U'U''|(\tilde{v}_0^i)'\rangle,
\end{aligned} \tag{14}$$

where the primes stand for derivatives with respect to Q. Similar expressions for the higher moments are more complicated but their derivation is straightforward.

After the first p moments have been evaluated, the envelope $\mathcal{I}_p$ may be obtained by solving the following set of equations

$$\int_{E_{min}}^{E_{max}} \mathcal{I}_p(E)E^q dE = \mu_q, \quad q = 1, 2, \ldots, p \tag{15}$$

with the parameters defining $\mathcal{I}_p$ as the unknowns. In some cases applying the least-square procedure may be more appropriate.

The convergence pattern (in terms of p) of this procedure strongly depends upon the choice of the trial function $\mathcal{I}_p$. Since many distributions are related to the normal one, the trial functions of the Gram-Charlier-type (denoted here as $\mathcal{I}_p^G$) belong to those most frequently used. Besides, using these expansions leads to a very simple formalism (23). However the Gram-Charlier expansions, though highly flexible, are appropriate only if the intensity distributions behave asymptotically as $\exp(-cE^2)$. Besides, they are frequently divergent. Therefore, in this paper, we introduce a trial function

$$\mathcal{I}_3^D(E) \sim (E-\varepsilon)^\alpha \exp\{-[c(E-\varepsilon)]^\beta\}, \quad E \in <\varepsilon, \infty>, \tag{16}$$

with adjustable parameters c, α and β and ε and the proportionality factor determined by the normalization condition. The corresponding moments are equal to

$$\mu_q(\mathcal{I}_3^D) = \sum_{k=0}^{q} \binom{q}{k} \varepsilon^{q-k} \Gamma\left(\frac{\alpha+k+1}{\beta}\right) \Gamma\left(\frac{\alpha+1}{\beta}\right)^{-1} c^{-k}. \tag{17}$$

4. Results

Two sets of calculations have been performed. In the first one, a model potential

$$V^M(Q) = \frac{\omega^2}{2a^2}\tan^2 aQ, \quad -\frac{\pi}{2a} < Q < \frac{\pi}{2a}. \tag{18}$$

introduced recently in a study on spectra of luminescence centers in some solids (20) has been considered. It approaches the harmonic oscillator potential if $a \longrightarrow 0$ and its eigenvalue problem is analytically solvable.

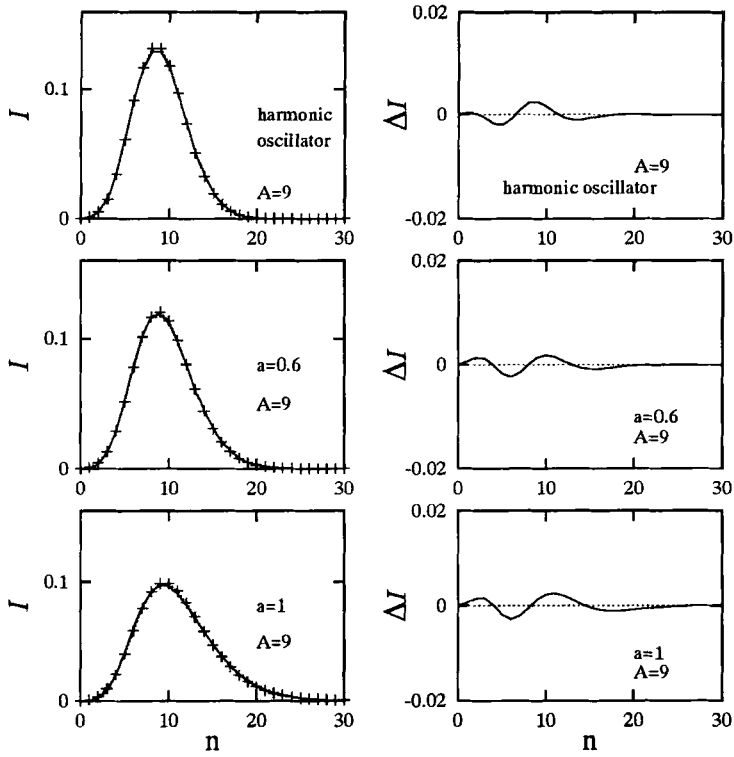

Figure 1: Envelopes $\mathcal{I}_3^D$ (solid lines) and the exact intensities (dotted lines) for the harmonic oscillators and for the model potentials defined in Eq. (18). On the right-hand-side the differences $\Delta\mathcal{I}$ between the exact and the evaluated intensities are shown.

Therefore this potential is particularly useful in model studies of the effects of a departure from harmonicity on spectra. As one can show, (18) the envelopes of the vibronic bands resulting from transitions between v_0^i corresponding to $V_i(Q) = V^M(Q)$ and v_n^f, $n = 0, 1, 2, \ldots$, corresponding to $V_f(Q) = V^M(Q - R)$ with $R - \frac{\pi}{2a} < Q < R + \frac{\pi}{2a}$ depend upon two parameters: $A = \omega R^2/2$ and a. The Gram-Charlier envelopes for these transitions have been reported in a previous paper (18). The envelopes obtained using the trial functions $\mathcal{I}_3^D$ are shown in Fig. 1. A comparison of the differences between the exact envelopes and the ones derived from $\mathcal{I}_3^G$ and from $\mathcal{I}_3^D$ is given in Fig. 2. Except for the harmonic oscillator, which is very well described in both cases, the envelopes derived from $\mathcal{I}_3^D$ are considerably better and the improvement increases with increasing departure from harmonicity.

In a second set of calculations we have studied two kinds of transitions in H_2 molecule: the absorption from the ground ro-vibrational state of $X\,^1\Sigma_g^+$ to all discrete levels of the first excited electronic state $B\,^1\Sigma_u^+$, and the emission from the ground ro-vibrational state of $B\,^1\Sigma_u^+$ to all discrete levels of the ground electronic state $X\,^1\Sigma_g^+$. The potentials and the transition moments have been taken from the numerically exact solutions of the electronic Schrödinger equation for H_2 obtained by Wolniewicz (21).

The value of ε (the limit of the envelope) has been put equal to the difference between the minimum of the potential energy curve of the final electronic state and the zeroth ro-vibrational energy of the initial electronic state. The other parameters defining the envelopes have been determined using the values of the first three moments, as defined in Eqs. (14). For the absorption $\varepsilon = 0.4081$ a.u., $\alpha = 2.682$, $c = 59.05$ a.u.$^{-1}$, $\beta = 1.1$. For the emission $\varepsilon = -0.4204$ a.u., $\alpha = 2.813$, $c = 9.978$ a.u.$^{-1}$, $\beta = 5.0$. The resulting standard deviations of the moment-determined intensities from the exact ones for the absorption and for the emission bands are, respectively, equal to 0.0019 and 0.0025. The absorption and the emission envelopes are compared with the exact intensities in Fig. 3. As one can see, in both cases the envelopes reproduce very well the shapes of the spectra. The Gram-Charlier results are very poor and are not displayed in the Figure. The standard deviations of the Gram-Charlier envelopes for $p = 2, 3, 4, 5$, in the case of the absorption, are equal to 0.007, 2.8, 0.8 and 0.4, respectively. The corresponding numbers for the emission are 0.008, 7.5, 4.5 and 4.6. The standard deviation of the four-moment Edgeworth distribution for the absorption is equal to 0.7 and for the emission – 12. Hence, the Gram-Charlier-type expansions are clearly divergent in this case.

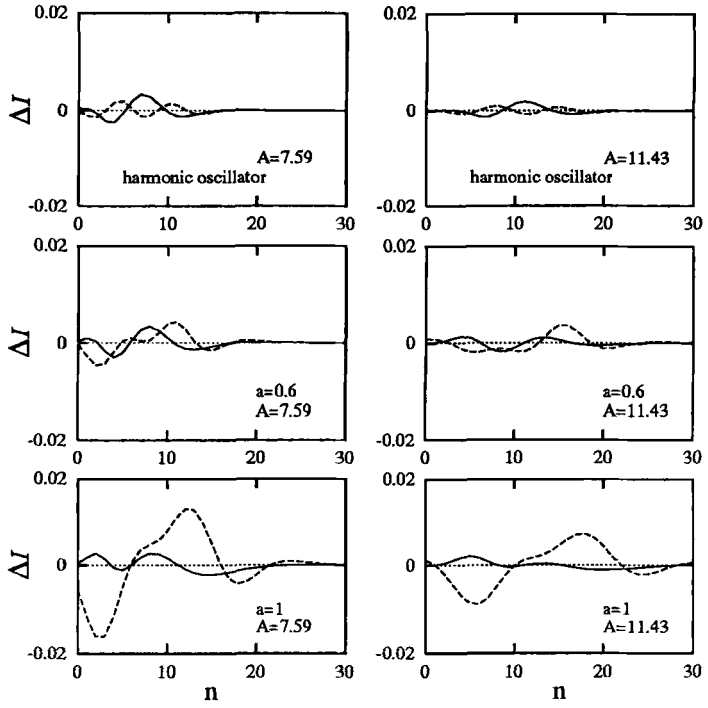

Figure 2: Differences between the exact and the evaluated intensities. The solid lines correspond to envelopes $\mathcal{I}_3^D$ and the broken lines to the Gram-Charlier ones.

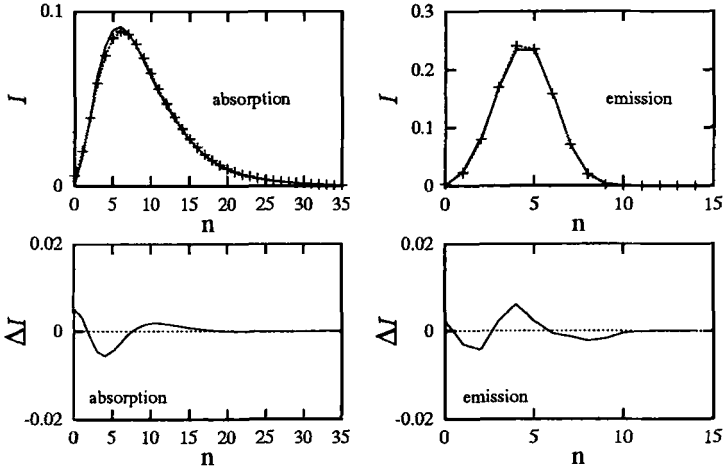

Figure 3: Envelopes $\mathcal{I}_3^D$ (solid lines) and the exact intensities (dotted lines) for $X\,^1\Sigma_g^+ \leftrightarrow B\,^1\Sigma_u^+$ transitions in H_2. Differences $\Delta\mathcal{I}$ between the exact and the evaluated intensities.

5. Summary

A method of determination of the envelopes of vibronic molecular spectra has been obtained by a generalization of a similar approach known in the atomic spectroscopy. Its application to diatomic molecules is very easy and has been illustrated by several examples. A simple way of taking into account the Q-dependence of the molecular transition moments has been described. The implementation of the method to more complex cases, involving multidimensional potential hypersurfaces, is straightforward though requires some numerical effort connected with the evaluation of multi-dimensional integrals.

6. Acknowledgements

The authors are indebted to F. Mrugała for several illuminating discussions, to L. Wolniewicz for supplying them with his H_2 computer code and to B. G. Wybourne for his critical reading the manuscript. The work has been supported by the Polish KBN, project No. 2 P03B 011 08.

References

(1) C. E. Porter, 1965 *Statistical Theories of Spectra: Fluctuations*, Academic, New York 1965.

(2) T. A. Brody, J. Flores, J. B. French, P. A. Mello, A. Pandey and S. S. M. Wong, Rev. Mod. Phys. **53**, 385 (1981).

(3) J. B. French and V. K. B. Kota, Ann. Rev. Nucl. Part. Sci., ed. J. D. Jackson (Palo Alto, CA: Annual Reviews 1982) p. 35.

(4) J. Bauche, C. Bauche-Arnoult and M. Klapisch, Adv. Atom. Molec. Phys. **23**, 132 (1988); J. Bauche and C. Bauche-Arnoult, Comp. Phys. Commun. **12**, 1 (1990); C. Bauche-Arnoult and J. Bauche, Physica Scripta **T40**, 58 (1992).

(5) R. Karazija, *Sums of Atomic Quantities and Mean Characteristics of Spectra*, Mokslas, Vilnius 1991, *in Russian.*

(6) G. H. F. Diercksen, W. P. Kraemer, T. N. Rescigno, B. V. McKoy, S. R. Langhoff and P. W. Langhoff, J. Chem. Phys. **76**, 1043 (1982).

(7) M. R. Hermann, G. H. F. Diercksen, B. W. Fatyga and P. W. Langhoff, Int. J. Quantum Chem. **18S**, 719 (1984).

(8) G. H. F. Diercksen and P. W. Langhoff, Chem. Phys. **112**, 227 (1987).

(9) G. H. F. Diercksen, M. R. Hermann, B. W. Fatyga and P. W. Langhoff, Chem. Phys. Letters **123**, 345 (1986).

(10) F. Müller-Plathe and G. H. F. Diercksen, Phys. Rev. A **40**, 696 (1989).

(11) F. Müller-Plathe and G. H. F. Diercksen, in *Proceedings of the 2-nd Brasilian School on Electronic Structure*, eds. F. Paixao, J. d'a Castro and S. Canuto, World Scientific, Singapore 1990, p. 1.

(12) E. Haller, H. Köppel and L. S. Cederbaum, Chem. Phys. Letters **101**, 215 (1983).

(13) R. Cimiraglia, A. Ferretti and N. K. Rahman, Chem. Phys. Letters **151**, 38 (1988) and references therein.

(14) M. Bancewicz, Chem. Phys. **203**, 93 (1996); J. Mol. Structure **356**, 231 (1955) and references therein.

(15) V. S. Ivanov and V. B. Sovkov, Opt. Spectrosc.**74**, 30, 52 (1993).

(16) M. S. Aleksandrov, V. S. Ivanov and V. B. Sovkov, Opt. Spectrosc.**74**, 42 (1993).

(17) J. Karwowski, Intern. J. Quantum Chem. **51**, 425 (1994).

(18) D. Bielińska-Wąż and J. Karwowski, Phys. Rev. **A 55** 1067 (1995).

(19) J. Karwowski, D. Bielińska-Wąż and J. Jurkowski, in *Symmetry & Structural Properties of Condensed Matter*, eds. T. Lulek, W. Florek and C. Wałcerz, World Scientific, Singapore 1995, p. 67.

(20) C. Zicovich - Wilson, J. Planelles, and W. Jaskólski, Intern. J. Quantum Chem. **50**, 429 (1994); M. Grinberg, W. Jaskólski, Cz. Koepke, J. Planelles, and M. Janowicz Phys. Rev. B **50**, 6504 (1994).

(21) L. Wolniewicz, J. Chem. Phys. **51**, 5002 (1969); **99**, 1851 (1993).

(22) C. Manneback, Physica, **17**, 1001 (1951).

(23) M. G. Kendall and A. Stuart, *The Advanced Theory of Statistics*, vol. 1 (Charles Griffin, London 1963).

(24) G. H. F. Diercksen and J. Karwowski, Comp. Phys. Commun. **47**, 83 (1987).

(25) G. H. F. Diercksen, W. Duch and J. Karwowski, Phys. Rev. A **41**, 3503 (1990).

(26) M. Bancewicz, G. H. F. Diercksen and J. Karwowski, Phys. Rev. A **40**, 5507 (1989).

Convergence of Symmetry-Adapted Perturbation Theory for the Interaction between Helium Atoms and between a Hydrogen Molecule and a Helium Atom

Tatiana Korona[1], Robert Moszynski[2], and Bogumił Jeziorski[3]

Department of Chemistry, University of Warsaw,
ul. Pasteura 1, 02-093 Warsaw, Poland

Abstract

Convergence properties of perturbation expansions for the interaction energy are investigated by performing high-order calculations for the interaction between helium atoms and between a hydrogen molecule and a helium atom. It is shown that for small intermonomer distances the standard Rayleigh-Schrödinger (polarization) expansion converges to a Pauli forbidden state of the dimer. At large separations the exchange component of the interaction energy is not recovered in a practically low order and an apparent convergence to the Coulomb part of the interaction energy is observed. The symmetrized Rayleigh-Schrödinger (SRS) theory provides in low order very accurate values of both the Coulomb and the exchange parts of the interaction energy for the physical, Pauli allowed state. In the region of the van der Waals minimum already the second-order treatment reproduces the full configuration interaction (FCI) energy with an error of a few percent. In very high orders the convergence of the SRS theory becomes extremely slow and the series appears to converge to a nonphysical limit very close to the exact interaction energy. The symmetry-adaptation characteristic of the Hirschfelder-Silbey (HS) theory is shown to correct this pathological behavior although the improved convergence is observed only in very high orders, so from the practical point of view the HS theory is not superior to the SRS approach. The HS series converges to the FCI interaction energy only if the latter is corrected for the basis set superposition error using the full counterpoise correction of Boys and Bernardi.

[1] tania@chem.uw.edu.pl, [2] rmoszyns@chem.uw.edu.pl, [3] jeziorsk@chem.uw.edu.pl

ADVANCES IN QUANTUM CHEMISTRY, VOLUME 28

0065-3276/97 $25.00

1. Introduction

Perturbation theory approach appears to be the most natural tool for theoretical investigations of weak intermolecular interactions (1). It provides the basis for present understanding of interactions between atoms and molecules, and defines the asymptotic constraints (via the multipole expansion (2, 3)) on the interaction potential. It is not surprising, then, that since the early 1970's the convergence properties of various perturbation expansions for the intermolecular interaction energies are subject of extensive theoretical studies (4)–(23).

It is known that the standard Rayleigh-Schrödinger (RS) perturbation theory (following Hirschfelder (24), referred to as the polarization approximation in this case) converges only asymptotically at large intermonomer distances R (15), and fails to reproduce in a finite order treatment those components of the dimer wave function which are due to the resonance tunneling of electrons between the interacting subsystems, *i.e.*, the components which make the total wave function of the dimer antisymmetric with respect to permutations of electrons between the interacting molecules.

Several symmetry-adapted perturbation theories (SAPT) have been proposed to remove the above deficiency (see Refs. (1, 15) for critical overviews). The existing SAPT approaches can be divided into two categories. In the first category, corresponding to the so-called *weak symmetry forcing* (10, 25), the antisymmetrizer appears only in the energy expressions. In the second class, corresponding to the *strong symmetry forcing* (10, 25) the symmetry operators enter the perturbation equations, complicating significantly their solution when the interacting monomers have more than two electrons.

Among various SAPT theories the symmetrized Rayleigh-Schrödinger (SRS) (10) and the Hirschfelder-Silbey (26) perturbation expansions were shown (15) to reproduce the correct asymptotics of the interaction energy and the correct form of the asymptotic expansion of the wave function (27). The so-called MSMA theory (28)–(30) also gives the correct asymptotics of the interaction energy (15) but it does not represent an improvement over the SRS theory. Despite some additional complications, the MSMA expansion is divergent even for the simplest *ungerade* states of H_2^+ and H_2 (10, 11, 22), while the SRS expansion remains convergent in these cases. For this reason the MSMA scheme will not be considered in the present paper.

The SRS perturbation theory is the simplest of all SAPT expansions proposed thus far, and in view of numerous recent applications to complexes of direct experimental interest (see Refs. (1, 31) for reviews) it is important to study the convergence properties of this expansion, and its applicability in low orders to interactions of many-electron systems. When

the strength of the perturbation is large (*e.g.*, at small intermonomer separations), the symmetry forcing characteristic to the SRS scheme may not be sufficient to ensure convergence in low orders, and an application of the HS theory may be necessary. Thus, the convergence properties of this expansion are also of interest. In particular, it is important to check whether the strong symmetry forcing employed in the HS approach leads to a better convergence in low orders.

Until now, the convergence of the SRS and HS expansions has been studied only for model one- and two-electron systems ($2p\sigma_u$ state of H_2^+ (9)–(11) and $b^3\Sigma_u^+$ state of H_2 (21, 22)). Both expansions were shown to converge satisfactorily for the investigated cases (10, 21). Unfortunately, an extrapolation of the convergence properties from the results for one and two-electron systems to real many-electron case is not straightforward. When at least three electrons are present the asymptotically degenerate states, which one has to simultaneously consider, include unphysical, Pauli-forbidden, states (4, 12), and it is not *a priori* clear if a given perturbation expansion will converge to a physical solution of the Schrödinger equation, or will be divergent.

In the present paper we investigate the convergence properties of the RS, SRS, and HS perturbation series for He_2 and HeH_2 molecules, *i.e.* for the interaction of two ground-state two-electron systems. These perturbation formalisms correspond to none, weak, and strong symmetry forcing, respectively. In Sec. II the perturbation equations of the RS, SRS, and HS theories are briefly summarized. In Sec. III the computational details of the calculations are presented. The numerical results are presented and discussed in Sec. IV.

2. Method

We consider the interaction of two closed-shell systems A and B. When the interaction between the monomers is neglected, the complex AB is described by the Hamiltonian $H_0 = H_A + H_B$, where H_A and H_B denote Hamiltonians for the monomers A and B, respectively. The corresponding wave function Ψ_0 and energy E_0 can be simply expressed in terms of wave functions and energies of the unperturbed monomers:

$$\Psi_0 = \Psi_A \Psi_B, \qquad E_0 = E_A + E_B, \tag{1}$$

where E_X and Ψ_X denote the ground state eigenvalue and eigenfunction of H_X, $X = A$ or B. When the interaction is switched on, the total Hamiltonian H for the dimer AB can be written as,

$$H = H_0 + V, \tag{2}$$

where the perturbation operator V collects all Coulombic potentials corresponding to interactions between electrons and nuclei associated with the monomer A on one side and those associated with the monomer B on the other. We will assume that the Hamiltonians H_A and H_B act on the coordinates of electrons 1, 2 and 3, 4, respectively. This means that the electrons 1 and 2 are assigned to the monomer A and the electrons 3 and 4 to the monomer B.

To define the perturbation expansions corresponding to various SAPT formalisms, it is useful to introduce a general concept of the *interpolation function* ${}^{\nu}\epsilon(\zeta)$ defined such that (11):

$$ {}^{\nu}\epsilon(0) = 0, \qquad {}^{\nu}\epsilon(1) = {}^{\nu}E_{\rm int}, \tag{3}$$

where the index ν labels the permutational symmetry of the state of interest at $\zeta = 1$. The perturbation expansion corresponding to a given symmetry adaptation scheme is then defined as a power series expansion of ${}^{\nu}\epsilon(\zeta)$,

$$ {}^{\nu}\epsilon(\zeta) = \sum_{n=1}^{\infty} \zeta^n \ {}^{\nu}E^{(n)}, \tag{4}$$

while the interaction energy ${}^{\nu}E_{\rm int}$ is obtained by summing the expansion (4) at $\zeta = 1$.

A general expression for interpolation functions corresponding to various symmetry adaptation schemes has been given in Ref. (11), and can be written as,

$$ {}^{\nu}\epsilon(\zeta) = \zeta \frac{\langle \Psi_0 | V \ {}^{\nu}\mathcal{G} \ {}^{\nu}\Psi(\zeta) \rangle}{\langle \Psi_0 | \ {}^{\nu}\mathcal{G} \ {}^{\nu}\Psi(\zeta) \rangle}, \tag{5}$$

where the wave function ${}^{\nu}\Psi(\zeta)$ is a solution of the equation,

$$ {}^{\nu}\Psi(\zeta) = \Psi_0 + R_0({}^{\nu}\epsilon(\zeta) - \zeta V) \ {}^{\nu}\mathcal{F} \ {}^{\nu}\Psi(\zeta), \tag{6}$$

subject to intermediate normalization condition $\langle \Psi_0 | \ {}^{\nu}\Psi(\zeta) \rangle = 1$, R_0 is the reduced resolvent of the Hamiltonian H_0, and ${}^{\nu}\mathcal{G}$ and ${}^{\nu}\mathcal{F}$ are operators enforcing the proper permutational symmetry.

When ${}^{\nu}\mathcal{G} = {}^{\nu}\mathcal{F} = 1$, *i.e.*, when no symmetry is enforced, the Taylor expansion of Eqs. (5) and (6) defines the Rayleigh-Schrödinger perturbation equations,

$$ \Psi_{\rm pol}^{(n)} = R_0(E_{\rm pol}^{(1)} - V)\Psi_{\rm pol}^{(n-1)} + \sum_{k=2}^{n-1} E_{\rm pol}^{(k)} R_0 \Psi_{\rm pol}^{(n-k)}, \tag{7}$$

$$ E_{\rm pol}^{(n)} = \langle \Psi_0 | V \Psi_{\rm pol}^{(n-1)} \rangle, \tag{8}$$

where, obviously, $E_{\rm pol}^{(n)}$ and $\Psi_{\rm pol}^{(n)}$ denote the perturbation corrections to the energy and wave function in the polarization approximation, and $\Psi_{\rm pol}^{(0)} \equiv \Psi_0$.

In the SRS perturbation theory the symmetry forcing operator appears only in the energy expression. Thus, in this formalism ${}^{\nu}\mathcal{F} = 1$ and ${}^{\nu}\mathcal{G} = {}^{\nu}\mathcal{A}$, where ${}^{\nu}\mathcal{A}$ is the projection operator on the appropriate representation of the symmetric group S_4. Moreover, the interpolation function ${}^{\nu}\epsilon(\zeta)$ appearing in Eq. (6) is not calculated from Eq. (5) but is taken directly from the RS theory (10, 21). The SRS perturbation corrections to the interaction energy, ${}^{\nu}E_{\rm SRS}^{(n)}$, are given by,

$$ {}^{\nu}E_{\rm SRS}^{(n)} = {}^{\nu}N_0[\langle\Psi_0|V\,{}^{\nu}\mathcal{A}\Psi_{\rm pol}^{(n-1)}\rangle - \sum_{k=1}^{n-1} {}^{\nu}E_{\rm SRS}^{(k)}\langle\Psi_0|\,{}^{\nu}\mathcal{A}\Psi_{\rm pol}^{(n-k)}\rangle], \qquad (9) $$

where ${}^{\nu}N_0 = \langle\Psi_0|\,{}^{\nu}\mathcal{A}\Psi_0\rangle^{-1}$.

The symmetry forcing employed in the Hirschfelder-Silbey theory is somewhat more complicated. In this approach, one simultaneously considers all eigenfunctions of the Hamiltonian H which are asymptotically degenerate with the physical solution of the Schrödinger equation for the dimer, *i.e.*, one considers the functions ${}^{\nu}\Psi$ with symmetry labels $\nu = 1, \ldots, f$ corresponding to all irreducible representations (irreps) of S_4 entering the induced product $[2] \otimes [2] \uparrow S_4$ (the spatial part of the zeroth-order wave function for He_2 and HeH_2 transforms according to the $[2] \otimes [2]$ representation of $S_2 \otimes S_2$). The corresponding symmetry forcing operators, given in Ref. (25), are ${}^{\nu}\mathcal{G} = {}^{\nu}\mathcal{F} = {}^{\nu}\mathcal{K}$, where

$$ {}^{\nu}\mathcal{K}({}^{1}\Psi, \ldots, {}^{f}\Psi) = {}^{\nu}\mathcal{A}\sum_{\mu=1}^{f} {}^{\mu}\Psi. \qquad (10) $$

Note that the symmetry forcing operator of the HS theory acts on f functions ${}^{\mu}\Psi$, *i.e.*, may be viewed as a (linear) function of f variables. Expanding Eqs. (5) and (6) in powers of ζ one obtains the following equations for the HS perturbation energies

$$ {}^{\nu}E_{\rm HS}^{(n)} = {}^{\nu}N_0[\langle\Psi_0|V\,{}^{\nu}\mathcal{A}F^{(n-1)}\rangle - \sum_{k=1}^{n-1} {}^{\nu}E_{\rm HS}^{(k)}\langle\Psi_0|\,{}^{\nu}\mathcal{A}F^{(n-k)}\rangle], \qquad (11) $$

$$ (H_0 - E_0)F^{(n)} = -VF^{(n-1)} + \sum_{k=1}^{n}\sum_{\nu=1}^{f} {}^{\nu}E_{\rm HS}^{(k)}\,{}^{\nu}\mathcal{A}F^{(n-k)}, \qquad (12) $$

where

$$ F^{(n)} = \frac{1}{f}\sum_{\mu=1}^{f} {}^{\mu}\Psi^{(n)}. \qquad (13) $$

For the interaction of two closed-shell two-electron monomers, the symmetry labels appearing in Eqs. (11) and (12) can be deduced from the induced product decomposition,

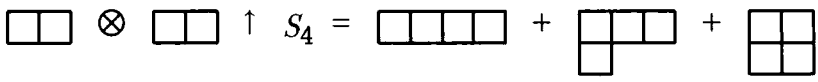

i.e., they correspond to the following irreps of S_4: [4] (the mathematical ground state), [31], and [2^2] (the physical ground state).

The definitions of the perturbation corrections to the interaction energy, as given by Eqs. (8), (9), and (11), involve *nonsymmetric* operators, like H_0, V, and R_0. These operators do not include all electrons in a fully symmetric way, so H_0, V, and R_0 must act in a larger space than the dimer Hilbert space $\mathcal{H}_{AB}$ adapted to a specific irrep of S_4. To use these operators we have to consider the space $\mathcal{H}_A \bigotimes \mathcal{H}_B$, the tensor product of Hilbert spaces $\mathcal{H}_A$ and $\mathcal{H}_B$ for the monomers A and B. For the interaction of two closed-shell two-electron systems this tensor product space should be adapted to the irreps of the $S_2 \otimes S_2$ group. In most of the quantum chemical applications the Hilbert spaces $\mathcal{H}_X$, $X = A$ and B, are constructed from one-electron spaces of finite dimension $\mathcal{L}_X$. In the particular case of two-electron systems in singlet states we have: $\mathcal{H}_X = \mathcal{L}_X \textcircled{S} \mathcal{L}_X$, where the symbol $\textcircled{S}$ denotes the symmetrized tensor product. We define the one-electron space $\mathcal{L}$ as the space spanned by the union of two atomic bases associated with the monomers in the dimer. The basis of the space $\mathcal{L}$ includes functions centered on all atoms in the dimer and, consequently, will be referred to as the *dimer-centered basis*. We assume that the same one-electron space $\mathcal{L}$ is used to construct the Hilbert spaces $\mathcal{H}_X$, $X = A$ and B, *i.e.*, $\mathcal{H}_X = \mathcal{L} \textcircled{S} \mathcal{L}$. In such case $\mathcal{H}_A \bigotimes \mathcal{H}_B$ can be represented as a direct sum of Hilbert spaces $\mathcal{H}_\nu$ adapted to the irreps entering the induced product $[2] \otimes [2] \uparrow S_4$, *i.e.*, $\mathcal{H}_A \bigotimes \mathcal{H}_B = \mathcal{H}_{[2^2]} \bigoplus \mathcal{H}_{[31]} \bigoplus \mathcal{H}_{[4]}$. This means that every function from $\mathcal{H}_\nu$, $\nu = [2^2]$, [31], or [4], can be expanded in terms of functions from $\mathcal{H}_A \bigotimes \mathcal{H}_B$.

In practice the perturbation equations are solved in a finite basis of suitably chosen configuration functions. It is well known (9) that SAPT expansions can converge to the variational energy obtained by minimizing the Rayleigh-Ritz functional within the space spanned by the configuration functions used in the perturbation calculations if and only if this set of configuration functions is stable under the symmetry projections ${}^{\nu}\mathcal{A}$. This condition is fulfilled when the atomic basis used to construct $\mathcal{H}_A$ and $\mathcal{H}_B$ is the full basis of the dimer. The eigenvalues (*i.e.* monomer energies) and the eigenfunctions of H_0 are then calculated in the dimer-centered basis. Thus, a perturbation theory in a finite basis can possibly converge only to the supermolecular interaction energy computed using the so-called

Boys-Bernardi counterpoise correction for the basis set superposition error (BSSE) (32). This means that the use of the Boys-Bernardi counterpoise correction is legitimate, in full agreement with the theoretical arguments and numerical results of Refs. (33)–(40).

In actual calculations for He_2 and HeH_2 we used configuration basis functions of the form,

$$\Psi_{klmn} = N_{kl}N_{mn}(1+P_{12})(1+P_{34})\psi_k(1)\psi_l(2)\psi_m(3)\psi_n(4), \qquad (14)$$

where P_{ij} permutes the spatial coordinates of electrons i and j, ψ_k and ψ_l (ψ_m and ψ_n) denote the Hartree-Fock orbitals of the monomer A (B) computed in the full basis of the dimer, and $N_{kl} = [2(1+\delta_{kl})]^{-1/2}$. The functions transforming according to [4], [31], and [2^2] irreps of S_4 can be obtained by applying the projection operators ${}^{\nu}\mathcal{A}$, $\nu = [4], [31], [2^2]$. The dimension of the tensor product space $\mathcal{H}_A \bigotimes \mathcal{H}_B$ is $M^2(M+1)^2/4$, while the dimensions of the spaces $\mathcal{H}_{[2^2]}$, $\mathcal{H}_{[31]}$, and $\mathcal{H}_{[4]}$ are $M^2(M^2-1)/12$, $M(M+2)(M^2-1)/8$, and $M(M+1)(M+2)(M+3)/24$, respectively, where M is the dimension of the orbital basis used to construct $\mathcal{H}_A$ and $\mathcal{H}_B$.

The projection operators ${}^{\nu}\mathcal{A}$ acting in $\mathcal{H}_A \bigotimes \mathcal{H}_B$ can be expressed via the single exchange ($\mathcal{P}_1$) and double exchange ($\mathcal{P}_2$) operators,

$$\mathcal{P}_1 = P_{13} + P_{24} + P_{14} + P_{23}\,, \qquad (15)$$

$$\mathcal{P}_2 = P_{13}\,P_{24}\,. \qquad (16)$$

Explicit expressions for ${}^{\nu}\mathcal{A}$, $\nu = [4], [31]$, and $[2^2]$, can be written as,

$${}^{1}\mathcal{A} = \tfrac{1}{6}(1+\mathcal{P}_1+\mathcal{P}_2) \quad \text{for} \quad [4]\,, \qquad (17)$$

$${}^{2}\mathcal{A} = \tfrac{1}{2}(1-\mathcal{P}_2) \quad \text{for} \quad [31]\,, \qquad (18)$$

$${}^{3}\mathcal{A} = \tfrac{1}{6}(2-\mathcal{P}_1+2\mathcal{P}_2) \quad \text{for} \quad [2^2]. \qquad (19)$$

3. Computational Details

High-order calculations of the RS, SRS, and HS interaction energies of He_2 and HeH_2 molecules were performed using a computer code specific for the interaction of two ground-state two-electron monomers. The perturbation corrections were calculated with finite basis sets from matrix equations obtained by converting Eqs. (7)–(9), (11), and (12) to the matrix form (*cf.* Refs. (9, 10)). Adaptation of the program to the symmetry of the point group C_{2v} reduced the number of configuration functions approximately by a factor of 4. This allowed us to perform high-order calculations in reasonably large basis sets (up to 102 orbitals). For the interaction of two helium atoms we used three basis sets: a $[7s3p2d1f]$ basis centered on the

nuclei – denoted by B66, a superposition of the B66 basis and a $[2s1p]$ basis centered on the midbond – denoted by B71, and a moderately large basis, denoted by B102, consisting of a $[7s5p3d1f]$ set centered on the nuclei and a $[3s2p1d]$ set centered on the midbond. The isotropic part of these basis sets was represented by a $7s$ contraction of the $16s$ basis set of Partridge (41). The nuclei-centered polarization part of the B71 basis consisted of two functions of p symmetry (3.04717, 0.759122) and one function of d symmetry (1.95910) with exponents optimized for the intra-atomic correlation (39), and one function of p symmetry (0.19427), one function of d symmetry (0.22896), and one function of f symmetry (0.18360) with exponents optimized for the dispersion energy (42). The basis centered on the midbond consisted of the two second most diffuse Partridge functions ($2s$ part) and one p function (0.5). The polarization part of the basis B102 was taken from Ref. (42). The midbond part consisted of the $3s2p$ set taken from the two second most diffuse functions of the nuclei-centered basis set and of one function of d symmetry (0.5). For the helium atom interacting with the hydrogen molecule we considered two basis sets. The small B44 basis consisted of a $[5s3p1d]$ basis on helium (43), and a $[4s2p]$ basis on hydrogen (44) supplemented with two s functions (0.2, 0.4) and one p function (0.3) centered on the midbond. The larger B83 basis was taken from Tao's paper (45) (in Ref. (45) this basis is denoted by $[6s4p] - \{3s3p2d1f\}$).

ATMOL package (46) was used to generate integrals in the atomic basis and the SCF vectors for the monomers. The integrals were transformed to the Hartree-Fock basis using the four-index transformation from the SAPT suite of codes (47). The program LUCIA from the MOLCAS package (48) and the Harrison-Zarrabian code (49) interfaced with ATMOL suite of programs were used to calculate supermolecular FCI interaction energies. The FCI interaction energies were corrected for BSSE using the counterpoise correction of Boys and Bernardi.

4. Numerical Results and Discussion

The convergence properties of the perturbation expansions considered in the previous section have been tested by performing large-order numerical calculations. Perturbation corrections to the interaction energy of He_2 and HeH_2 have been calculated up to and including the 50th order. For He_2 three interatomic distances have been considered: $R = 4$ bohr, $R = 5.6$ bohr, and $R = 7$ bohr. These separations correspond to the repulsive region, the van der Waals minimum, and the long-range attractive region in the He_2 interaction potential. In addition, for He_2 Rayleigh-Schrödinger perturbation theory calculations at $R = 1$ bohr were performed. The convergence of the SRS expansion for HeH_2 was studied only at $R = 6.5$ bohr,

i.e., in the region of the van der Waals minimum (R denotes here the distance between the helium atom and the center of mass of H_2). Additionally, we have looked at the convergence of the SRS series for different values of the angle θ between the line defined by the hydrogen atoms (separated by 1.449 bohr) and the vector joining the helium atom and the center of mass of H_2 ($\theta = 0°$ corresponds to the linear configuration). In this way we could check how well the SRS formalism reproduces the anisotropy of the interaction potential.

Table 1: Convergence of the Rayleigh-Schrödinger perturbation expansion for the interaction of two ground-state helium atoms at $R = 1.0$ and 5.6 bohr. The variational interaction energies of the fully symmetric state are equal to −1.01904 hartree and −166.5301 μhartree, respectively. The Coulomb energy for $R = 5.6$ bohr is equal to −77.4764 μhartree. The B66 and B71 basis sets were used for distances 1.0 and 5.6 bohr, respectively. $\Sigma(n)$ denotes the sum of perturbation corrections up to and including the nth-order and $\delta(n)$ the percent error of $\Sigma(n)$ with respect to the variational interaction energy. Energies are in hartree for $R = 1$ bohr, and in μhartree for $R = 5.6$ bohr.

	$R = 1.0$ bohr		$R = 5.6$ bohr	
n	$\Sigma(n)$	$\delta(n)$	$\Sigma(n)$	$\delta(n)$
1	−0.0822	−91.93	−5.510	−96.69
2	−0.4665	−54.22	−75.244	−54.82
3	−0.6299	−38.19	−74.668	−55.16
4	−0.7605	−25.37	−75.651	−54.57
5	−0.8446	−17.11	−76.042	−54.34
6	−0.9063	−11.07	−76.383	−54.13
7	−0.9478	−6.99	−76.632	−53.98
8	−0.9768	−4.14	−76.824	−53.87
9	−0.9959	−2.27	−76.972	−53.78
10	−1.0082	−1.06	−77.087	−53.71
15	−1.0226	0.35	−77.373	−53.54
20	−1.0200	0.09	−77.458	−53.49
25	−1.0191	0.00	−77.485	−53.47
30	−1.0190	−0.01	−77.495	−53.46
40	−1.0190	−0.00	−77.503	−53.46
50	−1.0190	0.00	−77.507	−53.46

We start the presentation of our results with the Rayleigh-Schrödinger perturbation theory. The results presented in Table 1 show that for small interatomic distances the RS perturbation expansion converges to the energy of the mathematical ground state of the dimer. This state is a Pauli forbidden solution of the Schrödinger equation, completely symmetric un-

der the exchange of spatial coordinates of electrons. At large R this solution is quasidegenerate with the physical ground state. The observed convergence pattern of the polarization expansion was predicted by Claverie 25 years ago (4). Claverie carried out an analysis of the permutation symmetry of the He_2 wave functions and found that only the fully symmetric, nodeless solution of the Schrödinger equation can correlate at $\zeta = 1$ with the unperturbed wave function at $\zeta = 0$ and, consequently, can be the limit of the RS perturbation series.

At distances corresponding to the van der Waals minimum the situation is different. Initially, the sum of the series approaches fast the Coulomb energy, Q, defined as,

$$Q = \frac{\sum_\nu f_\nu \, {}^\nu E_{\rm int}}{\sum_\nu f_\nu}, \tag{20}$$

where f_ν is the degeneracy of the state labeled by ν. After the value of the Coulomb energy is reproduced to a very good accuracy, the convergence deteriorates drastically and becomes extremely slow. Although the series do converge, the exchange part of the interaction energy is not recovered in a finite order. Indeed, an inspection of Table 1 shows that the sum of the perturbation series through the 20th order represents 99.98% of the Coulomb energy, while $E_{\rm pol}^{(21)} + \cdots + E_{\rm pol}^{(50)}$ reproduces only $\simeq 0.05\%$ of the exchange energy, ${}^1K$,

$${}^1K = {}^1E_{\rm int} - Q, \tag{21}$$

where ${}^1E_{\rm int}$ is the interaction energy for the mathematical ground state of He_2.

It is worth noting that the convergence pattern of the polarization series for He_2 is very similar to that found for H_2^+ (9) and H_2 (18). Thus, at the distances of the van der Waals minimum the Rayleigh-Schrödinger perturbation theory provides only a part of the interaction energy (15), and in practical applications symmetry-adapted perturbation formalisms must be used.

High-order SRS calculations are very computer time demanding if large basis sets are employed. The use of large basis sets is, however, necessary to check whether the observed convergence pattern persists in the limit of a complete basis. In the present paper high-n SRS and HS corrections to the interaction energy of the He dimer have been computed with the B71 basis. This basis reproduces 94% of the saturated value of the He_2 interaction potential at the minimum (50). To check the basis set dependence of the convergence pattern of the SRS series, we performed additional calculations in the B102 basis. The FCI interaction energy in this basis is rather close to the best theoretical value, and represents 98% of the exact result (50).

The results presented in Table 2 show that the convergence pattern of the SRS expansion for He_2 is rather basis set independent. Except for the

Table 2: Basis set dependence of the SRS interaction energy for the ground-state of a helium dimer at $R = 5.6$ bohr. $\Sigma(n)$ and $\delta(n)$ are defined as in Table 1. Energies are in μhartree.

	B71		B102	
n	$\Sigma(n)$	$\delta(n)$	$\Sigma(n)$	$\delta(n)$
2	-32.899	-0.11	-34.520	0.37
3	-31.976	-2.91	-33.382	-2.94
4	-32.442	-1.50	-33.914	-1.40
5	-32.533	-1.22	-33.987	-1.18
6	-32.635	-0.91	-34.094	-0.87
7	-32.704	-0.70	-34.162	-0.67
8	-32.758	-0.54	-34.217	-0.52
9	-32.798	-0.42	-34.257	-0.40
10	-32.829	-0.32	-34.288	-0.31
FCI	-32.935		-34.394	

second order the error of an nth order calculation remains approximately constant. The large difference in the second order is of no practical importance, since the error is anyway very small. It is worth noting that this error remains very small also in larger bases, *e.g.*, in basis sets of 147 and 159 functions it amounts to 0.52% and 0.48%, respectively (51).

The results of large-order calculations of the He_2 interaction energy at various R are presented in Table 3. Our numerical results clearly show that the SRS method is quite effective. Around the van der Waals minimum the convergence is fast and the error of the 10th order treatment amounts to -0.3%. Only at smaller distances this good convergence deteriorates somewhat, but even in this region the sum of SRS corrections through the 45th order reproduces the interaction energy within 0.06%.

It should be noted that the SRS expansion converges to an energy slightly different from the true physical value. As discussed in Refs. (10) and (21) the difference between the actual limit of the SRS expansion and the true interaction energy is the so-called residual exchange energy. An inspection of Table 3 shows that even in the repulsive region the residual exchange energy is smaller than 0.07% of the physical interaction energy.

In practical calculations for many-electron systems the SRS theory can be applied only through low order in V. Therefore, it is important to establish how much the low-order SRS energies differ from the low-order energies of the HS theory. The latter approach is free from the residual-exchange pathology and is expected to converge fast in high orders. As the results of Table 3 demonstrate, the SRS and HS energies are very close to

Table 3: Convergence of the symmetrized Rayleigh-Schrödinger and Hirschfelder-Silbey perturbation expansions for the interaction of two ground-state helium atoms at various interatomic distances. The B71 basis set was used. $\Sigma(n)$ and $\delta(n)$ are defined as in Table 1. Energies are in μhartree.

	$R = 4.0$ bohr		$R = 5.6$ bohr				$R = 7.0$ bohr	
n	$\Sigma(n)^a$	$\delta(n)^a$	$\Sigma(n)^a$	$\delta(n)^a$	$\Sigma(n)^b$	$\delta(n)^b$	$\Sigma(n)^a$	$\delta(n)^a$
2	1034.46	8.095	−32.899	−0.110	−32.899	−0.109	−14.450	0.545
3	1030.05	7.635	−31.976	−2.911	−31.977	−2.908	−14.341	−0.213
4	1009.45	5.482	−32.442	−1.498	−32.443	−1.495	−14.364	−0.055
5	998.71	4.359	−32.533	−1.222	−32.534	−1.218	−14.364	−0.053
6	989.81	3.430	−32.635	−0.913	−32.636	−0.909	−14.366	−0.037
7	983.05	2.724	−32.704	−0.702	−32.705	−0.698	−14.368	−0.028
8	977.75	2.170	−32.758	−0.539	−32.759	−0.535	−14.369	−0.021
9	973.60	1.736	−32.798	−0.416	−32.800	−0.412	−14.369	−0.016
10	970.34	1.395	−32.829	−0.321	−32.831	−0.317	−14.370	−0.012
15	961.82	0.505	−32.905	−0.093	−32.906	−0.089	−14.371	−0.003
20	959.09	0.220	−32.925	−0.030	−32.927	−0.026	−14.372	−0.001
25	958.17	0.123	−32.931	−0.012	−32.933	−0.008	−14.372	0.000
30	957.83	0.088	−32.933	−0.006	−32.934	−0.003	−14.372	0.000
35	957.70	0.074	−32.934	−0.004	−32.935	−0.001	−14.372	0.000
40	957.64	0.068	−32.934	−0.004	−32.935	0.000	−14.372	0.000
45	957.60	0.064	−32.934	−0.004	−32.935	0.000	−14.372	0.000
FCI	956.99		−32.935		−32.935		−14.372	

[a] SRS results.
[b] HS results.

each other, even in rather high orders. Significant differences between the SRS and HS energies show up only in the 20th and higher orders. Hence, the SRS method can be considered as an excellent approximation to the HS method. In fact, the SRS results presented in Table 3 show that a low order perturbation treatment employing weak symmetry forcing is able to reproduce the variational interaction energy to a very good accuracy. In the region of the van der Waals minimum the sum of corrections through the second order reproduces the exact interaction energy with errors smaller than 1%.

It should be stressed that the HS series converges to the supermolecular FCI interaction energy only if the latter is corrected for BSSE using the Boys-Bernardi prescription (32) (the uncorrected FCI interaction energy for $R = 5.6$ bohr amounts to -60.453 μhartree and is 1.8 times larger than the limit of the HS series). Thus, our results confirm the conclusions reached in Refs. (33)–(40) concerning the correctness of the counterpoise correction

of Boys and Bernardi.

Table 4: Convergence of the symmetrized Rayleigh-Schrödinger perturbation expansion for the interaction of a ground-state helium atom with a hydrogen molecule at $R = 6.5$ bohr. The B83 basis set was used. $\Sigma(n)$ and $\delta(n)$ are defined as in Table 1. Energies are in μhartree.

	$\theta = 0°$		$\theta = 90°$	
n	$\Sigma(n)$	$\delta(n)$	$\Sigma(n)$	$\delta(n)$
2	−46.256	−3.01	−41.163	−0.82
3	−44.771	−6.13	−39.710	−4.32
4	−45.844	−3.88	−40.407	−2.64
5	−46.047	−3.45	−40.507	−2.40
10	−46.979	−1.50	−41.076	−1.03
15	−47.364	−0.69	−41.310	−0.47
20	−47.537	−0.33	−41.414	−0.22
FCI	−47.693		−41.504	

The results of large-order SRS calculations for the linear and T-shaped geometries of the HeH_2 complex are presented in Table 4. An inspection of this table shows that also for this system the SRS expansion appears to be convergent. Compared to the He dimer case the convergence is slower. Also the error of the second order treatment is somewhat larger than for He_2: 3% and 0.8% for the linear and T geometries of the complex, respectively.

Similar results for other angles could not be obtained in the B83 basis due to the limitations of the FCI codes. Therefore, the convergence pattern of the SRS expansion for different angles θ was studied in a smaller, B44 basis. An inspection of Table 5 shows that the convergence of the SRS expansion for HeH_2 is rather independent of the angle θ. The error of the second-order approximation changes from 4% at $\theta = 0°$ to 2% at $\theta = 90°$, so the barrier height is reasonably well reproduced.

Since the convergence properties of the SRS perturbation expansion are satisfactory for weakly interacting systems like He_2 and HeH_2, it is interesting to analyse the importance of various contributions to the interaction energy computed through the second order. The SRS theory gives the correct asymptotics of the interaction energy (15), so each correction $E^{(n)}_{\rm SRS}$ can be decomposed as,

$$E^{(n)}_{\rm SRS} = E^{(n)}_{\rm pol} + E^{(n)}_{\rm exch}\,, \tag{22}$$

where $E^{(n)}_{\rm pol}$ are the polarization corrections defined by the standard RS perturbation theory, Eqs. (7) and (8), and $E^{(n)}_{\rm exch}$ are the exchange terms describing the effect of the resonance tunneling of electrons between the

Table 5: Convergence of the symmetrized Rayleigh-Schrödinger perturbation expansion for the interaction of a ground-state helium atom with a hydrogen molecule for different angles θ (R = 6.5 bohr). The B44 basis set was used. $\Sigma(n)$ and $\delta(n)$ are defined as in Table 1. Energies are in μhartree.

	$\theta = 0°$		$\theta = 30°$		$\theta = 60°$		$\theta = 90°$	
n	$\Sigma(n)$	$\delta(n)$	$\Sigma(n)$	$\delta(n)$	$\Sigma(n)$	$\delta(n)$	$\Sigma(n)$	$\delta(n)$
2	−41.349	−4.29	−39.754	−3.58	−36.943	−2.30	−35.608	−1.74
3	−40.341	−6.63	−38.707	−6.12	−35.861	−5.17	−34.523	−4.73
4	−41.263	−4.49	−39.528	−4.13	−36.510	−3.45	−35.100	−3.14
5	−41.524	−3.89	−39.752	−3.59	−36.674	−3.02	−35.239	−2.76
6	−41.801	−3.25	−39.996	−3.00	−36.862	−2.52	−35.405	−2.30
7	−42.013	−2.76	−40.183	−2.54	−37.007	−2.14	−35.531	−1.95
8	−42.193	−2.34	−40.342	−2.16	−37.130	−1.81	−35.639	−1.65
9	−42.343	−1.99	−40.474	−1.83	−37.233	−1.54	−35.730	−1.40
10	−42.470	−1.70	−40.586	−1.56	−37.320	−1.31	−35.806	−1.19
15	−42.867	−0.78	−40.936	−0.71	−37.590	−0.59	−36.044	−0.54
20	−43.046	−0.37	−41.093	−0.33	−37.710	−0.27	−36.149	−0.25
25	−43.128	−0.18	−41.165	−0.16	−37.765	−0.13	−36.196	−0.12
30	−43.166	−0.09	−41.198	−0.08	−37.790	−0.06	−36.218	−0.06
40	−43.193	−0.03	−41.221	−0.02	−37.807	−0.02	−36.233	−0.02
50	−43.199	−0.01	−41.226	−0.01	−37.811	−0.01	−36.236	−0.01
FCI	−43.204		−41.231		−37.814		−36.238	

interacting systems. The second-order SRS treatment yields the interaction energy as a sum of well defined contributions, such as the *electrostatic*, *exchange*, *induction*, and *dispersion* energies, which have a clear physical meaning resulting from the extension of the multipole expansion interpretation (2, 3). In particular, $E^{(1)}_{\rm pol}$ is the classical *electrostatic* energy fully accounting for the overlap (penetration) of the monomer charge distributions, and $E^{(2)}_{\rm pol}$ is the sum of the non-expanded classical *induction* and quantum mechanical *dispersion* energies,

$$E^{(2)}_{\rm pol} = E^{(2)}_{\rm ind} + E^{(2)}_{\rm disp}. \tag{23}$$

The second-order exchange energy is also split into an induction and a dispersion parts,

$$E^{(2)}_{\rm exch} = E^{(2)}_{\rm exch-ind} + E^{(2)}_{\rm exch-disp}, \tag{24}$$

where the *exchange-induction* energy ($E^{(2)}_{\rm exch-ind}$) and *exchange-dispersion* energy ($E^{(2)}_{\rm exch-disp}$) result from the antisymmetrization of those contributions to the perturbed wave function, which originate from the classical

induction and quantum mechanical dispersion interactions (52, 53), respectively. $E^{(2)}_{\mathrm{exch-ind}}$ and $E^{(2)}_{\mathrm{exch-disp}}$ can be interpreted as the coupling of the electron exchange with the induction and dispersion interactions, respectively.

The values of various contributions to the interaction potential of HeH_2 as a function of the angle θ are reported in Table 6. Similar results for He_2 are presented and discussed in Ref. (51). As expected, the interaction

Table 6: Anisotropy of the first and second-order contributions to the interaction energy of HeH_2 at $R = 6.5$ bohr. The B44 basis set was used. Energies are in μhartree.

	$\theta = 0°$	$\theta = 30°$	$\theta = 60°$	$\theta = 90°$
$E^{(1)}_{\mathrm{pol}}$	−9.430	−8.377	−6.603	−5.856
$E^{(1)}_{\mathrm{exch}}$	56.732	50.840	40.554	36.118
$E^{(2)}_{\mathrm{ind}}$	−2.923	−2.355	−1.616	−1.425
$E^{(2)}_{\mathrm{exch-ind}}$	2.291	2.027	1.581	1.395
$E^{(2)}_{\mathrm{disp}}$	−91.327	−84.842	−73.210	−67.928
$E^{(2)}_{\mathrm{exch-disp}}$	3.309	2.953	2.350	2.088
E_{int}	−41.349	−39.754	−36.943	−35.608

energy of the HeH_2 complex is dominated by the first-order exchange energy and the second-order dispersion energy. However, other contributions are nonnegligible. For instance, the electrostatic energy (which is of purely penetrational character in this case) represents as much as $\sim$ 20% of the interaction energy, while the second-order exchange component amounts to $\sim$ 10% of E_{int}. Thus, the final shape of the potential energy surface results from a delicate balance of various attractive and repulsive components. Indeed, the sum of all attractive terms represents 250% and 210% of E_{int} for $\theta = 0°$ and 90°, respectively, while the sum of all repulsive components amounts to 150% and 110% for the same angles, so the very good agreement between the FCI and the second-order SRS results, reached despite the large cancellations involved, is very gratifying.

Acknowledgement

This work was supported by the Polish Scientific Research Council (KBN), grant No. KBN 3 T09A 037 08. We thank Dr. K. Szalewicz for reading and commenting on this manuscript and Dr. H.L. Williams for performing part of the FCI calculations for HeH_2.

References

(1) B. Jeziorski, R. Moszynski, and K. Szalewicz, Chem. Rev. **94**, 1887 (1994).

(2) A.D. Buckingham, Adv. Chem. Phys. **12**, 107 (1967).

(3) P.E.S. Wormer, F. Mulder, and A. van der Avoird, Int. J. Quantum Chem. **11**, 959 (1977); A. van der Avoird, P.E.S. Wormer, F. Mulder, and R.M. Berns, Top. Curr. Chem. **93**, 1 (1980).

(4) P. Claverie, Int. J. Quantum Chem. **5**, 273 (1971).

(5) J.M. Schulman, J. Chem. Phys. **57**, 4413 (1972).

(6) P.R. Certain and W. Byers Brown, Int. J. Quantum Chem. **6**, 131 (1972); R. Ahlrichs and P. Claverie, Int. J. Quantum Chem. **6**, 1001 (1972).

(7) R. Ahlrichs, Chem. Phys. Lett. **18**, 67 (1973).

(8) W.N. Whitton and W. Byers Brown, Int. J. Quantum Chem. **10**, 71 (1976).

(9) G. Chalasinski, B. Jeziorski, and K. Szalewicz, Int. J. Quantum Chem. **11**, 247 (1977).

(10) B. Jeziorski, G. Chalasinski, and K. Szalewicz, Int. J. Quantum Chem. **14**, 271 (1978).

(11) B. Jeziorski, W.A. Schwalm, and K. Szalewicz, J. Chem. Phys. **73**, 6215 (1980).

(12) W. Kutzelnigg, J. Chem. Phys. **73**, 343 (1980).

(13) B. Jeziorski (1978), unpublished result quoted in Ref. (12).

(14) D.M. Chipman and J.O. Hirschfelder, J. Chem. Phys. **37**, 5164 (1980).

(15) B. Jeziorski and W. Kolos, in *Molecular Interactions*, edited by H. Ratajczak and W.J. Orville-Thomas, (Wiley, New York 1982), vol. 3, p. 1.

(16) W.H. Adams, Int. J. Quantum Chem. S **24**, 531 (1990).

(17) W.H. Adams, Int. J. Quantum Chem. S **25**, 165 (1991).

(18) T. Cwiok, B. Jeziorski, W. Kolos, R. Moszynski, J. Rychlewski, and K. Szalewicz, Chem. Phys. Lett. **195**, 67 (1992).

(19) W.H. Adams, J. Math. Chem. **10**, 1 (1992).

(20) W. Kutzelnigg, Chem. Phys. Lett. **195**, 77 (1992).

(21) T. Cwiok, B. Jeziorski, W. Kolos, R. Moszynski, and K. Szalewicz, J. Chem. Phys. **97**, 7555 (1992).

(22) T. Cwiok, B. Jeziorski, W. Kolos, R. Moszynski, and K. Szalewicz, J. Mol. Struct. (Theochem) **307**, 135 (1994).

(23) W.H. Adams, Chem. Phys. Lett. **229**, 472 (1994) .

(24) J. O. Hirschfelder, Chem. Phys. Lett. **1**, 325 (1967).

(25) B. Jeziorski and W. Kolos, Int. J. Quantum Chem. (Suppl. 1) **12**, 91 (1977).

(26) J.O. Hirschfelder and R. Silbey, J. Chem. Phys. **45**, 2188 (1966).

(27) R. Ahlrichs, Theor. Chim. Acta **41**, 7 (1976).

(28) W.J. Carr, Phys. Rev. **131**, 1947 (1963).

(29) J.N. Murrell and G. Shaw, J. Chem. Phys. **46**, 46 (1967).

(30) J.I. Musher and A.T. Amos, Phys. Rev. **164**, 31 (1967).

(31) A. van der Avoird, P.E.S. Wormer, and R. Moszynski, Chem. Rev. **94**, 1931 (1994); R. Moszynski, T.G.A. Heijmen, P.E.S. Wormer, and A. van der Avoird, Adv. Quantum Chem. – this issue.

(32) S.F. Boys and F. Bernardi, Mol. Phys. **19**, 553 (1970).

(33) M. Bulski and G. Chalasinski, Theor. Chim. Acta **44**, 399 (1977).

(34) M. Gutowski, J.H. van Lenthe, J. Verbeek, F.B. van Duijneveldt, and G. Chalasinski, Chem. Phys. Lett. **124**, 370 (1986).

(35) M. Gutowski, F.B. van Duijneveldt, G. Chalasinski, and L. Piela, Chem. Phys. Lett. **129**, 325 (1986).

(36) M. Gutowski, F.B. van Duijneveldt, G. Chalasinski, and L. Piela, Mol. Phys. **61**, 233 (1987).

(37) S.M. Cybulski and G. Chalasinski, Chem. Phys. Lett. **197**, 591 (1992).

(38) M. Gutowski and G. Chalasinski, J. Chem. Phys. **98**, 5540 (1993).

(39) M. Gutowski, J.G.C.M. van Duijneveldt-van der Rijdt, J.H. van Lenthe, and F.B. van Duijneveldt, J. Chem. Phys. **98**, 4728 (1993).

(40) F.B. van Duijneveldt, J.G.C.M. van Duijneveldt-van der Rijdt, J.H. van Lenthe, Chem. Rev. **94**, 1873 (1994).

(41) H. Partridge, J. Chem. Phys. **87**, 6643 (1987); NASA Technical Memorandum 89449; H. Partridge, J. Chem. Phys. **90**, 1043 (1989); NASA Technical Memorandum 101044; H. Partridge and K. Faegri, Jr., Theor. Chim. Acta **82**, 207 (1992); NASA Technical Memorandum 103918.

(42) M. Gutowski, J. Verbeek, J.H. van Lenthe, and G. Chalasinski, Chem. Phys. **111**, 271 (1987).

(43) H.L. Williams, K. Szalewicz, R. Moszynski, and B. Jeziorski, J. Chem. Phys. **103**, 4586 (1995).

(44) P. Hobza, B. Schneider, J. Sauer, P. Carsky, and R. Zahradnik, Chem. Phys. Lett. **134**, 418 (1987).

(45) F.-M. Tao, J. Chem. Phys. **100**, 4947 (1994).

(46) V.R. Saunders and M.F. Guest *ATMOL Program Package* (SERC Daresbury Laboratory, Daresbury, Great Britain).

(47) B. Jeziorski, R. Moszynski, A. Ratkiewicz, S. Rybak, K. Szalewicz, and H.L. Williams, in *Methods and Techniques in Computational Chemistry: METECC94, vol. B Medium-Size Systems*, edited by E. Clementi, (STEF, Cagliari 1993), p. 79.

(48) *MOLCAS version 2*, K. Anderson, M.P. Fülscher, R. Lindh, P.-Å. Malmqvist, J. Olsen, B.O. Roos, A.J. Sadlej, University of Lund, Sweden, and P.-O. Widmark, IBM Sweden 1991.

(49) R.J. Harrison and S. Zarrabian, Chem. Phys. Lett. **158**, 393 (1989).

(50) H.L. Williams, T. Korona, R. Bukowski, B. Jeziorski, and K. Szalewicz, Chem. Phys. Lett. – in press.

(51) T. Korona, H.L. Williams, R. Bukowski, B. Jeziorski, and K. Szalewicz, J. Chem. Phys. – submitted.

(52) G. Chalasinski and B. Jeziorski, Mol. Phys. **32**, 81 (1976).

(53) G. Chalasinski and B. Jeziorski, Theor. Chim. Acta **46**, 277 (1977).

Electron Affinity of SF_6

M. Klobukowski, G. H. F. Diercksen,[1] and

J. M. García de la Vega[2]

Department of Chemistry
University of Alberta
Edmonton, AB, Canada T6G 2G2

Abstract

Electron affinity of sulfur hexafluoride was studied using various density functionals and systematically expanded basis sets with polarization function exponents optimized in molecular environment. f-type polarization functions were found necessary to ensure convergence of both geometry and electron affinity. The ion was found to have octahedral symmetry, and the smallest value of electron affinity is only 1.40 eV (1.6 eV with zero-point energy correction).

[1] Max-Planck Institut für Astrophysik, Karl-Schwarzschild-Straße 1, D-85740 Garching, Germany.

[2] Departamento de Química Física Aplicada, Facultad de Ciencias, Universidad Autónoma de Madrid, 28049 Madrid, Spain.

ADVANCES IN QUANTUM CHEMISTRY, VOLUME 28

0065-3276/97 $25.00

1. Introduction

The adiabatic electron affinity of sulfur hexafluoride is defined (without the vibrational correction) as:

$$EA\,(\mathrm{SF_6}) = E_{tot}^{\mathrm{SF_6}}\left(r_e^{\mathrm{SF_6}}\right) - E_{tot}^{\mathrm{SF_6^-}}\left(r_e^{\mathrm{SF_6^-}}\right).$$

The total energies refer to electronic ground states, which in octahedral symmetry are $^1A_{1g}$ for SF_6 and $^2A_{1g}$ for SF_6^-. Electron affinity is positive if the molecular ion SF_6^- is *more* stable than SF_6. Electron affinity of SF_6 has been a subject of several studies, both experimental and theoretical. The past three decades of experimental studies attest the difficulty in the determination of this relatively small quantity, with values as small as $0.32\pm$ 0.15 eV (1) and as large as 1.49 ± 0.15 eV (2). However, two most recent experimental studies appear to agree that the electron affinity is about 1 eV. Kebarle and co-workers (3) derived $EA = 1.05 \pm 0.1$ eV from electron transfer equilibria. Chen *et al.* (4) established that $EA = 1.15 \pm 0.15$ eV in the studies of electron capture.

In theoretical work, much attention was focused on the electronic structure of the octahedral SF_6. The molecule was studied by Diercksen and co-workers who, using extensive basis sets as early as 1975, obtained $E_{tot}\,(\mathrm{SF_6}) = -993.8546$ E_h (at $r_{SF} = 1.5602$ Å) (5, 6). The total energy was lowered to $-994.252\,64$ E_h (at $r_{SF} = 1.561$ Å) by Klobukowski *et al.* (7) using extended basis set. Recent accurate calculations include the work of Gianturco *et al.*, who reported $E_{tot}\,(\mathrm{SF_6}) = -994.219\,709$ E_h (at $r_{SF} = 1.56026$ Å) (8), and calculations by von Niessen and co-workers (9) who reported the lowest total energy of $-994.373\,606$ E_h (at $r_{SF} = 1.5602$ Å).

Computational studies of the electron affinity of SF_6 show a large variation of results, undoubtedly due to the fact that the calculated electron affinity of SF_6 suffers from almost the same loss of accuracy as the weight of Coulson's Captain (10). Boring, using the MS – Xα method obtained $EA = 0.7$ eV (11). Hay, using very small basis set (without polarization functions on fluorine atoms) reported SCF value of $0.9 - 1.0$ eV (12). Tang and Callaway used a local density functional to find $EA = 1.19$ eV (13). Klobukowski *et al.* (7) found that in the limit of a large basis set the Hartree-Fock method gives a negative value of the electron affinity and thus demonstrated that the ability of SF_6 to attract an electron is due to electron correlation effects.[1] Sakai and co-workers performed a hybrid study in which the electron correlation correction to electron affinity (1.36 eV) was estimated using a very small basis set and then added to the negative value (-0.34 eV) obtained by Klobukowski (7) with an extended basis set to yield $EA = 1.02$ eV (14). The latest density-functional result was reported

[1] Negative, rather than zero, electron affinities result from using finite basis sets.

by Gutsev, who, using local spin density method to calculate equilibrium geometry of the two systems and adding non-local terms to improve total energy found the surprisingly large value of $EA = 3.44$ eV without the zero-point energy correction (15). In this work a triple-zeta STO basis equipped with two d-type polarization functions per each atom was used. Richman and Banerjee (16), in a careful study with very large basis sets and a limited CAS SCF found $EA = -0.63$ eV, only a slight improvement over their Hartree-Fock value of -0.68 eV. Finally, Cheung *at al.* used the G92(MP2) procedure and estimated electron affinity value of 1.04 eV (17). In these calculations octahedral symmetry was assumed for both the neutral molecule and its anion (only Richman and Banerjee studied lower symmetries), and usually only a single basis set was used.

Calculation of the electronic structure of both SF_6 and SF_6^- is complicated by the fact that the single Hartree-Fock determinant may be an inadequate zeroth-order reference function, as may be seen from the values of C_0 (the weight of the Hartree-Fock configuration) based on the MP2 results (UMP2 for the ion), which are collected in Table 1.

Table 1: Approximate values of C_0

Basis	SF_6	SF_6^-
6-311+G(d)	0.88	0.87
6-311+G(2df)	0.87	0.85

The density functional methods do not require a definition of the of zeroth-order space and were shown to give very good values of electron affinity for other systems (18). However, the recent value of electron affinity computed within the density-functional approach is so large that it poses the question whether the density functional approach was deficient or the functionals were inadequate. Furthermore, given that no evaluation of the energy Hessian was performed, the true geometry of SF_6^- could be lower than octahedral, as suggested by Gutsev (15), with the octahedral stationary point being a saddle point on the potential energy surface of SF_6^-.

As several density functionals became available in the Gaussian program (19, 20), it became possible to study their effect on the computed value of electron affinity with systematically enlarged basis sets. The plan of the present work is as follows: (a) initial calculations were done using the Hartree-Fock methods (RHF, the restricted Hartree-Fock; ROHF, the restricted open-shell Hartree-Fock; UHF, the unrestricted open-shell Hartree-Fock), and various non-local density functionals, defined in Table 2, with several standard basis sets (Section 2); (b) a large, saturated *sp* basis set was systematically enlarged by adding polarization functions with exponents optimized in molecular Hartree-Fock and density-functional cal-

Table 2: Key for density functionals

Key	Usual abbreviation	Description
DF1	BLYP	Becke exchange functional (Slater exchange plus correction involving the gradient of electron density) (21). Lee, Yang, Parr correlation functional with local and non-local (gradient-dependent) terms (22).
DF2	BP86	Becke exchange functional. Correlation functional of Perdew, includes gradient corrections (23, 24).
DF3	B3LYP	Becke's 3-parameter hybrid exchange functional (25) (as implemented in Gaussian 92 (19) and Gaussian 94 (20)) and Lee, Yang, Parr correlation functional.
DF4	B3PW91	Exchange functional as above with Perdew-Wang gradient-corrected correlation functional (26).

culations, in order to reach the limit of the molecular basis set (Section 3); (c) calculations of the structures and electron affinities using the large basis sets, followed by the evaluation of the energy hessian to establish the symmetry of the ion and to estimate the zero-point energy correction to electron affinity (Section 4).

2. Calculations using standard basis sets

The initial calculations were done using four library basis sets available in the programs Gaussian 92/DFT (19) and Gaussian 94 (20). The symbols used to denote these basis sets in the present work are shown in Table 3; the last row of the Table shows the number of contracted functions generated in the molecular calculations. These basis sets are similar to those which have

Table 3: Key for standard basis sets

Key:	A1	A2	A3	A4
Basis:	6-311G(d)	6-311+G(d)	6-311+G(2d)	6-311+G(2df)
Size:	134	162	197	246

been routinely used study the efficacy of the density functional methods (27, 28, 29, 30). It should be noted that despite the notation, the 6-311G basis set is a TZV basis set only in the p space, while it displays only DZV quality in the s space (31).

Table 4: Optimized bond length in SF_6 (in Å)

Method	Basis set			
	A1	A2	A3	A4
RHF	1.5467	1.5479	1.5374	1.5301
DF1	1.6380	1.6438	1.6271	1.6143
DF2	1.6248	1.6290	1.6137	1.6022
DF3	1.6034	1.6068	1.5923	1.5818
DF4	1.5949	1.5975	1.5842	1.5743

The equilibrium internuclear distances r_{SF} for SF_6 are shown in Table 4. They exhibit rather modest variation with the basis set (about 0.02 Å) and slightly larger change with the density functional (about 0.04 Å). The RHF values are too small, while the DF4 result is closest to the experimental value of $r_{SF} = 1.5622(7)$ Å (32). The sulfur-fluorine distances in SF_6^-, collected in Table 5, show similar variation with both basis set and density functional as SF_6. The ROHF and UHF results are fairly close despite the contamination of the UHF doublet wavefunction by higher multiplicities as revealed by the value of $\mathcal{S}^2 = 0.77 - 0.78$. Much greater variation

Table 5: Optimized bond length in SF_6^- (in Å)

Method	Basis set			
	A1	A2	A3	A4
ROHF	1.6980	1.6963	1.6884	1.6768
UHF	1.7037	1.7024	1.6940	1.6818
DF1	1.7898	1.8023	1.7888	1.7737
DF2	1.7743	1.7832	1.7709	1.7567
DF3	1.7542	1.7608	1.7495	1.7358
DF4	1.7439	1.7483	1.7385	1.7252

with basis sets and density functionals can be seen in the values of electron affinity, presented in Table 6. The basis A2 seems to favor the anion, thus leading to a positive electron affinity already at the Hartree-Fock level. The density functional methods make SF_6^- more stable than SF_6 for all basis sets. The most recent functional, denoted here as DF4, gives in conjunction with the largest basis set A4 the value of electron affinity which is about half of the value reported by Gutsev (15). Values similar to that obtained by Gutsev (about 3.5 eV) are obtained with density functionals DF1 and DF2 and the A2 and A3 basis sets (i.e. the basis sets without f-type functions). Electron affinity depends strongly on both the basis set and the density

Table 6: Electron affinity of SF_6 (in eV)

Method	Basis set			
	A1	A2	A3	A4
ROHF	-0.12	0.11	-0.64	-1.19
UHF	0.09	0.31	-0.46	-1.03
DF1	2.98	3.76	3.13	2.70
DF2	2.88	3.52	2.88	2.44
DF3	2.55	3.15	2.48	2.01
DF4	2.30	2.79	2.12	1.65

functional used. Selecting a basis set which fortuitously favors the ion may bring about a positive electron affinity already at the ROHF/UHF level. The data in Table 6 show that the best value of electron affinity which, without the ZPE correction, is 0.5 eV larger than the experimental result, is obtained by the combination of a large basis set which includes f-type functions with the most recently proposed density functionals.

3. Development of extended basis sets

Conclusions about the performance of density functional methods are frequently based on calculations utilizing relatively small basis sets (27, 28, 29, 30). However, as stressed by Andzelm and Wimmer (33), while the standard basis sets may bring about reasonable molecular geometries when used in the density functional calculations, they are frequently inadequate for the evaluation of energy differences. Furthermore, the results obtained

Table 7: Results obtained with 6-31G(3df) basis set

Method	System	r_e/Å	EA/eV
DF1	SF_6	1.6028	1.13
	SF_6^-	1.7526	
DF2	SF_6	1.5937	1.10
	SF_6^-	1.7412	

with standard basis sets suffer from the fact that the polarization functions, essential for satisfactory representation of electron density, were determined in the atomic calculations, usually for neutral atoms, and may be far from optimal for anions. In addition to that, the polarization functions used with some of the smaller basis sets may in fact act as stand-ins for an inadequate underlying *sp* basis set.

It should be kept in mind that a standard basis set *might* bring about excellent agreement with experiment. For example, using the 6-31G(3df) basis set (see Table 7) one gets nearly perfect agreement with the experimental value of electron affinity – and a good example of the "right answer for wrong reasons" (34, 35). In order to eliminate the basis set effects from the discussion of the merits of the density functional approach it is necessary to perform calculations to the basis set limit.

Table 8: Definition of polarization sets (PS).

PS	Composition[a]		System	Method	Optimized exponents		
1	S($\widetilde{1d}$)	F($\widetilde{1d}$)			d(S)	d(F)	
			SF_6	RHF	0.804	0.704	
			SF_6	DF1	0.825	0.650	
			SF_6^-	DF1	0.727	0.579	
2	S($\widetilde{2d}$)	F($1d$)			d(S)		
			SF_6	RHF	3.3	0.7	
			SF_6	DF1	3.3	0.7	
			SF_6^-	DF1	2.3	0.5	
3	S($2d$)	F($\widetilde{2d}$)			d(F)		
			SF_6	RHF	2.2	0.6	
			SF_6	DF1	1.6	0.5	
			SF_6^-	DF1	1.6	0.5	
4	S($\widetilde{3d}$)	F($2d$)				d(S)	
			SF_6	RHF	7.97	2.17	0.59
			SF_6	DF1	7.46	2.07	0.58
			SF_6^-	DF1	6.53	1.81	0.50
5	S($3d$)	F($\widetilde{3d}$)				d(F)	
			SF_6	RHF	2.52	1.21	0.58
			SF_6	DF1	2.75	1.18	0.51
			SF_6^-	DF1	2.22	1.03	0.48
6	S($3d\widetilde{1f}$)	F($3d\widetilde{1f}$)			f(S)	f(F)	
			SF_6	RHF	0.8	0.9	
			SF_6	DF1	0.8	0.9	
			SF_6^-	DF1	0.7	0.8	
7	S($3d1f\widetilde{1g}$)	F($3d1f$)			g(S)		
			SF_6	RHF	0.8		
			SF_6	DF1	0.8		
			SF_6^-	DF1	0.8		

[a] optimized functions are marked by $\widetilde{\ }$

In the present work, in order to avoid optimization of the *sp* basis set in the density functional calculations, the *sp* space was spanned by the

large well-balanced basis sets (36). The basis sets chosen, $(19s, 13p)$ for sulfur and $(15s, 9p)$ for fluorine were used with minimal contraction of the tightest few functions leading to contracted sets of $[15s.10p]$ for sulfur and $[12s.7p]$ for fluorine. The fluorine basis set was augmented by the diffuse p-type function with exponent of 0.0531. In the atomic Hartree-Fock calculations these basis sets give the following energies (in atomic units): $E_{tot}[\ \mathrm{F}\ (^2P)] = -99.409\,27$ $(-99.409\,44)$, $E_{tot}[\ \mathrm{F}^-\ (^1S)] = -99.459\,26$ $(-99.459\,45)$, $E_{tot}[\ \mathrm{S}\ (^3P)] = -397.504\,81$ $(-397.504\,90)$, $E_{tot}[\ \mathrm{S}^-\ (^2P)] = -397.536\,60$ $(-397.538\,43)$ (the numerical Hartree-Fock energies are given in parentheses). This sp basis set was systematically expanded by the addition of polarization functions. Their exponents were optimized in molecular energy calculations at fixed geometry: $r_{SF} = 1.56$ Å for SF_6, and $r_{SF} = 1.70$ Å for SF_6^-. The optimized polarization sets are shown in Table 8. In the Table, the symbol $\tilde{}$ indicates the polarization function(s) which were optimized in a given polarization set. The exponents of the remaining functions were taken from a preceding polarization set. For example, in the first polarization set (PS1) the two polarization functions, d(S) and d(F) were optimized simultaneously in the RHF and DF1 calculations for SF_6 and in the DF1 calculations for SF_6^-. In the next set (PS2), two d-type functions for sulfur were optimized while keeping the single d-type function on fluorine from the PS1 set. When more than two polarization functions were optimized (as in PS4 and PS5), the even-tempered formula was used. It is worth noticing that the exponents for SF_6 calculated with the RHF method do not differ greatly from the ones determined in the density functional calculations; this may indicate that good polarization exponents for density functional calculations may be chosen in the Hartree-Fock optimization. The values of the exponents for single and

Table 9: Total energies (in atomic units) of SF_6 and SF_6^- and their convergence ΔE with the basis set (see Table 10 for basis set labels)

Basis	SF_6 (RHF)	ΔE^a	SF_6 (DF1)	ΔE^a	SF_6^- (DF1)	ΔE^a
B0	-993.905721		-997.181371		-997.407336	
B1	-994.317547	-0.4118	-997.427102	-0.2457	-997.544863	-0.1375
B2	-994.355516	-0.0380	-997.463329	-0.0362	-997.565973	-0.0211
B3	-994.393654	-0.0381	-997.489322	-0.0260	-997.579782	-0.0138
B4	-994.397304	-0.0036	-997.493294	-0.0040	-997.583720	-0.0039
B5	-994.400265	-0.0030	-997.495109	-0.0018	-997.584913	-0.0012

[a] see text for the definition

double d-type polarization functions in the RHF calculations (0.8 and {3.3,

0.7}) are slightly larger than the values (0.7 and {2.0, 0.55}) recommended by Magnusson and Schaefer (37) for use with smaller *sp* basis sets. The effectiveness of consecutive expansions of the basis set may be estimated from the lowering of the total energy $\Delta E(B_i) = E_{tot}(B_{i-1}) - E_{tot}(B_i)$. Convergence of total energies with the basis set size is shown in Table 9. It is interesting to note that the density functional energies appear to converge faster than the RHF energies. The largest effect is seen for the first *d*-type function. The second *d* and the first *f*-type functions bring about comparable energy improvements. The third *d* function and the single *g*-type function have only negligible effects. The B3 basis may be considered to be effectively converged.

Polarization space was optimized further, with $2f$ functions optimized for both sulfur and fluorine. However, the improvement of energy when going from S($3d1f$)F($3d1f$) to S($3d\widetilde{2f}$)F($3d1f$) was only about 0.0003 E_h. Similarly, the energy gain which resulted from expanding S($3d1f$) F($3d1f$) to S($3d1f$)F($3d\widetilde{2f}$) was $0.004 - 0.008$ E_h, depending on the method. These improvements were considered insignificant, and the basis sets containing two *f*-type functions per atom were not used.

4. Calculations with optimized basis sets

Key to the optimized basis sets is shown in Table 10; the symbol B0 is used to denote the unpolarized *sp* basis set. In the ROHF and UHF calculations for SF_6^-, the polarization sets used were the ones determined for the ion in the DF1 calculations.

Table 10: Key for optimized basis sets

Basis key:	B1	B2	B3	B4	B5
PS[a]:	(1)	(2,3)	(2,3,6)	(4,5,6)	(4,5,6,7)
Polarization:	($1d$, $1d$)	($2d$, $2d$)	($2d1f$, $2d1f$)	($3d1f$, $3d1f$)	($3d1f1g$, $3d1f$)
Size:	278	313	362	397	406

[a] numbers in parentheses indicate the polarization set as defined in Table 8

The equilibrium sulfur-fluorine distances are shown in Table 11. It is satisfying to see that results converged to within 0.001 Å are obtained already with the B3 basis set. However, the best value (DF4 and B5) is still about 0.008 Å longer than the experimental bond length. The calculated bond lengths in SF_6^- are collected in Table 12. Again, the B3 results are converged to within 0.002 Å. Experimental value of the bond length in SF_6^- is not known, but on the basis of the present work it may be

Table 11: Optimized bond length in SF_6 (in Å)

Method	Basis set					
	B0	B1	B2	B3	B4	B5
RHF	1.6554	1.5408	1.5336	1.5288	1.5291	1.5281
DF1	1.7916	1.6279	1.6163	1.6092	1.6092	1.6083
DF2	1.7721	1.6141	1.6038	1.5973	1.5973	1.5965
DF3	1.7435	1.5949	1.5848	1.5784	1.5783	1.5774
DF4	1.7311	1.5861	1.5770	1.5709	1.5709	1.5701

Table 12: Optimized bond length in SF_6^- (in Å)

Method	Basis set					
	B0	B1	B2	B3	B4	B5
ROHF	1.7774	1.6877	1.6818	1.6710	1.6736	1.6727
UHF	1.7789	1.6925	1.6867	1.6755	1.6782	1.6772
DF1	1.9066	1.7851	1.7758	1.7687	1.7662	1.7653
DF2	1.8865	1.7672	1.7589	1.7522	1.7498	1.7489
DF3	1.8598	1.7472	1.7389	1.7323	1.7300	1.7291
DF4	1.8471	1.7358	1.7284	1.7219	1.7198	1.7189

expected to be about 1.72 Å.

The electron affinities calculated with the extended, optimized basis sets are shown in Table 13. First of all, the results clearly show that at the Hartree-Fock level (ROHF or UHF) the SF_6 molecule is destabilized after the addition of an electron. All calculated values of electron affinity decrease systematically with the expansion of basis set. Furthermore, the combination of the most recent functionals (DF4) gives a value of $EA =$

Table 13: Electron affinity of SF_6 (in eV)

Method	Basis set					
	B0	B1	B2	B3	B4	B5
ROHF	4.11	−0.63	−1.04	−1.45	−1.44	−1.46
UHF	4.43	−0.46	−0.87	−1.28	−1.28	−1.31
DF1	6.15	3.21	2.79	2.46	2.46	2.44
DF2	6.05	2.94	2.53	2.19	2.20	2.18
DF3	6.03	2.55	2.21	1.77	1.78	1.76
DF4	5.76	2.18	1.75	1.39	1.40	1.38

Table 14: Vibrational frequencies (in cm^{-1})

Method	Mode					
	t_{2u}	t_{2g}	t_{1u}	e_g	a_{1g}	t_{1u}
			SF_6			
DF1	309	470	548	563	674	835
Experiment (38)	344	522	614	639	769	940
Experiment (39)	347	524	614	643	775	939
			SF_6^-			
DF1	211	307	177	382	536	594

1.4 eV, which is only about 30% larger than the experimental one.

This value of electron affinity, calculated from the bottom of the potential energy well, must be corrected for the zero-point energy (ZPE) effects. It may be expected that the normal modes of the anion will be softer than in SF_6 and the ZPE correction will increase the computed value of electron affinity. In order to establish the magnitude of ZPE and determine the character of the stationary point for the anion, harmonic vibrational analysis was performed. Due to limited computer resources, only the DF1 calculations were done using the extended, $(3dlf, 3dlf)$ polarized basis set. Zero-point energies were found to be 0.51 eV and 0.32 eV for SF_6 and SF_6^-, respectively; the ZPE correction to the computed value of electron affinity is thus about 0.2 eV, and the ZPE-corrected value of electron affinity is 1.6 eV.

The vibrational frequencies for SF_6 and SF_6^- are collected in Table 14 together with the experimental data for SF_6 (38, 39). Only the t_{1u} modes are infrared active. Their calculated intensities are 15 and 397 km mol^{-1} for SF_6 and 80 and 485 km mol^{-1} for SF_6^-. For SF_6, the calculated harmonic frequencies are smaller than the experimental values. All frequencies are positive, indicating that the stationary points are genuine minima both for SF_6 and for SF_6^-.

5. Summary

The results obtained in the present work show that there is room and need for the improvement of density functionals as the present, ZPE-corrected, value of electron affinity is still about 0.5 eV (about 50%) larger than the experimental one. It may be expected that the development of better functionals could bring about better agreement with the experimental electron affinity without the need to postulate that experimental measurements sample the excited states of the ion. Contrary to the occasionally expressed

opinion (40), density functional calculations could become a reliable tool in the computational studies of electron affinities; however, their quality may be fully appreciated only after any adverse basis set effects were eliminated by performing the calculations *ad limitem*. In contrast to the conventional post-Hartree-Fock calculations such as CAS SCF, (MR)CI, or CC, approaching the basis-set limit within the density functional approach could be a feasible task (41).

The ultimate quality of computed electron affinity depends on both the basis set used and the density functionals employed. Large basis sets are needed for accurate predictions of electron affinity in SF_6; in particular, at least one *f*-type function is required. With their exponents optimized in the molecular environment, the polarization set consisting of two *d*-type and one *f*-type functions is sufficient. It is worth noticing that the addition of the second *d*-type function lowers the value of electron affinity by about 0.4 eV, while the *f*-type functions increases the reduction by an additional 0.3 eV. The combined reduction amounts to about 0.7 eV and is achieved by the differential lowering of the energy of SF_6. Within a given basis set, replacing Becke's exchange functional (21) with the hybrid functional (25) reduces the value of electron affinity by about 0.6 eV. Additional reduction of about 0.4 eV results from replacing the Lee, Yang, and Parr correlation functional (22) with the Perdew-Wang functional (26). (It may be noted that Becke's hybrid functional (25) was designed in conjunction with the Perdew-Wang functional.) The combined effect of improved functionals and better basis sets is to bring about better agreement with experiment.

The stationary point in octahedral symmetry is a genuine minimum on potential energy surface of SF_6^-. This does not eliminate the possibility of the existence of local minima of lower symmetry with lower energy (which would increase the value of electron affinity).

6. Acknowledgments

One of us (M.K.) acknowledges discussions with Professor Paul Kebarle and Dr. Gennady Gutsev. This work was partly supported by a Research Grant OGP0046770 from the Natural Sciences and Engineering Research Council of Canada.

References

(1) M. M. Hubers and J. Los: *Chem. Phys.* **10**, 235-259 (1975).

(2) J. Kay and F. M. Page: *Trans. Faraday Soc.* **60**, 1042-1046 (1964).

(3) E. P. Gimsrud, S. Chowdhury, and P. Kebarle: *J. Chem. Phys.* **83**, 1059-1068 (1985).

(4) E. C. M. Chen, L.-R. Shuie, E. D. D'sa, C. F. Batten, and W. E. Wentworth: *J. Chem. Phys.* **88**, 4711-4719 (1988).

(5) W. von Niessen, L. S. Cederbaum, G. H. F. Diercksen, and G. Hohlneicher: *Chem. Phys.* **11**, 399-407 (1975).

(6) W. von Niessen, W. P. Kraemer, and G. H. F. Diercksen: *Chem. Phys. Lett.* **63**, 65-68 (1979).

(7) M. Klobukowski, Z. Barandiaran, L. Seijo, and S. Huzinaga: *J. Chem. Phys.* **86**, 1637-1638 (1987).

(8) F. A. Gianturco, R. R. Lucchese, and N. Sanna: *J. Chem. Phys.* **102**, 5743-5751 (1995).

(9) D. M. P. Holland, M. A. MacDonald, P. Baltzer, L. Karlsson, M. Lundqvist, B. Wanneberg, and W. von Niessen: *Chem. Phys.* **192**, 333-353 (1995).

(10) C. A. Coulson: *Valence* (1st ed.), Oxford University Press, Oxford (1952), p. 88.

(11) M. Boring: *Chem. Phys. Lett.* **46**, 242- (1977).

(12) P. J. Hay: *J. Chem. Phys.* **76**, 502-504 (1982).

(13) R. Tang and J. Callaway: *J. Chem. Phys.* **84**, 6854-6860 (1986).

(14) E. Miyoshi, Y. Sakai, and S. Miyoshi: *J. Chem. Phys.* **88**, 1470-1471 (1988).

(15) G. I. Gutsev: *Int. J. Mass Spectrom. Ion Proc.* **115**, 185-192 (1992).

(16) K. W. Richman and A. Banerjee: *Int. J. Quantum Chem.* **S27**, 759-767 (1993).

(17) Y.-S. Cheung, Y.-J. Chen, C. Y. Ng, S.-W. Chiu, and W.-K. Li: *J. Am. Chem. Soc.* **117**, 9725-9733 (1995).

(18) T. Ziegler and G. L. Gutsev: *J. Chem. Phys.* **96**, 7623-7632 (1992).

(19) Gaussian 92/DFT, Revision F.2, M. J. Frisch, G. W. Trucks, H. B. Schlegel, P. M. W. Gill, B. G. Johnson, M. W. Wong, J. B. Foresman, M. A. Robb, M. Head-Gordon, E. S. Replogle, R. Gomperts, J. L. Andres, K. Raghavachari, J. S. Binkley, C. Gonzalez, R. L. Martin, D. J. Fox, D. J. Defrees, J. Baker, J. J. P. Stewart, and J. A. Pople, Gaussian, Inc., Pittsburgh PA, 1993.

(20) Gaussian 94, Revision B.3, M. J. Frisch, G. W. Trucks, H. B. Schlegel, P. M. W. Gill, B. G. Johnson, M. A. Robb, J. R. Cheeseman, T. Keith, G. A. Petersson, J. A. Montgomery, K. Raghavachari, M. A. Al-Laham, V. G. Zakrzewski, J. V. Ortiz, J. B. Foresman, C. Y. Peng, P. Y. Ayala, W. Chen, M. W. Wong, J. L. Andres, E. S. Replogle, R. Gomperts, R. L. Martin, D. J. Fox, J. S. Binkley, D. J. Defrees, J. Baker, J. P. Stewart, M. Head-Gordon, C. Gonzalez, and J. A. Pople, Gaussian, Inc., Pittsburgh PA, 1995.

(21) A. Becke: *Phys. Rev. A* **38**, 3098-3100 (1988).

(22) C. Lee, W. Yang, and R. G. Parr: *Phys. Rev. B* **37**, 785-789 (1988).

(23) J. P. Perdew: *Phys. Rev. B* **33**, 8822-8824 (1986).

(24) J. P. Perdew, and A. Zunger: *Phys. Rev. B* **23**, 5048-5079 (1981).

(25) A. Becke: *J. Chem. Phys.* **98**, 5648-5652 (1993).

(26) J. P. Perdew and Y. Wang: *Phys. Rev. B* **45**, 13244-13249 (1992).

(27) P. M. W. Gill, B. G. Johnson, and J. A. Pople: *Int. J. Quantum Chem.* **26**, 319-331 (1992).

(28) B. G. Johnson, P. M. W. Gill, and J. A. Pople: *J. Chem. Phys.* **98**, 5612-5626 (1993).

(29) C. Sosa and C. Lee: *J. Chem. Phys.* **98**, 8004-8011 (1993).

(30) R. H. Hertwig and W. Koch: *J. Comp. Chem.* **16**, 576-585 (1995).

(31) R. S. Grev and H. F. Schaefer III: *J. Chem. Phys.* **91**, 7305-7306 (1989).

(32) B. R. Miller and M. Fink: *J. Chem. Phys.* **75**, 5326-5328 (1981).

(33) J. W. Andzelm and E. Wimmer: *J. Chem. Phys.* **96**, 1280-1303 (1992).

(34) E. R. Davidson: *Rev. Comput. Chem.* **1**, 373-382 (1990).

(35) P. R. Taylor: *Lecture Notes in Quantum Chemistry* (B. O. Roos, Ed.), Springer-Verlag, Berlin (1992), pp. 325-412.

(36) M. Klobukowski: *Can. J. Chem.* **72**, 1741-1752 (1994).

(37) E. Magnusson and H. F. Schaefer III: *J. Chem. Phys.* **83**, 5721-5726 (1985).

(38) G. Herzberg: *Molecular spectra and molecular structure* Van Nostrand, Princeton, vol. III, p. 644 (1967).

(39) K. Nakamoto: *Infrared and Raman spectra of inorganic and coordination compounds* Wiley, New York, p. 150 (1986).

(40) K. K. Irikura: *J. Chem. Phys.* **102**, 5357-5367 (1995).

(41) N. C. Handy, *Lecture Notes in Quantum Chemistry II* (B. O. Roos, Ed.), Springer-Verlag, Berlin (1994), pp. 99-124.

The Oxonium Rydberg Radical: Electronic Transitions

C. Lavín and I. Martin

Departamento de Química Física

Facultad de Ciencias; Universidad de Valladolid

47005 Valladolid, Spain

Abstract

The Quantum Defect Orbital (QDO) method has been applied to the study of transition probabilities in the oxonium Rydberg radical H_3O. Absorption oscillator strengths and Einstein emission coefficients are reported and compared with the results of an earlier, simplified, molecular version of QDO method.

ADVANCES IN QUANTUM CHEMISTRY, VOLUME 28

0065-3276/97 $25.00

1. Introduction

Rydberg states form an important class of excited electronic states in atomic and molecular systems (1). At present, there is a renewed interest in high energy states which is stimulated by general problems of space research. A particularly interesting class of molecules in this context is that of "Rydberg molecules" (2), for which the ground electronic state is unstable but all the excited states have Rydberg character. They possess long lifetimes compared to rotational or vibrational periods, and their corresponding cation is quite stable. A number of diatomic and polyatomic Rydberg molecules have recently been observed in astrophysical regions (3). They also are of more general chemical interest since some of them have already been detected as short-lived intermediates in several chemical reactions (4).

The first polyatomic Rydberg molecule experimentally observed and studied by Herzberg (5) and Herzberg and co-workers (6) was H_3. Since then, only a few polyatomic Rydberg molecules have been identified, such as the ammonium (7) and oxonium (8,9) radicals. Because of the large proton affinity of some the second-row hydrides, some of which have been observed in interstellar regions (10), the corresponding cations are expected to be stable. The addition of an electron to the cations, a favorable process in the aforementioned regions (11), would yield the corresponding Rydberg radicals. However, the spectra of most of these radicals has not been obtained in the laboratory, with the exception of ammonium, NH_4. The theoretical determination of these spectra becomes, thus, a requisite for diagnosing astrophysical observations as well as for establishing the mechanisms of important chemical reactions that take place on the Earth.

The relevance of the oxonium Rydberg radical in astrophysically important regions has manifested itself in the detection of two transitions attributed to H_3O^+ by Wooten et al. (12) and by van Dishoek et al. (13). Some theoretical models assume a non-negligible yield for the electron capture process of H_3O^+ and, hence, the existence of H_3O in interstellar clouds and nebulae. Turner (3) has more recently included H_3O in a group of molecules present in interstellar media. Also, a possible mechanism for the formation of either H_3O^+ or H_3O in interstellar regions would be a heterogeneous catalysis reaction taking place on the surface of dust grains after H_2O had been adsorbed, as very recently suggested by Howe and co-workers (14).

The first evidence for the existence of H_3O dates from as far back as 1955 and 1964, when Sworski (15) identified this radical in his kinetic study of the radiolysis of water. A few years later, Melton and Joy (16) claimed to have detected H_3O by mass spectrometry in an experiment in which an

electron beam interacted with water vapor. A more recent technique for obtaining Rydberg radicals consists of an electron capture process of their parent ion in a collision with a beam of metal atoms whose ionization energy must be of the same order of magnitude as the electron affinity of the Rydberg cation (8,9). The neutral Rydberg radical and the ionized metal atom are the resulting fragments. In the particular experiments performed on H_3O^+, this ion is first produced by the chemical ionization of water, or of water mixed with molecular hydrogen. Then the Rydberg ions are accelerated and focused into a neutralization chamber that contains atomic potassium at low pressure (8,9).

In diagnosing astrophysical observations, the availability of reliable theoretical transition probabilities is essential, since they can allow the determination of molecular abundances in the different regions explored, in addition to electron temperatures and densities. In the laboratory, the experimental study of Rydberg series in molecules constitutes a relatively recent development in experimental spectroscopy. A number of ab initio calculations have so far been carried out on Rydberg molecules, such as the frequently-quoted Hartree-Fock (HF) study of H_3 by King and Morokuma (17), the self-consistent field frozen-core calculation with floating-spherical-Slater-type orbitals (FSSO) on the second-row Rydberg hydrides by Raynor and Herschbach (18), and the more recent extensive-Gaussian-basis set calculation on H_3 by Diercksen et al. (19). This comprehensive study has brought out the problem encoutered by ab initio procedures when applied to Rydberg molecules, even the most sophisticated ones: Diercksen and co-workers found the energy ordering of the Rydberg levels of H_3 to be basis-dependent. An additional and important problem when ab initio procedures are employed to calculate transition probabilities was pointed out by Oddershede (20) in the context of molecular astrophysics. This author recalls that the methods based on the variational principle yield wavefunctions of rather less quality than the energies they provide. Additionally, in configuration interaction (CI) methods, it is standard usage to perform separate energy optimization on individual states (often using different basis sets). The states so obtained are non-orthogonal, and the calculation of transition matrix elements between them is not a trivial problem. Given this situation, we considered the adequacy of modeling the molecular Rydberg states with a semi-empirical method that had proven successful for atomic Rydberg states, on the grounds that an electron in a sufficiently excited molecular Rydberg state can be expected to possess a quasi-hydrogenic character (with the spherical atomic core replaced by a molecular cation which imposes "internal crystal field" splittings according to its symmetry).

In a previous study on the Rydberg transition probabilities in H_3O, a simplified QDO model, in which only the radial part of the orbital is explicitly defined, has been used (21). In a subsequent study on NH_4 and

H_2F Rydberg radicals, an improved approach, in which both the radial and the angular parts of the orbital are determined, has been formulated (22). This improved approach has been very recently applied to the recalculation of the oscillator strengths of H_3 (23), the results being superior in quality to those of our earlier calculation (24). In the present paper, the new QDO approach has been applied to study the Rydberg spectrum of H_3O.

2. Computational procedure

The QDO wavefunctions are represented by orbitals which are solutions of a one-electron Schrödinger equation

$$[-\frac{1}{2}\Delta + V(r,\vartheta,\varphi)_M]\psi(r,\vartheta,\varphi)_{n\mu\nu} = E_{n\mu}\psi(r,\vartheta,\varphi)_{n\mu\nu}, \quad (1)$$

where V_M is an effective potential of the molecular core. The solutions to the above equation can be written as follows

$$\psi(r,\vartheta,\varphi)_{n\mu\nu} = \frac{1}{r}R(r)_{n\mu}\,\Xi(\vartheta,\varphi)_{\mu\nu}, \quad (2)$$

n and l are, respectively, the principal and the orbital angular momentum quantum numbers, μ and ν label different wavefunctions corresponding to the same (n,l) pair. The radial part of the wavefunction is obtained from the equation

$$[-\frac{d^2}{2dr^2} + \frac{l(l+1)}{2r^2} + V(r)_a]R(r)_a = E_a R(r)_a, \quad (3)$$

where a stands for (n,l,μ). The effective central field potential is defined as

$$V(r)_a = \frac{(c - \delta_a)(2l + c - \delta_a + 1)}{2r^2} - \frac{1}{r}, \quad (4)$$

Solutions of this equation are related to the Kummer functions (21). The parameter δ_a is the quantum defect and *c* is an integer chosen to ensure the normalizability of the orbitals and their correct nodal pattern -the number of radial nodes is equal to *n-l-c-1*.

The mathematically alowed values of c are determined by the following inequality (21):

$$\delta - l - \frac{3}{2} < c \leq n - l - 1, \tag{5}$$

The quantum defect, δ_a, corresponding to a given state, is related to the energy eigenvalue through the following equation,

$$E_a = T - \frac{1}{2(n_a - \delta_a)^2}, \tag{6}$$

where T is the ionization energy. Since usually experimental energies are only known for very few transitions and since their assignment is frequently uncertain, in many cases transition energies are taken from theoretical calculations or even from extrapolation formulae (24)

In the case of spherically symmetric systems, the pairs of indices μ and ν correspondig to the magnetic quantum numbers *m=-l, -l+1,..., l* and $\Xi(\vartheta, \varphi)_{l\mu\nu}$ are equal to the spherical harmonics $Y(\vartheta, \varphi)_{lm}$. In the case of molecules the angular part of the QDO wavefunction may be expressed as a symmetry-adapted combination of spherical harmonics. Index μ in this case identifies the irreducible representation of the appropiate symmetry group and ν labels the basis functions of this representation. For H_3O the molecular point-group symmetry is C_{3v}. In this case Y_{00} corresponds to the totally symmetric representation $A_1(s)$, Y_{10} -to $A_1(p)$ and Y_{20} -to $A_1(d)$. The functions $Y_{1\pm1}$, $Y_{2\pm1}$ and $Y_{2\pm2}$ span the representations E(p) and E(d). The combinations of the spherical harmonics which form bases for the irreducible representations may readily be constructed using standard techniques (25). One of the main advantages of this procedure is that is leads to closed-form analytic expressions for the transition integrals

The absorption oscillator strength for a transition between two states *a* and *b* may be expressed as

$$f(a \rightarrow b) = \frac{2}{3} (E_b - E_a)\, Q\{a \rightarrow b\}\, |R_{ab}|^2, \quad (7)$$

where Q{a-b}, referred as the *angular factors*, result from the angular integration, and the radial transition moment integrals are defined as

$$R_{ab} = \langle R_a(r) | r | R_b(r) \rangle. \quad (8)$$

The values of Q{a-b} for the group C_{3v} are collected in Table I.

Table I. Values of non-zero angular factors Q{a-b} for *l*=0, 1, 2

C_{3v}	Q {A_1(s) - A_1(p)} = 1/3
	Q {A_1(s) - E(p)} = 2/3
	Q {E(p) - A_1(s)} = 1/3
	Q {A_1(p) - A_1(d)} = 4/15
	Q {A_1(p) - E(d)} = 2/5
	Q {E(p) - E(d)} = 1/5
	Q {E(p) - E(d)} = 2/5

The Einstein transition probabilities for spontaneous emission are related to the absorption oscillator strengths through the well-known expression,

$$A_{ba} = 6.6702.10^{15}\, \lambda^{-2}\, (g_a / g_b)\, f_{ab}, \quad (9)$$

where the wavelength for the transition, λ, is in Angstroms, and A_{ba} is expressed in seconds^{-1}. g_a and g_b are, respectively, the statistical weights of the initial and final states in the absorption process.

3. Results and analysis

In our calculations on H_3O, we have adopted the C_{3v} pyramidal geometry predicted by Raynor and Herschbach (18) with the procedure we mention in the Introduction, in which the bond lengths are 1.824 bohrs and the bond angle is 116°. This geometry is in good agreement with that of an earlier calculation by Diercksen et al. (26) and with the nuclear magnetic resonance results obtained by Symons (27). Given the lack of experimental energy data for the Rydberg states, we have employed the quantum defects and ionization potential also reported by Raynor and Herschbach (18), whose spectral study of this radical is the only one that we have found in the literature. The quantum defects for H_3O, together with those of its united atom limit, Na (28), are collected in Table II. The internal crystal field splittings displayed by the energy levels of the radical due to the symmetry of the molecular core are reflected in its quantum defects.

Table II. Rydberg states of H_3O at C_{3v} geometry: excitation energies (second column) and the corresponding quantum defects (third column). Data for the united atom limit (sodium) are also included (the last column).

State	E (eV)[a]	FSSO[a]	Na[b]
1 A_1 (3s)	0.00	1.2959	1.3729
3 A_1 (4s)	2.92	1.2255	1.3571
6 A_1 (5s)	3.64	1.3875	1.3527
1 E (3p)	1.88	0.7993	0.8829
2 A_1 (3p)	2.26	0.6332	
4 E (4p)	3.46	0.6703	0.8669
5 A_1 (4p)	3.52	0.5827	
2 E (3d)	3.01	0.1492	0.0103
3 E (3d)	3.29	-0.1204	
4 A_1 (3d)	3.23	-0.0581	
5 E (4d)	3.72	0.2397	0.0123
6 E (4d)	3.82	0.0277	
7 A_1 (4d)	3.85	-0.0393	

[a] Raynor and Herschbach (18)
[b] Moore (28)

As previously done (23), in the present work we have chosen $c = \min(n_l) - l - 1$, where $\min(n_l)$ stands for the lowest n value corresponding to the given l. For example, if $l = 0,1,2$, then $\min(n_l) = 3$.Whith this choice the radial wavefunctions are nodeless for $n = l$.

Given the similarities observed between the spectra of the Rydberg radicals, for those it has been possible to measure, and those of their united atom limit, we have considered it most interesting to calculate f-values and Einstein emission coefficients for those transitions whose wavelengths fall within the range of those of the most prominent transitions of sodium. Thus, the most promising spectral bands for the identification of H_3O would fall into two main regions: 5000-7000 Å and 9000-12000 Å. Additional transitions which may be of practical interest are those belonging to the same Rydberg series as the ones which give rise to the former.

We have collected our results, in Tables III to V, together with those of the FSSO calculations (18) grouped by the symmetry of the initial and final states involved in the transition. This has been done with the purpose of showing that the QDO calculations reflect the expected decrease in the transition probability as the transition energy increases within a given Rydberg series. The magnitude of the QDO oscillator strengths displays an abrupt decrease along a given Rydberg series as the principal quantum number of the upper state increases. This fact can be explained in terms of a decrease in the overlap between the initial and final states, which becames so substantial at high-energy transitions that is no longer compensated by the corresponding increase in the transition energy. A Rydberg series is characterized by the symmetry of the upper and lower states and by their angular momentum quantum number in the united atom limit. A more careful inspection of Raynor and Herschbach's tables (18) has lead us to recalculate some of their data. This is why some of the results we now include in the present tables under the FSSO heading (18) do not exactly coincide with those included in our former study of the H_3O (29). Our present QDO f-values and Einstein coefficients resemble better than the previous ones (29) the revised FSSO data, in particular, for the strongest transitions. However, in Raynor and Herschbach's results, the decreasing intensity along a Rydberg series is often not observed. The lack of experimental intensities makes us difficult to make any definite judgement on the quality of the QDO transition probabilities over that of the other theoretical results (18). However, in calculations on other Rydberg molecules (24), for which a relatively large body of comparative data was available, including some experimental intensities, the performance of the QDO method has been quite satisfactory over that of ab initio procedures.

Table III. Absorption oscillator strengths and Einstein emission coefficients (in units of 10^7/s) for the 3s-np (n=3-10) electronic transitions in H_3O. f-values are multiplied by 10^3.

Transition	f(QDO)[a]	f(FSSO)[b]	A(QDO)[a]	A(FSSO)[b]
$1A_1(3s) - 2A_1(3p)$	297	293	6.55	6.48
$1A_1(3s) - 5A_1(4p)$	24.5		1.32	
$1A_1(3s) - 8A_1(5p)$	7.07		0.49	
$1A_1(3s) - 11A_1(6p)$	3.08		0.24	
$1A_1(3s) - 14A_1(7p)$	1.64		0.13	
$1A_1(3s) - 17A_1(8p)$	0.99		0.08	
$1A_1(3s) - 20A_1(9p)$	0.65		0.06	
$1A_1(3s) - 23A_1(10p)$	0.45		0.04	
$1A_1(3s) - 1E(3p)$	523	739	3.99	5.64
$1A_1(3s) - 4E(4p)$	31.2		0.81	
$1A_1(3s) - 7E(5p)$	7.92		0.27	
$1A_1(3s) - 10E(6p)$	3.25		0.12	
$1A_1(3s) - 13E(7p)$	1.68		0.07	
$1A_1(3s) - 16E(8p)$	0.99		0.04	
$1A_1(3s) - 19E(9p)$	0.64		0.03	
$1A_1(3s) - 22E(10p)$	0.44		0.02	

[a] This work
[b] Raynor and Herschbach (18)

Table IV. Absorption oscillator strengths and Einstein emission coefficients (in units of 10^7/s) for the 3p-ns (n=4-10) electronic transitions in H_3O. f-values are multiplied by 10^3.

Transition	f(QDO)[a]	f(FSSO)[b]	A(QDO)[a]	A(FSSO)[b]
$2A_1(3p) - 3A_1(4s)$	183	305	0.35	0.58
$2A_1(3p) - 6A_1(5s)$	0.44		0.004	
$2A_1(3p) - 9A_1(6s)$	0.08	71	0.001	0.98
$2A_1(3p) - 12A_1(7s)$	0.03		0.0006	
$2A_1(3p) - 15A_1(8s)$	0.02		0.0003	
$2A_1(3p) - 18A_1(9s)$	0.01		0.0002	
$2A_1(3p) - 21A_1(10s)$	0.01		0.0001	
$1E(3p) - 3A_1(4s)$	171	162	1.61	1.53
$1E(3p) - 6A_1(5s)$	7.01	70	0.19	1.90
$1E(3p) - 9A_1(6s)$	1.92	64	0.08	2.63
$1E(3p) - 12A_1(7s)$	0.83	15	0.04	0.72
$1E(3p) - 15A_1(8s)$	0.45		0.02	
$1E(3p) - 18A_1(9s)$	0.27		0.02	
$1E(3p) - 21A_1(10s)$	0.18		0.01	

[a] This work

[b] Raynor and Herschbach (18)

Table V. Absorption oscillator strengths and Einstein emission coefficients (in units of 10^7/s) for the 3p-nd (n=3-6) electronic transitions in H_3O. f-values are multiplied by 10^3.

Transition	f(QDO)[a]	f(FSSO)[b]	A(QDO)[a]	A(FSSO)[b]
$2A_1(3p) - 4A_1(3d)$	325	248	1.34	1.02
$2A_1(3p) - 7A_1(4d)$	17.8		0.20	
$2A_1(3p) - 10A_1(5d)$	4.41	32.8	0.07	0.51
$2A_1(3p) - 13A_1(6d)$	1.78	48.5	0.03	0.89
$2A_1(3p) - 16A_1(7d)$	0.91		0.02	
$2A_1(3p) - 3E(3d)$	503	509	0.96	0.97
$2A_1(3p) - 6E(4d)$	16.6		0.09	
$2A_1(3p) - 9E(5d)$	3.50		0.03	
$2A_1(3p) - 12E(6d)$	1.30	79	0.01	0.72
$2A_1(3p) - 15E(7d)$	0.63		0.006	
$1E(3p) - 4A_1(3d)$	79.6	106	1.27	1.68
$1E(3p) - 7A_1(4d)$	8.99	54.6	0.30	1.85
$1E(3p) - 10A_1(5d)$	2.84	12.3	0.13	0.55
$1E(3p) - 13A_1(6d)$	1.29		0.07	
$1E(3p) - 16A_1(7d)$	0.71		0.04	
1E(3p) - 3E(3d)	477	260	3.59	1.96
1E(3p) - 6E(4d)	42.5	73.0	0.70	1.2
1E(3p) - 9E(5d)	12.5	31.2	0.28	0.69
1E(3p) - 12E(6d)	5.47	29.3	0.14	0.75
1E(3p) - 15E(7d)	2.95		0.08	
1E(3p) - 2E(3d)	222	483	1.24	2.7
1E(3p) - 5E(4d)	5.49	39.8	0.08	0.59
1E(3p) - 8E(5d)	1.03	32.6	0.02	0.69
1E(3p) - 11E(6d)	0.36		0.009	
1E(3p) - 14E(7d)	0.17		0.005	

[a] This work

[b] Raynor and Herschbach (18)

It should be mentioned here that even though some transitions are theoretically predicted to have large transition probabilities, they may in practice be rather weak if the upper state is severely predissociated or is not significantly populated during the electron capture process that forms the Rydberg molecule from its parent cation.

Regarding Table V a remark is in order: what Raynor and Herschbach classify as the 10E(5d)-1E(3p) transition in their Table IV (18) can be no other than the $10A_1$(5d)-1E(3p) transition, if their rather confusing data presentation is carefully scrutinized.

4. Concluding remarks

The overall quality of the present results seems to be better than of the ones obtained using the simplified approach (29). In the latter one, the angular parts of the orbitals are not explicitly defined, with the value of Q in Eq. (7) being set equal to 1, and the molecular selection rules for the electronic transitions being assumed to be valid. Then, the intensities of the transitions are determined by the values of the radial integrals R_{ab}. In the present approach, both radial and angular parts of the QDO wavefunctions are determined according to Eq.(2), with $\Xi(\vartheta,\varphi)$ being expressed as a linear combination of Y_{lm}. In consequence, transitions between Rydberg states for which the difference between the l values is other that ± 1 are forbidden. This is certainly a drawback of our present formulation, though these transitions are usually very weak. This is, however compensated by allowing for an analytic wavefunction describing the molecular Rydberg electron.. The use of this method may serve as an alternative to expensive ab initio procedures, which are not always reliable.

Acknowledgements

This work has been supported by the D.G.I.C.Y.T. of the Spanish Ministry of Education and Science, under Project No.PB94-1234-C03-03.

References

(1) A.B.F.Duncan, "Rydberg series in atoms and molecules", Academic Press: New York, 1971.
(2) G.Herzberg, Ann.Rev.Phys.Chem. 1987, **38**, 27, and references therein.
(3) B.E.Turner, Symp.Int.Astron.Union 1992, **150**, 181.
(4) M.E.Jacox, J.Phys.Chem.Ref.Data, Monograph 3, 1994.
(5) G.Herzberg, J.Chem.Phys. 1979, **70**, 4806 .
(6) I.Dabrowski, G.Herzberg, Can.J.Phys. 1980, **58**, 1238; G.Herzberg and J. K. G. Watson, Can. J. Phys. 1980, **58**, 1250; G. Herzberg, H. Lew, J. Sloan, and J.K.G. Watson, Can. J. Phys. 1981, **59**, 428; G.Herzberg, Discuss. Faraday Soc. 1981, **71**, 165.
(7) G.Herzberg, J.J. Hougen, J.Mol.Spectrosc. 1983, **97**, 430; G.Herzberg, J.Mol.Struct. **113**, 1 (1984).
(8) B.W.Willians, R.F.Porter, J.Chem.Phys. 1980, **73**, 5598.
(9) G.I.Gellene, R.F.Porter, J.Chem.Phys. 1984, **81**, 5570.
(10) W.W.Duley, D.A.Williams, "Interstellar Chemistry", Academic Press: London 1984.
(11) M.Guelin, in "Molecules in Physics, Chemistry and Biology", Maruani, J.; Ed., Kluwer: Dordrecht, 1988.
(12) H. A.Wootlen, J. G.Mangum, B.E.Turner, M.Bogey, F.Boulanger, F. Combes, P.J. Encrenaz, M. Gerin, Astrophys. J.Letters, as reported by B.E.Turner 1992.
(13) E.van Dishoek, T.C.Phillip, as reported by B.E.Turner, 1992.
(14) D.A. Howe, J.M. Rawlings, D.A. Williams, in "Advances in Atomic, Molecular and Optical Physics". Bates, D., Bederson, B. Eds., Academic Press: New York, 1994.
(15) T.J.Sworski, J.Chem.Soc. 1955, **77**, 4689; 1964, **86**, 5034.
(16) C.E.Melton, H.W.Joy, J.Chem.Phys. 1967, **46**, 4275.
(17) H.F.King, K.Morokuma, J.Chem.Phys. 1979, **71**, 3213.
(18) S.Raynor, D.R.Herschbach, J.Phys.Chem. 1982, **86**, 3592.
(19) G.H.F.Diercksen, W.Duch, J.Karwowski, Chem.Phys.Lett. 1990, **168**, 69.
(20) J.Oddershede, in "Molecular Astrophysics", Diercksen, G.H.F., Huebner, W.F., Langhoff, P.W., Eds., Reidel: Dordrecht, 1984.
(21) G. Simons, J. Chem. Phys. 1974 , **60**, 645; I. Martin, G. Simons, J.Chem.Phys. 1975, **62**, 4799; Mol.Phys. 1976, **32**, 1017.
(22) I.Martin, C. Lavín, M.Velasco, M.O.Martin, J.Karwowski, G. H. F. Diercksen, Chem.Phys. 1996, **202**, 307.

(23) I.Martin, C.Lavín, J.Karwowski, Chem.Phys.Lett., in press.
(24) I.Martin, J. Karwowski, G.H.F. Diercksen, C.Lavín, Int. J.Quant. Chem. 1993, Symp.**27**, 723.
(25) M.Weissbluth, "Atoms and Molecules", Academic Press: New York, 1978.
(26) G.F.H.Diercksen, W.P.Kraemer, B.O.Roos, Theor.Chim.Acta 1975, **36**, 249.
(27) M.C.R.Symons, J.Am.Chem.Soc. 1980, **102**, 3982.
(28) C.E.Moore, Nat. Bur. Stds. Ref. Data Section, Circ.no 35, Washington, D.C., 1971.
(29) I.Martin, P.Campo, C.Lavín, Int.J.Quant.Chem.Symp. 1995, **29**, 631.

An *ab initio* study of four-membered rings. Boranes HBXYBH; (X, Y = C, N, O)

Borislava Batandjieva, Ingrid Miadoková

and Ivan Cernušák*

Department of Physical Chemistry, Faculty of Science Comenius University, Mlynská dolina CH-1, SK-84215 Bratislava, Slovakia.

*E-mail: cernusak@fns.uniba.sk

Dedicated to Professor Geerd H.F. Diercksen, in honor of his 60th birthday

Abstract

A prediction of four-membered cyclic boranes is presented. Structure and bonding of planar and puckered rings optimized at MBPT(2)/PVDZ level are discussed. Singlet-triplet gaps and thermodynamic stabilities of the rings based on Coupled Cluster calculations are given.

ADVANCES IN QUANTUM CHEMISTRY, VOLUME 28

0065-3276/97 $25.00

1. Introduction

Hydrocarbon-based conjugated polymers are subject of systematic experimental and theoretical studies due to their potential applicability in semiconductor technology. The crucial quantity of interest is the band gap that influences the electrical conductivity of the material. In principle, there are two ways to tune this gap: either by doping with light metals (1-3) or substituting carbon by heteroatom while conserving the π-system of the polymer (4-7). Success of the latter possibility relies on knowledge of molecular structures representing the building blocks of the polymer. This can be accomplished by quantum chemical calculations. Until recently, the polymers used in band gap engineering were compounds based on traditional five- or six-membered π-systems (polypyrrole, polythiophene, polyperelene or poly-*p*-phenylene). Four-membered rings represent challenging and provoking material: they consist of less number of atoms and, hence, the number of possibilities to arrange them in the ring is smaller. One can construct the heteropolymer by altering the electron-acceptor moiety with electron-donor one (7). The local geometry is quite sensitive to the presence of heteroatom that may cause puckering and hence loss of delocalized π-electron states.

Tanaka et al. (4) and Yamanaka et al. (5) investigated in detail electronic behavior of boron heteroatoms in polymer models. They pointed out that boron-substituted fragments exhibited interesting properties and suggested that further investigation of its role in different environments is required. As the first step before pursuing the study of suitable extended systems we decided to investigate the thermodynamic stability of various boron-containing four-membered rings in their singlet and triplet states. This area offered a wealth of questions to answer.

Four-membered rings containing boron have attracted some attention in the last two decades (8-10). Our motivation was: what happens if one feeds the electron "deficient" diborane B_2H_2 with some "electron-rich" π-system? How would act in this role two isoelectronic diatomics, carbon monoxide and nitrogen molecule? B_2H_2 combined with CO or N_2 is interesting since diborane was predicted to be in $^3\Sigma_g$ ground state (11), while both diatomics are singlets. What state will the resulting rings prefer? Chemical intuition suggests that the singlets

may prevail since the diatomics can sacrifice part of theirs π-system to couple with both unpaired electrons in B_2H_2. How would the structure and bonding depend on the sequence of the atoms in the ring? There are in principle two possibilities: either with 'diagonally opposed positions' (1,3 dibora-isomers) or 'neighboring positions' for boron atoms (1,2 dibora-isomers). Recently, we have investigated isomers of borane BH bound with CN^-, CO and CF^+ (12) and the results have shown that one can view these new species as compounds rather than complexes. Turning our curiosity to B_2H_2 combined with CO or N_2 is an extension of our previous studies (13) and another example of the interesting *"complex or compound"* problem. We note that to date the structures investigated in this study are known neither theoretically nor experimentally.

2. Computational details

Approximate geometries of the structures are sketched in the following Scheme.

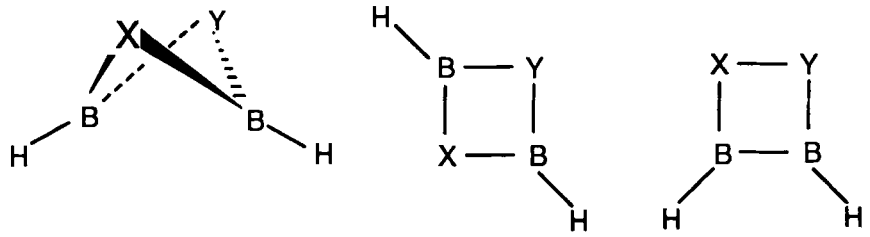

1a, **3a**, **1b**, **3b** **2a**, **2b**, **4b**

(**1** - 2,4,1-diboroxetan-3-ylidene, **2** - 2,3,1-diboroxetan-4-ylidene, **3** - 1,3-didehydro-1,3-diaza-2,4-diboretane, **4** - 3,4-dibora-1,2-diazetine; **a** - singlet, **b** - triplet).

We have adopted the following computational strategy in gradient geometry optimizations (14). Initial geometries and Hessians were obtained at the SCF level with the PVDZ basis set (15). Final geometry tuning was performed at the MBPT(2)/PVDZ level, for some molecules also at the MBPT(2)/PVTZ level (15). Core electrons were frozen in correlated optimizations. To confirm the true

minima on the potential energy surface the stationary points were checked against the frequency calculations at the final optimization level. Single point, frozen-core coupled cluster (CC) (16, 17) calculations (CCSD+T(CCSD) (18) and CCSD(T) (19)) were performed at these stationary points to evaluate relative energies. UHF reference was used for the triplet states. For each system the largest T_1 and T_2 amplitudes from CC-calculation were checked to judge the adequacy of the single-reference approach. Where possible, the electronic energies were converted to thermodynamic quantities ΔH_{298K} and ΔG_{298K} within the rigid-rotor harmonic-oscillator model.

Usually, it is reasonable to optimize the geometry at the simplest correlated level and to compute energy differences (within single-point calculation technique) with a more elaborate method. Recently, Espinosa-García and Corchado have shown that for reaction energies one can expect partial compensation or reduction of energy errors introduced by this approach (20). Their arguments are based on the comparison of the SCF/STO-3G and the MBPT(2)/6-31G(d,p) results for the minimum energy path of the reaction $NH_3+H \rightarrow NH_2+H_2$. In our approach we are using even softer change in the computational level, that is, the same basis set but different correlated level. Thus, assuming that the potential energy surfaces MBPT(2)/PVDZ and CCSD+T(CCSD)/PVDZ lie quite close to each other, the corresponding errors in relative energies could be acceptably small. The performance of basis sets used in the evaluation of energies was tested for the series of dissociation energies of diatomics (21,22). Thus, more accumulated data on various types of reactions are desirable. In the main body of the paper we present the theoretical predictions of the structure and energetics of four-membered rings based mostly on CC/PVDZ data and compare them, where possible, with CC/PVTZ ones.

Table 1

Selected MBPT(2)/PVDZ-optimized bond lengths (Å), bond- and dihedral angles (deg) [a].

		BO	CB	BH	∠BCB	∠BOB	∠BCBO
1a	$^1A'$	1.465	1.507	1.190	80.90	83.74	41.68
		1.464	*1.505*	*1.189*	*80.89*	*83.71*	*41.70*
1b	$^3B_1$	1.435	1.566	1.197	82.10	91.81	0.0
		1.424	*1.552*	*1.182*	*82.38*	*91.74*	*0.0*

		BO	CB	BH	∠BBC	∠BBO	∠OBBC
2a	^1A	1.466	1.620	1.194[b]	79.71	79.89	32.67
				1.195[c]			
2b	^3A	1.491	1.536	1.198[b]	67.29	95.89	19.96
				1.189[c]			

		NN	BN	BH	∠BNB	∠NBN	∠BNBN
3a	^1A	1.853	1.458	1.189	84.75	78.93	41.31
		1.823	*1.446*	*1.175*	*85.34*	*78.16*	*41.53*
3b	^3A	1.614	1.473	1.183	113.31	66.44	5.62
		1.482	*1.435*	*1.165*	*117.10*	*62.18*	*9.51*

		BB	NN	BN	HB	∠BBN	∠NNB	∠BNNB
4b	$^3A_2$	1.615	1.210	1.750	1.194	83.36	96.64	0.0
		1.594	*1.197*	*1.736*	*1.178*	*83.44*	*96.56*	*0.0*

[a] All data referring to PVTZ basis set are displayed in italics; [b] adjacent to oxygen; [c] adjacent to carbon;

3. Results and discussion

The geometries of the rings are in Table 1, the total energies in Tables 2 and 3. Since there is virtually no difference between CCSD+T(CCSD) CCSD(T) energies, we present only the former in Tables 2 and 3. For CBH we have investigated also the lowest singlet and triplet states (23). The final relative energies and S-T gaps for CH_2B_2O are presented in Tables 4 and 5 and for $B_2H_2N_2$ in Tables 6 and 7. We have calculated also triplet states for the geometries of **1a** and **3a** (single point calculations denoted as **1b/a** and **3b/a**) to evaluate the vertical S-T gaps in order to distinguish geometrical and electronic factors.

The PVDZ bonds are longer than PVTZ ones by 0.01-0.02Å and these differences are slightly smaller in the rings than in subsystems. One can treat them as acceptable, keeping in mind the contraction scheme for PVDZ - [3s2p1d]. Prediction of bond angles and torsions for the rings is even less sensitive when going from PVDZ to PVTZ.

Bonding. The classification of bonds in the rings based on bond lengths can assist in resolving the question whether these systems are 'compounds' or merely 'complexes'. Unfortunately, not all bonding environments (similar to those presented here) are tabulated in the literature (24, 25). Single BO experimental bond length ranges from 1.205 to 1.367Å. Our results for **1a** and **1b** indicate elongated BO-bonds (by 0.1-0.2Å), mostly the result of ring strain, with subsequent puckering and C...O lone-pair repulsion. Theoretical BC data match satisfactorily with the experimental single BC-bonds (1.56-1.65Å). BN bonds range from 1.43 to 1.47Å, while the experimental single BN bonds are larger (1.55-1.61Å). Clearly, our values for the ring match better with experimental ones from borazine $B_3H_6N_3$ (1.44Å) or *"inorganic benzene"*. Comparison of iso-electronic **1a** and **3a** shows that the former can be less stable than the latter. Simple qualitative MO analysis reveals that **1a** has puckered-carbene electronic structure with unbalanced lone pairs, two on O and one on C. In contrast to CH_2B_2O, nitrogen isomer **3a** has only two lone pairs, it gains additional stabilization due to

Table 2

Total energies [E/E(h)] and ZPV corrections [kJ/mol] of the rings.

-SCF	-MBPT(2)	-CCSD	-CCSD+ T(CCSD)	ZPV
		1a		
163.18307	163.64230	163.67241	163.69746	84.8
163.23127	*163.79851*	*163.81959*	*163.85350*	-
		1b/a		
163.05253	163.48963	163.52343	163.54451	-
		1b		
163.22668	163.63994	163.67500	163.69187	85.7
163.27451	*163.79015*	*163.81893*	*163.84426*	-
		2a		
163.11861	163.57079	163.60584	163.62939	79.7
		2b		
163.14393	163.58130	163.61515	163.63608	81.8
		3a		
159.40101	159.88827	159.90862	159.93554	87.1
159.44576	*160.03783*	*160.04922*	*160.08556*	-
		3b/a		
159.15352	159.66032	159.67563	159.70861	-
		3b		
159.29030	159.78631	159.79982	159.82680	b
159.34281	*159.92839*	*159.93717*	*159.97095*	-
		4b		
159.29738	159.74485	159.77162	159.79236	83.3

[a] All data referring to PVTZ basis set are displayed in italics; [b] harmonic approximation gave no imaginary frequency but for one stretching vibration lead to artificially large wavenumber.

Table 3

Total energies [E/E(h)] and ZPV corrections [kJ/mol] of the fragments [a].

-SCF	-MBPT(2)	-CCSD	-CCSD+ T(CCSD)	ZPV
		B_2H_2		
50.42570	50.55208	50.58186	50.58627	56.0
50.43904	*50.59491*	*50.62250*	*50.62911*	*56.4*
		CO		
112.74669	13.03681	113.04380	113.05668	12.6
112.77889	*113.13565*	*113.13834*	*113.15711*	*12.7*
		N_2		
108.94670	109.26295	109.26327	109.27699	13.0
108.97966	*109.35776*	*109.35460*	*109.37461*	*13.13*
		CBH[b]		
62.95688	63.10563	63.13618	63.14217	31.4
62.97095	*63.17383*	*63.20257*	*63.21175*	-
		HBO		
100.17238	100.44233	100.44940	100.46065	37.9
100.20307	*100.53534*	*100.53819*	*100.55460*	*37.5*
		HBN[c]		
79.60163	79.80561	79.83136	79.84126	36.4
79.62446	*79.87580*	*79.89769*	*79.91173*	*35.5*

[a] All data referring to PVTZ basis set are displayed in italics; [b] $^3\Sigma^-$ state, [c] $^2\Sigma$ state

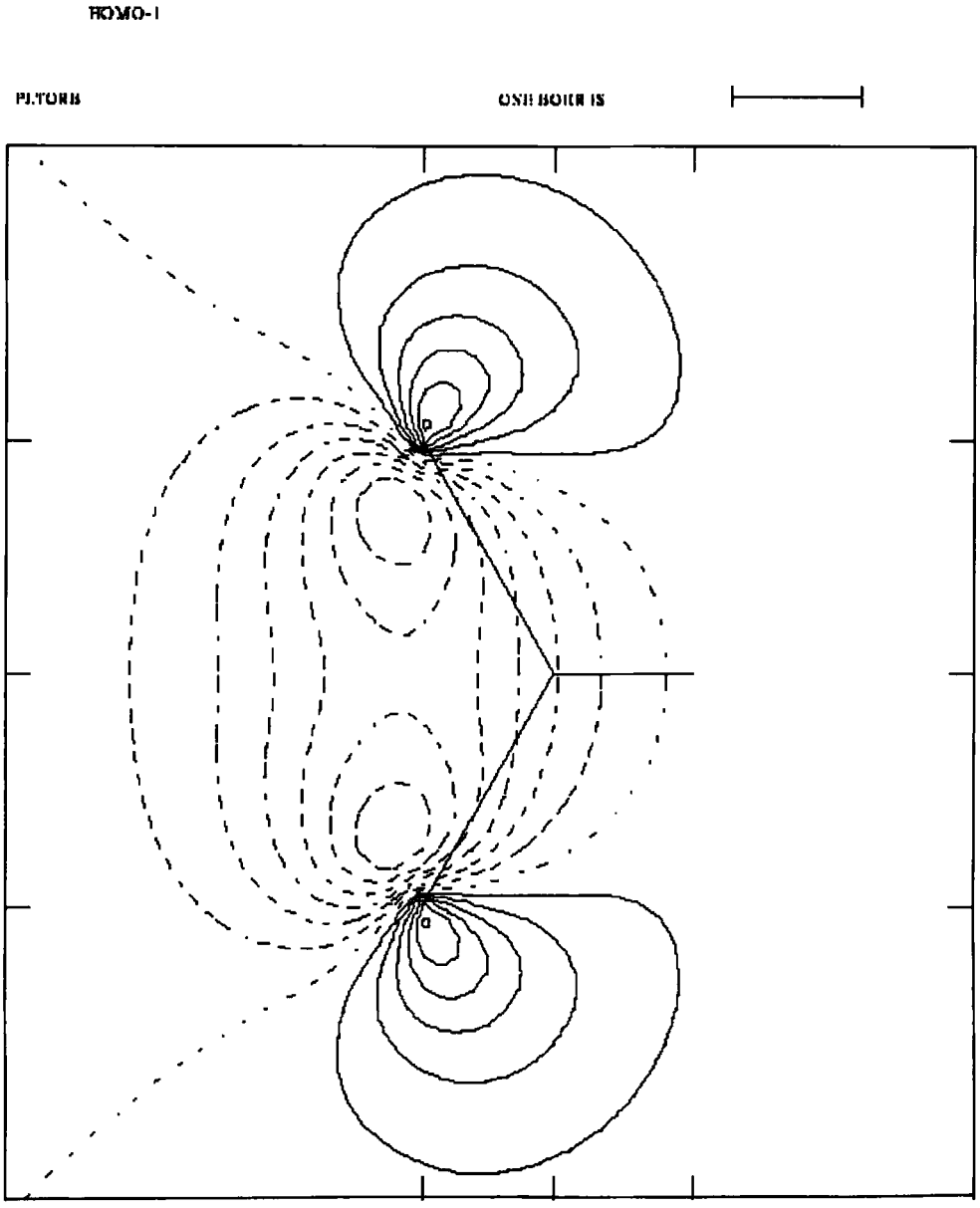

Figure 1. HOMO-1 of $B_2H_2N_2$, projection on YZ plane bisecting the molecule along NN direction. Plotted using PLTORB utility from GAMESS graphical package (26).

better π-electrons delocalization, the corresponding MO extends over the BNBN skeleton. This MO is the mixture of π-contribution from p_z AO's on BNBN and σ-contribution from p_y AO's in NN direction (Fig. 1). Though the systems **3a** and **3b** formally satisfy Huckel's 4n+2 rule, **3a** can be defined as "quasi-aromatic" since it is not planar and, consequently, does not posses pure π-orbitals. These stabilizing effects are missing in CH_2B_2O. The reaction energies correlate with these findings. However, all singlet states are significantly puckered which partly deteriorates the conjugation and delocalization over the ring. The orbital picture in **1b** is close to **1a** with one exception, instead of the carbene lone pair there are in α-set three, almost equivalent, highest occupied MO's, $C(\pi_y)$, $C(\pi_z)$ and $C(\pi_x)$, with orbital energies -0.4143, -0.4638 and -0.4457 hartree, respectively.

The 1,3-interactions may in extreme cases (singlets) lead to bicyclo structures with 1,3-σ bonding (8b). However, such a bonding was neither observed (1,3-atomic distances are too large) nor confirmed by overlap populations. On the other hand, the triplet states are planar or tend to be so. Structure **4b** resembles a complex $B_2H_2...N_2$, since the BN bonds are substantially elongated, 1.750Å (PVDZ) and 1.736Å (PVTZ) and the BN-overlap population (0.166) drops down significantly with respect to **3a** (0.451) or **3b** (0.428). Since the NN bond in **4b** (1.210Å) falls within the experimental range of single NN bonds (1.16-1.26 Å) we can conclude that in **4b** a strong π-donation from N-atoms takes place. The delocalization is common feature for all triplets - the MBPT(2)/PVDZ dipole moments are generally lower 0.579D (**1b**), 0.480 (**2b**), 0.165D (**3b**), 0.383D (**4b**), while those for singlets are substantially higher: 2.071D (**1a**), 1.882 (**2a**), 1.909D (**3a**).

CH_2B_2O isomers. The rearrangement **2**→**1** is favored by 173 (singlet) and 142 (triplet) kJ/mol at 298K. Correlation has negligible stabilizing effect for singlet's but slightly larger destabilizing effect for triplet's rearrangement, respectively. Larger correlation effect in **2b**→**1b** can be partially explained in terms of different spin density. For **1b** it is concentrated on carbon (1.89au) while for **2b**

Table 4

Rearrangement and S-T gaps for CH_2B_2O isomers (kJ/mol) [a].

	2a→**1a** (1)	**2b**→**1b** (2)	**1a**→**1b** (3)		**2a**→**2b** (4)
SCF	-169.3	-217.3	-114.5	*-113.5*	-66.5
MBPT(2)	-187.7	-154.0	6.2	*22.0*	-27.6
CCSD	-174.8	-157.1	-6.8	*1.7*	-24.5
CCSD+T(CCSD)	-178.7	-146.5	14.7	*24.3*	-17.6

[a] All data referring to PVTZ basis set are displayed in italics;

Table 5

Reaction energies of formation of CH_2B_2O isomers (kJ/mol).

$^3\Sigma$ CBH + $^1\Sigma$ HBO → ^{1}A' CH_2B_2O (**1a**) (5)

$^3\Sigma_g$ B_2H_2 + $^1\Sigma_g$ CO → ^{1}A' CH_2B_2O (**1a**) (6)

	(5)		(6)	
SCF	-141.3	*-150.3*	-28.1	*-35.0*
MBPT(2)	-247.7	*-234.6*	-140.2	*-178.4*
CCSD	-228.0	*-207.0*	-122.8	*-154.3*
CCSD+T(CCSD)	-248.5	*-228.8*	-143.1	*-176.7*
ΔH_{298K}	-237.0	-	-131.2	
ΔG_{298K}	-191.0	-	-86.9	

[a] All data referring to PVTZ basis set are displayed in italics;

it is delocalized over the B(0.66au)-C(0.87au)-O(0.33au) moiety. The S-T gap for **1a**→**1b** is slightly enhanced upon the basis set extension. One can split the CCSD+T(CCSD) S-T gap into vertical contribution, **1a**→**1b/a**, representing electronic factor (401.6 kJ/mol) and relaxation, **1b/a**→**1b**, representing geometric factor (-386.9 kJ/mol). The SCF contributions for these processes have opposite

Table 6

Rearrangement and S-T gaps for $B_2H_2N_2$ isomers (kJ/mol) [a]

	4b→3b (7)	**3a→4b** (8)	**3a→3b** (9)	
SCF	18.6	272.1	290.7	*270.3*
MBPT(2)	-66.4	334.1	267.7	*287.3*
CCSD	-31.0	316.6	285.7	*294.2*
CCSD+T(CCSD)	-42.7	328.2	285.5	300.*9*

[a] All data referring to PVTZ basis set are displayed in italics;

signs and partially cancel, while the correlation ones are both positive. Therefore, the overall SCF and correlation contributions (reaction (3)) are opposite and almost cancel leading to rather small gaps. Though the singlet state is preferred for **1** and triplet for **2**, the relatively small S-T gaps suggest that both states could coexist in the gas phase. Formation of **1** from three-atomic fragments is more favorable than from diborane and CO, the corresponding difference in ΔG's is ~100kJ/mol for both states. In other words, one can decompose **1** into B_2H_2 and CO more easily than to CBH and HBO. Correlation contributions, which are quite large for all reactions, have destabilizing effect for S-T gaps and stabilizing effect for rearrangement and ring formation. The tripleexcitations become more important in the latter process, due to the redistribution of electrons during bond-making in the rings. Curiously, MBPT(2) data do not differ too much from CCSD+T(CCSD) due to fortunate cancellation of higher order contributions.

$B_2H_2N_2$ isomers. The S-T gaps are significantly larger than for CO-isomers, ruling out the importance of triplets. However, there is different interplay between electronic and geometrical factors in the total CCSD+T(CCSD) S-T gap.

Table 7

Formation of $B_2H_2N_2$ isomers from radicals (kJ/mol) [a].

$^2\Sigma$ 2HBN $\rightarrow$ ^{1}A $B_2H_2N_2$ (3a) (10)

$^1\Sigma^+$ N_2 + $^3\Sigma_g$ B_2H_2 $\rightarrow$ ^{1}A $B_2H_2N_2$ (3a) (11)

	(10)		(11)	
SCF	-519.2	*-516.8*	-75.1	*-71.0*
MBPT(2)	-727.4	*-751.5*	-192.3	*-223.6*
CCSD	-645.6	*-666.4*	-166.7	*-189.4*
CCSD+T(CCSD)	-664.3	*-688.2*	-189.8	*-214.9*
ΔH_{298K}	-667.7		-176.2	
ΔG_{298K}	-618.9		-131.4	

[a] All data referring to PVTZ basis set are displayed in italics;

The positive vertical contribution 3a→3b/a (595.8 kJ/mol) is almost twice as large as the negative geometry relaxation 3b/a→3a (-310.3 kJ/mol). Moreover, the correlation effects partially cancel in these processes leaving the SCF to be the dominant contribution. Complex 4b can be treated as an intermediate in one of the possible channels in formation of 1,3-diazo-2,4-diboretidine. It may easily convert to 3b or 3a (Table 7) since such a process is the transition *complex* → *compound*, provided that it is formed in process ($^1\Sigma^+$) N_2 +($^3\Sigma_g$) B_2H_2 → ($^3A_2$) $B_2H_2N_2$. However, direct path from HBN radicals to 3a (and to 3b) is thermodynamically more favorable. Reactions including diborane and N_2 are less exothermic for singlet, similarly as for CH_2B_2O and even endothermic for triplets. The correlation contributions for $B_2H_2N_2$ isomers have stabilizing effect in rearrangement reactions and also during

ring formation. The most stable ring among all isomers is **3a**, formation of one BN bond is accompanied by remarkable energy release ~310kJ/mol. In contrast to CH_2B_2O isomers, MBPT(2) data are more scattered and deviate significantly from CCSD+T(CCSD) ones.

4. Summary

In our study we suggest various new four-membered isoelectronic rings formed from BH, C, O and N. Theory predicts remarkable differences in structure and stability between CO- and N_2-isomers. Generally, MBPT(2) reaction energies are scattered, especially for $B_2H_2N_2$ isomers, and can not be recommended even for reliable estimates of reaction energies. Singlet $B_2H_2N_2$ 1,3-isomer is far more stable with respect to three-atomic fragments than the corresponding CH_2B_2O one due to the stabilizing effect of the π-like MO in $B_2H_2N_2$ and destabilizing effect of carbene lone pair on C in CH_2B_2O. Absence of dramatic differences for CCSD-+T(CCSD) and CCSD(T) data signals that the single reference CC approach is sufficient for these systems. The deviation between PVDZ and PVTZ basis sets in relative energies range from 10 to 30 kJ/mol and can be critical for the cases where small absolute values take place and qualitative decisions are expected. Work is in progress on PN- and SiC-isomers and we expect a variety of new species and complexes to arise.

5. Acknowledgments

This research was carried out with the support of the COST action D3/0003/94 and the Slovak Grant Agency grant #1/1455/94. I.C. wants to thank Prof. H. Lischka for hospitality, discussions and computer support from ITC-RC, Vienna University. Stimulating conversations with Prof. V. Bonaciæ-Koutecký and Prof. R. Zahradník are acknowledged. The full description of geometries is available from WWW page http://www.qch.fns.uniba.sk/~cernusak /ic_index.shtml.

References

(1) *Conjugated Polymers: The Novell Science and Technology of Highly Conducting and Nonlinear Optically Active Materials*, edited by J.-L. Brédas and R. Silbey (Kluwer, Dordrecht, 1991).

(2) S. Irle and H. Lischka, J. Chem. Phys. **103,** 1508 (1995).

(3) N.C. Greenham, S.C. Moratti, D.D.C. Bradley R.H. Friend and A.B. Holmes, Nature **345,** 628 (1993).

(4) K. Tanaka, S. Yamanaka, K. Ueda, S. Takeda and T. Yamabe, Synth. Met. **20,** 333 (1987).

(5) S. Yamanaka, T. Inoue, T. Aoyagi, T. Komatsu, Synth. Met. **46,** 221 (1992).

(6) E.E. Havinga, W. ten Hoeve and H. Wynberg, Synth. Met. **55-57,** 299 (1993).

(7) G. Brocks, J. Chem. Phys. **102,** 2522 (1995).

(8) a) K. Krogh-Jespersen, D. Cremer, J.D. Dill, J.A. Pople, P.v.R. Schleyer, J.Amer.Chem Soc. **103,** 2589 (1981); b) P.H.M. Budzelaar, E. Kraka, D. Cremer, P.V.R. Schleyer, J. Amer. Chem Soc. **108,** 561 (1986); c) M. Bühl, Schleyer, M.A. Ibrahim, T. Clark, J.Amer.Chem Soc. **113,** 2466 (1991).

(9) V. Bonaciæ-Koutecký, K. Schöffel, J. Michl, J.Amer.Chem Soc. **111,** 6140 (1989).

(10) C. Liang and L. C. Allen, J.Amer.Chem Soc. **113,** 1878 (1989).

(11) L.A. Curtiss and J.A. Pople: J. Chem. Phys. **91,** 4809 (1989).

(12) A. Pappová, C. A. Deakyne, A. Skancke, I. Cernušák, J. F. Liebman, Mol. Phys. (accepted for publication 1996).

(13) a) I. Cernušák, S. Beck, and Bartlett, R.J., J. Phys. Chem. **96,** 10284 (1992); b)I. Cernušák, M. Urban; P. Ertl, R.J. Bartlett, J. Am. Chem. Soc. **114,** 10955 (1992); c) I. Cernušák, M. Urban; J.F. Stanton, R.J. Bartlett, J. Phys. Chem. **98,** 8653 (1994); d) I. Cernušák and H. Lischka, Chem. Phys. Lett. **241,** 261 (1995).

(14) GAUSSIAN 94, Rev. B, M.J. Frisch, G.W. Trucks, H.B. Schlegel, P.M.W. Gill, B.G. Johnson, M.A. Robb, J.R. Cheeseman, T. Keith, G.A. Petersson, J.A. Montgomery, K. Raghavachari, M.A. Al-Laham, V.G. Zakrzewski,

J.V. Ortiz, J.B. Foresman, J. Cioslowski, B.B. Stefanov, E.S. Replogle, R. Gomperts, R.L. Martin, D.J. Fox, J.S. Binkley, D.J. DeFrees, J. Baker, J.P. Stewart. M. Head-Gordon, C. Gonzales, J.A. Pople 1955 (Pittsburgh, PA: Gaussian).

(15) T.H. Dunning, Jr.: J. Chem. Phys. **90,** 1007 (1989).

(16) J.F. Stanton, J. Gauss, J.D. Watts, W.J. Lauderdale; R.J. Bartlett: ACES-II A quantum chemical program package, Int. J. Quantum. Chem. Symp. **26,** 879 (1992).

(17) M. Urban, I. Cernušák, V. Kellö, J. Noga in *Methods in Computational Chemistry*, Wilson S., Ed.; Plenum Press, 1987, Vol.1, pp 117-250.

(18) M. Urban, J. Noga; S. J. Cole and R. J. Bartlett, J. Chem. Phys. **83,** 4041 (1985).

(19) K. Raghavachari, G.W. Trucks, and J.A. Pople and M. Head-Gordon, Chem. Phys. Letters **157,** 479(1989).

(20). J. Espinosa-García and J.C. Corchado, J. Phys. Chem. **99,** 8613 (1995).

(21) D.E. Woon and Thom H. Dunning, Jr., J. Chem. Phys. **99,** 1914 (1993).

(22) K.A. Peterson, R.A. Kendall and Thom H. Dunning, Jr., J. Chem. Phys. **99,** 9790 (1993).

(23) B.T. Luke, J.A. Pople and P.v.R. Schleyer, Chem. Phys. Lett. **122,** 19 (1985).

(24) Handbook of Chemistry and Physics, 61st edition, R.C. Weast, Ed., CRC Press, Boca Raton, 1980.

(25) International Tables for Crystallography, vol. C, ed. A.J.C. Wilson, Kluwer Academic Publishers, Dordrecht 1992.

(26) M.W. Schmidt, K.K. Baldridge, J.A. Boatz, J.H. Jensen, S. Koseki, M.S. Gordon, K.A. Nguyen, T.L. Windus, S.T. Elbert, GAMESS-US, Release September 1993. See also QCPE Bulletin **10,** 52 (1990).

SiN_2 and SiN_4 Molecules: An ab Initio Study of Molecular and Electronic Structure, Stability, and IR Activity

Rudolf Janoschek

Institut für Theoretische Chemie

Karl-Franzens-Universität Graz

Mozartgasse 14

A-8010 Graz

Austria

Abstract

The geometries, vibrational wave numbers and absorption intensities, and complexation energies of SiN_2 and SiN_4 have been calculated by second order Moeller-Plesset perturbation theory (MP2), single and double excitation coupled cluster method (CCSD), and the gradient corrected exchange-correlation density functionals (B3LYP). The electronic structures have been studied applying the natural bond orbitals analysis (NBO). A hitherto ignored pair of strong bands near 2000 cm^{-1} in the IR spectrum of SiN_2 is assigned to the NN stretching modes of the novel compound SiN_4.

ADVANCES IN QUANTUM CHEMISTRY, VOLUME 28

0065-3276/97 $25.00

1. Introduction

The SiN_2 molecule has been detected spectroscopically in 1970 and is known to be the product of various photochemical processes, where small silicon and nitrogen containing systems are involved (1). Experience has shown that elemental nitrogen in the matrix may cause dramatic shifts of UV and IR absorption bands for the systems under investigation (2, 3). Furthermore, nitrogen in the matrix can make vibrational bands vanish and generate new bands (1). The crucial question is as follows: Can these spectroscopical shifts be interpreted as "matrix effects" on the target system, or are they due to the formation of yet unknown species? This question is a challenge for the computational chemist. In a first step, the target system should be analysed by means of quantum chemical calculations to identify all bands that originate from the SiN_2 system. The second step is the identification of proper systems which might be the sources for unidentified bands.

For the spectroscopically identified SiN_2, even the first computational step addressed above exhibits a dramatic history. In 1988, a series of hitherto successfully applied computational methods failed for the assignment of observed vibrational wave numbers (4). These methods are open-shell Hartree-Fock, configuration interaction including singly and doubly excited configurations (CISD), and complete active space multiconfiguration SCF (CASSCF). This list of unsuccessful methods (for SiN_2) will be completed in this work by the second order Moeller-Plesset perturbation theory (MP2). All these methods yielded a loosely bound Si...N_2 complex with vibrational wave numbers of roughly 2500 and < 100 cm^{-1} instead of the spectroscopical values of 1731 and 485 cm^{-1}, respectively. Later, in 1992, the density functional theory (DFT) as well as the coupled cluster method (CCSD) were presented to be sufficiently sophisticated theoretical approaches, which are suitable for the assignment of vibrational wave numbers to the linear SiN_2 system in its $^3\Sigma^-$ groundstate (5-7). According to these investigations the vibrational wave numbers of 1731 and 485 cm^{-1} are now ascertained to correspond to the NN and SiN stretching modes, respectively.

The additional statement of Milligan and Jacox (1) "a strongly absorbing pair of peaks at 2012 and 2026 cm^{-1} dominated the product spectrum. None of these absorptions shifted in N_2:SiD_4 experiments,

suggesting that the species responsible for them does not contain hydrogen" has been ignored ever since. It is interesting to note that this pair of peaks has been considered neither in the above mentioned theoretical papers nor in subsequent experimental papers. The aim of this study is, therefore, to present a consistent assignment of this pair of peaks near 2000 cm^{-1} which cannot be attributed to SiH stretching modes.

2. Computational Methods

Three computational methods, which can be seen as representatives of successful periods of computational chemistry, were applied to the systems SiN_2 and SiN_4. These are the second order Moeller-Plesset perturbation theory (MP2/6-31G(d)), the single and double excitation coupled cluster method (CCSD/6-31G(d)), and the gradient corrected exchange-correlation density functionals (B3LYP/6-311G(2d)). Exploratory calculations on N_2 and SiN_2 with both basis sets have shown, that the standard basis set 6-31G(d) describes the properties under discussion correctly. For the cost effective density functional (DF) method a basis set reduction is unnecessary. The results of Hartree-Fock (HF) and complete active space multiconfiguration SCF (CASSCF) are not reported anew, since their failure in the description of SiN_2 is already documented in the literature (4). The calculated properties are energy minimum geometries and harmonic vibrational wave numbers. Absorption intensities are presented for the MP2 as well as B3LYP calculated vibrations. In addition, complexation energies of the systems were calculated at the three levels of theory. For the most reliable computational method (B3LYP) the "basis set superposition error" (BSE) for the complexation energy of $SiN_2 \rightarrow Si + N_2$ resulted to be as low as 2 kJ mol^{-1}. This correction is lower than 2% and is, therefore, omitted in the discussion of the results. The ab initio calculations, described in this work, have been carried out at the computer center of the University of Graz on an SGI computer employing the GAUSSIAN 94, Revision B.3 programs (8). The natural bond orbital analysis (NBO) was applied to find the best possible resonance Lewis structures for the

systems. Then, the NBO's were allowed to delocalize forming the natural localized molecular orbitals (NLMO) which are suitable for the discussion of delocalization stabilization. The NBO analysis of the target systems has been performed by means of the HF/6-311G(d) density employing the G94NBO program (9).

3. Computational Results

In Table 1 the geometries for N_2, SiN_2, and SiN_4 are presented. The bond distance for N_2 is more than 0.03 Å too long at the MP2/6-31G(d) level compared to the experimental value. The linear triplet ground state ($^3\Sigma^-$) of SiN_2 (**1a**) appears as a loosely bound complex at the MP2/6-31G(d) level. The CCSD/6-31G(d) approach yields two minima on the same energy hypersurface with almost identical energies, which can be characterized by a long and a short SiN distance of 2.829 Å and 1.828 Å, respectively. A single minimum with an SiN distance of 1.754 Å and an elongated NN bond of 1.140 Å was found at the B3LYP/6-311G(2d) level of theory. The UHF reference determinant is used in all three types of calculation for the SiN_2 triplet state. The spin contamination is not serious ($<S^2>$ ~ 2.05). A cyclic SiN_2 (**1b**) could also be of interest for the assignment of unidentified bands. The geometry of the (**1b**) singlet state ($^1A_1$) is quite insensitive to the computational methods.

1a

1b

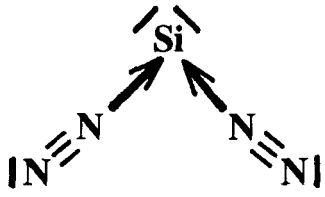

2a

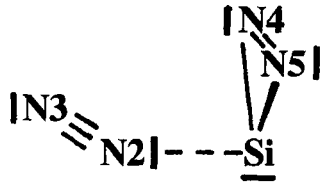

2b

The study of SiN_4 has been initiated by matrix spectroscopists (10). Two geometries **2a** and **2b** in the singlet state are presented in Table 1. All three computational approaches provide a uniform description. The SiN interaction in **2a** can be compared with that of **1a** at the B3LYP level. The structure **2b** represents a weak SiN interaction at all levels of theory. The attempt to optimize a linear N_2SiN_2 triplet geometry ($D_{\infty h}$) resulted in a transition structure for the colinear N_2 exchange:

$$N_2 + SiN_2 - N_2Si + N_2$$

The height of the E+ZPE barrier at the B3LYP level resulted to be 49 kJ mol^{-1}. An unsymmetrical N_2SiN_2 ($C_{\infty v}$) triplet structure could not be found.

The calculated harmonic vibrational wave numbers and absorption intensities are given in Table 2. The N_2 molecule is an unusual example where the MP2 method yields a much to low wave number for the stretching vibration. The wave numbers and absorption intensities of SiN_2 (**1a**) reflect the differences between a weak complex (low SiN stretching and SiNN bending wave numbers) obtained with MP2 and CCSD, and a tightly bound system as resulting from B3LYP. In addition, MP2 failed even for a proper NN stretching vibration in **1a** with an unrealistically high value of 3463 cm^{-1}. In contrast to **1a**, the cyclic structure **1b** can be described with comparable accuracy at any level of sophistication. The same is true for the SiN_4 structure **2a**. For the latter system all computational approaches yield a pair of slightly degenerate NN stretching vibrations near 2000 cm^{-1}, which can be assigned to the unidentified bands at 2012 and 2026 cm^{-1}. The absorption intensities of these both peaks are much stronger than all other transitions, which is in agreement with the experimental observation that these peaks dominate the spectrum and further corroborate this assignment. The SiN_4 structure **2b** is a sample for a

weak complex where the wave numbers indicate the fragments **1b** and N_2. No absorption in the IR spectrum can be found to justify structure **2b**.

Table 1. Optimized geometries (Å, deg) of N_2, SiN_2 (**1a**: $C_{\infty v}$, $^3\Sigma^-$; **1b**: C_{2v}, $^1A_1$), and SiN_4 (**2a**: C_{2v}, $^1A_1$; **2b**: C_s, $^1A'$).

	MP2/ 6-31G(d)	CCSD/ 6-31G(d)	B3LYP/ 6-311G(2d)
N_2			
NN[a]	1.131	1.114	1.091
SiN_2 (**1a**)			
SiN	2.889	2.829/1.828	1.754
NN	1.121	1.113/1.142	1.140
SiN_2 (**1b**)			
SiN	1.869	1.843	1.835
NN	1.258	1.251	1.237
SiN_4 (**2a**)			
SiN	1.854	1.910	1.846
NN	1.154	1.129	1.118
NSiN	81.4	80.7	83.8
NNSi	169.7	169.9	167.9
SiN_4 (**2b**)			
SiN2	3.018	3.198	3.157
SiN4	1.878	1.847	1.841
N2N3	1.130	1.113	1.091
N4N5	1.254	1.250	1.234
SiN2N3	175.0	174.2	178.4
N2SiN4	82.9	82.2	87.4

[a]Experimental value 1.098 Å.

The trend of the NN distances in N_2, SiN_4 (**2a**), and SiN_2 (**1a**) with the values 1.091, 1.118, and 1.140 Å excellently agrees with that of the NN

stretching wave numbers 2438, 2071/2163, and 1820 cm^{-1} at the B3LYP level.

Table 2. Harmonic vibrational wave numbers (cm^{-1}) and absolute IR absorption intensities (km mol^{-1}) (in parentheses).

	Experiment	MP2/ 6-31G(d)	CCSD/ 6-31G(d)	B3LYP/ 6-311G(2d)
N_2	2331	2174	2412	2438
SiN_2 (**1a**)		73 (0)	79/302	334 (0)
	485	92 (4)	88/303	512 (16)
	1731	3463 (95)	2414/1924	1820 (692)
SiN_2 (**1b**)		542 (2)	591	585 (0)
		717 (22)	742	736 (18)
		1483 (85)	1556	1524 (114)
SiN_4 (**2a**)		118 (0)	113	121 (1)
		301 (3)	205	301 (1)
		313 (1)	274	334 (0)
		370 (0)	304	403 (3)
		425 (6)	343	413 (0)
		451 (32)	355	414 (22)
		518 (5)	460	522 (10)
	2012	2032 (268)	2077	2071 (863)
	2026	2052 (786)	2215	2163 (252)
SiN_4 (**2b**)		43 (1)	38	36 (1)
		54 (0)	51	40 (0)
		77 (5)	68	53 (3)
		116 (3)	100	100 (5)
		140 (0)	114	112 (0)
		526 (2)	584	574 (0)
		707 (22)	737	730 (19)
		1498 (90)	1567	1537 (120)
		2175 (1)	2417	2441 (0)

The relative energies in Table 3 do not exhibit any clear cut trend with respect to the computational approaches employed. As mentioned above the MP2 method is unable to describe a truely bound SiN_2 (**1a**) complex. However, SiN_2 appears to be weakly bound at the CCSD level (-3.6 kJ mol^{-1}), and the inclusion of triple excitations in a single point CCSD(T) calculation increases the amount of complexation energy slightly to -12.7 kJ mol^{-1}. At the B3LYP level, the complex exhibits a significant stability of -71.5 kJ mol^{-1}. The lowest energy on the SiN_4 singlet hypersurface is found for structure **2b** at the MP2 and CCSD levels of theory. Thus, the relative energies E+ZPE for **1b** + N_2, **2a**, and **2b** are 33.1, 70.2, and 27.5 kJ mol^{-1}, respectively, at the CCSD level. In contrast, **2a** is the lowest SiN_4 singlet structure at the B3LYP level, 19.7 kJ mol^{-1} below **2b**. There is reason enough to trust in the B3LYP computed results which predict SiN_4 (**2a**) as the lowest lying structure and, therefore, justify the assignment of the IR bands near 2000 cm^{-1}.

Table 3. Energies E+ZPE (h) and relative energies Δ(E+ZPE) (kJ mol^{-1}) of the singlet (S) and triplet (T) SiN_2 and SiN_4 systems.

		MP2/ 6-31G(d)	CCSD/ 6-31G(d)	B3LYP/ 6-311G(2d)
Si + N_2	T	0.0[a]	0.0[b]	0.0[c]
SiN_2 (**1a**)	T	-0.3	-3.6[g]	-71.5
SiN_2 (**1b**)	S	24.3	33.1	-21.7
Si + $2N_2$	T	0.0[d]	0.0[e]	0.0[f]
SiN_2 (**1a**) + N_2	T	-0.3	-3.6[g]	-71.5
SiN_2 (**1b**) + N_2	S	24.3	33.1	-21.7
SiN_4 (**2a**)	S	27.8	70.2	-44.3
SiN_4 (**2b**)	S	15.9	27.5	-24.6

[a]-398.123000; [b]-398.138618; [c]-398.948461; [d]-507.373324; [e]-507.388917; [f]-508.502799; [g]short SiN distance

The electronic structures of the SiN_2 and SiN_4 systems can be characterized by means of the natural bond orbitals analysis (NBO). For the linear triplet SiN_2 (**1a**) the SiN interaction is a donor bond formed by the nitrogen lone pair which is polarized 11% toward Si. The unpaired electrons at Si (3p) are delocalized to the antibonding NN π*-orbitals and are both polarized 28% toward N_2. The formula sketched for the cyclic singlet SiN_2 (**1b**) is a good Lewis structure with respect to the occupation numbers of the NBO's. In contrast to the SiC_2 molecule (11), no stabilizing three-center π-orbital can be found in SiN_2. Nevertheless, the strain energy of 152 kJ mol^{-1} in SiN_2, according to the homodesmic equation (MP2/6-31G(d))

1b + H_2N-NH_2 + H_3Si-SiH_3 → $Si(NH_2)_2$ + $H_3SiN{=}NSiH_3$

is surprisingly low. The SiN_4 structure **2a** is a highly delocalized system. Starting from the Si which adopts two electron pairs 3s and 3px (the x axis is perpendicular to the plane of the molecule) in the valence state, two Si←N donor bonds can be formed. Either of them is polarized 11% toward Si. The 3px lone pair on Si is strongly delocalized to the antibonding NN π*-orbitals and is polarized 34% toward the nitrogens. The NBO analysis revealed two isolated systems, **1b** and N_2, in the search for a Lewis structure for **2b**. Consequently, only **2a** can be regarded as a compound in the sense of valency.

4. Conclusions

The list of unsuccessful computational methods for the calculation of vibrational wave numbers for N_2 and SiN_2 (**1a**) was extended from HF, CASSCF, and CISD to MP2. Density functional theory (DFT) in the B3LYP framework yielded vibrational wave numbers 5% above experimental values throughout. Only CCSD(T) results are closer to the experiment (6), but the B3LYP method is a better candidate for the investigation of larger systems.

The lowest lying singlet SiN_4 isomer **2a** is suggested for the assignment of the hitherto ignored pair of strong bands near 2000 cm^{-1} in the IR spectrum of SiN_2 (**1a**).

The electronic structures of the SiN_2 and SiN_4 systems, as

turned out from the natural bond orbitals analysis (NBO), revealed Si←N donor bonds accompanied by π-electron delocalization from Si to the antibonding NN π*-orbitals. These effects are present only in the structures **1a** and **2a** of SiN_2 and SiN_4, respectively. Therefore, these formulae do not represent good Lewis structures.

Acknowledgment. The author is indebted to Dr. Josef Kalcher for useful discussions.

References

(1) D. E. Milligan, M. E. Jacox, *J. Chem. Phys.* **52**, 2594 (1970).

(2) G. Maier, G. Mihm, H. P. Reisenauer, D. Littmann, *Chem. Ber.* **117**, 2369 (1984).

(3) R. R. Lembke, R. F. Ferrante, W. Weltner, *J. Am. Chem. Soc.* **99**, 416 (1977).

(4) R. L. DeKock, R. S. Grev, H. F. Schaefer III, *J. Chem. Phys.* **89**, 3016 (1988).

(5) D. A. Dixon, R. L. DeKock, *J. Chem. Phys.* **97**, 1157 (1992).

(6) I. S. Ignatyev, H. F. Schaefer III, *J. Phys. Chem.* **96**, 7632 (1992).

(7) C. W. Murray, G. J. Laming, N. C. Handy, R. D. Amos, *J. Phys. Chem.* **97**, 1868 (1993).

(8) GAUSSIAN 94, Revision B.3. M. J. Frisch, G. W. Trucks, H. B. Schlegel, P. M. W. Gill, B. G. Johnson, M. A. Robb, J. R. Cheeseman, T. Keith, G. A. Petersson, J. A. Montgomery, K. Raghavachari, M. A. Al-Laham, V. G. Zakrzewski, J. V. Ortiz, J. B. Foresman, C. Y. Peng, P. Y. Ayala, W. Chen, M.

W. Wong, J. L. Andres, E. S. Replogle, R. Gomperts, R. L. Martin, D. J. Fox, J. S. Binkley, D. J. Defrees, J. Baker, J. P. Stewart, M. Head-Gordon, C. Gonzalez, and J. A. Pople, Gaussian, Inc., Pittsburgh PA, 1995.

(9) E. D. Glendening, A. E. Reed, J. E. Carpenter, F. Weinhold, NBO Version 3.1, Wisconsin, 1988.

(10) J. Glatthaar, G. Maier, Justus-Liebig-Universität Giessen, personal communication, 1995.

(11) G. Maier, H. Pacl, H. P. Reisenauer, A. Meudt, R. Janoschek, *J. Am. Chem. Soc.* **117**, 12712 (1995).

A Sternheimer-like response property of the bromine molecule: electric field dependence of the Br field gradient

P.W. Fowler, S.A. Peebles and A.C. Legon

Department of Chemistry, University of Exeter, Stocker Road, Exeter EX4 4QD, UK

Abstract

The generalised polarisability describing the response to an applied field of the electric field gradient at a nucleus in Br_2 is calculated *ab initio*. A value of 110.55 a_0^{-1} is found at the self-consistent -field level. This is about half the value derived by modelling the measured nuclear quadrupole coupling constants of the ammonia-bromine complex.

ADVANCES IN QUANTUM CHEMISTRY, VOLUME 28

0065-3276/97 $25.00

1. Introduction

Response properties have central rôles in the theories describing intermolecular forces and the behaviour of molecules in external fields. It was recently demonstrated(1) that one such property which can be calculated *ab initio* is also accessible from the measured nuclear quadrupole coupling constants χ of weak complexes. The linear response of the electric field gradient $\mathbf{V}^{\mathrm{X}}$ at a nucleus X in a molecule X_2 to an external electric field $\mathbf{F}$ is a tensor quantity $g^{\mathrm{X}}_{\alpha\beta,\gamma} = (\partial V^{\mathrm{X}}_{\alpha\beta}/\partial F_\gamma)$ of which the axial component $g^{\mathrm{X}}_{zz,z}$ can be determined from the variation of the coupling constants $\chi(\mathrm{X})$ along a series of complexes $\mathrm{B}\cdots\mathrm{X}_2$. The property $g^{\mathrm{Cl}}_{zz,z}$ for Cl in Cl_2 has been determined in this way. It is the purpose of the present note to report an *ab initio* calculation of the corresponding property of Br in Br_2 and to compare it with the empirical value extracted from measurements on the rotational spectrum of the complex $H_3N\cdots Br_2$(2).

The paper is divided into sections as follows. First, *ab initio* calculations on Br_2 and then some approximate supermolecule calculations on $H_3N\cdots Br_2$ are reported. Then the Townes-Dailey model for nuclear quadrupole coupling constants and its connection with response theory are briefly reprised. Finally the model is applied to the complex $H_3N\cdots Br_2$, and empirical and *ab initio* results are compared.

2. Ab initio calculations on Br_2

All calculations were performed at the SCF level, using the Exeter version of the Modena SYSMO program(3). The energy, quadrupole moment and electric field gradients at the nuclei were calculated at the experimental r_0 bondlength (2.28326Å(4)) using the polarised Br basis of contracted gaussian functions that was designed by Sadlej(5) to give an accurate account of electric properties. This basis in its spherical-gaussian form has 74 functions per Br centre with a contraction pattern (15s12p9d4f) → [9s7p4d2f]. Polarisability and the electric field response tensors were calculated by application of finite perturbations, either uniform fields or field gradients, as appropriate. Some calculations were also performed at a longer bondlength (increased by 0.05Å) in order to estimate the effect of the stretching of the bromine molecule observed in its complex with ammonia. The same basis, in combination with the polarised set for first-row atoms(6) was also used for rigid-monomer supermolecule calculations on the ammonia complex $H_3N\cdots Br_2$.

The calculated SCF energy is −5144.743325 E_h at the experimental r_0 bondlength. At this geometry the calculated quadrupole moment is $\Theta_{\|} = +3.9179\ ea_0^2$. Values of +3.55, +3.48, and +3.39 ea_0^2 have been found

with smaller basis sets(7, 8, 9); zero-point effects and electron correlation contributions are predicted to be very small for this property of Br_2(9).

The dipole polarisability calculated in the present basis has components $\alpha_{\parallel} = 62.38$ and $\alpha_{\perp} = 34.52$, giving a mean value of $\overline{\alpha} = 43.81$ and $\Delta\alpha = 27.87$, all in units of $e^2a_0^2E_h^{-1} \approx 1.648778 \times 10^{-41}$ $C^2m^2J^{-1}$. These values are all close to the CHF results reported in ref (9) where correlation effects were estimated and found to lower $\alpha_{\parallel}$ by ~ 0.9 and raise $\alpha_{\perp}$ by ~ 1.6 $e^2a_0^2E_h^{-1}$, respectively, and zero-point vibrational effects were predicted to give increases in both $\Delta\alpha$ and $\overline{\alpha}$ by only ~ 0.1 $e^2a_0^2E_h^{-1}$. The present value of $\overline{\alpha}$ is within the spread of values obtained from measurement of the refractive index of the gas(10) (43.4 $e^2a_0^2E_h^{-1}$) and the liquid(11) (46.6 $e^2a_0^2E_h^{-1}$) and the radio-frequency dielectric constant of the vapour(12) (47.2 $e^2a_0^2E_h^{-1}$), all as quoted in ref. (9). Some further remarks on polarisability values are made in ref. (8).

In the present calculation the electric field gradient at each Br nucleus is $V_{zz} = -11.2679$ a.u. (1 a.u. of electric field gradient $= e/4\pi\epsilon_0a_0^3 \approx 9.71736 \times 10^{21}$ Vm^{-2}). The observable is not the field gradient, but the nuclear quadrupole coupling constant χ(Br). The conversion equation for a nucleus of quadrupole moment Q is

$$(\chi/\text{MHz}) \approx -2.349651(Q/\text{fm}^2)(V_{zz}/\text{a.u.}) \qquad (1)$$

Tabulated values(13) of $Q(^{79}\text{Br}) = 33.1(4)$ fm^2 and $Q(^{81}\text{Br}) = 27.6(4)$ fm^2 give predicted coupling constants with this basis of $\chi(^{79}\text{Br}) = 876.341$ MHz and $\chi(^{81}\text{Br}) = 730.726$ MHz, the former being 8% larger than the experimental $\chi(^{79}\text{Br})$ for free Br_2 of 810.0(5) MHz(14). If the tabulated nuclear quadrupole moments are accepted, this implies a similar overestimation in the magnitude of V_{zz}. Although the ratio $Q(^{79}\text{Br})/Q(^{81}\text{Br})$ is well established from rotational spectroscopy(15), it has been suggested(16) that the tabulated value of $Q(^{79}\text{Br})$ is too high and that the lower experimental value of 30.8(18) fm^2 obtained by King and Jaccarino(17) is more accurate than the value of 33.1(4) fm^2. If this lower value were accepted, the 8% overestimate $|V_{zz}|$ would be reduced to an overshoot of less than 1%.

The extension to molecules of the Sternheimer treatment of electric field gradients at nuclei within electron distributions immersed in external fields is made by representing $V_{zz}(\text{X})$ as a Taylor series in the perturbing field and its gradients(18, 19). In a notation that we have used before(19, 20, 21), the series for a nucleus in a linear molecule, making a fixed choice of origin, is

$$V_{zz}(\text{X}) = V_{zz}^0(\text{X}) + g_{zz,z}(\text{X})F_z + (1+\frac{3}{2}g_{zz,zz}(\text{X}))F_{zz} + \frac{5}{2}g_{zz,zzz}(\text{X})F_{zzz} + \ldots \qquad (2)$$

where V_{zz}^0 is the permanent value of the gradient at the nucleus, $g_{zz,z}$ the linear response to a uniform field, and the bracketed term $(1 + \frac{3}{2}g_{zz,zz}(\text{X}))$

plays the rôle of a Sternheimer antishielding factor. Equation (2) implies a definite choice of origin: the tensors for each nucleus describe the response of its local electric field gradient to an external field and its derivatives evaluated at a particular point within the molecule. The natural choice for a homonuclear diatomic molecule such as Br_2 is at the centre of symmetry, the midpoint of the bond. With this choice the two sites have equal and opposite values of all terms $g_{zz,z\ldots z}(X)$ with odd numbers of subscripts, but equal values of all terms with even numbers of subscripts. Thus, $g_{zz,z}(Br_i) = -g_{zz,z}(Br_o)$ but $g_{zz,zz}(Br_i) = +g_{zz,zz}(Br_o)$ for the 'inner' and 'outer' bromine sites Br_i and Br_o (where the positive z axis runs from the bond midpoint to the outer nucleus so that the coordinates of inner and outer nuclei are equal and opposite).

Finite perturbation calculations give a value of $g_{zz,z}(Br_i) = 110.55\ a_0^{-1}$, which is independent of origin. There is a second independent component of the tensor $g_{xz,z}$: this is much smaller than the axial component and in the present basis is $2.298\ a_0^{-1}$. The response to external field gradients is described by $g_{zz,\alpha\beta}$ and, for an origin at the bond midpoint, the present basis gives a value of $g_{zz,zz}(Br_i) = 20.38$ for the axial component. The full antishielding term is therefore $(1 + \frac{3}{2}g_{zz,zz}(Br)) = 31.58$, representing a thirty-fold amplification at each nucleus of a field gradient applied to the molecule. For an origin at the nucleus itself the calculated antishielding component $g_{zz,zz}(Br@Br)$ would be 179.38, a change of $\frac{R}{3}g_{zz,z}$ arising from the origin dependence of the quadrupole operator(19).

There appears to be no literature value of $g_{zz,z}(Br)$ for Br in Br_2 for direct comparison. A comparison with an empirical value extracted from the rotational spectrum of the complex $H_3N\cdots Br_2$ will be made in the following section. The small contribution of the transverse term $g_{xz,z}$ to the tensor is a feature that has been seen in previous calculations, e.g. for Cl in Cl_2(18, 20). The magnitude of the calculated term is compatible with the $98.6\ a_0^{-1}$ found at the SCF level in our recent calculations(22) on $g_{zz,z}$ for Br in BrCl. In the case of BrCl, the combined effects of electron correlation and relativistic corrections are predicted to give a fall of 12% in this property.

At the extended bondlength of 2.333264 Å, the electric field gradients are 2% larger in magnitude (V_{zz} changing to $-11.5131\ e/4\pi\epsilon_0 a_0^3$), the quadrupole moment and axial dipole polarisability increase by 5% (to $4.1306\ ea_0^2$ and $65.39\ e^2a_0^2E_h^{-1}$, respectively), and $g_{zz,z}(Br)$ increases by 8% (to $119.23\ a_0^{-1}$).

3. Ab initio calculations on $H_3N\cdots Br_2$

In order to provide some theoretical under-pinning for the analysis of nuclear quadrupole coupling constants in the complex, a series of supermolecule calculations were carried out for $H_3N\cdots Br_2$. Basis sets were as described above. The two monomers were frozen at their experimental equilibrium geometries and the geometries were restricted to axially symmetric configurations with atoms in the order $H_3\cdots N\cdots Br\text{-}Br$.

Curves for the energy, dipole moment, field gradient at N and field gradients at the two Br atoms were computed and are shown in Figure 1. Although these SCF calculations which neglect both electron correlation/dispersion interactions and monomer relaxation are undoubtedly crude, they are expected to give a reasonable qualitative picture of the trends in properties with monomer separation. The potential curve has a minimum at a distance of $\sim 5.6\ a_o$ (~ 2.96 Å) between N and Br_i; the experimental separation is somewhat shorter, at 2.72 Å. As the monomers approach more closely the dipole moment rises monotonically, with a computed dipole enhancement of $0.59\ ea_0$ (1.50 D) at the SCF minimum and $0.83\ ea_0$ (2.12 D) at the experimental separation.

The nitrogen field gradient shows little change until close to the minimum, as does the average of the field gradients at bromine. Inner and outer sites show the opposed trends typical of complexes $B\cdots X_2$, with the magnitude $|V_{zz}|$ rising at Br_i and falling at Br_o in near cancellation. Again, the onset of significant change is close to the equilibrium separation. At the SCF minimum the inner, outer and average bromine field gradients are 1.049, 0.906 and 0.977 times the value for the free Br_2 molecule in this basis; at the experimental separation of 2.72 Å these ratios are 1.070, 0.860 and 0.965, respectively. The ratio $\chi(Br_i)/\chi(Br_o)$ is 1.158 at 2.96 Å and 1.244 at 2.72 Å; these values bracket the experimental ratio of 1.22616. The significance of these results will be discussed further in the final section.

4. The Townes-Dailey model

Measured nuclear quadrupole coupling constants $\chi(X)$ for complexes $B\cdots X_2$ have been interpreted using the Townes-Dailey model(23). After allowing for zero-point angular oscillation of X_2, it is found that the effect of complexation is to increase the magnitude of the equilibrium field gradient and coupling constant at the inner and reduce them at the outer X nucleus(24). The model ascribes this change to a charge shift within the X_2 moiety; the same change is described in the more detailed long-range model as a polarisation of the Br_2 molecule(1).

The Townes-Dailey model is as follows. An isolated molecule X_2 has a coupling constant $\chi_0(X)$. If *inter*molecular charge transfer and the effects of

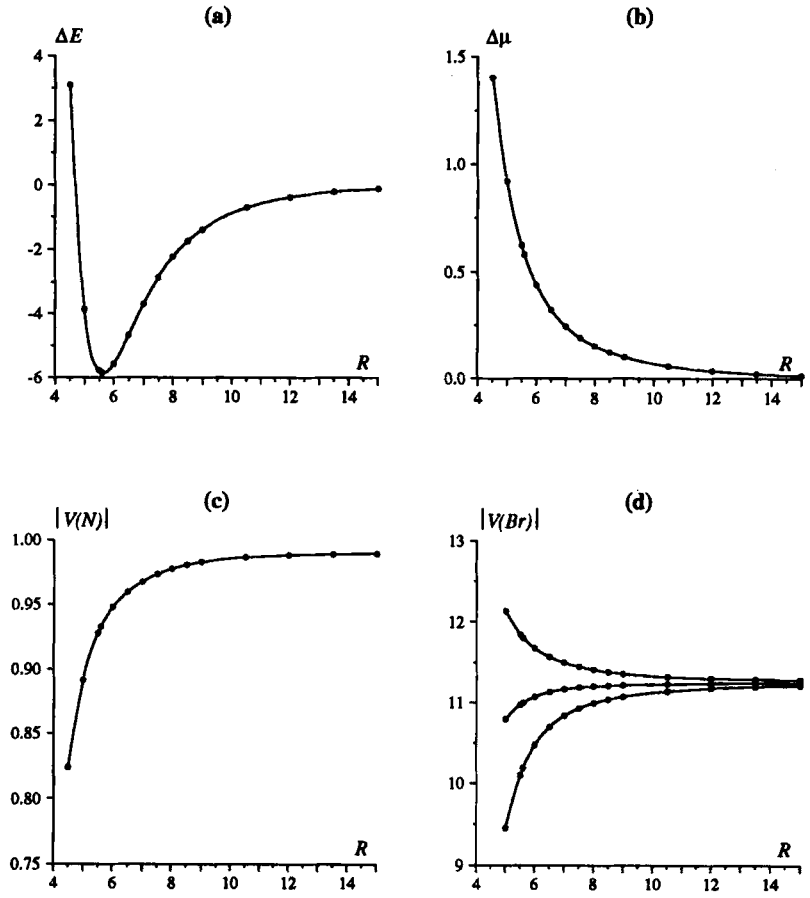

Figure 1: Variation with intermolecular separation of calculated energy and electric properties of the complex $H_3N\cdots Br_2$. The plots (a) to (d) show the results of rigid-monomer SCF supermolecule calculations as described in the text. The properties are (a) the energy (E) in millihartree, (b) dipole moment enhancement ($\Delta\mu$) in ea_0, electric field gradients at (c) nitrogen ($|V(N)|$) and (d) bromine ($|V(Br)|$) in atomic units, all displayed as functions of the distance R (in bohr) between N and the nearer Br atom. In (d), the top curve represents the electric field gradient at the inner bromine and the bottom curve the gradient at the outer; the middle curve is the mean of the two.

any increase in bond length on formation of the complex in its equilibrium geometry can be neglected, the perturbation to the electronic structure of X_2 can be crudely modelled by a transfer of a fraction δ of an np_z valence electron from inner to outer X atoms. This causes changes of $+\chi_A(X)\delta$ at X_i and $-\chi_A(X)\delta$ at X_o, where χ_A is the coupling constant for the free atom, which is taken to be equal to χ_0.

The zero-point average coupling constants, referred to the a inertial axis of the complex, are therefore

$$\chi_{aa}(X_i) = (1+\delta)\chi_0(X)\langle\frac{1}{2}(3\cos^2\beta - 1)\rangle \tag{3}$$

$$\chi_{aa}(X_o) = (1-\delta)\chi_0(X)\langle\frac{1}{2}(3\cos^2\beta - 1)\rangle \tag{4}$$

where β is the instantaneous angle between the molecular axis of X_2 axis and the a axis of the complex, and the angular brackets denote the average. The fractional number of electrons transferred from one end of X_2 to the other when $B\cdots X_2$ is formed can be extracted as the equilibrium(24) quantity

$$\delta = [\chi_{aa}(X_i) - \chi_{aa}(X_o)]/[\chi_{aa}(X_i) + \chi_{aa}(X_o)] \tag{5}$$

and the averaging term $\langle\frac{1}{2}(3\cos^2\beta - 1)\rangle$ can then be found from the sum $\chi_{aa}(X_i) + \chi_{aa}(X_o)$.

In a purely inductive model of the interaction of B with X_2, where both monomers preserve their identities but each is polarised by the electric field of the other, the field gradients at the inner and outer X nuclei are given by (2) and therefore(1)

$$\delta = \frac{g_{zz,z}(X_i)F_z}{V^0_{zz}(X)}\{1 - \frac{(1+\frac{3}{2}g_{zz,zz}(X_i))}{V^0_{zz}(X)}F_{zz}\ldots\} \approx \frac{g_{zz,z}(X_i)F_z}{V^0_{zz}(X)} \tag{6}$$

5. An empirical value for the response tensor $g_{zz,z}$(Br)

In the complex $H_3N\cdots Br_2$, the measured average coupling constants are(2) $\chi(^{79}B_i) = 852.494(4)$ MHz, $\chi(^{79}B_o) = 695.253(5)$ MHz, leading to $\delta = 0.102$. The supermolecule calculations described earlier give bracketing values of $\delta = 0.073$ (SCF minimum) and $\delta = 0.109$ (experimental separation).

The field at a distance of 3.8875 Å along the C_3 axis from the nitrogen atom of ammonia, i.e. at the position of the Br_2 midpoint of the complex, can be estimated using a distributed-multipole (DMA) model(25, 26). The field F_z is found to be −0.00469 a.u. and its gradient F_{zz} is +0.00205 a.u., with z running from B to Br_i to Br_o. Comparison of (5) and (6) gives

an empirical estimate of the relative sensitivity to field of the electric field gradient at Br in Br_2:

$$|\frac{g_{zz,z}(\mathrm{Br})}{V^0_{zz}(\mathrm{Br})}| = |\frac{d\chi(\mathrm{Br})/dF_z}{\chi(\mathrm{Br})}| = 21.7 \quad \text{a.u.} \tag{7}$$

The empirical estimate of the response coefficient $|g_{zz,z}(\mathrm{Br})|$ is therefore $\sim$ 230 a.u. and the estimate of the ratio is just over twice the 110.55/11.2679 = 9.81 a.u. obtained from the SCF calculations. This discrepancy is larger than was found for Cl in Cl_2, where the experimental ratio was about 150% of the calculated(1), but agreement is closer than for Cl in HCl, where the experimental response coefficient(27) was three times the calculated property(18, 20).

Some error in the *ab initio* ratio is anticipated from the non-correlated, non-relativistic nature of the calculation, as mentioned earlier. Small errors could also arise from neglected terms of the model: the SCF response coefficients and DMA field gradient indicate that the Sternheimer term in the curly brackets in (6) would contribute less than $\sim$ 0.5%; comparison of perturbation and supermolecule calculations suggests that the total contribution of all missing higher terms would be 3.5% or less. A model incorporating distributed response tensors for the X_2 molecule might be therefore be expected to recover most of the Townes-Dailey charge shift, but at the expense of the simple interpretation in terms of a single 'polarisability' on each atom. Additional errors of some few per cent in the DMA estimate of the electric field arising from the ammonia partner would not be surprising. The Townes-Dailey model as described above also neglects the effect of the changes in bondlength on the properties of X_2. The direct effect on χ_0 of the estimated lengthening(2) of 0.05 Å is, as we have seen, likely to be small, and the combined effect of the changes in $g_{zz,z}$ and χ would raise the *ab initio* ratio by just 6% to 10.36 a.u.

More difficult to quantify is the extent to which the premise of a vanishing degree of intermolecular charge transfer holds for this relatively strong complex. The long-range electrostatic/inductive model has had many successes(25, 26, 28) and should be not jettisoned prematurely, but it may be that this complex is close to the limit of validity of the model. A useful experimental test would be the measurement of the nuclear coupling constants of Br_2 in some more weakly bound complex and the extraction of a second empirical estimate of $g_{zz,z}/V_{zz}$.

In conclusion, the comparison that can be made so far is not free of all ambiguity but supports at least the order of magnitude of the *ab initio* response tensor $g_{zz,z}(\mathrm{Br})$. Tandem experimental and theoretical studies for a wider range of systems of this novel probe of the polarisability of an electron distribution should reveal the extent of transferability and the chemical implications of this property.

References

[1] P. W. Fowler, S. A. Peebles and A. C. Legon, Mol. Phys. (in press) (1996).

[2] H. I. Bloemink and A. C. Legon, J. Chem. Phys. **103,** 876 (1995).

[3] P. Lazzeretti and R. Zanasi, SYSMO package, University of Modena, Italy 1994.

[4] R. F. Barrow, T. C. Clark, J. A. Coxon and K. K. Lee, J. Mol. Spectrosc. **51,** 428 (1974).

[5] A. J. Sadlej, Theor. Chim. Acta **81,** 45 (1991).

[6] A. J. Sadlej, Coll. Czech. Chem. Comm. **53,** 1995 (1988).

[7] P. A. Straub and A. D. McLean, Theor. Chim. Acta **32,** 227 (1974).

[8] J. Dougherty and M. A. Spackman, Mol. Phys. **82,** 193 (1994).

[9] E. F. Archibong and A. J. Thakkar, Chem. Phys. Lett. **201,** 485 (1993).

[10] E. A. Moelwyn-Hughes, Physical Chemistry, Pergamon Press, Oxford 1961 (2nd edition, p. 383)

[11] A. Donaldson and A. D. Caplin, Phil. Mag. B **54,** 231 (1986).

[12] K. F. Luft, Z. Physik **84,** 767 (1933).

[13] P. Pyykkö and J. Li, Nuclear Quadrupole Moments, Report HUKI1-92, University of Helsinki, Helsinki (1992).

[14] N. Bettin, H. Knöckel and E. Tiemann, Chem. Phys. Lett. **80,** 386 (1981).

[15] A. C. Legon and J. C. Thorn, Chem. Phys. Lett. **215,** 554 (1993).

[16] V. Kellö and A. J. Sadlej, Mol. Phys. (in press).

[17] J. G. King and V. Jaccarino, Phys. Rev. **94,** 1610 (1954).

[18] S. Engström, H. Wennerström, B. Jonssön, and G. Karlström, Molec. Phys. **34,** 813 (1977).

[19] P. W. Fowler, P. Lazzeretti, E. Steiner, and R. Zanasi, Chem. Phys. **133,** 221 (1989).

[20] J. Baker, A. D. Buckingham, P. W. Fowler, P. Lazzeretti, E. Steiner and R. Zanasi, J. Chem. Soc. Faraday Trans. 2 **85,** 901 (1989).

[21] A. D. Buckingham, P. W. Fowler, A. C. Legon, S. A. Peebles, and E. Steiner, Chem. Phys. Lett. **232,** 437 (1995).

[22] P. W. Fowler, S. A. Peebles, A. C. Legon and A. J. Sadlej, (to be published).

[23] See C. H. Townes and A. L. Schawlow, Microwave Spectroscopy McGraw-Hill, New York ch. 9 (1955).

[24] A. C. Legon, Chem. Phys. Letters **237,** 291 (1995) and references therein.

[25] A. D. Buckingham and P. W. Fowler, J. Chem. Phys. **79,** 6426 (1983).

[26] A. D. Buckingham and P. W. Fowler, Can. J. Chem. **63,** 2018 (1985).

[27] A. C. Legon, and D. J. Millen, Proc. Roy. Soc. London A **417,** 21 (1988).

[28] A. D. Buckingham, P. W. Fowler and A. J. Stone, Int. Rev. Phys. Chem. **5,** 107 (1986).

Molecular Properties of Boron-Coinage Metal Dimers: BCu, BAg, BAu [1]

Maria Barysz[2], Miroslav Urban[3]

[2]Max–Planck–Institut für Astrophysik, Garching, Germany[2]

[3]Department of Physical Chemistry, Comenius University, 84215 Bratislava, Slovak Republic

Abstract

Spectroscopic constants and dipole moment curves of the coinage metal diatomic molecules with boron , BCu, BAg, and BAu were investigated using high-level-correlated methods combined with quasi-relativistic Douglas–Kroll (No–pair) spin averaged approximation.

[1]This paper is dedicated to Professor Geerd H. F. Diercksen to mark his 60th birthday and to thank him cordially for all scientific support, collaboration and friendship..

[2]Permanent address: Department of Chemistry, University of Silesia, ul. Szkolna 9, PL–40 006 Katowice, Poland

ADVANCES IN QUANTUM CHEMISTRY, VOLUME 28

0065-3276/97 $25.00

1. Introduction

Dimers of metal atoms are the simplest building blocks useful in understanding of properties of bulk solids and alloys. The knowledge about the nature of the bonding between metals and other elements is directly related to properties of many industrially important materials and catalysts, especially when transition metals are involved(1). Experimental investigations of simple molecules involving metal atoms are principally oriented towards the question of their very existence (2) rather than concerned with the determination of their molecular properties. Hence, the importance of the theoretical work leading to the systematization, generalization, and prediction of properties of such molecules can hardly be overestimated. Of particular importance seem to be systematic investigations in the series of related atoms, as e.g. in the series of the coinage atoms which are studied in the present paper. Considerable attention has already been devoted to experimental (3, 4) and theoretical (5, 6) investigations of compounds of copper with different atoms, including aluminum. However, no systematic study of such dimers over the whole series of the coinage metals seems to be available. Such investigations are both interesting and challenging for theoreticians. One should note that already the properties of the coinage metal atoms, Cu, Ag, Au, show quite interesting patterns which reflect certain specific features of the electron correlation and relativistic effects within the series (7–11). The same holds for the series of the coinage metal hydrides (12, 13). Atomic properties like ionization potentials, electron affinities, atomic polarizabilities etc., are relevant for the explanation of the chemical behaviour of chemical compounds of these metals. Moreover, it is only the relativistic effects which can elucidate why the behaviour of the gold atom is different from that of the other members in the series. Of importance is the fact that highly sophisticated theoretical methods capable of simultaneously considering the electron correlation correlation and relativistic effects can be used to study diatomic molecules formed by the coinage metals and provide results in a good agreement with experiment. For example, the Coupled Cluster (CC) methods (14, 15) or Complete Active Space Self Consistent Field (CASSCF) method (16) followed by the second order perturbation correction (CASPT2) (17) recover a substantial portion of the electron correlation effects. These methods combined with quasirelativistic schemes based on the No–pair (Np) Douglas Kroll (DK) transformation of the Dirac hamiltonian (18, 19) result in IP's and EA's of Cu, Ag, Au in reasonably good agreement with experiment(8, 11, 19). Also atomic polarizabilities resulting from CC, CASPT2 and DK calculations show systematic patterns and are mutually consistent (10, 13, 20). All this gives a good basis for the credibility of molecular data predicted by high–level–correlated quasirelativistic theoretical calculations.

The usefullness of theoretical ab initio methods in elucidating the bonding character and molecular properties of mixed dimers of the coinage metal atoms was convincingly demonstrated in the case of AlCu. The theoretical results appear to compete with reliable experimental data (6). We did not find any theoretical calculations on dimers composed of the coinage metals and the boron atom. Since the valence electronic structure of the boron atom is similar to that of aluminum, one can expect the bonding situation in BMe compounds analogous to that found to be responsible for the bonding in AlCu, i.e. the σ(2p-ns) bond (3, 5, 6) and the $^1\Sigma^+$ ground state. Anther motivation for the present work is the very interesting chemistry of boron compounds and, from the theoretical point of view, the role of relativistic effects which are expected to significantly influence the bonding in the series BCu, BAg, BAu.

2. Basis sets and computational methods

Basis sets and quasi-relativistic methods

The non–relativistic PolMe (9) and quasirelativistic NpPolMe (10) basis sets were used in calculations reported in this paper. The size of the [uncontractd/contracted] sets for B, Cu, Ag, and Au is [10.6.4./5.3.2], [16.12.6.4/9.7.3.2], [19.15.9.4/11.9.5.2], and [21.17.11.9/13.11.7.4], respectively. The PolMe basis sets were systematically generated for use in nonrelativistic SCF and correlated calculations of electric properties (10, 21). They also proved to be successful in calculations of IP's and EA's (8, 22). Nonrelativistic PolMe basis sets can be used in quasirelativistic calculations in which the Mass-Velocity and Darwin (MVD) terms are considered (23). This follows from the fact that in the MVD approximation one uses the approximate relativistic hamiltonian as an external perturbation with the nonrelativistic wave function as a reference. At the SCF and CASSCF levels one can obtain the MVD quasi-relativistic correction as an expectation value of the MVD operator. In perturbative CASPT2 and CC methods one needs to use the MVD operator as an external perturbation either within the finite field approach or by the analytical derivative schems. The first approach leads to certain numerical accuracy problems.

The NpPolMe basis sets were developed recently (10) for the investigation of relativistic effects using the DK transformed hamiltonian (13, 18–20). This is the spin-averaged no-pair approximation which reduces the 4-component relativistic one-electron hamiltonian to a 1-component form without introducing strongly singular operators. NpPolMe basis sets indirectly incorporate some relativistic effects on the wave function. Let us note that both PolMe and NpPolMe contracted sets share the same exponents of primitive Gaussians. Contraction coefficients are, however,

different, even if the contraction scheme is essentially the same for both basis sets. Still, however, one can approximately estimate the relativistic contribution by comparing non-relativistic results (either SCF, CASSCF, CC, or CASPT2) calculated with PolMe basis sets and quasirelativistic DK data obtained with NpPolMe basis sets. Such a comparison is reasonable (10, 20) although, strictly speaking, only nonrelativistic and DK calculations with completely uncontracted basis sets would give the true DK relativistic contribution. The use of a fully uncontracted basis set is, obviously, not practical for molecular calculations. Another possibility of estimating the relativistic contribution would be to use the MVD approach and the PolMe basis sets for both nonrelativistic and relativistic calculations. This, however, is not applicable to atoms as heavy as gold (8, 13).

Correlated methods

Two different sets of theoretical methods were used at the correlated level of approximation for molecular wave functions. The CASSCF method (16) is well established as being capable of recovering most of the non-dynamical correlation effects (near-degeneracy effects) and is suitable for the use over the full range of the potential energy surface. Usually, the dynamical correlation is not covered satisfactorily in CASSCF. A substantial portion of the dynamical correlation can be accounted for in the subsequent CASPT2 calculation. The CASPT2 method (17) is the second order approach to dynamical correlation with a single reference state given by a multiconfigurational (multideterminant) wave function.

The selection of the active space in CASSCF and CASPT2 calculations is by no means trivial. In the present case we assumed that: (i) the selected active space should at least represent the valence bonding and antibonding σ orbitals in BMe, (ii) the corresponding CAS scheme must lead to correct dissociation products (B: ^2P, Me: ^2S) and should be well balanced along the potential curve up to the dissociation limit, (iii) the CAS scheme should account for as much dynamical correlation as possible, and (iv) the same active space can be employed for all molecules in the series, i.e., BCu, BAg, and BAu.

We did some preliminary calculations for BCu (which still could be treated with rather large active spaces) with different partitioning of the orbital space in CAS calculations. The notation is: (frozen|inactive|active; n el) for orbital subspaces and n correlated electrons in the active space. The C2v symmetry was used in all computations. For most distances the wave function has definitively a two configuration form. The smallest active space considered is (0000|9331|2000; 2 el) in the CASSCF calculation while in the subsequent CASPT2 calculation we used the (6220|3111|2000; 2 el) space. The best would be to choose as the active space the valence orbitals of boron (2110) and the 3d,4s and the correlating 4d shell for Cu (5222).

This results in the active space (7332) with 14 correlated electrons, which is, unfortunately, too big to handle. It produces over 10^6 determinants in the CAS wave function. For BCu the tractable active space was the one in which the $2p_\pi$(B) orbitals were eliminated from the active space, and the 2s(B) orbital was shifted to the inactive space, i.e. (0000|7220|6222; 12 el). Thus, this partitioning of the orbital space in CASSCF calculations includes the optimization of the 1s,2s of B and 1s,2s,2p,3s,3p orbitals of Cu in the inactive subspace, and σ,σ^* bond orbitals and 3d,4s,and 4d orbitals of Cu in the active subspace. The 2s(B) is then activated at the level of CASPT2 approximation which follows the CASSCF step. The partitioning in CASPT2 is thus (6220|1000|6222; 12 el) with 1s of B, 1s,2s,2p, 3s, 3p of Cu frozen, 2s(B) inactive, and σ,σ^* , 3d, 4s, 4d (Cu) active. Unfortunately this partitioning can not be used for the whole series of BMe molecules. The pattern of correlating orbitals for BAg and BAu is different from that for BCu. The major contribution comes from the correlation effects on boron while that on the heavy metal is less important. Moreover, for Ag and Au the (n-1)d shell of the heavy atom has as the principal correlating shell the f orbitals (angular correlation). With all valence orbitals on boron, (n-1)d, ns, and the correlating f shell on the heavy atom one would need to use the active space (7442) for 14 electrons, which generates prohibitively large number of configurations in the CI expansion. The only possibility applicable to all molecules BCu, BAg, and BAu is to use the active space comprising the valence orbitals of B and the ns orbital of the heavy atom, i.e. (3110) for 4 electrons. All subsequent CASSCF and CASPT2 results are calculated with this active space.

The comparison of basic quantities representing BCu, i.e. its equilibrium bond distance, dissociation energy, and the harmonic vibrational frequency for these active spaces, calculated from a limited number of interatomic distances, is presented in Table 1. These results correspond to quasirelativistic DK CASSCF and DK CASPT2 levels of approximation. With the extension of the active space we observe a decrease of R_e at the CASSCF level and increase of R_e at the level of the CASPT2 method. The CASSCF values of D_e and ω_e increase with the active space size and they decrease in the CASPT2 method with ω_e being insensitive to the increase of the active space from (3110) to (6222). This preliminary investigation of the selection of the active space gives us some confidence in the results obtained with relatively small active space.

In CC calculations we used well established CCSD(T) method (24) in which the single and double excitations are considered iteratively, while triples are calculated in a perturbative way using the converged CCSD single and double excitation amplitudes. In CC calculations we correlated 2s and 2p electrons of boron and either (n-1)d electrons and ns electrons of the coinage metal or (n-1)p, (n-1)d, and ns electrons of the coinage metal.

Table 1
DK no-pair CASSCF and CASPT2 calculations for BCu with NpPol basis sets. A comparison of different active spaces.

		CASSCF	
Frozen	(0000)	(0000)	(0000)
Inactive	(9331)	(8331)	(7220)
Active	(2000; 2*el*)	(3110; 4*el*)	(6222; 12*el*)
$R_e(\AA)$	2.176	2.191	2.017
$D_e(eV)$	0.96	1.02	1.33
$we(cm^{-1})$	339	343	406
		CASPT2	
Frozen	(6220)	(6220)	(6220)
Inactive	(3111)	(2111)	(1000)
Active	(2000; 2*el*)	(3110; 4*el*)	(6222; 12*el*)
$R_e(\AA)$	1.840	1.866	1.889
$D_e(eV)$	2.48	2.35	2.25
$\omega_e(cm^{-1})$	601	560	562

Computer programs were MOLCAS 3 program system (25) for SCF, CASSCF, and CASPT2 calculations and the program TITAN for closed shell calculations (26) . The new version of the COMENIUS program was used for open shell CCSD(T) calculations based on the spin adapted singly and doubly excited amplitudes (15, 27–29). These codes were supplemented by the generator of the no-pair hamiltonian written by B. A. Hess in all DK calculations.

3. Results and discussion

Spectroscopic constants of BCu, BAg, and BAu molecules are presented in Tables 2–4. The potential energy curves around the minima are shown in Figure 1. For all molecules the correlation effects are very important. Some bonding is, however, obtained already at the CASSCF level without any dynamic electron correlation being taken into accounts. The analysis of molecular orbitals clearly shows that the bonding is mainly due to relatively strong single σ bond orbital arising predominantly from 2p(B) and ns(Me) orbitals. One also finds quite significant contribution from 2s(B) and very little contribution from (n-1)p(Me) orbitals. This is fully compatible with the description of the bonding situation in AlCu (3, 5, 6).

Table 2
Spectroscopic constants of BCu. The (3110) active space with 4 correlated electrons was used in CAS calculations. In CC calculations 14 or 20 electrons were correlated.

	$R_e(\AA)$	$D_e(eV)$	$\omega_e(cm^{-1})$	$\omega_e x_e(cm^{-1})$	$B_e(cm^{-1})$
Nonrelativistic					
$CASSCF$	2.249	1.073	320	3.27	0.3555
$CASPT2$	1.910	2.806	518	4.25	0.4932
Relativistic					
$CASSCF + MVD$	2.188	1.019	343	3.45	0.3757
$No-pairDK$					
$CASSCF$	2.189	1.017	341	3.66	0.3753
$CASPT2$	1.865	2.354	563	4.34	0.5169
$CCSD-14$	1.959	1.893	497	3.53	0.4689
$CCSD(T)-14$	1.917	1.430	544	4.29	0.4895
$CCSD-20$	1.947	1.986	509	3.56	0.4748
$CCSD(T)-20$	1.909	1.522	555	4.33	0.4939

Table 3
Spectroscopic constants of BAg. The (3110) active space with 4 correlated electrons was used in CAS calculations. In CC calculations 14 or 20 electrons were correlated.

	$R_e(\AA)$	$D_e(eV)$	$\omega_e(cm^{-1})$	$\omega_e x_e(cm^{-1})$	$B_e(cm^{-1})$
Nonrelativistic					
$CASSCF$	2.547	0.655	261	3.00	0.2604
$CASPT2$	2.258	1.248	341	2.32	0.3313
Relativistic					
$CASSCF + MVD$	2.397	0.833	296	2.50	0.2940
$No-pairDK$					
$CASSCF$	2.384	0.850	302	3.22	0.2972
$CASPT2$	2.098	1.684	425	3.41	0.3833
$CCSD-14$	2.173	1.403	404	2.58	0.3576
$CCSD(T)-14$	2.144	0.774	416	3.01	0.3674
$CCSD-20$	2.147	1.507	423	2.75	0.3664
$CCSD(T)-20$	2.115	0.910	440	3.26	0.3775

Table 4
Spectroscopic constants of BAu. The (3110) active space with 4 correlated electrons was used in CAS calculations. In CC calculations 14 or 20 electrons were correlated.

	$R_e(\AA)$	$D_e(eV)$	$\omega_e(cm^{-1})$	$\omega_e x_e(cm^{-1})$	$B_e(cm^{-1})$
Nonrelativistic					
$CASSCF$	2.546	0.708	266	2.95	0.2495
$CASPT2$	2.256	1.261	362	3.06	0.3177
Relativistic					
$CASSCF + MVD$	2.119	1.588	447	3.91	0.3601
$No-pairDK$					
$CASSCF$	2.062	2.078	521	3.93	0.3802
$CASPT2$	1.931	3.519	676	4.76	0.4338
$CCSD-14$	1.972	3.107	633	3.96	0.4159
$CCSD(T)-14$	1.965	2.529	649	4.04	0.4187
$CCSD-20$	1.967	3.248	646	3.94	0.4181
$CCSD(T)-20$	1.960	2.709	663	4.01	0.4210

It has been found in the case of the coinage metal hydrides (12) that relativity induces some *sd* hybrides into the σ_s orbital of AuH. In contrast to this finding we do not observe any *sd* hybridization in the BAu molecule. Both correlation and relativistic effect strengthen the bond. Results of CC calculations with 14 and 20 correlated electrons (i.e. not including or including (n-1)p electrons of the metal atom) are quite close to each other. However, the observed differences are by no means negligibe. Once again, the most sensitive is the dissociation energy where, e.g., for BAu the difference is about 0.1 eV at both CCSD and CCSD(T) levels of approximation. The importance of relativistic contributions for the shape of the potential energy curves of BCu, BAg, and BAu is clearly demonstrated by plots presented in Figure 1. The analysis of individual contributions is displayed in Table 5. In BAu the relativistic contribution is larger than the correlation contribution and for its dissociation energy the relativistic term, the correlation term and the mixed (correlation–relativistic) term are all of the same sign. For the equilibrium distance the mixed term partly compensates the shortenting of the

The comparison of the two correlated methods, CASPT2 and CCSD(T) shows relatively good agreement for R_e , ω_e , and B_e and significant differences for D_e and $\omega_e x_e$. bond resulting from both correlation and relativistic contributions.

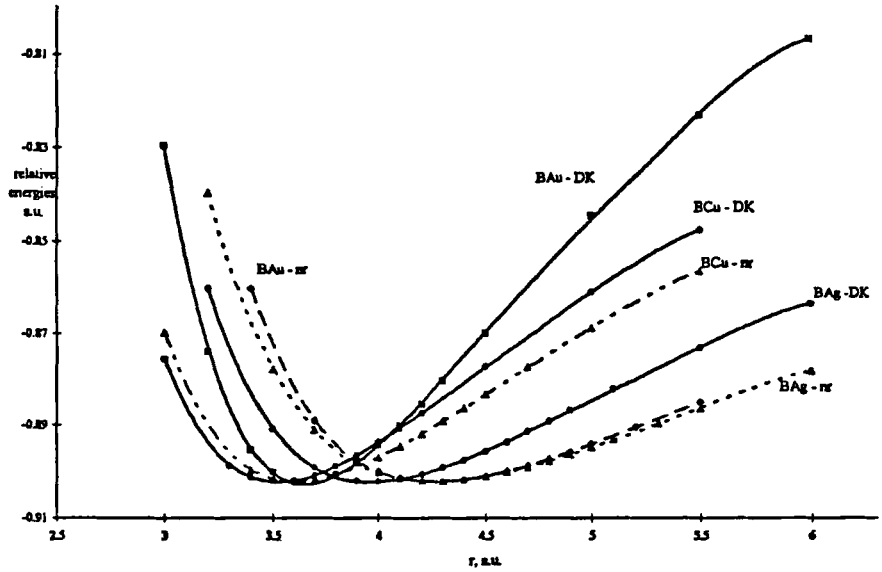

Fig.1. CASPT2 potencial energy curves of BCu, BAg, and BAu.

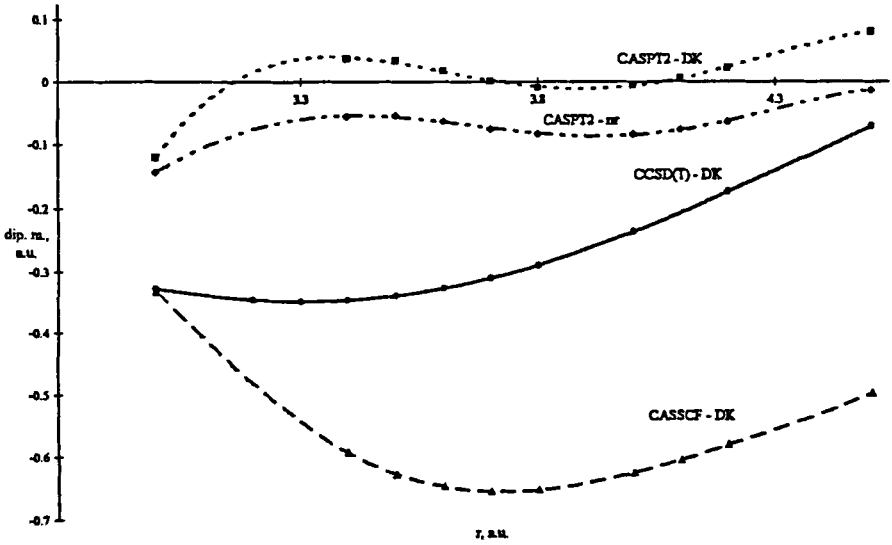

Fig.2. Dipole moment curves of BCu.

Table 5
Correlation, relativistic and mixed contributions to R_e and D_e of BCu, BAg and BAu (data from CASSCF, CASPT2 and no-pair DK calculations) relative to the corresponding nonrelativistic CASSCF values (100%).

	BCu		*BAg*		*BAu*	
	R_e	D_e	R_e	D_e	R_e	D_e
CASSCF(100%)	2.249	1.07	2.547	0.66	2.546	0.71
corr.con.	−0.339	+1.73	−0.289	+0.59	−0.290	+0.55
(%)	15	162	11	91	11	78
rel.con.	−0.060	−0.06	−0.163	+0.20	−0.484	+1.37
(%)	2.7	5	6	30	19	194
mixed term	+0.015	−0.396	+0.003	+0.240	+0.159	+0.888
(%)	.6	37	.1	37	6	125

One can expect that the $\omega_e x_e$ constant is better represented by the CASSCF and CASPT2 wave functions since these methods are applicable over the whole range of distances (our calculations have been carried out for distances through 20 a.u.). In contrast, the single reference CC methods are not expected to be well behaved for distances larger than about 1.5 of R_e, i.e., larger than 5.0 - 5.5 a.u. Then, the multirefence character of the wave function deteriorates the quality of CC results. The convergence is worse and the τ_1 diagnostic (30) increases. The dissociation energy is, however, calculated from energies at the equilibrium distance, where the wave function is very well represented by a single determinant reference and from energies of the separated atoms (using the ROHF reference with spin adapted amplitudes in CCSD, see Ref. (28)). Since three valence electrons at the boron atom and either 11 (n-1)d ns or 17 (n-1)p (n-1)d, ns electrons of the coinage atoms are correlated at the equal footing, the CC results are expected to be more reliable in the case of the dissociation energy. This is also supported by the decrease of the dissociation energy with the increasing active space and the number of correlated electrons for the test case of BCu with CASPT2 (see Table 1). Large contributions to the difference between CASPT2 and CCSD(T) dissociation energies seem to arise from triple excitations (see Tables 2–4).

The dipole moment curves are presented in Figures 2–4 . The positive sign of the dipole moment means the polarity B(+)Me(-). The relativistically calculated CASPT2-DK curves differ considerably from their nonrelativistic counterparts. Moreover, the CASPT2-DK and CCSD(T)-DK

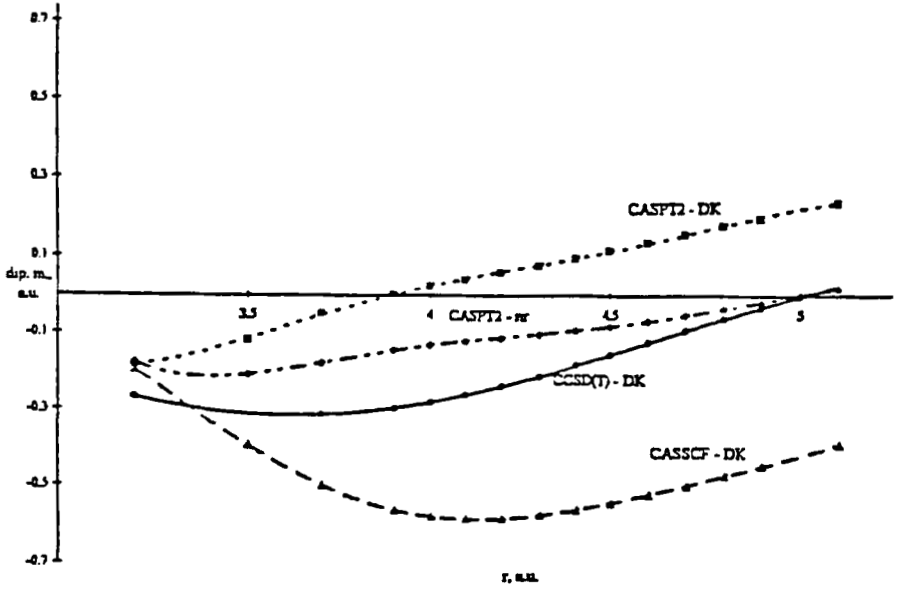

Fig.3. Dipole moment curves of BAg.

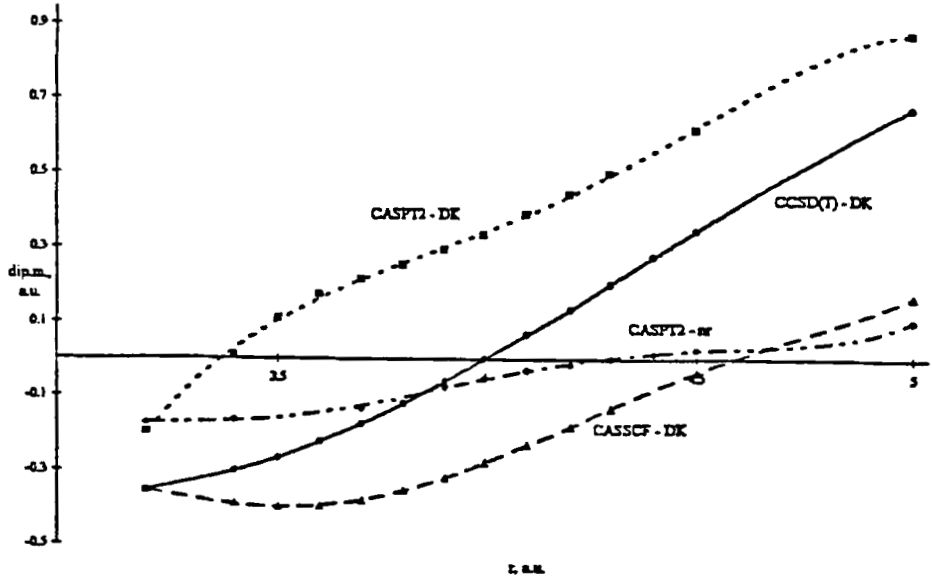

Fig.4. Dipole moment curves of BAu.

curves differ considerably from each other. This reflects the larger sensitivity of the dipole moment (charge distribution) to the level of including the electron correlation effects. However, at least for BAg and BAu, the overall shape of the CASPT2-DK and CCSD(T)-DK curves is similar. For presumably most reliable CCSD(T) method and 20 correlated electrons the first derivatives of the dipole moment with respect to the bond lenghts in the vicinity of the equilibrium are: 0.15 a.u. for BCu , 0.20 a.u. for BAg, and 0.49 a.u. for BAu. More interesting than the absolute values are the trends in the series: the CASPT2-DK dipole moment curve oscillates around zero value for BCu and the CASPT2-DK curve for BAg is only slightly positive for distances longer than 3.9 a.u. In the relativistic approximation the equilibrium distance of BAg is 3.965 a.u. for CASPT2-DK and slightly larger for CCSD(T)-DK. The CCSD(T)-DK dipole moment of BAg is negative up to the distance of 5 a.u. Quite different are the calculated dipole moments for the BAu molecule. The CASPT2-DK values are positive for distances above 3.4 a.u. (the equilibrium distance is 3.649 a.u.) and for CCSD(T) they are positive for distances larger than 4.0 a.u. This different behaviour of the dipole moment curves gives a key for the explanation of relativistic effects on the bond in the BAu molecule, which (i) has a shorter equilibrium distance than the BAg molecule, (ii) has the highest dissociation energy of all three molecules, and also (iii) has the largest harmonic vibrational frequency in the series. This indicates that in BAu the flow of electrons in the formation of the bond is different from that in BAg and BCu. In contrast to BCu and BAg, the transfer of electrons in BAu, at least for long enough interatomic separations, is in the direction from B to Au. This charge transfer is compatible with the relativistic enhancement of the electron affinity of the gold atom (8, 11, 19). In the CCSD(T) approximation with 17 correlated electrons EA of Au is 1.161 eV while the corresponding DK value amounts to 2.229 eV. For Cu and Ag this relativistic effect is much smaller (8). Quite instructive is the comparison of the CASSCF Mulliken charges for BAg and BAu obtained for instance, at the distance of 4.5 a.u. (2.38 Å, an arbitrary bond distance in between the relativistic and nonrelativistic energy minima for both molecules): With the nonrelativistic CASSCF one finds a negative charge at Ag(-0.06el) whereas the CASSCF-DK method gives the formal charge of -0.13el. In BAu the charges are Au(-0.08el) for nonrelativistic CASSCF and Au(-0.47el) for CASSCF-DK. The idea of the charge transfer was used in the interpretation of the mechanism of the interaction of Cu and Ag with the water molecule for different configurations of the complex (31) (see also (32, 33)).

Another effect which should be considered is the relativistic shrinkage of the ns valence shell of the metal. This can contribute to the valence repulsion (making it weaker), although, on the other hand, this may also reduce the overlap between the boron 2p orbital and the ns orbital of the

metal. Once the atoms are close enough, the weaker valence repulsion prevails and brings about stronger attraction at shorter distances. The relativistic decrease of the polarizability (10) may influence the dispersion interaction but this effect is very small in comparison to other forces in the region of the equilibrium.

Some of our results for BAu can be compared to experiment (2) but no experimental data seem to be available for BCu and BAg. To the best of our knowledge no other theoretical ab initio data are available as well. Experimental dissociation enthalpy for the process BAu(g) $\leftrightarrow$ B(g) + A(g) varies from 337.8±16 kJ/mole [3.50±0.17 eV] to 364±11 [3.77±0.11 eV] and 356.5±20.9 [3.70±0.22 eV] (2, 34, 35, 36). The corresponding value with respect to the 298 K reference temperature is given as 368±11 kJ/mole [3.81±0.11 eV] (34). These values agree quite well with our CASPT2 values, but are much higher than CCSD(T) values although the later are considered to be more reliable. The bond lenghts and vibrational frequencies were only very roughly estimated using empirical formulae and vary from 1.91 Å, 2.11 Å up to 2.35 Å for R_e and 989 cm^{-1}, 650 cm^{-1}, and 554 cm^{-1} for ω_e. To compare our theoretical data with experimental reaction enthalpies more precisely, we need to add to our values some corrections. The zero point vibrational energy (ZPE) for BCu with CASPT2 and CCSD(T) (20 correlated electrons) are practically identical, 0.035 and 0.034 eV, respectively. With thermal vibrational correction, 0.005 eV, the change of translational and rotational energy and the PδV term for 298 K, all these corrections give the final enthalpy of the reaction BCu(g) $\leftrightarrow$ B(g) + Cu(g) identical to within 0.005 eV with D_e listed in Table 2. The same holds for BAg and BAu with the ZPE (CASPT2) values of 0.026 eV and 0.042 eV, respectively. Almost the same values are obtained with the CCSD(T) method. Thus, the above mentioned comparison of our theoretical results with experiment for BAu does not change upon adding different corrections. Our data for BCu and BAg may predict their spectroscopic constants.

4. Conclusions

The three molecules , BCu BAg, and BAu are stable species with a singlet $^1\Sigma^+$ ground state. The strong binding in these molecules arises mainly due to a σ bond formed mainly by 2p(B) and ns(Me) orbitals with the significant contribution from the 2s(B) orbital. Both relativistic (mainly in the BAu molecule) and correlation effects must be considered very carefully if reasonably accurate results are to be obtained. Although a qualitative description of the studied molecules is already achieved at the level of the non–relativistic SCF approximation, any quantitative data can only follow from high–level–correlated calculations with relativistic effects being taken

into account for heavier atoms. The relativistic effects change the order of dissociation energies. According to CASPT2-DK and CCSD(T)-DK (20 correlated electrons) methods most stable is BAu with the corresponding dissociation energies of 3.52 eV and 2.71 eV, followed by BCu (2.35 eV and 1.52 eV) . The least stable is BAg (D_e is 1.68 and 0.91 eV with CASPT2-DK and CCSD(T)-DK, respectively). The nonrelativistic CASPT2 values are 1.261 eV (BAu), 2.81 eV (BCu) and 1.25 eV (BAg). Using the CASSCF and CASPT2 data one concludes that the pure correlation effects increase the dissociation energy of BCu by a factor of 2.6. When both correlation and relativistic effects are considered simultaneously, D_e increases by a factor of 2.2. In BAg these factors are 1.9 and 2.6; with BAu the relativistic effect dominates, the respective factors being 1.8 and 5.0. The charge distribution in BCu and BAg is different from that in BAu. In contrast to BCu and BAg, the polarity of BAu indicates, at least for distance longer than the equilibrium separation, a shift of electrons from boron to the gold atom. This different behaviour is connected to the relativistic increase of the electron affinity of the gold atom. The relativistic shrinkage of the ns valence shell electrons also makes the bond stronger.

5. Acknowledgements

A part of calculations reported in this paper has been carried out at the Department of Theoretical Chemistry of the University of Lund. One of us (MB) wishes to acknowledge the financial support from the Committee for Scientific Research (KBN) extended to her under the research grant KBN No. 2P30310407. MU thanks the Slovak grant agency for support of this work, under contract No. 1/1455/1994.

References

[1] S. R. Langhoff and C. W. Bauschlicher, Ann. Rev. Phys. Chem. **39,** (1988).

[2] D. Fischer, G. Hönes, I. Kreuzbichler, U. Neu-ecker and B. Schwager, in:*Gmelin Handbuch of Inorganic and Organometallic Chemistry: Au, Gold, Supplement Vol. B2* ed. R. Keirn (Springer Verlag, Berlin, 1994), pp 246-248.

[3] M. F. Cai, S. J. Tsay, T. P. Dzugan, K. Pak and V. E. Bondybey, J. Phys. Chem. **94,** 1313 (1990).

[4] J. M. Behm, C. A. Carrington, J. D. Landberg and M. D. Morse, J. Chem. Phys. **99,** 6394 (1993).

[5] C. W. Bauschlicher, S. R. Langhoff, H. Partridge and S. P. Walch, J. Chem. Phys. **86,** 5603 (1987).

[6] M. Bär and R. Ahlrichs, Chem. Phys. Letters **91,** 241 (1991).

[7] P. Pyykkö, Chem. Rev. **88,** 563 (1988).

[8] P. Neogrády, V. Kellö, M. Urban and A. J. Sadlej, Int. J. Quantum Chem., submitted

[9] P. Neogrády, V. Kellö, M. Urban and A. J. Sadlej, Theoret. Chim. Acta **93,** 101 (1996).

[10] V. Kellö and A. J. Sadlej. Theoret. Chim. Acta in press.

[11] P. Schwerdtfeger M. Dolg, W. H. E. Schwarz, G. A. Bowmaker and P. D. W. Boyd, J. Chem. Phys. **91,** 1762 (1989).

[12] C. L. Collins, K. G. Dyall and H. F. Schaefer III, J. Chem. Phys. **102,** 2024 (1995)

[13] V. Kellö, A. J. Sadlej and B. A. Hess. J. Chem. Phys., in press.

[14] M. Urban, I. Černušák, V. Kellö and J. Noga, in: *Methods in Computational Chemistry, Vol. 1*, ed. S. Wilson (Plenum Press, New York, N. Y., 1987), pp.117 - 250; R. J. Bartlett, J. Phys. Chem. 93, 1697 (1990); J. Paldus, in: *Relativistic and Electron Correlation Effects in Molecules and Solids*, ed. G. L. Malli (NATO ASI Series, Plenum, 1993) pp. 207 - 282.

[15] T. J. Lee and G. E. Scuseria, in: *Quantum Mechanical Electronic Structure Calculations with Chemical Accuracy*, ed. S. R. Langhoff (Kluwer Academic Publ., Dordrecht, 1995), pp. 47 - 108.

[16] B. O. Roos. Adv. Chem. Phys. **69,** 399 (1987).

[17] K. Andersson, P. A. Malmquist, B. O. Roos, A. J. Sadlej and K. Wolinski, J. Chem. Phys. **94,** 5483 (1990); K. Andersson, P. A. Malmquist, B. O. Roos, J. Chem. Phys. **96,** 1218 (1992).

[18] M. Douglas and N. M. Kroll, Ann. Phys. **82,** 89 (1974); J. Sucher, Phys. Rev. **A22,** 348 (1980); B. A. Hess, Phys. Rev. **A33,** 3742 (1986); B. A. Hess and P. Chandra, Phys. Scr. **36,** 412 (1987).

[19] U. Kaldor and B. A. Hess, Chem. Phys. Letters **230,** 1 (1994).

[20] V. Kellö, M. Urban and A. J. Sadlej. Chem. Phys. Letters **253,** 383 (1996).

[21] A. J. Sadlej, Collection Czechoslov. Chem. Commun. **53,** 1995 (1988); Theoret. Chim. Acta **79,** , 123 (1991).

[22] M. Urban, R. J. Bartlett and S. A. Alexander, Int. J. Quantum Chem. Symp. **26,** 271 (1992).

[23] V. Kellö and A. J. Sadlej, J. Chem. Phys. **93,** 8112 (1990); R. D. Kowan and D. C. Griffin, J. Opt. Soc. Am. **66,** 1010 (1976); R. L. Martin, J. Chem. Phys. **87,** 750 (1983).

[24] M. Urban, J. Noga, S. J. Cole and R. J. Bartlett, J. Chem. Phys. **83,** 4041 (1985); K. Raghavachari, G. W. Trucks, J. A. Pople and M. Head-Gordon, Chem. Phys. Letters **157,** 479 (1989).

[25] K. Andersson, M. R. A. Blomberg, M. Fülscher, V. Kellö, R. Lindh, P.-A. Malmquist, J. Noga, J. Olsen, B. O. Roos, A. J. Sadlej, P. E. M. Siegbahn, M. Urban and P.-O. Widmark, Molcas System of Qantum Chemistry Programs, Release 3. Theoretical Chemistry, University of Lund, Lund, Sweden and IBM Sweden (1994).

[26] T. J. Lee, A. P. Rendell and P. R. Taylor, J. Chem. Phys. **94,** 5463 (1990).

[27] J. D. Watts, J. Gauss and R. J. Bartlett, J. Chem. Phys. **98,** 8718 (1993).

[28] P. Neogrády, M. Urban and I. Hubač, J. Chem. Phys. **97,** 5074 (1992); J. Chem. Phys. **100,** 3706 (1994); P. Neogrády and M. Urban, Int. J. Quantum Chem. **97,** 187 (1995).

[29] P. J. Knowles, C. Hampel and H. J. Werner, J. Chem. Phys. **99,** 5219 (1993).

[30] T. J. Lee and P. R. Taylor, Int. J. Quantum Chem. Symp. **23,** 199 (1989).

[31] P. Neogrády, M. Urban and A. J. Sadlej, Theochem. **332,** 197 (1995).

[32] P. Schwerdtfeger and G. A. Bowmaker, J. Chem. Phys. **100,** 4487 (1994).

[33] J. Hrušák, W. Koch and H. Schwarz, J. Chem. Phys. **100,** 3898 (1994).

[34] K. A. Gingerich, J. Chem. Phys. **54,** 2646 (1971).

[35] K. A. Gingerich, Z. Naturforsch. **24a** 293 (1969).

[36] A. Vander Auwera-Mahieu, R. Peeters, N. S. McIntyre and J. Drowart, Trans. Faraday Soc. **66,** 809 (1970).

DECADES OF THEORETICAL WORK ON PROTONATED HYDRATES

E. Kochanski, R. Kelterbaum, S. Klein, M. M. Rohmer, A. Rahmouni[1],

UPR 139 du CNRS, Laboratoires de Chimie Théorique et de Chimie Quantique, Université Louis Pasteur, Institut Le Bel, BP 296, 67008 Strasbourg, France

Abstract :

Theoretical studies on protonated hydrates (PH) are illustrative of the progress realized in theoretical chemistry over several decades. The evolution of such studies is presented. The main methods used (quantum chemistry, Monte Carlo or Molecular Dynamics calculations...) and the problems encountered are briefly recalled. Some of the results obtained are commented.

---

[1]present address : Laboratoire de Chimie Théorique, Ecole Normale Supérieure de Saïda, Route de Mascara, BP 138, Cité En-Nasr, 20 002 Saïda, Algérie

ADVANCES IN QUANTUM CHEMISTRY, VOLUME 28

0065-3276/97 $25.00

1. Introduction

Protonated hydrates (PH) are probably among the most important systems encountered in chemistry. They can be found in solid, liquid or gas phase and have been observed in the atmosphere and in the interstellar medium. Many experimental and theoretical studies appeared on these hydrates since the hypothesis of the existence of an oxonium ion in 1907 (1), leading to hundreds of publications. This is not surprising since a great deal of chemical, physical and biological phenomena are related to the protonated water clusters, involving a wide range of problems. This motivated a large amount of theoretical treatments quite illustrative of the general progress realized in Theoretical Chemistry. We first recall briefly the historical evolution of the theoretical studies on these topics, and then present the main methods used in this field. Finally, we comment some of the results obtained.

2. Historical evolution of theoretical studies on PH

The first theoretical papers, mainly related with explaining the abnormal mobility of water (2-4), are based on simple models. Protonated hydrates were, in fact, considered within a more general treatment of liquids or solids. The first quantum chemistry calculations appeared in the sixties (5,6) and were concerned with H_3O^+. Its geometry was not yet well known and a planar (5) or a pyramidal structure (6) has been proposed. As we shall discuss below, the determination of the geometry of the oxonium ion was not trivial. Experimental determinations of the structure appeared only in 1980, and then in 1985 (7).

In the seventies, most of the 37 papers (8-24) that we report are quantum chemical calculations, mainly on $H_5O_2^+$ (8-14,20) or H_3O^+(14-20) and a few on larger clusters with n=4-6 (8,9). However these last calculations are not accurate, obtained either from semi-empirical methods (8) or with small basis sets (DZ , 4-31G) and at the SCF level in ab initio calculations (9). The first accurate CI calculations definitely establish the pyramidal geometry of the oxonium ion (15,16). The first ab initio determination of the barrier in $H_5O_2^+$ appeared in 1970 (10). An attempt was made to study the effect of CI on this barrier (11) and the abnormal polarizability of $H_5O_2^+$ (12). At the end of this decade appeared the first CI ab initio calculation on the excited states of H_3O^+ (19) and the first CNDO calculations on excited states of larger clusters (20). In parallel to these quantum chemistry studies, a kinetic model (21) treats large systems with n=20 and 26, a polarisation model (22) is proposed, and a study on the liquid uses a continuum model (23).

The eighties have been very productive, with 63 theoretical papers collected in the literature (7b, 25-55). The methods used and the properties studied are much various than in the previous decade. More information and a

better accuracy are available on H_3O^+ (7b, 25, 27, 29ac, 31-33, 35, 37, 40, 48, 50, 52, 53) or $H_5O_2^+$ (26-29, 32, 34, 35, 37, 38, 41, 44, 45b, 46-48, 50-53), mainly from ab initio calculations. A paper appears on the excited states of H_3O^+ (54). Quantum chemistry calculations are also available on larger systems, from ab initio studies but also from semi-empirical determinations (28a, 29d, 34, 38, 41, 45-48, 51-53, 55). Let us also mention the work using a cavity model by Karlstöm (53).The proton transfer is largely dominant among the problems treated (28, 34, 35, 37, 41, 51-53). New analytical models are proposed describing the interaction between H_3O^+ and H_2O (29acd, 36, 43, 50), including implicitly (50) or explicitly (29d) non additive terms. The first Monte Carlo calculations on these systems appeared in this decade, based on a kinetic model in 1980 (30) for n = 21, or using the analytical potentials mentioned above generally coupled with the MCY potential for the water-water interaction (56). In these cases, the systems studied have 1 to 9 water molecules (29be), 21 (43) and 20 to 22 or 27 to 29 (42) water molecules. At the end of this decade appeared the first Molecular Dynamics studies (49-50).

The nineties are even more productive than the previous decades. At this date, 48 theoretical publications have already been published (57-88). Among them, 11 are based on the DFT method (59g, 68, 70, 75-77, 82, 85, 86), eventually associated to MD calculations(75), and essentially within the last two years. This rise of the DFT approach in this field is perhaps one of the most striking features of this period. Work on H_3O^+ in its ground (58, 60, 62-65, 67, 69-70, 72-73, 76-77, 82, 86-87) and excited (59i, 79) state or on $H_5O_2^+$ (57, 59a-dh, 60, 61, 63, 64, 66-70, 72, 76-78, 82-84, 86-87) still appears, but larger systems are more and more often considered (57, 59-61, 63-64, 66, 67, 69, 71-72, 74-76, 80-81, 85, 87) and the choice of the methods used is larger. Analytical models (59abef, 67a) have been proposed, based on a polarizable model (67a) or including explicitly three-body contributions (59ef). They can be used for minimization of structures, but more generally they are associated to Monte Carlo (59abdhj) or MD (67b) calculations. Studies involving a large amount of water molecules : 21 (67b, 71, 74, 75a), 32 (75bc), 28, 40 and 50 (59h) have been published. Proton transfer remains a subject of interest for a large amount of papers (59g, 64, 66, 68, 70, 72, 75, 77, 80, 81, 83, 86, 87).

3. Theoretical treatments and Techniques

The previous section shows that the methods and techniques used in the treatments of these systems can be decomposed into 4 categories : Quantum chemistry calculations, analytical models, Monte Carlo and Molecular Dynamics studies (based on analytical models or DFT). We shall not discuss the huge amount of work concerning the water system alone and will consider only the cases involving an ion and water molecules.

3.1 Quantum chemistry treatments

3.1.1 Supermolecules, cavity model, perturbation treatments

Most of the general methods developed for isolated molecules have been used to treat PH as **supermolecules** : HF, CI, CEPA, MPn, MRD-CI, CC, DFT, etc... They can use semi-empirical or, more often, ab initio wave functions. Let us notice that MP2 is mostly used in the last decade. Among the emerging methods, let us mention CASPT2 calculations on the excited states of H_3O^+(59i) and DFT studies more or less arbitrarily included in quantum chemistry treatments. VB calculations are found in only one case.

Recently, a new category of methods, the **cavity model,** has been proposed to account for the solvent effect. Molecules or supermolecules are embedded in a cavity surrounded by a dielectric continuum, the solvent being represented by its static dielectric constant. The molecules (supermolecules) polarize the continuum. As a consequence this creates an electrostatic potential in the cavity. This reaction potential interacts with the molecules (supermolecules). This effect can be taken into account through an interaction operator. The usual SCF scheme is modified into a SCRF (self consistent reaction field) scheme, and similar modifications can be implemented beyond the SCF level. Several studies based on this category of methods have been published on protonated hydrates. They account for the solvent effect on the filling of the first solvation shell (53, 69), the charges (69, 76) and the energy barrier to proton transfer (53, 76).

The **perturbation theory** has been used to describe the dispersion energy between the oxonium ion and one water molecule (29a), a comparison between different approaches (TDCHF, MBPT, semi-empirical) being available for two water molecules (59c). The perturbation theory has also been used to determine three-body interactions (59ef).

The quantum chemistry studies published on protonated hydrates at the end of the last decade reveal two interesting features. One is a strong need for more information about many-body contributions, closely related to the use of analytical potential in modellisation techniques. The other is the sudden break-through of the DFT method in this field. These two points deserve a particular attention and are developed in the next two sections.

3.1.2 The many-body problem

The many-body contributions are automatically taken into account in the supermolecule treatment, whatever the method. In the perturbation theory, the different terms are developed and computed independently. The analytical potentials used to optimize geometries or in Monte Carlo and Molecular Dynamic treatments are quite often deduced from approximations of the perturbation terms. During a long time, they were limited to the pair

approximation, more or less artificially adapted to obtain an agreement with experimental data. In the course of the last decade, it has been seen that the role of the non-additive contributions may be crucial, even when they are not energetically large. More information on these terms was thus necessary and could be obtained from quantum chemistry. This motivated studies, both from the supermolecule treatment and the perturbation theory.

The intermolecular energy can be decomposed in the following way :

$$E = \sum_{i}^{N}\sum_{j<i}^{N} E^{(2)}(X_i,X_j) + \sum_{i}^{N}\sum_{j<i}^{N}\sum_{k<j<i}^{N} E^{(3)}(X_i,X_j,X_k) + \ldots E^{(N)}(X_i,\ldots X_N)$$

In a supermolecule treatment, the many body terms may be obtained from calculation performed on the total system and on the different components of this system (isolated molecules, set of two molecules, three molecules, four molecules, etc...). For instance, if we call $E_{(X)}$ the energy of the system or of the sub-systems, the three-body non-additive contribution for a set of three molecules A, B, C is :

$$\Delta E^{3\text{-body}}_{\text{non add}} = E_{(ABC)} - E_{(AB)} - E_{(AC)} - E_{(BC)} + E_{(A)} + E_{(B)} + E_{(C)}$$

Table I : Energetic contributions in Kcal/mole for $H_3O^+(H_2O)_6$; (total energy : -95. 24 kcal/mole; 5-,6-,7-body : +0.09 kcal/mole)

pair		3-body		4-body	
I w1 w2	Sum of cont.	I w1 w2	Sum of cont.	I w1 w2	Sum of cont.
1 1 0	-78.185	**1 2 0**	**+11.747**	1 3 0	-0.268
1 0 1	-17.052	1 1 1	-0.465	1 2 1	+0.158
0 2 0	+ 3.416	1 0 2	+1.245	1 1 2	-0.402
0 1 1	-7.070	0 3 0	-0.075	1 0 3	-0.031
0 0 2	-6.157	0 2 1	-0.057	0 3 1	+0.000
		0 1 2	-1.618	0 2 2	+0.074
		0 0 3	-0.578	0 1 3	-0.015
tot	**-105.05**	**tot**	**+10.200**	**tot**	**-0.480**

I, w1 and w2 refer to the ion I and to the first (w1) or second (w2) solvation shells water molecules, with numbers 0 to 3.

The order of magnitude of these terms is given in Table I on the example of $H_3O^+(H_2O)_6$ at the SCF level. The geometric configuration considered (denoted by (3+3)PYR in Ref. (59c)) has 3 water molecules in the first solvation shell and 3 others in the second shell, the oxonium ion being pyramidal. We see that the three-body contribution arising from the ion and two water molecules of the first shell (term 120) is largely dominant (12% of the total energy). The three-body contributions arising from the water molecules alone (terms 0w1w2) represent only 20% of the previous one and 2% of the total energy. The four-body forces represent only 0.5% of the total

energy, the part due to the water molecules alone being 0.06%. The higher order terms are negligible.

The dominant terms being the three-body ion-water-water interactions, these terms have been studied more precisely. In the supermolecule approach, at SCF level, $\Delta E^{SCF}_{non\ add} \sim \Delta E^{1st}_{non\ add} + \Delta E^{deloc}_{non\ add}$ if we start the SCF calculations with the SCF vectors of the monomers, $\Delta E^{1st}_{non\ add}$ being the contribution obtained at the first iteration of the calculation and $\Delta E^{deloc}_{non\ add}$ the contribution due to the following iterations till convergency is reached. Δ means that these values are obtained from differences between numbers, which are generally of similar magnitude. This decomposition is close to that proposed in Ref. (89), which calls deformation energy a term equivalent to $\Delta E^{deloc}_{non\ add}$.

In a perturbation scheme to second order (59ef), if $E^{exch}_{non\ add}$ is the first-order exchange term, $E^{ind}_{non\ add}$ a second-order induction contribution, and $E^{ind\text{-}exch}_{non\ add}$ a second-order exchange term, $E^{(2)}_{non\ add} = E^{exch}_{non\ add} + E^{ind}_{non\ add} + E^{ind\text{-}exch}_{non\ add}$. The non-additive dispersion energy is a third order term which can be neglected for polar systems.

Approximate equivalencies between the two approaches lead to :

$$\Delta E^{1st}_{non\ add} \approx E^{exch}_{non\ add} \text{ and } \Delta E^{deloc}_{non\ add} \approx E^{ind}_{non\ add} + E^{ind\text{-}exch}_{non\ add}$$

These expressions allowed to show (59ef) that the last term, $E^{ind\text{-}exch}_{non\ add}$, may be important though it is generally neglected.

3.1.3 Break-through of the DFT approach in this field

The use of the DFT approach in the treatment of such systems is very recent. It is perhaps one of the most striking features noted in the nineties. A few studies appeared on water in 1992, and the first work on $H_5O_2^+$ in 1993 (68, 70). Nine papers have been published on protonated hydrates in 1994 and 1995 (59g, 75-77, 82, 85, 86). As recalled in Ref. 75c the standard DFT techniques based on the local density approximation are not adequate to describe weak interactions. Great progress has been made possible by the use of non local terms. Except in the work of Ref. (75) where there is no correction for the correlation term (only the exchange correlation term is considered), most programs include a correction for the correlation and the exchange correlation. The corrections most often used (90-92) are those proposed by Perdew (90) or Lee-Yang-Parr (91) for the correlation and by Becke (92a-c) for the exchange-correlation term (leading to the notation BP or BLYP). However, it is noted (86) that such corrections lead to an overestimation of the OH bond length by about 0.015Å. The role of the exact exchange term is underlined by Becke

(92de) and it is shown (86) that such a correction gives OH bond lengths in agreement with MP2 determinations.

3.2 Analytical models

Several analytical models have been proposed to describe the interaction between the proton (22, 67a) or the oxonium ion (29a, 36, 43, 50, 67a) and a water molecule. They differ by the terms considered, their analytical description and the way to parametrize them. The polarizable model of Ref. (22) considers the entities H^+ and O^{2-}, with an induction term modified to account for the linear polarization response. In ref. (67a), the water is represented by four charges, interacting either through a hard-core in the case of the proton, or with a four charges oxonium ion. In this polarizable model, an induction term is added to a 12-6 (repulsion and dispersion) atom-atom potential, the parameters fitting gas phase data. In Ref. (29a), a 12-1-6 (repulsion, electrostatic, dispersion) atom-atom expression fits an ab initio surface of the dimer. In Ref. (36), an induction term is added to an $\exp\text{-}r^{-1}$ expression (repulsion, electrostatic) to fit a HF surface of the dimer. In Ref. (43), a HF surface of the dimer is fitted by a 8-4-3-1 atom-atom expression. In Ref. (50), an induction term is added to a 12-1-6 atom-atom expression, the parameters fitting gas phase energies. In this last case, the induction term accounts for many-body interactions by considering up to 5 nearest neighbors, according to the philosophy of the polarizable models described above (22, 67a), while three-body contributions are explicitly included in Refs. (59ef).

3.3 Monte Carlo treatments

Three groups have performed Monte Carlo calculations on these systems : Kochanski et al. (29be, 59abdgh), Nagashima et al. (42) and Fornili et al. (43). Recently, another work uses MC treatment in complement of MD calculations to treat the proton transfer as a jump (81). The first need is potentials. Ref. (42) used the Byers Brown expression (36) to treat clusters involving 20 to 22 or 27 to 29 water molecules. Ref. (43) used the potential described in section 3.2. Refs. (29be, 59abd) use the potential (29a), eventually completed with three-body components (29d), while Refs. (59ghj) couple the pair potential of ref. (43) and refined description of three-body forces given in refs. (59ef). The effect of the three-body contribution will be commented in the section "results". It is worth to mention also some other problems in Monte Carlo calculations :

- Though equilibrium calculations should not be necessary for these clusters since we can easily build a reasonable starting geometrical configuration, it is wise to discard the first steps of the simulation, which can depend on the choice of the starting point.

- the convergency may be tricky. For such systems, there is no real benefit to use an umbrella technique. A very large number of configurations (several millions) must be included to guarantee the convergency of the calculations.
- the size of the box must be carefully estimated : if it is too small the cluster is too concentrated, if it is too large some water molecules can escape the cluster and we obtain a mixing of n and n+1 clusters which cannot be characterized.
- a comparison between simulations performed with either a box or a sphere shows that the box allows a disymmetry in the shape of the cluster, due to the possibility that some water molecules locate in the corners. The energy can thus be lower in the case of a sphere, because of smaller distances between the water molecules and the ion. However, it is then necessary to increase the size of the volume to avoid some artefact in the potentials. It is thus not clear if there would be an advantage to work with a sphere or a box.

3.4 Molecular Dynamics

As in the case of the Monte Carlo treatments, this category of methods requires potentials. The first Molecular Dynamics studies on these clusters appear in the late eighties, involving the small $H_3O^+(H_2O)_3$ system and based on a pair approximation in 1987 (49), including the polarization of the water for 216 molecules in 1988 (50). In 1993, the use of a hydronium (oxonium) and a proton model in studies of $H^+(H_2O)_{20}$ and $H^+(H_2O)_{21}$ leads to a four coordinated H_3O^+ ion (67b). In recent studies on the proton transfer, MD calculations are coupled with a MC (81) or a DFT (75bc, 82) approach. In the last work (82), both electrons and nuclei are treated quantum mechanically (all quantum Molecular Dynamics AQMD). As will be seen in section 4, the quantum nature of the hydrogen atoms affects the properties studied (82). More general comments about these various results will be given in section 4.

4. The Results

4.1 Most stable structures

The determination of the most stable structures may be delicate, even for small clusters. We shall discuss a few examples.

H_3O^+ : many studies are concerned with H_3O^+. The planar structure found in the first ab initio quantum chemistry calculations of the ground state was due to the neglect of polarization functions. A polarized basis set leads to a slightly pyramidal structure, in agreement with the experimental data. The distances at SCF level (ranging from 0.959Å (16) to 0.969Å (35)) are slightly smaller than when the correlation is included (0.972Å (16), 0.973Å (31), 0.980Å (58)). The

SCF angles (112.5°(18), 113.5°(16), 113.2°(31), 113.1(35)) generally decrease when the correlation contribution is included (111.6°(16, 31), 112.7°(58)), the more recent value (58) being curiously larger than expected. Planar structures are found for the first singlet and triplet excited states (19, 54, 79, 59i).

$H_5O_2^+$: Since the first ab initio study by Kraemer and Diercksen in 1970 (10), many other determinations have been proposed. The proton may be attached to one water molecule or at midpoint between the two water molecules. The energy difference between both structures is small (around 0.4-0.6 kcal/mole (10, 37, 78)), favoring an easy proton tranfer. In the most recent study (78) extended basis sets and different treatments of the correlation contribution are considered. It is shown that the most stable structure has a C_s symmetry at SCF level and a C_2 symmetry at the higher level of theory. In both cases, the energy difference does not exceed 0.4 kcal/mole.

$H_9O_4^+$: This cluster has not been the source of special theoretical difficulties. All studies agree that the Eigen structure is very stable, corresponding to some "magic number" cluster features. It is illustrated by the first shell of Figure 1a.

$H_{11}O_5^+$: This cluster is interesting, not only for itself but also in relation with the filling of the first solvation shell in larger clusters. In a recent paper (59g) 10 geometries have been studied from Monte Carlo and DFT calculations. Three of them will be discussed here and are shown in Figure 1.

Figure 1 : 3 structures of $H_{11}O_5^+$

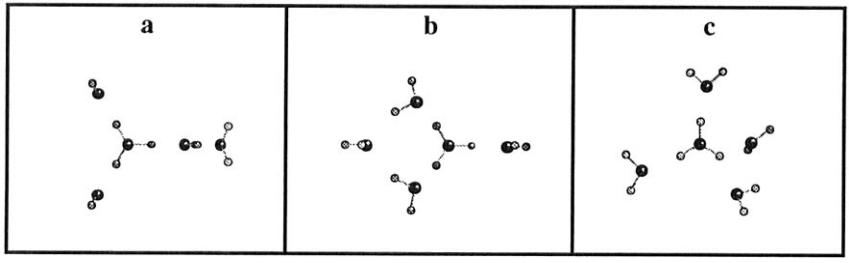

In Figure 1, a) is the Eigen structure, with 3 water molecules in the first solvation shell and b) a cyclic structure proposed on the basis of experimental data (94c, 95). These structures will be discussed in the present section. c) is found for large clusters in Monte Carlo calculations based on the pair approximation, with four water molecules in the first solvation shell. This structure will be discussed in the following sections.

The results published in Ref. (59g) for the structures a) and b) are recalled in columns 1-3 of Table 2, and completed by columns 4-8. The geometries g1 and g2 are taken from Ref. (59g), obtained either from a Monte Carlo treatment or DFT calculations; g3. is a complete optimization at MP2 level,

using a DZP basis set. In this case, the BSSE is corrected (column 5), while this correction is not done for large basis sets (columns 2-3, 6-8).

The Table 2 shows that structures a and b are very close in energy at any level of the methods (MC, DFT, SCF, MP2). The cyclic geometry b) is generally slightly more stable than the Eigen structure a), but these relative stabilities are inverted when the Zero Point Energy is accounted for (column 3) and when the MP2 results are corrected for the BSSE. Only very high accuracy determinations could establish the absolute minimum. This confirms the point already discussed in Ref. (59g) and suggested in (94b) : an equilibrium population of different structures may be found in solution, different experimental conditions and environment favoring different structures.

Table 2 : Energy differences in Kcal/mole

	1	2	3	4	5	6	7	8
Conf geom basis	MC g1	DFT g2 ext	DFT$_{zpe}$ g2 ext	MP2 g3 DZP	MP2,c g3 DZP	SCF g1 large	SCF g2 large	SCF g3 large
a	2.13	1.68	0	1.13	0	1.38	0.16	0.09
b	0	0	0.06	0	0.55	0	0	0

g1 : only the intermolecular parameters are optimized in a Monte Carlo treatment modified to minimize the energy at low temperature

g2 : complete optimization of the geometrical parameters in a DFT calculation

g3 : complete optimization of the geometrical parameters at MP2 level; results corrected for the BSSE in column "MP2,c", not in column "MP2"

basis sets : "ext" (59g); "DZP" (29a); "large" (96)

$H^+(H_2O)_{21}^+$: The system $H^+(H_2O)_{21}^+$ has been the subject of many studies since its abnormal behaviour has been reported (93). In 1974, Searcy et al. proposed that the proton is associated to a water clathrate (21). Further theoretical studies generally consider the proton located either on the surface (30, 74, 75a) or inside (24, 36, 42, 67b, 71) a dodecahedron, though other geometries could be compatible with experimental data (67b). Monte Carlo calculations considering water molecules and an oxonium ion (59h) have shown that several structures are close in energy. Among them a dodecahedron and other compact structures have been considered, with an oxonium ion located either inside or on the surface. The configurations with the oxonium ion on the surface are more stable than when the ion is located inside. A decomposition of the energetic contributions shows that the dodecahedron alone is more stable than the other structures, but its stability is counterbalanced by the ion/water and three-body interactions. It is thus very difficult to determine the absolute minimum. Furthermore, it is noted that the most stable structures have 11 free hydrogen atoms while only ten are found in a recent experimental work (95b).

All these studies on the most stable structures of various clusters show that many geometries are very close in energy. Two features can thus be drawn. The first one is that only extremely accurate calculations could definitely establish where is the absolute minimum. The second idea is that we may assume, as suggested in previous work (94b, 59g), that an equilibrium population of several different structures can be found in solution, these structures being differently stabilized according to the experimental conditions.

4.2 Statistical distribution of the molecules

Interesting information can be obtained from maps of the Monte Carlo statistical distribution of the molecules in a cluster as illustrated by Figure 2.

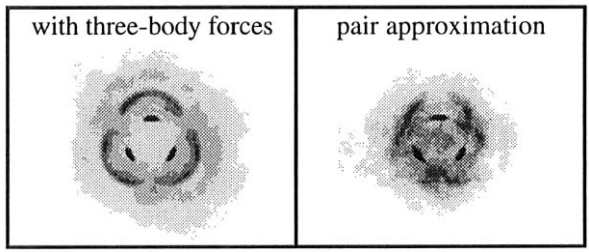

Figure 2 : Statistical distribution of the water molecules in a cluster $H_3O^+(H_2O)_{20}$

The reliability of the statistical distribution is strongly depending on the quality of the analytical potentials used. The present example shows the effect of the neglect of three-body interactions (59j). On the left side, these contributions are included. The first solvation shell, described by three black spots, corresponds to water molecules of an Eigen-type structure (see Figure 1a). The second shell is clearly defined, corresponding to water molecules bonded to the water molecules of the first shell. There are nearly no water molecules in the center of the map and between the black spots of the first shell on this left side figure. On the right side, obtained in the pair approximation, the shells are overlapping. This is due to configurations shown in Figure 1c) which are strongly stabilized by the neglect of three-body interactions. This explains that the pair approximation can overestimate coordination numbers.

4.3 Exchange of water molecules between different solvation shells

The previous comments suggest that an exchange between water molecules of the fist two shells would be artificially favored by the pair approximation, while it should not be easy when three-body contributions are included. This is confirmed when we follow the position of each water molecule during a

simulation in Monte Carlo calculations (59j). It is also shown that an exchange of the water molecules in the upper shells (59j) should be easy.

4.4 Evolution of the clusters with their size

The statistical distribution maps are a good tool to study the evolution of the clusters with their size. This has been presented in a previous work (59h) and is briefly recalled here. Clusters of N water molecules around an oxonium ion are considered for N increasing from 3 (first solvation shell filled) to 28. We can see the progressive formation and filling of the different solvation shells. The maps are drawn in three orthogonal planes, allowing a spatial view. For N=10, the water molecules are mainly in the region located below the base of the oxonium ion pyramid : first shell water molecules are H-bonded to the three H atoms of the oxonium, and second shell water molecules are H-bonded to water molecules of the first one. The filling of the second shell, only partial for N=10, progressively increases with increasing N. The spatial development of this shell progresses toward the plane of the H atoms of the oxonium ion (N=20) and gradually above this plane (already seen for N=25). For N=40, the oxonium ion is nearly embedded within a net of water molecules, which becomes about complete for N=50. We can thus find water molecules above the oxonium ion, but they are not in the first solvation shell as proposed in some work.

4.5 Clustering energies

We already discussed the question of the clustering energies in Refs. (59hj). The experimental clustering energies are strongly decreasing from about 32 kcal/mole for N=1 to 11.5-12.5 kcal/mole for N=4 (94b, 97, 99). The values available for the following clusters involving up to 28 water molecules show a plateau when N is larger than 8 (95, 98). To our knowledge, our Monte Carlo calculations (59hj) are the only theoretical determinations available for the plateau region. They lie between the two series of experimental data, even in the pair approximation which has only a minor effect in this part of the curve.

The effect of the temperature and the low values obtained in Ref. (98) have already been commented (59hj, 95d). As seen from simulations at 200, 250 and 300K, the clustering energies decrease with decreasing temperatures. If we consider the plateau between N=10 and 20 molecules, we obtain an average value of 7.32, 7.96 and 9.02 kcal/mole for 300, 250 and 200 K. This underlines the difficulty to compare with experimental determinations where the temperature is often not well known. An additional point has been recently stressed. The most recent study (78) on $H_5O_2^+$, using a CCSD(T) correlation treatment with a TZ2Pf basis, predicts an energy of 33.4 kcal/mole after the zero point vibrational energy correction. The most accurate experimental determinations (97c, 94b) are slightly smaller. This calculation is commented in ref. (84) where it is argued that the vibrational, rotational and translational

contributions above 100 K must be added, leading to 35.0 kcal/mole. This last value is in agreement with previous theoretical determinations (34.6 kcal/mole (44)) and an other experimental data (35.0 kcal/mole (32b)).

Many theoretical determinations have been proposed for small clusters. In Monte Carlo calculations, we showed the crucial role of the three-body interactions to describe clusters with N=2 and 3 (59hj). For ab initio quantum chemistry calculations, it is seen that small basis sets systematically overestimate the clustering energies (9, 52). In this case, the Zero-Point Energy correction is large (9), and seems less important with larger basis sets (63b). The role of the correlation contribution is not clear and seems to depend on the clusters considered (52, 63b, 69). The other determinations, from semi-empirical quantum chemical methods (8, 55) or analytical models (22, 50, 67a) are of variable accuracy.

4.6 The proton transfer problem

The last, and very important illustration of the progress in theoretical chemistry is the treatment of the proton transfer problem. Most of the work on this subject before 1995 was devoted to the determination of the most stable structures and the barriers (references can be found in the historical section 2). In an early paper , Conway et al. in 1956 (4) suggested that the rotation of water molecules was the rate determining reaction, preceded and succeeded by fast tunneling of protons. They concluded that, though the rapid proton interchange precludes any permanent individuality of a given H_3O^+ entity, the proton spends a much longer time with a definite molecule than as a proton migrating one. Indeed, that was the justification of our own work on protonated hydrates based on an oxonium ion with water molecules. This was the only information of this nature till 1995. Recent work by Tuckerman et al. (75bc) from Molecular Dynamics and the DFT approximation confirms this hypothesis and states that 60% of the excess proton is associated with the oxonium ion in MD trajectory configurations, though not obligatory sequential, while it could not be assigned to a unique oxygen atom in 40% of the cases. They propose that the second shell plays a role in the mechanism. The conversion between $H_9O_4^+$ and $H_5O_2^+$ being easy, a newly formed $H_9O_4^+$ conformation may retain a memory of the former $H_5O_2^+$ state reflected in the structure of the second solvation shell. This would explain that two of the three ligands H_2O in the $H_9O_4^+$ structure are hydrogen-bonded to three second-neighbors of the H_3O^+ while the third H_2O is H-bonded to two H_2O only. This gives an average coordination number of 3.67 for an oxygen, resulting from 4 in two H-bonds and 3 in the third one. Agmon (80) proposed a mechanism of the tropotropic mobility, which would be compatible with the trajectories of Ref. (75bc). In this description the rate limiting step is the cleavage of a H-bond. This cannot occur in the extra strong bond of the first shell. The process would begin by the cleavage of a H-bond in the second solvation shell, then the moving of the

proton and a hydrogen-bond formation in its back. Let us also mention that a recent molecular dynamics study account for the proton transfer by means of a hopping mechanism treated via Monte Carlo calculations (81). In complement to these studies, another MD work coupled with DFT potential underlines the importance of considering the quantum nature of the hydrogen atoms in such treatments (82). AQMD simulations performed at 150K show a broadening of distributions concerning the position of the proton in $H_5O_2^+$ when the nuclei are treated quantum mechanically, reflecting a shallow potential energy surface for motion of the "bonding" proton. Their results (82) suggest that the potential barrier for the proton transfer, which collapses for small intermolecular distances, should rather favor configurations of the type $H_3O^+{\cdot}H_2O$ at higher temperatures.

5. Conclusion

This short and very limited review gives an idea of the wide variety and complexity of the problems encountered in the study of protonated hydrates. This selection of topics is illustrative of the new possibilities offered by the present developments of theoretical treatments and shows the progress realised in this field, especially within the last few years. Besides the improvement of the accuracy of some of the methods used, in particular to treat the correlation contribution to the intermolecular energies, other categories of methods of lower accuracy bring other kinds of information. This has been exemplified by the results obtained from Monte Carlo and Molecular Dynamics calculations based on the use of DFT or analytical potentials. Though great care must be taken to the possibility of artefacts due to the approximations included in these treatments, such work is complementary to more accurate determinations. We can expect all these methods to be more and more coupled in the near future.

Acknowledgements

The CNRS is acknowledged for computer facilities. In particular a part of the calculations has been performed on the Cray C98 at IDRIS, project 940306. It is a great pleasure to dedicate this paper to Geerd Diercksen and I wish to thank him for his decisive role in the building of the European ab initio Community.

References

(1) A. Hantzsch, K. S. Caldwell, Z. Physik. Chem. **58**, 575 (1907); H. Goldschmitt, O. Udby, Z. Physik. Chem. **60**, 728 (1907). As underlined in Refs. 6ab the monohydrated proton should be called "oxonium" ion following the rules for chemical nomenclature accepted by IUPAC. Indeed, it is more coherent with the definition of the "onium" group than the name "hydronium", which is very often

used. This point has been commented again in Ref. 100 (page 394), which specifies that names such as 'hydroxonium" or "hydronium" should be avoided.
(2) J.D. Bernal, R.H. Fowler, J. Chem. Phys. **1**, 515 (1933).
(3) E. Wicke, M. Eigen, Th. Ackermann, Z. Physik. Chem. **1**, 340 (1954); M. Eigen, L. De Maeyer, Proc. Roy. Soc. **a247**, 505 (1958); M. Eigen, Angew. Chem. **75**, 489 (1963).
(4) B. E. Conway, J. O'M. Bockris, H. Linton, J. Chem. Phys. **24**, 834 (1956).
(5) R. Grahn, Arkiv Physik **19**, 147 (1961); R. Grahn, Arkiv Physik **21**, 1 (1962); J. W. Moskowitz, M. C. Harrisson, J. Chem. Phys. **43**, 3550 (1965).
(6) a) D. Bishop, J. Chem. Phys. **43**, 4453 (1965); b) B. D. Joshi, J. Chem. Phys. **47**, 2793 (1967); c) A. C. Hopkinson, N. K. Holbrook, K. Yates, I. G. Csizmadia, J. Chem. Phys. **49**, 3596 (1968).
(7) a) M. C. R. Symons, J. Am. Chem. Soc. **102**, 3982 (1980); 133. b) T. J. Sears, P. R. Bunker, P. B. Davies, S. A. Johnson, V. Spirko, J. Chem. Phys. **83**, 2676 (1985).
(8) M. de Paz, S. Ehrenson, L. Friedman, J. Chem. Phys. **52**, 3362 (1970).
(9) a) M. D. Newton, S. Ehrenson, J. Am. Chem. Soc. **93**, 4971 (1971); b) M. D. Newton, J. Chem. Phys. **67**, 5535 (1977); c) J. H. Busch, J. R. de la Vega, J. Am. Chem. Soc. **99**, 2397 (1977).
10) W. P. Kraemer, G. H. F. Diercksen, Chem. Phys. Lett. **5**, 463 (1970).
(11) W. Meyer, W. Jakubetz, P. Schuster, Chem. Phys. Lett. **21**, 97 (1973).
(12) R. Janoschek, E. G. Weidemann, H. Pfeiffer, G. Zundel, J. Am. Chem. Soc. **94**, 2387 (1972).
(13) P. Schuster, Theoret. Chim. Acta **19**, 212 (1970); M. C. Flanigan, J. R. de la Vega, Chem. Phys. Lett. **21**, 521 (1973).
14) P. A. Kollman, L. C. Allen, J. Am. Chem. Soc. **92**, 6101 (1970); G. Alagona, R. Cimiraglia, U. Lamanna, Theoret. Chim. Acta **29**, 93 (1973); J. J. Delpuech, G. Serratrice, A. Strich, A. Veillard, Mol. Phys. **29**, 849 (1975); P. Schuster, W. Jakubetz, W. Marius, Topics in Current Chemistry **60**, 1 (1975).
(15) H. Lischka, Theoret. Chim. Acta **31**, 39 (1973); H. Lischka, V. Dyczmons, Chem. Phys. Lett. **23**, 167 (1973); R. Ahlrichs, F. Driessler, H. Lischka, V. Staemmler, W. Kutzelnigg, J. Chem. Phys. **62**, 1235 (1975).
(16) G. H. F. Diercksen, W. P. Kraemer, B. O. Roos, Theoret. Chim. Acta **36**, 249 (1975)
(17) W. A. Lathan, W. J. Hehre, L. A. Curtiss, J. A. Pople, J. Am. Chem. Soc. **93**, 6377 (1971); R. A. Gangi, R. F. W. Bader, Chem. Phys. Lett. **11**, 216 (1971); G. H. F. Diercksen, W. P. Kraemer, Theoret. Chim. Acta **23**, 387 (1972); M. Fournier, M. Allavena, A. Potier, J. Chim. Phys. **69**, 1520 (1972); J. Almlöf, U. Wahlgren, Theoret. Chim. Acta **28**, 161 (1973); P. C. Hariharan, J. A. Pople, Mol. Phys. **27**, 209 (1974); M. Allavena, E. Le Clec'h, J. Mol. Struct. **22**, 265 (1974); M. Fournier, M. Allavena, Theoret. Chim. Acta **42**, 145 (1976); M. E. Schwartz, Chem. Phys. Lett. **40**, 1 (1976); R. E. Kari, I. G. Csizmadia, J. Am. Chem. Soc. **99**, 4539 (1977); P. C. Hiberty, C. Leforestier, J. Am. Chem. Soc. **100**, 2012 (1978); J. A. Pappas, J. Am. Chem. Soc. **101**, 561 (1979).
(18) P. A. Kollman, C. F. Bender, Chem. Phys. Lett. **21**, 271 (1973).
(19) R.C. Raffenetti, H.J.T. Preston, J.J. Kaufman, Chem. Phys. Lett. **46**, 513 (1977).
(20) T. F. Thomas, T. L. Rose, J. F. Paulson, J. Chem. Phys. **71**, 552 (1979).
(21) J. Q. Searcy, J. B. Fenn, J. Chem. Phys. **61**, 5282 (1974); J. Q. Searcy, J. Chem. Phys. **63**, 4114 (1975).

(22) F. H. Stillinger, C. W. David, J. Chem. Phys. **69**, 1473 (1978).
(23) A. Warshel, J. Phys. Chem. **83**, 1640 (1979).
(24) J. L. Kassner, Jr, D. E. Hagen, J. Chem. Phys. **64**, 1860 (1976).
(25) W. I. Ferguson, N. C. Handy, Chem. Phys. Lett. **71**, 95 (1980); M. F. Guest, S. Wilson, Chem. Phys. Lett. **72**, 49 (1980); A. Greenberg, R. Winkler, B. L. Smith, J. F. Liebman, J. Chem. Educ. **59**, 367 (1982); P. Botschwina, P. Rosmus, E. A. Reinsch, Chem. Phys. Lett. **102**, 299 (1983); J. E. Del Bene, H. D. Mettee, M. J. Frisch, B. T. Luke, J. A. Pople, J. Phys. Chem. **87**, 3279 (1983); P. Botschwina, J. Chem. Phys. **84**, 6523 (1986); D.J. Swanton, G.B. Bacskay, N.S. Hush, Chem. Phys. **107**, 9 (1986); W.A. Sokalski, A. Sawaryn, J. Chem. Phys. **87**, 526 (1987); D. J. DeFrees, A. D. McLean, J. Comp. Chem. **7**, 321 (1986); C. A. Deakyne, J. Phys. Chem. **90**, 6625 (1986); J. A. Pople, L. A. Curtiss, J. Phys. Chem. **91**, 155 (1987); A. E. Howard, U. C. Singh, M. Billeter, P. A. Kollman, J. Am. Chem. Soc. **110**, 6984 (1988).
(26) P. J. Desmeules, L. C. Allen, J. Chem. Phys. **72**, 4731 (1980); S. G. Lias, J. Phys. Chem. **88**, 4401 (1984); L. M. Bass, M. T. Bowers, J. Chem. Phys. **86**, 2611 (1987); J. E. Del Bene, J. Comp. Chem. **8**, 810 (1987); J. E. Del Bene, J. Phys. Chem. **92**, 2874 (1988).
(27) S. Yamabe, T. Minato, K. Hirao, J. Chem. Phys. **80**, 1576 (1984); C. I. Ratcliffe, J. A. Ripmeester, J. S. Tse, Chem. Phys. Lett. **120**, 427 (1985); J. E. Del Bene, M. J. Frisch, J. A. Pople, J. Phys. Chem. **89**, 3669 (1985).
(28) a) S. Scheiner, J. Am. Chem. Soc. **103**, 315 (1981); b) S. Scheiner, J. Phys. Chem. **86**, 376 (1982); c) S. Scheiner, J. Chem. Phys. **77**, 4039 (1982); d) S. Scheiner, M. M. Szczesniak, L. D. Bigham, Int. J. Quantum Chem. **XXIII**, 739 (1983); e) S. Scheiner, P. Redfern, J. Phys. Chem. **90**, 2969 (1986); f) S. Scheiner, R. Wang, L. Wang, Int. J. Quantum Chem. **16** (QB Sym), 211 (1989); g) E. A. Hillenbrand, S. Scheiner, J. Am. Chem. Soc. **106**, 6266 (1984); h) G. E. Scuseria, A. C. Scheiner, T. J. Lee, J. E. Rice, H. F. Schaefer III, J. Chem. Phys. **86**, 2881 (1987).
(29) a) E. Kochanski, Nouv. J. Chim. **8**, 605 (1984); b) E. Kochanski, J. Am. Chem. Soc. **107**, 7869 (1985); c) E. Kochanski, Chem. Phys. Lett. **130**, 291 (1986); d) E. Kochanski, Chem. Phys. Lett. **133**, 143 (1987); e) E. Kochanski, A. Rahmouni, J. Chim. Phys. **86**, 995 (1989).
(30) P. M. Holland, A. W. Castleman, Jr, J. Chem. Phys. **72**, 5984 (1980).
(31) W. R. Rodwell, L. Radom, J. Am. Chem. Soc. **103**, 2865 (1981).
(32) a) K. Hirao, M. Sano, S. Yamabe, Chem. Phys. Lett. **87**, 181 (1982);
b) K. Hiraoka, H. Takimoto, S. Yamabe, J. Phys. Chem. **90**, 5910 (1986).
(33) a) V. Spirko, P. R. Bunker, J. Mol. Spect. **95**, 226 (1982); b) P. R. Bunker, W. P. Kraemer, V. Spirko, J. Mol. Spect. **101**, 180 (1983).
(34) J. R. de la Vega, Acc. Chem. Res. **15**, 185 (1982).
(35) H. Z. Cao, M. Allavena, O. Tapia, E. M. Elveth, Chem. Phys. Lett. **96**, 458 (1983).
(36) I. P. Buffey, W. Byers Brown, Chem. Phys. Lett. **109**, 59 (1984).
(37) A. Potier, J. M. Leclercq, M. Allavena, J. Phys. Chem. **88**, 1125 (1984).
(38) K. Y. Burstein, A. N. Isaev, Theoret. Chim. Acta **64**, 397 (1984).
(39) C. E. Klots, J. Phys. Chem. **88**, 4407 (1984).
(40) N. Shida, K. Tanaka, K. Ohno, Chem. Phys. Lett. **104**, 575 (1984).
(41) M. A. Muniz, J. Bertran, J. L. Andrés, M. Duran, A. Lledos, J. Chem. Soc. Faraday Trans. **81**, 1547 (1985).

(42) U. Nagashima, H. Shinohara, N. Nishi, H. Tanaka, J. Chem. Phys. **84**, 209 (1986).
(43) S. L. Fornili, M. Migliore, M. A. Palazzo, Chem. Phys. Lett. **125**, 419 (1986).
(44) M. J. Frisch, J. E. Del Bene, J. S. Binkley, H. F. Schaefer III, J. Chem. Phys. **84**, 2279 (1986).
(45) a) M. Okumura, L. I. Yeh, J. D. Myers, Y. T. Lee, J. Chem. Phys. **85**, 2328 (1986); b) L. I. Yeh, M. Okumura, J. D. Myers, J. M. Price, Y. T. Lee, J. Chem. Phys. **91**, 7319 (1989).
(46) G. R. J. Williams, J. Mol. Struct. (Theochem) **138**, 333 (1986).
(47) C. A. Reynolds, C. Thomson, J. Quantum Chem. : Quantum Biol. Symp. **12**, 263 (1986).
(48) C. A. Deakyne, M. Meot-Ner, C. L. Campbell, M. G. Hughes, S. P. Murphy, J. Chem. Phys. **84**, 4958 (1986).
(49) U. C. Singh, F. K. Brown, P. A. Bash, P. A. Kollman, J. Am. Chem. Soc. **109**, 1607 (1987).
(50) Y. Guissani, B. Guillot, S. Bratos, J. Chem. Phys. **88**, 5850 (1988).
(51) J. Y. Choi, E. R. Davidson, I. Lee, J. Comp. Chem. **10**, 163 (1988).
(52) D. Peeters, G. Leroy, Bull. Soc. Chim. Belg. **97**, 931 (1988).
(53) G. Karlström, J. Phys. Chem. **92**, 1318 (1988).
(54) P. Ertl, J. Leska, Collect. Czech. Chem. Comm. **51**, 738 (1986).
(55) J. Waite, M.G. Papadopoulos, Z. Naturforsch. **43a**, 253 (1988).
(56) O. Matsuoka, E. Clementi, M. Yoshimine, J. Chem. Phys., **64**, 2314 (1976)
(57) C. K. Lutrus, D. E. Hagen, S. H. Suck Salk, Atmospheric Environment **24A**, 1397 (1990).
(58) J.E. Del Bene, I. Shavitt, J. Phys. Chem. **94**, 5514 (1990).
(59) a) E. Kochanski, A. Rahmouni, R. Wiest, in "Modelling of Molecular Structures and Properties", Ed. J. L. Rivail, Studies in Physical and Theoretical Chemistry (Elsevier) **71**, 303 (1990); b) E. Kochanski, A. Rahmouni, R. Wiest, J. Chim. Phys. **87**, 917 (1990); c) A. Rahmouni, E. Kochanski, R. Wiest, P. E. S. Wormer, J. Langlet, J. Chem. Phys. **93**, 6648 (1990); d) E. Kochanski, A. Rahmouni, R. Kelterbaum, R. Wiest, P. E. S. Wormer, J. Langlet, J. Chim. Phys. **88**, 2451 (1991); e) R. Kelterbaum, N. Turki, A. Rahmouni, E. Kochanski, J. Chem. Phys. **100**, 1589 (1994); f) R. Kelterbaum, N. Turki, A. Rahmouni, E. Kochanski, J. Mol. Struct. (Theochem) **314**, 191 (1994); g) G. Corongiu, R. Kelterbaum, E. Kochanski, J. Phys. Chem. **99**, 8038 (1995); h) R. Kelterbaum, E. Kochanski, J. Phys. Chem. **99**, 12493 (1995); i) S. Klein, E. Kochanski, A. Strich, Chem. Phys. Lett., submitted; j) R. Kelterbaum, E. Kochanski, J. Mol. Struct. (Theochem), in press.
(60) M. Okumura, L. I. Yeh, J. D. Myers, Y. T. Lee, J. Phys. Chem. **94**, 3416 (1990).
(61) C. A. Chatzidimitriou-Dreismann, E. J. Brändas, Int. J. Quantum Chem. **XXXVII**, 155 (1990);192. C. A. Chatzidimitriou-Dreismann, E. J. Brändas, Ber. Bunsenges. Phys. Chem. **95**, 263 (1991).
(62) S. Roszak, P. C. Hariharan, J. J. Kaufman, W. S. Koski, J. Comp. Chem. **11**, 1076 (1990).
(63) a) E. P. F. Lee, J. M. Dyke, A. E. Wilders, P. Watts, Mol. Phys. **71**, 207 (1990); b) E. P. F. Lee, J. M. Dyke, Mol. Phys. **73**, 375 (1991).
(64) D. Peeters, G. Leroy, J. Mol. Struct. (Theochem) **209**, 263 (1990).
(65) R. F. W. Bader, J. R. Cheeseman, K. E. Laidig, K. B. Wiberg, C. Breneman, J. Am. Chem. Soc. **112**, 6530 (1990).

(66) E. S. Kryachko, Chem. Phys. **143**, 359 (1990).
(67) a) R. E. Kozack, P. C. Jordan, J. Chem. Phys. **96**, 3131 (1992);
b) R. E. Kozak, P. C. Jordan, J. Chem. Phys. **99**, 2978 (1993).
(68) C. Lee, D. Vanderbilt, Chem. Phys. Lett. **210**, 279 (1993).
(69) I. Tunon, E. Silla, J. Bertran, J. Phys. Chem. **97**, 5547 (1993).
(70) C. Mijoule, Z. Latajka, D. Borgis, Chem. Phys. Lett. **208**, 364 (1993).
(71) M. W. Jurema, K. N. Kirschner, G. C. Shields, J. Comp. Chem. **14**, 1327 (1993).
(72) T. Komatsuzaki, I. Ohmine, Chem. Phys. **180**, 239 (1994).
(73) S. P. A. Sauer, V. Spirko, I. Paidarova, J. Oddershede, Chem. Phys. **184**, 1 (1994).
(74) A. Khan, Chem. Phys. Lett. **217**, 443 (1994).
(75) a) K. Laasonen, M. L. Klein, J. Phys. Chem. **98**, 10079 (1994); b) M. Tuckermann, K. Laasonen, M. Sprik, M. Parrinello, J. Phys. Chem. **99**, 5749 (1995); c) M. Tuckermann, K. Laasonen, M. Sprik, M. Parrinello, J. Chem. Phys. **103**, 150 (1995).
(76) D. Wei, D.R. Salahub, J. Chem. Phys. **101**, 7633 (1994).
(77) R.V. Stanton, K.M. Metz, Jr., J. Chem. Phys. **101**, 6658 (1994).
(78) Y. Xie, R.B. Remington, H.F. Schaeffer III, J. Chem. Phys. **101**, 4878 (1994).
(79) a) F. Di Giacomo, F.A. Gianturco, F. Raganelli, F. Schneider, J. Chem. Phys. **101**, 3952 (1994); b)F.A. Gianturco, F. Raganelli, F. Di Giacomo, F. Schneider, J. Phys. Chem. **99**, 64 (1995).
(80) N. Agmon, Chem. Phys. Lett. **244**, 456 (1995).
(81) R.G. Schmidt, J. Brickmann, Solid State Ionics **77**, 3 (1995).
(82) H.-P. Cheng, R.N. Barnett, U. Landmann, Chem. Phys. Lett. **237**, 161 (1995).
(83) a) A. Lami, G. Villani, Chem. Phys. Lett. **238**, 137 (1995);
b) A. Lami, G. Villani, Theochem (J. Molec. Structure) **330**, 307 (1995).
(84) A.T. Pudzianowski, J. Chem. Phys. **102**, 7761 (1995).
(85) C. Lee, C. Sosa, J.J. Novoa, J. Chem. Phys. **103**, 4360 (1995).
(86) V. Barone, L. Orlandini, C. Adamo, Int. J. Quantum Chem. **56**, 697 (1995).
(87) J. Lobaugh, G.A. Voth, J. Chem. Phys. **104**, 2056 (1996).
(88) A.S. Edison, L. Markley, . Weinhold, J. Phys. Chem. **99**, 8013 (1995).
(89) a) G. Chalasinski, M. M. Szczesniak, P. Cieplak., S. Scheiner, J. Chem. Phys., **94**, 2873 (1991); b) G. Chalasinski, S. M. Cybulski, M. M. Szczesniak, S. Scheiner J. Chem. Phys., **91**, 7048 (1989); c) M. M. Szczesniak, G. Chalasinski, S. M. Cybulski, S. Scheiner, J. Chem. Phys. **93**, 4243 (1990); d) M.M. Szczesniak, R. A. Kendall, G. Chalasinski, J. Chem. Phys., **95**, 5169 (1991).
(90) J.P. Perdew, Phys. Rev. **B33**, 8822 (1986); ibid, Erratum **34**, 7406 (1986); J.P. Perdew, Phys. Rev. Lett. **55**, 1665 (1985); J.P. Perdew, Y. Wang, Phys. Rev., **B33**, 8800 (1986); J.P. Perdew, A. Zunger, Phys. Rev. **B 23**, 5048 (1981)
(91) C. Lee, W. Yang, R. G. Parr, Phys **B 37**, 785 (1988)
(92) A.D. Becke, a) J. Chem. Phys., **88**, 1053 (1988); b) J. Chem. Phys. **96**, 2155 (1992); c) Phys. Rev., **A38,** 3098 (1988); d) J. Chem. Phys., **98,** 1372 (1993); e) J. Chem. Phys., **98**, 5648 (1993)
(93) S. S. Lin, Rev. Sci. Instrum **44**, 516 (1973).
(94) a) M. Meot-Ner, J. Am. Chem. Soc. 106, 1265 (1984); b) M. Meot-Ner, C. V. Speller, J. Phys. Chem. **90**, 6616 (1986); c) M. S. El-Shall, G. M. Daly, J. Gao, M. Meot-Ner, L. W. Sieck, J. Phys. Chem. **96**, 507 (1992).
(95) a) S. Wei, W. B. Tzeng, R. G. Keesee, A. W. Castleman, Jr, J. Am. Chem. Soc. **113**, 1960 (1991); b) S. Wei, Z. Shi, A. W. Castleman, Jr, J. Chem. Phys. **94**,

3268 (1991); c) S. Wei, W.B. Tzeng, A.W. Castleman, Jr., Chem. Phys. Lett. **178,** 411 (1991); d) Z. Shi, J. V. Ford, S. Wei, A. W. Castleman, Jr, J. Chem. Phys. **99**, 8009 (1993).

(96) A. J. Sadlej, Coll. Czech. Chem. Commun. **53**, 1995 (1988)

(97) a) P. Kebarle, S. K. Searles, A. Zolla, J. Scarborough, M. Arshadi, J. Am. Chem. Soc. **89**, 6393 (1967); b) A. J. Cunningham, J. D. Payzant, J. Am. Chem. Soc. **94**, 7627 (1972); c) Y. K. Lau, S. Ikuta, P. Kerbale, J. Am. Chem. Soc. **104**, 1462 (1982).

(98) T. F. Magnera, D. E. David, J. Michl, Chem. Phys. Lett. **182**, 363 (1991).

(99) N. F. Dalleska, K. Honma, P. B. Armentrout, J. Am. Chem. Soc. **115**, 12125 (1993).

(100) J. O. Lundgren, I. Olovsson, in :*The Hydrogen Bond*, ed. P. Schuster, G. Zundel, C. Sandorfy, North Holland, **2**, 471 (1976).

Density Functional Theory: A Useful Tool for the Study of Free Radicals

Oscar N. Ventura, Martina Kieninger and Kenneth Irving

MTC-Lab, University of Uruguay
CC 1157, 11800 Montevideo, Uruguay

Abstract

The application of density functional theory (DFT) to the study of the structure and reactivity of some molecules with unpaired electrons (radicals) performed by our group is presented. The results describe the application of LSD, gradient corrected and hybrid DFT methods to several small molecules. On average the results are as good as highly-correlated post-Hartree-Fock methods, but still some problems remain to be solved

ADVANCES IN QUANTUM CHEMISTRY, VOLUME 28

0065-3276/97 $25.00

1. Introduction

The computational chemistry community has dedicated a lot of attention in recent years to the application of density functional methods (DFT) to molecular systems (for general reviews see ref. (1)). This is due, on one hand, to the accuracy that the more sophisticated of these methods can exhibit, usually comparable to highly-correlated post-Hartree-Fock methodologies. On the other hand, for the same degree of accuracy, DFT methods scale much more slowly with the size N of the system than conventional correlated *ab initio* methods and are therefore applicable to the study of larger systems.

DFT methods as applied nowadays to molecular systems, are based on the demonstration by Kohn and Sham (KS) (2) that the exact ground state density and energy of a many-electron system may be found through the self-consistent solution of a one-particle set of equations similar to Hartree-Fock (HF). In the KS-equations one replaces the HF exchange potential by the functional derivative $v_{xc,\sigma}(r) = \delta E_{xc} / \delta\rho_\sigma(r)$ where E_{xc} is the exchange-correlation energy, a function of the spin-up and spin-down *(i.e.* σ) electronic densities (ρ) (1). This exchange-correlation energy accounts for exchange and coulombic terms, dynamical and non-dynamical correlation energy and the residual kinetic energy (*i.e.* the difference between the exact kinetic energy and that obtained from the one particle occupation of the natural spin-orbitals). The derivation of ever more precise exchange-correlation functionals has been one of the very important tasks in the last years, and it is briefly summarized in what follows.

The simplest approximation, employed for very many years until the most recent developments, is known as Local Spin Density Approximation (LSDA) and does not depend on the gradients of the electronic density but only on the electronic density itself. One of the variants of LSDA, commonly employed in the applications to molecular systems in the last years, is the one called SVWN. In this exchange-correlation functional, the exchange is provided by Slater's formula (3) for the uniform electron gas, whereas the correlation is evaluated according to the expression derived by Vosko, Wilk and Nusair (4) from an interpolation of previous Monte-Carlo results for the spin-polarized homogeneous electron gas

$$\varepsilon_c(r_s) = A\left\{\ln\frac{x^2}{X(x)} + \frac{2b}{Q}\tan^{-1}\frac{Q}{2x+b}\right\} - \frac{Abx_o}{X(x_o)}\left[\ln\frac{(x-x_o)^2}{X(x)} + \frac{2(b+2x_o)}{Q}\tan^{-1}\frac{Q}{2x+b}\right]$$

where $X(x)=x^2+bx+c$, $Q=(4c-b^2)^{1/2}$ and x_o, b and c are adjustable parameters.

Generalized gradient approximations (GGA), in which the exchange-correlation functional depends on the electronic density and, at least, on its gradient, were developed in more recent times (5-12). A guide for "comparison shopping" of

gradient-corrected DFT methods has been provided recently by Perdew and Burke (13). Among exchange functionals, the ones better known are called PW86 (7) and PW91 (14), due to Perdew and associates, and B88 (9) due to Becke. In this last case, for instance, the LDA exchange is complemented with a term depending on the gradient of the density, designed in such a way that the exchange energy density has the correct -1/r asymptotic behavior. It has the form

$$-\beta \sum_{\sigma} \rho_{\sigma}^{4/3}(r) \frac{x_{\sigma}^{2}}{1 + 6\beta x_{\sigma} \sinh^{-1}(x_{\sigma})}$$

where $x_{\sigma} = |\nabla \rho_{\sigma}| / \rho_{\sigma}$. According to the available experience (13) the three exchange potentials tend to give similar results. An example of an exchange potential with a dependence on higher derivatives of the electronic density is that of Becke and Roussel (15) which also depends on $|\nabla^2 \rho|$ and was designed to model the shape of the HF exchange hole.

The exchange potentials mentioned before have been combined with different correlation potentials, in particular PW86 or PW91 and that of Lee, Yang and Parr (10). The combinations of such exchange and correlation potentials have become well known in the literature of the last years as BLYP (=B88+LYP), BP86, BP91, etc. It is important to mention that although LYP seems to be the most popular correlation functional in recent years, it is PW91 the one that seems to be more accurate (13).

Recently, Becke has derived theoretically the need to include part of the Hartree-Fock exact exchange (*i.e.* non-local effects) in the exchange functional to improve the predictions of the gradient-corrected DFT methods (16,17). Becke (17) proposed the functional

$$E_{xc} = E_{xc}^{LSDA} + a_0(E_x^{exact} - E_x^{LSDA}) + a_x \Delta E_X^{88} + a_c \Delta E_c^{PW91}$$

where E_{xc}^{LSDA} is the local spin-density exchange-correlation energy, E_x^{exact} is the exact (HF) exchange energy, ΔE_x^{B88} is Becke's 1988 gradient correction for exchange and ΔE_c^{PW91} is Perdew and Wang 1991 gradient correction for correlation. This method is normally called B3PW91. The correlation correction in this Adiabatic Connection Functional (ACM) can be changed to PW86 or LYP, generating respectively B3P86 or B3LYP. This last method has been immensely popular since its coding in the Gaussian series of programs.

Gradient corrected DFT methods, specially the ACM versions, have been very successful in the prediction of different molecular properties. In the following we will give some examples of this behavior. One interesting study has been

published by Hertwig and Koch (18) on the diatomic homonuclear molecules of the three first rows of the periodic table. They found that for all these 21 molecules and using a relatively small basis set, the performance of DFT methods was superior to HF, MP2 (Møller-Plesset perturbation theory at second order), or CISD (configuration interaction including singles and doubles). Particularly, no pathological cases, such as the group 2 dimers (Be_2, Mg_2, Ca_2) were observed. Edgecombe and Becke (19) studied recently the difficult Cr_2 molecule and found that they were able to reproduce the double-well potential energy curve suggested by other theoretical studies and experiment. In general, it seems that the performance of DFT methods (at least in its more modern versions) with respect to non-weakly bound molecules is satisfactory, as shown, for instance by the study of Martin *et al* (20) on the performance of B3LYP for geometries and harmonic frequencies. It has usually been found that the basis set convergence of DFT methods is faster than that of conventional *ab initio* methods (this was found, for instance, by Martin *et al* (20) and by Kristyán (21)). Other properties of molecular systems have also been studied. So, for instance, Smith and Radom (22) studied gas-phase acidities of some molecules containing first- and second-row atoms and found that the DFT methods could behave as accurately as Pople's G2 or G2(MP2) (23) model chemistries. Analogously, Barone (24) used DFT methods successfully to study the structure, epr parameters and reactivity of organic radicals. Solà *et al* (25) performed a comparative analysis of density distributions derived from DFT and conventional *ab initio* methods. Many other examples of the application of these methods to strongly bound molecules can be found in the literature for this and last years. Some consideration has been given to weakly bound interactions (Hobza *et al* (26), Lundqvist *et al* (27) and others) but the results, although good for hydrogen-bonded systems, seem not conclusive for other weak interactions.

Chemical reactions have also been studied from the DFT point of view. For instance, Barone and Adamo (28) studied the water-assisted isomerization of formaldehyde radical cation employing LDA and B3LYP. More recently, Jursic and Zdravkovski (29) studied a more complicated reaction, the conrotatory ring opening of cyclobutene and derivatives, using BLYP methods and found reasonable results, while Jursic (30) determined that B3LYP and B3P86 are adequate tools for the study of proton transfer between neutral and radical molecules. Other proton transfer reactions were study by Barone and associates (31) who investigated typical hydrogen bonded systems including water and ammonia. They also found that use of the hybrid DFT methods (ACM) significantly improved the agreement with experiment and post-HF results. Andzelm and associates (32) made similar studies on several chemical reactions involving small molecules. They have shown that sometimes DFT methods underestimate reaction barrier heights, specially when radicals and H are invoved. In particular, they found that for the reaction $OH + H_2 \rightarrow H_2O + H$ most gradient-corrected DFT methods produce wrong results (the energy of the TS is *below* that of the reactants) while the use of ACM produces reasonable results (33). Recently Nachtigall *et al* (34) have studied some reactions

and activation energies for Si-Si bond cleavage and H2 elimination from silanes and found that B3LYP gives reaction and activation energies close to experimental and to those from QCISD(T) (35) calculations. Some doubts remain, however, concerning transition states (36).

In this paper we will refer specifically to the application of DFT methods to problems involving radicals. These open-shell molecules are more difficult to treat than closed shell ones at the conventional level due to the often inaccurate HF reference configuration. Conventional *ab initio* calculations of radicals is often complicated by spin contamination, a problem showed to be less severe in DFT calculations (24,37). Therefore, it is useful to apply this methodology to the determination of structure and reactivity of radicals.

2. Geometrical Structure of Simple Radicals

2.1 Diatomic Molecules

Spin contamination is a severe problem in conventional *ab initio* calculations on radicals. For instance, spin contamination can have a large effect on calculated vibrational frequencies, as proved by Jensen (38), and certainly severely reduces the rate of convergence of the Møller-Plesset series (UMP2, UMP3, UMP4) (39), leading in some cases to poor energies for radicals with low-lying unfilled orbitals. Surprisingly, even small diatomic molecules can exhibit that type of pathological behavior. Tozer *et al* (39) derived formulas for open-shell restricted Møller-Plesset theory, and in that some paper studied several diatomic radicals containing first row atoms. For most of them they obtained relatively good agreement with the experimental results, but for some cases this agreement was definitely poor (for instance, FO, F_2^+, BN, etc). More sophisticated calculations on some of these diatomic molecules were done recently by Peterson (40), using the correlation consistent (cc) basis sets of Dunning (41) at the MRCI level.

Based on the knowledge that spin contamination in DFT is usually much smaller than in conventional *ab initio* calculations (37), we decided to apply B3LYP to construct the potential energy curves for some of these diatomic molecules and to compare the results with those already published in the literature (42). Some of these results are shown in Table 1. Here are reported only the results obtained by us at the B3LYP/6-311+G(2df) level, other results can be seen in the original reference. One can see that B3LYP performs better than MP4, either in its unrestricted or restricted versions, and as well as QCISD(T), CCSD(T) or MRCI. In fact, if one calculates the vibrationally-averaged bond distances r_e, the resemblance with experiment is even more striking. Using the order given in Table 1, the r_e, calculated using B3LYP are (experimental bond distances in parenthesis):

Table 1
Comparison of the equilibrium bond distances (r_e, in Å) for several diatomic molecules as obtained with different methods (39,42).

	UMP4	RMP4	QCISD(T)	RCCSD(T)	MRCI	MRCI+Q	UB3LYP	EXP
BN	1.320	1.353	1.335	1.332	1.333	1.349	1.317	1.329
CN	1.136	1.197	1.177	1.178	1.185	1.195	1.164	1.172
CO^+	1.099	1.143	1.123	1.122	1.107	1.132	1.107	1.115
NO	1.142	1.174	1.162	1.159	1.157	1.160	1.147	1.151
O2	1.231	1.246	1.218	1.217	1.217	1.211	1.207	1.208
O_2^+	1.153	1.161	1.127	1.126	1.144	1.134	1.108	1.116
OF	1.352	1.375	1.379	1.372	1.364	1.359	1.348	1.354
F_2^+	1.359	1.365	1.330	1.327	1.308	1.334	1.290	1.305
r.m.s.	0.010	0.010	0.005	0.004	0.004	0.006	0.003	

1.322(1.329), 1.167(1.172), 1.112(1.115), 1.151(1.151), 1.209(1.208), 1.112(1.116), 1.353(1.354) and 1.296(1.305) Å, with an r.m.s. of only 0.002 Å. In general, restricted and unrestricted B3LYP calculations led to the same values of r_e (within 1mÅ) except in the case of BN. In this case, the UB3LYP calculation led to the first excited state, with a bond distance of 1.235 Å, while the restricted B3LYP calculation led to the correct ground state curve, with a minimum at 1.317 Å.

2.2 Molecules in Astrophysics

Some of the small radicals studied during the past year have importance in astrophysics. An example is MgNC, the first Mg-containing molecule identified in space. Guélin *et al* (43) reported in 1986 the discovery of a new "non-terrestrial" molecule in the envelope of the carbon star IRC+10216. The molecule was linear or slightly asymmetric and had an odd number of electrons, *i.e.* it was a radical. They found a rotational constant of 5966.8 MHz and hypothesized that this molecule could be HSiCC, HCCSi or HSCC. After some theoretical investigation of these molecules by Largo-Cabrerizo and Flores (44) who demonstrated that they have smaller rotational constants than the observed ones, Kawaguchi *et al* (45) detected the linear MgNC radical for the first time by laboratory microwave spectroscopy, assigning six of the lines reported by Guélin *et al* (43). This experimental work was suggested by previous theoretical calculations by Bauschlicher, Langhoff and Partridge (46) on Be, Mg, Ca and Ba cyanides. They showed that all these molecules are linear and that the isocyanide (MNC) structure is always more stable than the cyanide (MCN) one by 0.3 to 0.5 eV. More recently, Ishii *et al* (47) reanalyzed the structures of MgNC and MgCN as well as the

transition state between them and reduced sections of the potential energy surface, using SDCI with a TZ2P basis set.

We have performed LSDA and B3LYP calculations, using the 6-311+G(3df) basis set, on the three structures MgNC, MgCN and the transition state that interconnects them (TS). To provide further comparison with conventional *ab initio* calculations, we also performed MP2 and Complete Basis Set (CBS (48)) calculations. These last are alternative "model chemistries" similar to the G2 or G2(MP2) methods of Pople *et al* (23). A subset of the results obtained are shown in Tables 2 and 3.

One can see that B3LYP geometries for MgNC and MgCN are in agreement with those of SDCI. Both MP2 and SVWN give a too large CN bond in MgNC, while SVWN gives also a too short MgN bond length. More important, both MP2 and SVWN predict erroneously that MgCN is more stable than MgNC, against the results of SDCI, MRCI and CBS-Q calculations. Also in disagreement with the other methods is the height of the TS, which is too short by 2 to 3 kcal/mol in MP2 and SVWN. B3LYP, on the contrary, does not exhibit anyone of these drawbacks, to the point that both the stability of MgNC with respect to MgCN and the height of the TS are in fair to excellent agreement with the configuration-interaction results. This method predicts also an equilibrium rotational constant which is completely similar to the one found at the SDCI level, implying then that B3LYP is useful for the study of this type of metal-organic bond (49).

3. Thermodynamics

In the previous section we saw that B3LYP was able to describe properly the relative energy of MgCN with respect to MgNC. We further investigated thermodynamics, by employing B3LYP in the calculation of heats of reaction and heats of formation. For this study we chose several compounds containing the FO bond, specially the FO_2 radical, a species that has attracted much interest in several fields, for instance in atmospheric chemistry (50). FO_2 can be formed by reaction of free fluorine with molecular oxygen, $F + O_2 + M \rightarrow FO_2 + M$, or ozone, $F + O_3 + M \rightarrow FO_2$ + products. Experimentally, it is known that FO_2 is bent (51) with a long F-O bond (r_{FO}=1.649 ± 0.013 Å, r_{OO}= 1.200 ± 0.013 Å, θ_{FOO} = 111.19 ± 0.36 °). The structure results from the weak interaction between F and O, also shown by the small value of the F-O stretching frequency (52) (579 cm^{-1}), and the relatively unperturbed O-O stretching frequency (52,53) (1487 cm^{-1} *vs* 1580 cm^{-1} in O_2). Spectrokinetic studies of the gas-phase equilibrium $F + O_2 \rightarrow FO_2$ between 295 and 359 K were performed by Pagsberg *et al* (54), who found a value of $\Delta H^0_{r,298}$ = -12.62 ± 0.50 kcal/mol and heat of formation of FO_2 $\Delta H^0_{f,298}$ = 6.24 ± 0.50 kcal/mol. Other recent experimental value of the heat of formation is the one by Lyman and

Table 2
Comparison of the equilibrium bond distances (in Å) and angles (in deg) for MgNC, MgCN, and TS according to the different methods of calculation [(a)].

	MgNC		MgCN		Transition State		
Method	**r(MgN)**	**r(NC)**	**r(MgC)**	**r(CN)**	**r(MgC)**	**r(CN)**	**θ**
MP2	1.945	1.183	2.075	1.166	2.065	1.178	102.66
SVWN	1.848	1.180	1.956	1.159	1.933	1.166	113.21
B3LYP	1.941	1.173	2.081	1.158	2.079	1.166	102.32
SDCI(b)	1.945	1.170					
SDCI(c)	1.937	1.169	2.080	1.154			

(a) MP2 and B3LYP calculations were performed employing the 6-311+G(3df) basis set. (b) SDCI/TZ2P calculations of Ishii *et al* (47). (c) SDCI/TZ2P of Bauschlicher *et al* (46)

Table 3
Comparison of the relative energy (in kcal/mol) with respect to MgNC and of the equilibrium (B_e) and ground-state (B_0) rotational constants (in MHz) of MgNC as obtained with the different methods [(a)]

Method	**ΔE(MgCN)**	**ΔE(TS)**	**B_e(MgNC)**	**B_0(MgNC)**
MP2	-0.14	+5.10	5844.7	5901.6
SVWN	-0.81	+4.51		
B3LYP	+2.14	+7.46	5893.7	5950.6
SDCI(b)	+2.57	+7.47	5882.8	5939.7
MRCI-SDQ(c)	+2.72	+7.47		
CBS-Q (c)	+1.75			
Experimental				5966.9

(a) MP2 and B3LYP calculations were performed employing the 6-311+G(3df) basis set. (b) SDCI/TZ2P calculations of Ishii *et al* (47). (c) this work

Holland (55) who got $\Delta H^0_{f,298}$=5.49 kcal/mol. From this value, Francisco *et al* (56) have calculated a $\Delta H^0_{f,0}$ of 5.93 kcal/mol.

Several theoretical studies were performed on the FO_2 radical. The best and more recent one is that by Francisco *et al* (56). References to previous work on the subject are given there. The calculation of $\Delta H^0_{r,0}$ for the direct reaction proved to be exceedingly difficult and inaccurate. Therefore, the authors studied also some other isodesmic and/or isogyric reactions, namely

$$FO_2 + HO \rightarrow HO_2 + FO$$

$$FO_2 + H_2O \rightarrow HO_2 + FOH$$
$$FO_2 + 3F \rightarrow 2O + 2F_2$$

where errors due to defects in the basis set and inadequate correlation cancel.

At the post-Hartree-Fock level, the F-O bond in FO_2 is extremely difficult to describe (56), even worse than in the cases of the FO radical (57) or the F_2O_2 molecule(58). At the best theoretical level employed, *i.e.* QCISD(T)/6-311G(d,p)//QCISD(T)/6-311G(d,p), the calculations still produced an F-O bond length too long by about 0.06 Å, while $\Delta H^0_{r,0}$ for the direct reaction is in error by about 6 kcal/mol (-5.6 vs -11.68 kcal/mol (54)). However, considering the isodesmic reactions above (for which *ab initio* $\Delta H^0_{r,0}$ are more in agreement with experiment) they estimated the heat of formation $\Delta H^0_{f,0}(FO_2)$ as 8.9 ± 3 kcal/mol. This result is more in agreement with that reported by CODATA (59) (12 ± 3 kcal/mol) than with the one in the JANAF thermochemical tables (53) (3 ± 5 kcal/mol). It is also larger than the value obtained from the $\Delta H^0_{f,298}$ determined by Pagsberg et al (54) or Lyman and Holland (55).

Some of our results (60) obtained using B3LYP are summarized in Tables 4 to 6. The first point to notice is that while all theoretical methods give reasonable FO distances for FO, this is not so for FO_2. MP4 gives completely erroneous values both for the FO and OO bonds, while B3LYP is reasonably similar both to QCISD and experiment. Residual differences of B3LYP with respect to experiment are surely due to anharmonicity (notice how the vibrationally averaged FO bond in FO agrees perfectly well with the experimental value). Some other important results are shown in Table 5. None of the conventional *ab initio* methods applied up to now is able to describe properly the direct reaction of formation of FO_2. Extreme cases are seeing for perturbative methods which predict the reaction to be *endothermic*. B3LYP, on the contrary, performs perfectly well for this reaction. Furthermore, for the reactions presented in this Table, B3LYP has the smallest r.m.s. error. Finally, in Table 6 are given the heats of formation of four molecules involving the FO bond, obtained as averages of several reactions. It is obvious that the behavior of B3LYP is good and systematic, *i.e.* not limited to just one reaction but to a whole set of them involving species with an FO bond.

4. Reactivity

4.1 Isomerization of $HXCO^{\cdot +}$

Møller-Plesset perturbation theory at second order (MP2) (61) is the easiest and most popular way of including correlation energy after a Hartree-Fock calcula-

Table 4
Comparison of the equilibrium structures for FO and FO_2 as obtained with different methods [(a)]

	Method	r(FO), Å	r(OO), Å	θ, deg
FO	B3LYP/6-311+G(3df)	1.346 (1.353) [(b)]		
	MP4SDTQ/6-311+G(2d)	1.349		
	QCISD(T)/6-311G(d)	1.365		
	Experimental[(c)]	1.3579		
FO_2	B3LYP/6-311+G(3df)	1.626	1.184	111.1
	MP4SDTQ/6-311+G(2d)	1.389	1.245	110.6
	QCISD(T)/6-311G(d)	1.709	1.198	111.8
	Experimental	1.649	1.200	111.2

(a) B3LYP calculations from ref. (60); others from refs. (57) and (56). (b) Vibrationally averaged r_e; (c) CRC Handbook of Chemistry and Physics, 1995.

Table 5
Heats of Reaction (in kcal/mol) for reaction involving FO_2 (values for the reaction $H + O_2$ -> HO_2 is also shown for the purpose of comparison).

Reaction	UMP4	QCISD(T)	G1	B3LYP	Exp.
F + O2 -> FO_2	+12.7	-1.98	-5.6	-11.1	-11.68
FO_2 + HO -> HO_2 + FOH	+1.39	+13.4		+12.7	+16.59
FO_2 + H_2O -> HO_2 + FOH	+18.2	+31.3		+32.6	+35.77
FO_2 + 3F -> 2O + $2F_2$		+55.3		+63.3	+56.62
H + O_2 -> HO_2	-40.4	-42.3		-47.8	-47.4
r.m.s. error	8.6	2.5		1.7	

Table 6
Heats of Formation (in kcal/mol) for molecules involving the FO bond (60).

Species	B3LYP	Experimental	Other theoretical calcs.
FOH	-19.0	-22.8±1, -19.9±1	-20.8±1
FO	25.4	26±10, 26.6±4, 27.2±2	27.8±1
FO_2	7.2	6.68±0.5, 3±5, 12±3, 5.93±1.5	8.9±3
F_2O_2	8.2	5.47±0.40, 6.82±0.40	

Table 7
Isomerization energies (in kcal/mol) for the reaction $XHCO^{+\cdot}$ -> $XCOH^{+\cdot}$ calculated with several DFT and conventional *ab initio* methods (67). Values in parenthesis imply that the geometry of the molecules were not optimized at that level.

Method	X=H	X=F	X=Cl
HF	-32.4	-2.13	-2.55
MP2	+5.60	+62.4	+56.5
QCISD	-25.9	(+29.9)	(+20.0)
BVWN	-34.4	+33.7	+13.5
BLYP	-33.2	+38.2	+17.7
B3LYP	-26.5	+36.9	+28.1
G1	-24.4	+35.4	+28.0
G2	-23.4	+38.7	+29.7

tion. Being a perturbative procedure, its success relies on the rapid convergence of the perturbation expansion. Several cases where this prerequisite is not met are known (for instance, due to spin-contamination, as explained previously). One interesting example, provided by Ma *et al* (62) concerns the energy of isomerization of the formaldehyde radical cation ($H_2CO^{+\cdot}$) to hydroxymethylene ($HCOH^{+\cdot}$) radical cation, where MP2, either restricted or unrestricted, fails even in reproducing the sign of the energy difference. The authors showed that this failure is related to the slow convergence of the perturbation series, specially for the $H_2CO^{+\cdot}$ species.

We have been working in the last years on radical cations derived from hydrogen-bonded complexes of aldehydes (63-66) and we were interested in this failure of MP2 theory described by Ma *et al* (62). We showed that there was no failure in the MP2 description of the complexes of formaldehyde with water (64), mainly because no $H_2CO^{+\cdot}$ moiety was present. This is because there is a proton transfer in the $H_2O.H_2CO^{+\cdot}$ cation radical, so that the equilibrium structure can be represented as $(H_3O)^+.HCO^{\cdot}$. Consequently, no MP2 failure was observed. These facts were confirmed by Barone and Adamo (28) who repeated some of our *ab initio* calculations (63). They showed also (24,28) that DFT at the B3LYP level is very accurate in the prediction of the isomerization energy of $H_2CO^{+\cdot}$ (27.6 kJ/mol *vs* an experimentally derived value of 25 kJ/mol). Also the activation energy, underestimated at the MP2 level, is in agreement with the most precise QCISD calculations performed in (28).

Therefore, we made some DFT calculations (67) on the species $XHCO^{+\cdot}$ comparing the results with conventional QCISD, G1 and G2 methods. The results are shown in Table 7. The main result obtained is that, at least for X=H, the B3LYP results are as good as the QCISD ones. QCISD optimizations were not possible

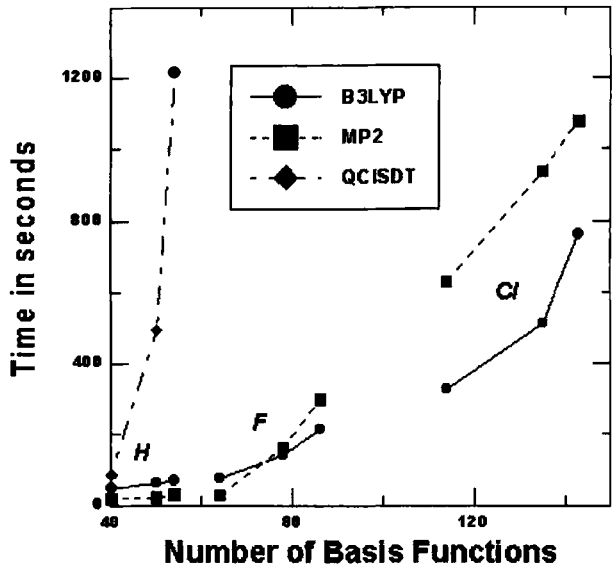

Figure 1: Time necessary for the energy of each geometry cycle, at the QCISD, MP2 and B3LYP level with progressively larger basis sets.

with our present resources for X=F and X=Cl and the results obtained with less acurate geometries are not so good. G2 alculations demonstrate that the B3LYP results are precise. It was also described in this paper how much faster the B3LYP calculations are with respect to QCISD (see Fig. 1) and that, for a certain number of functions, they are even faster than MP2 (notice that MP2 results are completely wrong in the three cases).

4.2 Transition states

As said in the Introduction, one of the pending problems of DFT methods are some transition states, particularly those of radical and specially those involving H atoms. In an effort to look for well-defined and well-undestood systems in which this failure can be quantified, we performed DFT calculations on the reaction Li + HF -> LiF + H (68). This reaction has been extensively studied experimentally(69-72) and theoretically (73-77). It exhibits a deep well (72) in the entrance channel, corresponding to a non-linear (73-77) LiFH complex, with an experimental stabilization energy of about 300 meV (29.0 kJ/mol) and enthalpy of about 317 meV (30.6 kJ/mol) (72). Theoretically, energies for this complex were calculated at 10.2 kJ/mol(73), 19.3 kJ/mol(74), 28.9 kJ/mol (75), 21.6 kJ/mol (76), and 28 kJ/mol (77) in several papers. The reaction proceeds via a highly non-linear

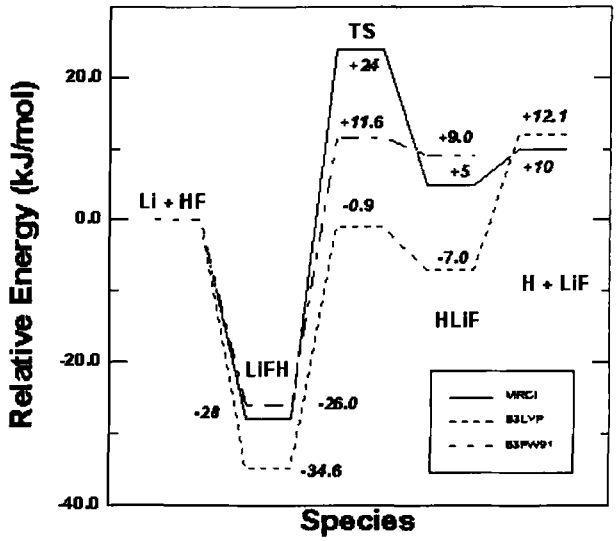

Figure 2: Relative energy of the species in the Li + HF reaction according to three different methods of calculation.

transition state (73-77) which has been calculated at 42 kJ/mol in the older CI calculation of Chen and Schaefer (74) or at 24 kJ/mol in the more recent MRDCI calculation of Aguado *et al* (77) (reduced to 8.5 kJ/mol when zero-point energies are taken into account). No experimental value of the energy of activation exists, but an estimation of the height of the barrier may be obtained from the experimental work of Lee *et al* (69). In fact, they observed products at a nominal collision energy as low as 2.2 kcal/mol (9.2 kJ/mol) which implies either a low barrier (as the calculations of Aguado *et al* (77) suggest) or that tunelling through a higher barrier is playing an important role in this system. The subject is even more complicated by the fact that in the opinion of some of the previous theoretical studies (Balint-Kurti and Yardley (73), Chen and Schaefer (74), Suárez et al (78)) the barrier located on the reaction surface is due to an avoided crossing between the surfaces corresponding to the ionic ($Li^+ + HF^-$) and covalent (Li + HF) structures.

Eventually, the reaction proceeds past the transition state to the products, LiF + H, which are enthalpically 4.6 ± 8 kJ/mol (69) below the reactants, a value to be compared with the recent theoretically calculated exoergicity(77) of about 9 kJ/mol for this reaction. A weak product complex HLiF has been pointed out by Chen and Schaefer (74) and calculated by Aguado *et al* (77) to lie at an energy of 5 kJ/mol below the separated H + LiF products.

We have performed B3LYP and B3PW91 calculations using the 6-311++G(3df,3pd) basis set, comparing the results with those of Aguado *et al* (77)

at the MRCI level. These data are displayed in Fig. 2. Here one can observe that both DFT methods underestimate by a large margin the height of the transition state. For all non-ACM methods this underestimation is even larger, in all cases studied the energy of the TS being below the energy of the reactants. The fact that B3PW91 corrects B3LYP by more than 12 kJ/mol shows how it is not irrelevant to change the correlation functional in the ACM methods. B3PW91 is still far from the value of the barrier obtained with MRCI methods, but shows encouraging improvement over B3LYP which has being up to now the ACM method of choice.

5. Conclusions

Several radical systems have been studied and it has been shown that ACM methods (either B3LYP or B3PW91) are a powerful tool for the prediction of the structure and reactivity of free radicals. Some problems still remain in the description of transition states of reactions of H-radicals, but it is still too soon to say whether this is a fatal drawback of the method or this can be corrected. At the same time, more experience is needed to know whether other, non-detected errors still exist within the realm of DFT.

6. Acknowledgments

This paper is dedicated to Prof. Geerd H. F. Diercksen on the ocassion of his 60th anniversary. The authors want to acknowledge the hospitality of Prof. Diercksen in his laboratory at Garching bei München during the course of many years. The authors want to thank also Prof. S. Suhai, DKFZ, Heidelberg, for valuable discussions concerning some of the topics in this paper. The research reviewed here has been supported by grants from the European Union, the International Bank for Development and Conicyt-Uruguay. One of the authors (ONV) thanks the Alexander von Humboldt-Stifftung for a fellowship stay in Germany, where part of the work reported here has been performed.

References

(1) (a) R. G. Parr, W. Yang, *Density Functional Theory of Atoms and Molecules*, Oxford University Press, New York, 1989.(b) R. M. Dreizler, E. K. U. Gross, *Density Functional Theory*, Springer-Verlag, Berlin, 1990. (c) N. C. Handy, Lecture Notes in Chemistry **64**, 91 (1994). (e) J.

Labanowski, J. Andzelm, Eds., *Density Functional Methods in Chemistry*, Springer-Verlag, Berlin, 1991.
(2) W. Kohn, L. J. Sham, Phys. Rev. A **140**, 1133, (1965).
(3) J. C. Slater, *Quantum Theory of Molecules and Solids*, McGraw-Hill, New York, 1974.
(4) S. H. Vosko, L. Wilk, M. Nusair, Can. J. Phys. **58**, 1200 (1980).
(5) (a) D. C. Langreth, M. Mehl, M. J. Phys. Rev. B **28**, 1809 (1983). (b) C. D. Hu, D. C. Langreth, Phys. Scr. **32**, 391 (1985).
(6) J. P. Perdew, Phys. Rev. Lett. **55**, 1665 (1985); **55**, 2370 (1985).
(7) J. P. Perdew, Y. Wang, Phys. Rev. B **33**, 8800 (1986); **40**, 3399 (1989)
(8) J. P. Perdew, Phys. Rev. B **33**, 8822 (1986); **34**, 7406 (1986).
(9) A. D. Becke, Phys. Rev. A **38**, 3098 (1988).
(10) C. Lee, W. Yang, R. G. Parr, Phys. Rev. B **37**, 785 (1988).
(11) L. C. Wilson, M. Levy, Phys. Rev. B **41**, 12930 (1990).
(12) J. P. Perdew, Physica B **172**, 1 (1991).
(13) J. P. Perdew, K. Burke, Int. J. Quantum Chem. **57**, 309 (1996).
(14) J. P. Perdew, J. A. Chevary, S. H. Vosko, K. A. Jackson, M. R. Pederson, D. J. Singh, C. Fiolhais, Phys. Rev. B **46**, 6671 (1992); **48**, 4978 (1993).
(15) (a) A. D. Becke, M. R. Roussel, Phys. Rev. A **39**, 3761 (1989). (b) R. Neumann, N. C. Handy, Chem. Phys. Lett. **246**, 381 (1995).
(16) A. D. Becke, J. Chem. Phys. **98**, 1372 (1993).
(17) A. D. Becke, J. Chem. Phys. **98**, 5648 (1993).
(18) R. H. Hertwig, W. Koch, J. Comput. Chem. **16**, 576 (1995).
(19) K. E. Edgecombe, A. D. Becke, Chem. Phys. Lett. **244**, 427 (1995).
(20) J. M. L. Martin, J. El-Yazal, J.-P. François, Mol. Phys. **86**, 1437 (1995).
(21) S. Kristyán, Chem. Phys. Lett. **247**, 101 (1995).
(22) B. J. Smith, L. Radom, Chem. Phys. Lett. **245**, 123 (1995).
(23) (a) L. A. Curtiss, K. Raghavachari, G. W. Trucks, J. A. Pople, J. Chem. Phys. **94**, 7221 (1991). (b) L. A. Curtiss, K. Raghavachari, J. A. Pople, J. Chem. Phys. **98**, 1293 (1993).
(24) V. Barone, Theor. Chim. Acta **91**, 113 (1995).
(25) M. Solà, J. Mestres, R. Carbó, M. Duran, J. Chem. Phys. **104**, 636 (1996).
(26) P. Hobza, J. Šponer, T. Reschel, J. Comput. Chem. **16**, 1315 (1995).
(27) B. I. Lundqvist, Y. Andersson, H. Shao, S. Chan, D. C. Langreth, Int. J. Quantum Chem. **56**, 247 (1995).
(28) V. Barone, C. Adamo, Chem. Phys. Lett. **224**, 432 (1994).
(29) B. S. Jursic, Z. Zdravkovski, Int. J. Quantum Chem. **56**, 115 (1995).
(30) B. S. Jursic, Chem. Phys. Lett. **244**, 263 (1995).
(31) V. Barone, L. Orlandini, C. Adamo, Int. J. Quantum Chem. **56**, 697 (1995).
(32) (a) J. Andzelm, J. Baker, A. Scheiner, M. Wrinn, Int. J. Quantum Chem. **56**, 733 (1995). (b) J. Baker, M. Muir, J. Andzelm, J. Chem. Phys. 102, 2063 (1995).
(33) J. Baker, J.Andzelm, M. Muir, P. R. Taylor, Chem. Phys. Lett. 237, **53** (1995).

(34) P. Nachtigall, K. D. Jordan, A. Smith, H. Jónsson, J. Chem. Phys. **104**, 148 (1996).
(35) J. A. Pople, M. Head-Gordon, K. Raghavachari, J. Chem. Phys. **87**, 5968 (1987).
(36) (a) B. G. Johnson, C. A. Gonzalez, P. M. W. Gill, J. A. Pople, Chem. Phys. Lett. **221**, 100 (1994). (b) S. Gronert, G. L. Merrill, S. R. Kass, J. Org. Chem. **60**, 488 (1995).
(37) (a) G. J. Laming, N. C. Handy, R. Amos, Mol. Phys. **80**, 1121 (1993). (b) J. Baker, A. Scheiner, J. Andzelm, Chem. Phys. Lett. **216**, 380 (1993). (c) L. A. Ericsson, O. L. Malkina, V. G. Malkin, D. Salahub, J. Chem. Phys. **100**, 5066 (1994).
(38) F. Jensen, Chem. Phys. Lett. **169**, 519 (1990).
(39) D. J. Tozer, N. C. Handy, R. D. Amos, J. A. Pople, R. H. Nobes, Y. Xie, H. F. Schaefer, III, Mol. Phys. **79**, 777 (1993).
(40) K. A. Peterson, J. Chem. Phys. **102**, 262 (1995).
(41) (a) T. H. Dunning, Jr., J. Chem. Phys. **90**, 1007 (1989). (b) R. A. Kendall, T. H. Dunning, Jr., R. J. Harrison, J. Chem. Phys. **96**, 6796 (1992). (c) D. E. Woon, T. H. Dunning, Jr., J. Chem. Phys. **98**, 1358 (1993).
(42) K. Irving, O. N. Ventura, to be published.
(43) M. Guélin, J. Cernicharo, C. Kahane, J. Gomez-Gonzalez, Astron. Astrophys. **157,** L17 (1986).
(44) A. Largo-Cabrerizo, J. R. Flores, Chem. Phys. Lett. **147**, 90 (1988).
(45) K. Kawaguchi, E. Kagi, T. Hirano, S. Takano, S. Saito, Atrophys. J. **406**, L39 (1993).
(46) C. W. Bauschlicher, Jr., S. R. Langhoff, H. Partridge, Chem. Phys. Lett. **115**, 124 (1985).
(47) K. Ishii, T. Hirano, U. Nagashima, B. Weis, K. Yamashita, Astrophys. J. **410**, L43 (1993); *ibid*, J. Mol. Struct. Theochem **305**, 117 (1994).
(48) (a) M. R. Nyden, G. A. Petersson, J. Chem. Phys. **75**, 1843 (1981). (b) G. A. Petersson, M. A. Al-Laham, J. Chem. Phys. **94**, 6081 (1991). (c) G. A. Petersson, T. Tensfeldt, J. A. Montgomery, J. Chem. Phys. **94**, 6091 (1991). (d) J. A. Montgomery, J. W. Ochterski, G. A. Petersson, J. Chem. Phys. **101**, 5900 (1994)
(49) O. N. Ventura, K. Irving, M. Kieninger, L. Sandoval, N. Aquino, A. Palma, The Molecular Modeling e-Conference (TMMeC), **1**, P128 (1996).
(50) J. S. Francisco, A. N. Goldstein, Z. Li, Y. Zhao and I. H. Williams, J. Phys. Chem. **94**, 4791 (1990).
(51) C. Yamada and E. Hirota, J. Chem. Phys. **80**, 4694 (1984).
(52) A. R. W. McKellar, J. B. Burkholder, A. Sinha and C. J. Howard, J. Mol. Spectrosc. **125**, 288 (1987).
(53) M. W. Chase, Jr., C. A. Davies, J. R. Downey, Jr., D. J. Frurip, R. A. McDonald, A. Syverud, *JANAF Thermochemical Tables*, 3rd Ed, J. Phys. Chem. Ref. Data, Supl. No. 1, Vol. 14 (1985).

(54) P. Pagsberg, E. Ratajczak, A. Sillesen, J. T. Jodkowski, Chem. Phys. Letters **141**, 88 (1987).
(55) J. L. Lyman, R. Holland, J. Phys. Chem. **92**, 7232 (1988).
(56) J. S. Francisco, Y. Zhao, W. A. Lester, Jr., I. H. Williams, J. Chem. Phys. **96**, 2861 (1992).
(57) Y. Zhao, J. S. Francisco, Chem. Phys. Letters **167**, 285 (1990).
(58) (a) K. Raghavachari, G. W. Trucks, Chem. Phys. Letters **162**, 511 (1989). (b) D. A. Dixon, J. Andzelm, G. Fitzgerald, E. Wimmer, J. Phys. Chem. **95**, 9197 (1991). (c) R. D. Amos, C. W. Murray, N. C. Handy, Chem. Phys. Letters **202**, 489 (1993).
(59) CODATA Task Group on Chemical Kinetics, D. L. Baulch, R. A. Cox, P. J. Crutxen, R. F. Hampson, Jr., J. A. Kerr, J. Troe, R. T. Watson, J. Phys. Chem. Ref. Data **13**, 1259 (1984).
(60) O. N. Ventura, M. Kieninger, Chem. Phys. Lett. **245**, 488 (1995).
(61) (a) C. Møller, M. S. Plesset, Phys. Rev. **46**, 618 (1934). (b) R. Krishnan, M. J. Frisch, J. A. Pople, J. Chem. Phys. **72**, 4244 (1980).
(62) N. L. Ma, B. J. Smith, L. Radom, Chem. Phys. Lett. **193**, 386 (1992).
(63) E. L. Coitiño, A. Lledos, R. Serra, J. Bertran, O. N. Ventura, J. Am. Chem. Soc. **115**, 9121 (1993).
(64) E. L. Coitiño, O. N. Ventura, Chem. Phys. Letters **202**, 429 (1993).
(65) A. Pereira, E. L. Coitiño, O. N. Ventura, J. Mol. Struct. Theochem **314**, 31 (1994).
(66) E. L. Coitiño, A. Pereira, O. N. Ventura, J. Chem. Phys. **102**, 2833 (1995).
(67) O. N. Ventura, M. Kieninger, E. L. Coitiño, J. Comput. Chem., in press.
(68) O. N. Ventura, Mol. Phys., in press.
(69) C. H. Becker, P. Casavechia, P. W. Tiedermann, J. J. Valentini, Y. T. Lee, J. Chem. Phys. **73**, 2833 (1980).
(70) Y. T. Lee, Ber. Bunsenges. Physik. Chem.,**86**, 378 (1982).
(71) H. J. Loesch, E. Stenzel, B. Wüstenbecker, J. Chem. Phys., **95**, 3841(1991).
(72) H. J. Loesch, R. Stienkemeier, J. Chem. Phys., **98**, 9570; **99**, 9598 (1993).
(73) G. G. Balint-Kurti, R. N. Yardley, Faraday Discuss. Chem. Soc., **62**, 77 (1977).
(74) M. M. L. Chen, H. F. Schaefer III, J. Chem. Phys., **72**, 4376 (1980).
(75) P. Palmieri, A. Laganà, J. Chem. Phys., **91**, 7303 (1989).
(76) B. Berning, H.-J. Werner, ref. 10 in the second paper of ref. (72).
(77) A. Aguado, C. Suárez, M. Paniagua, Chem. Phys., **201**, 107 (1995) and references 6-25 therein.
(78) C. Suárez, A. Aguado, M. Paniagua, Chem. Phys., **178**, 357 (1993).

Guesses - Hunches - Formulae - Discoveries

B. G. Wybourne

Instytut Fizyki, Uniwersytet Mikołaja Kopernika
ul. Grudziądzka 5/7, 87-100 Toruń, Poland

Abstract

A number of examples of informed guesses and hunches leading to discoveries and unanticipated theorems are given.

ADVANCES IN QUANTUM CHEMISTRY, VOLUME 28

0065-3276/97 $25.00

1. Introduction

One of the most remarkable discoveries in all of atomic physics came as the result of a guess followed by a hunch that the guess was right and the formula highly suggestive but only much later was the discovery confirmed. I refer, of course, to Balmer's incredible guess that the wavelengths of the spectral lines of the hydrogen atom could be represented by simple formula in terms of integers. Balmer's guess was pure numerology based upon knowing the wavelengths of just three lines, his hunch was that his result would extend to other spectral lines of hydrogen. Balmer was unable to give any rational basis to his hunch but his discovery was to lead to a new age in atomic physics, in the hands of Niels Bohr. Few have made such momentous and far reaching discoveries and yet the process of discovery often involves guesses and hunches in a way inconsistent with most philosophical discussions of the so-called scientific method. Herein I propose to give a few examples of of guesses based upon very limited data that have led to unanticipated theorems of relevance to problems in chemistry and physics.

2. Spinors and the rotation groups

The rotation groups $SO(n)$ play an important role in many areas of chemistry and physics. The full rotation group $O(n)$ possess a basic spin representation Δ of degree $2^{[\frac{n}{2}]}$ which is irreducible under $O(n) \rightarrow SO(n)$ if n is *odd* or reducible into a pair of conjugate irreps $\Delta_{\pm}$. In 1935 Brauer and Weyl(1) gave a complete resolution of the Kronecker square of the basic spinor irreps of $SO(n)$ into their symmetric and antisymmetric components. Further results were obtained by Littlewood(2)–(4) by exploiting known automorphisms and isomorphisms for the $n = 3 \ldots 8$ cases but he noted(4) "The construction of the concomitants of degree higher than 2 in 10 or more variables would appear to present a formidable problem". Nevertheless, in 1981 a complete solution for the resolution of the third powers was obtained by King, Luan Dehuai and Wybourne(5) following upon an observation by the author. For the even rotation groups $SO(2\nu)$ one uses difference characters such that

$$\Delta'' = \Delta_+ - \Delta_-$$

The problem was then to resolve the Kronecker cube of Δ''. One had the special cases for $\Delta'' \otimes \{21\}$

$$\begin{array}{ll} SO(4) & -\Delta''([1] - [0]) \\ SO(6) & -\Delta''([1^2] - [1]) \\ SO(8) & -\Delta''([1^3] - [1^2] - [0]) \end{array}$$

$$SO(10) \qquad -\Delta''([1^4]-[1^3]-[1]+[0])$$

¿From this limited data could one guess the general result? The first clue was my observation that the dimensions of the terms enclosed in curved brackets was in each case $3^{\nu-1}$. The second guess was to note the combinatorial identity

$$3^{\nu-1} = \sum_x \left\{ \binom{2\nu}{\nu-1-6x} - \binom{2\nu}{\nu-2-6x} - \binom{2\nu}{\nu-4-6x} + \binom{2\nu}{\nu-5-6x} \right\}$$

which is consistent with the general result

$$\Delta'' \otimes \{21\} = \Delta'' \sum_x (-[1^{\nu-1-6x}] + [1^{\nu-2-6x}] + [1^{\nu-4-6x}] - [1^{\nu-5-6x}])$$

This result together with some similar results yielded the final solution.

3. Reduced notation and the symmetric group

The symmetric group $S(n)$ is of fundamental importance in quantum chemistry as well in nuclear models and symplectic models of mesoscopic systems. One wishes to discuss the properties of the symmetric group for general n and concentrate on stable results that are essentially $n-$independent. Here the reduced notation(6)–(9) proves to be very useful. The tensor irreps $\{\lambda\}$ of $S(n)$ are labelled by ordered partitions(λ) of integers where $\lambda \vdash n$. In reduced notation the label $\{\lambda_1, \lambda_2, \ldots, \lambda_p\}$ for $S(n)$ is replaced by $\langle \lambda_2, \ldots, \lambda_p \rangle$. Kronecker products can then be fully developed in a $n-$independent manner and readily programmed. Thus one finds, for example, the terms arising in the reduced Kronecker product $\langle 21 \rangle * \langle 2^2 \rangle$ are

$$\begin{aligned} &<51> + <5> + <43> + <421> + 3<42> + 3<41^2> + 5<41> + 3<4> \\ &+ <3^21> + 2<3^2> + <32^2> + <321^2> + 6<321> + 7<32> + 3<31^3> + 8<31^2> \\ &+ 8<31> + 3<3> + <2^31> + 2<2^3> + 3<2^21^2> + 7<2^21> + 5<2^2> + <21^4> \\ &+ 5<21^3> + 8<21^2> + 6<21> + 2<2> + <1^5> + 3<1^4> + 3<1^3> + 2<1^2> \\ &+ <1> \end{aligned}$$

Looking at the above list one is immediately struck by the observation that the list is self-associated. That is every partition (λ) in the list either has a conjugate partner $(\tilde{\lambda})$ where the rows and columns of the Young frame of the partition (λ) have been interchanged or the partition (λ) is self-conjugate. Some Kronecker products are self-associated while others are not. Is there

a general theorem that would tell us immediately which products are self-associated? We note that the partition (21) is an example of a *staircase partition* (staircase partitions have the general form $(a, a-1, a-2, \ldots, 1)$) while the partition (2^2) is self-conjugate. These observations led to the general theorem(10)

Theorem For H defined by $\langle\lambda\rangle * \langle\nu\rangle = \langle H\rangle$ to be self-associated, it is necessary and sufficient that one of the partitions be a staircase partition and the other be at least self-conjugate.

One may also resolve symmetrised powers of irreps of $S(n)$ in reduced notaion. For example, one finds that the terms in $\langle 21\rangle \otimes \{21\}$ are

$$
\begin{array}{lllllll}
<71> & +2<7> & +<621> & +5<62> & +5<61^2> & +17<61> & +14<6> \\
+<54> & +2<531> & +9<53> & +<52^2> & +2<521^2> & +20<521> & +45<52> \\
+<51^4> & +10<51^3> & +47<51^2> & +81<51> & +45<5> & +<4^21> & +5<4^2> \\
+3<432> & +3<431^2> & +25<431> & +47<43> & +3<42^21> & +20<42^2> & +2<421^3> \\
+30<421^2> & +118<421> & +149<42> & +10<41^4> & +64<41^3> & +163<41^2> & +185<41> \\
+78<4> & +3<3^221> & +16<3^22> & +<3^21^3> & +20<3^21^2> & +73<3^21> & +82<3^2> \\
+<32^3> & +2<32^21^2> & +25<32^21> & +73<32^2> & +<321^4> & +20<321^3> & +118<321^2> \\
+270<321> & +235<32> & +5<31^5> & +47<31^4> & +163<31^3> & +280<31^2> & +240<31> \\
+83<3> & +<2^41> & +5<2^4> & +9<2^31^2> & +47<2^31> & +82<2^3> & +5<2^21^4> \\
+45<2^21^3> & +149<2^21^2> & +235<2^21> & +162<2^2> & +<21^6> & +17<21^5> & +81<21^4> \\
+185<21^3> & +240<21^2> & +173<21> & +55<2> & +2<1^7> & +14<1^6> & +45<1^5> \\
+78<1^4> & +83<1^3> & +55<1^2> & +19<1> & +2<0> & &
\end{array}
$$

Again one observes that the list is self-associated and again one is led to a new and unanticipated theorem(10)

Theorem If $\langle\lambda\rangle \otimes \{\mu\} = \langle H\rangle$, where (λ) and (μ) are staircase partitions, then H is self-associated.

4. Kronecker products for two-row shapes

The Pauli exclusion principle limits interest in quantum chemistry to just those irreps of $S(n)$ involving partitions whose Young frames having at most two rows. Thus in forming Kronecker products only irreps having at most two rows can yield physical states. In the case of reduced Kronecker products interest is restricted to one-part partitions. Consider the case of $\langle 5\rangle * \langle 4\rangle$ whose one-part content is

$$
<9> \quad +<8> \quad +2<7> \quad +2<6> \quad +3<5> \quad +2<4> \quad +2<3> \quad +<2> \quad +<1>
$$

The first thing one notices is that the multiplicity distribution is unimodal.

Is this a general feature? Indeed one finds(10) that if we write

$$\langle k\rangle * \langle \ell\rangle = \sum_{\lambda} c^{\langle m\rangle}_{\langle k\rangle\langle \ell\rangle} \langle \lambda\rangle$$

then the coefficients $c^{\langle m\rangle}_{\langle k\rangle\langle \ell\rangle}$ are given by

$$\begin{aligned} c^{\langle m\rangle}_{\langle k\rangle\langle \ell\rangle} &= \frac{1}{2}(\ell - k + m + 2) \quad \text{for} \quad k > m \\ c^{\langle m\rangle}_{\langle k\rangle\langle \ell\rangle} &= \frac{1}{2}(k + \ell - m + 2) \quad \text{for} \quad m \geq k \end{aligned}$$

and the coefficients exhibit the symmetry

$$c^{\langle m\rangle}_{\langle k\rangle\langle \ell\rangle} = c^{\langle 2k-m\rangle}_{\langle k\rangle\langle \ell\rangle}$$

The above results give a complete description of the symmetric group Kronecker products needed in quantum chemistry. Results for specific values of n are found from the reduced results by simply prefixing the reduced labels $\langle k\rangle$, $\langle \ell\rangle$, $\langle m\rangle$ to give $\{n-k,k\}$, $\{n-\ell,\ell\}$ and $\{n-m,m\}$ respectively and remembering that for an irrep $\{p,q\}$ is non-standard if $p < q$ and must be made standard by use of the modification rule(4)

$$\{p,q\} \equiv -\{q-1,p+1\} \qquad \text{if} \quad q > p$$

Thus for $S(18)$ we obtain for $\{13\ ,5\} * \{14\ ,4\}$

$\{17\ 1\} + \{16\ 2\} + 2\{15\ 3\} + 2\{14\ 4\} + 3\{13\ 5\} + 2\{12\ 6\} + 2\{11\ 7\} + \{10\ 8\} + \{9^2\}$

whereas for $S(12)$ we obtain for $\{7,5\} * \{8,4\}$ just

$\{11\ 1\} + \{10\ 2\} + 2\{93\} + \{84\} + 2\{75\}$

5. n–NonInteracting Particles in a Harmonic Oscillator Potential

As a last topic I would like to briefly consider some problems that arise when one wishes to describe the states of n–noninteracting spin $\frac{1}{2}$ particles in an isotropic d–dimensional harmonic oscillator potential, a common starting point in a variety of nuclear and mesoscopic models(13),(14). For a single particle there are two infinite sets of states, those of even parity and those of odd parity(15). These two sets of states span a single infinite dimensional irrep Δ of the metapletic group $Mp(2d)$ which is the covering group of the

non-compact symplectic group $Sp(2d,R)$. Under $Mp(2n) \rightarrow Sp(2d,R)$ one has(11),(12)

$$\Delta \rightarrow \langle \frac{1}{2}(0) \rangle + \langle \frac{1}{2}(1) \rangle$$

The group $Sp(2d,R)$ has a maximal compact subgroup $U(d)$ such that under $Sp(2d,R) \rightarrow U(d)$ we have

$$\begin{aligned} \langle \frac{1}{2}(0) \rangle &\rightarrow \varepsilon^{\frac{1}{2}} \cdot M_+ \\ \langle \frac{1}{2}(1) \rangle &\rightarrow \varepsilon^{\frac{1}{2}} \cdot M_- \end{aligned}$$

where M_+ and M_- are effectively the even and odd terms in the infinite $S-$function series(4),(5),(16),(17)

$$M = \sum_{m=0}^{\infty} \{m\}$$

A number of problems arise in studying the properties of infinite dimensional irreps of $Sp(2d,R)$ in order to make practical applications. These include evaluating Kronecker products and resolving symmetrised powers of the basic irreps $\langle \frac{1}{2}(0) \rangle$ and $\langle \frac{1}{2}(1) \rangle$. The Kronecker products have been discussed elsewhere(11)–(13). The resolution of the symmetrised powers of the basic irreps is a particularly difficult problem and until now no general results have been known. The symmetrised squares of the basic irreps of $Sp(2d,R)$ have recently been studied in some detail for various values of d and up to terms of weight 20. This led me to guess that in general

$$\begin{aligned} < \frac{1}{2}; (0) > \otimes \{2\} &= \sum_{i=0}^{\infty} < 1; (0+4i) > \\ < \frac{1}{2}; (0) > \otimes \{1^2\} &= \sum_{i=0}^{\infty} < 1; (2+4i) > \\ < \frac{1}{2}; (1) > \otimes \{2\} &= \sum_{i=0}^{\infty} < 1; (2+4i) > \\ < \frac{1}{2}; (1) > \otimes \{1^2\} &= < 1; (1^2) > + \sum_{i=0}^{\infty} < 1; (4+4i) > \end{aligned}$$

holds for all $Sp(2d,R)$ with $d \geq 2$. For $d = 1$ the irrep $< 1; (1^2) >$ in the last equation must be deleted. But this would imply a hitherto unknown identity for symmetrised powers of the infinite $S-$function series, namely,

$$M_+ \otimes \{1^2\} = M_- \otimes \{2\}$$

which was readily proved. The equality

$$< \frac{1}{2}; (0) > \otimes \{1^2\} \equiv < \frac{1}{2}; (1) > \otimes \{2\}$$

has a surprising, and seemingly unnoticed, feature. The left-hand-side describes the $S = 1$ states formed by placing two of the fermions in even parity orbitals while the right-hand-side describes the $S = 0$ states formed by placing two particles in odd parity orbitals. This implies there is a one-to-one mapping between the orbital states for these two sets of states. Indeed, if one enumerates the two-particle $LS-$states for an isotropic three-dimensional isotropic harmonic oscillator potential formed by having one particle in the $n = 0$ $s-$orbital and a second in the $n = 2$ $s-$ or $d-$orbital one finds the spectroscopic terms ${}^{3.1}SD$ while placing both particles in the $n = 1$ $p-$orbital yields the spectroscopic terms ${}^3P$ and ${}^1SD$. Clearly the map ${}^3(SD) \rightarrow {}^1(SD)$ exists as predicted.

6. Concluding remarks

I have tried in the preceding remarks to show that sometimes guesses and hunches can sometimes lead to unexpected discoveries. Patterns can sometimes be discerned if we exercise our human imagination. Of course ultimately we must move to demonstrate the validity of our guesses and hunches.

7. Acknowledgements

It has been a real pleasure to be able to participate in celebrating Geerd Diercksen's 60th. Geerd has given leadership in both science and in the organisation of science from which many of us have benefitted. I have also appreciated Geerd for his sense of humour and basic humanity. I apologise for the lack of keywords in the title of this paper.

This work has been partially funded by a grant from the Polish KBN. The calculations used were derived from data produced by the programme SCHUR(18).

References

(1) Brauer, R., Weyl, H. : *Am. J. Math.* ***57***, 425 (1935).

(2) Littlewood, D. E.:*Proc. Lond. Math. Soc.* ***49***, 307 (1947).

(3) Littlewood, D. E.:*Proc. Lond. Math. Soc.* ***50***, 349 (1948).

(4) Littlewood, D. E.:*The theory of group characters* 2nd edn Oxford: Clarendon (1950).

(5) King, R. C., Luan Dehuai, Wybourne, B. G.: *J. Phys. A: Math. Gen.* ***14***, 2509 (1981).

(6) Murnaghan, F. D.:*Am. J. Math.* ***60***, 761 (1938).

(7) Littlewood, D. E.:*Can. J. Math.* ***10***, 1 (1958).

(8) Littlewood, D. E.:*Can. J. Math.* ***10***, 17 (1958).

(9) Butler, P. H., King, R. C.: *J. Math. Phys.* ***14***, 1176 (1973).

(10) Scharf, T., Thibon, J-Y., Wybourne, B. G.:*J. Phys. A: Math. Gen.* ***26***, 7461 (1993).

(11) Rowe, D. J., Wybourne, B. G., Butler, P. H.: *J. Phys. A: Math. Gen.* ***18***, 939-53 (1985).

(12) King, R. C. , Wybourne, B. G. : *J. Phys. A: Math. Gen.* ***18***, 3113-39 (1985).

(13) Grudziński, K. , Wybourne, B. G. : in *Symmetry and Structural Properties of Condensed Matter*, Ed. T. Lulek, W. Florek & S. Wałcerz, World Scientific, Singapore pp 469-83 (1995).

(14) Wybourne, B. G. : *Rept. Math. Phys.* ***34***, 9-16 (1994).

(15) Wybourne, B. G. : *Classical groups for physicists* New York: Wiley Interscience (1974).

(16) Wybourne, B. G. : *Symmetry principles and atomic spectroscopy* New York: Wiley Interscience (1970).

(17) Wybourne, B. G. : in *Symmetry and Structural Properties of Condensed Matter*, Ed. W. Florek, D. Lipiński, & T. Lulek, World Scientific, Singapore pp 79-100 (1993).

(18) Details can be found at http://www.phys.uni.torun.pl/~bgw or http://scm.vnet.net/Christensen.html

Applying Artificial Intelligence in Physical Chemistry

F.J. Smith[1], M. Sullivan, J. Collis and S. Loughlin

Department of Computer Science

The Queen's University

Belfast BT7 1NN Northern Ireland

Abstract

Databases of scientific data, such as tables of vapour pressures of gases or of intermolecular forces, can be used for the storage and retrieval of data in Physical Chemistry. Knowledge bases can be used to store not only scientific data but also the laws relating to physical sciences. However, if such a knowledge base is coupled with an Artificial Intelligence system, together they are able to solve quantitative problems directly by linking together code, formulas and data in the correct sequence to obtain solutions. Such a system has been proposed by Diercksen for Quantitative Chemistry. A pilot system, called QPS, has been developed at the Queen's University of Belfast and the system has demonstrated it's capability to solve many simple problems in the physical sciences.

[1] FJ.Smith@qub.ac.uk

ADVANCES IN QUANTUM CHEMISTRY, VOLUME 28

0065-3276/97 $25.00

1. Introduction

The application of the principles of Artificial Intelligence has been proposed by Diercksen to build an Expert System in Quantitative Chemistry(1). One of Diercksen's primary goals for such a system is to :

"[Provide] the novice user with a program, which can give him realistic results for a property of interest with an evaluation of their accuracy and significance."

This paper describes the design of a pilot system which demonstrates the feasibility of this concept; data items are numerical data and computations are achieved by the evaluation of relatively simple equations. However the principle concepts of this pilot system are the same as those needed in Diercksen's proposal, with wave functions as data and programs or modules replacing equations. The background to this system is now explained.

When data items are obtained from a conventional database system in science, whether through a query language or through a data manipulation language, the information is usually processed by other software in order to perform problem solving. In some databases the data items are factual rather than numerical, and the software is based on logical expert system techniques (2, 3). However, in physical chemistry the data are usually numerical in nature (4) and the software used to manipulate the data is frequently written in FORTRAN. In a very simple example, a chemist might want the mass, M, of the contents of a cylindrical beaker of known diameter, d, filled to a depth, l, with ethyl alcohol. The program would find the density, ρ, of ethyl alcohol from the database and calculate the weight from the two equations.

$$d = 2r \qquad M = \pi \rho r^2 l$$

Lists of formulas are found in almost any text book in the physical sciences. The symbols within these equations refer to scientific quantities, some of which are data items stored in a database. In this project we put both formulas and data into a single knowledge base. This type of knowledge is sometimes referred to as basic knowledge (5) or quantitative knowledge (6). The resulting system has all of the characteristics of a scientific database, but in addition it can carry out manipulations of the data to solve problems by automatically searching in the knowledge base for the sequence of formulas needed to solve a problem. These formulas must then be executed in the correct order and should retrieve data from the knowl-

edge base when necessary.

Before describing this process further, we first analyse the nature of quantitative knowledge and then describe how it can be represented in an object-oriented framework within our pilot system, called QPS (Quantitative Problem Solver).

2. Nature of Knowledge

We define quantitative scientific knowledge as the combination of numerical data and formulas. A quantity can be a geometrical quantity like area or volume, or a physical quantity like mass or viscosity. A geometrical quantity is a variable which depends on the geometrical shape under consideration. Physical quantities can be categorised into constant properties and variables. Physical constants are the universal constants of nature, such as Boltzmann's constant ($k = 1.380658\ 10^{-23} JK^{-1}$). Physical properties are quantities which hold different values for different substances (or elements) in different states, for example, the Critical Volume ($m^3 \cdot mol^{-1}$) $72.5\ 10^{-6}$ of Ammonia. The physical constants and physical properties are held in a database. Physical variables (sometimes called state variables) are independent variables which describe the state of a physical system, such as temperature (T) or pressure (P). The variables (including geometric values) are either specified by a user or computed by the system.

Quantities are normally identified by symbols. In certain cases a single symbol may be used to represent two or more different quantities; for example the symbol ρ is used to represent density or resistivity. QPS resolves these ambiguities by analysing the units with which the quantity is specified.

A formula describes the relationship between quantities and is expressed in the form of a mathematical equation. It represents a physical law describing a phenomenon or fact. An example of this is Boyle's Law;

$$PV = nRT$$

where P, V, and T are the pressure, volume and temperature of a gas and R is a constant. Some relatively simple sets of sample data and formulas are shown in Tables 1 and 2.

Table 1: Some sample data on properties of gases

Gas	*Critical Temp (K)*	*Critical Pressure (Pa)*	*Critical Density (kg*
Helium(4)	5.3	$2.29\ 10^5$	69.3
Helium(3)	3.34	$1.17\ 10^5$	41.3
Hydrogen	33.3	$13.0\ 10^5$	31.0
Deuterium	38.4	$16.6\ 10^5$	66.3
Nitrogen	126.2	$33.9\ 10^5$	311
Oxygen	154.8	$50.8\ 10^5$	410
Water	647.4	$221.2\ 10^5$	320

Table 2: Some simple formulas from the QPS knowledge base for Molecular Physics

$p = \frac{1}{3}mn\bar{c}^2$	$\rho = mn$
$\frac{1}{2}m\bar{c}^2 = \frac{3}{2}kT$	$p = nkT$
$c_p = c_v = \frac{k}{m}$	$\gamma = \frac{c_p}{c_v}$
$\gamma = 1 + \frac{2}{s}$	$\frac{1}{l} = 4\sqrt{2}\pi r^2 n$
$\eta = \frac{1}{2}a\rho l\bar{c}$	$\lambda = \frac{1}{2}bpl\bar{c}c_v$

3. Related Work

Although many software tools have been written to perform scientific computations, almost all have required their creators to encode the solutions to the problems. An alternative approach is for the software to use Artificial Intelligence techniques to autonomously seek a solution without human intervention. Early examples include MECHO by Bundy et al (3) and ISSAC by Novak (7). MECHO was developed to solve problems in Mechanics. In ISSAC formulas describing the relationship between objects in a problem were represented as procedures attached to a "Canonical Object Frame". There were also several systems developed in the area of Artificial Intelligence for solving problems in Geometry (e.g. Welham (8)). Though these systems were powerful in exploiting the domain knowledge and facilitate specification of the problem in natural language, their usage was restricted to highly specific domains.

Recently Tyugu et al (9) developed a system called PRIZ for general problem solving. Tyugu suggested the use of "Computational Models" which are special kinds of semantic networks for representing quantities in Mathematics and Physics and formulas relating these quantities. In Belfast a system called "Belfast Scientific Database System" was developed for storage of a wide range of data on science and technology (10). A special feature of this system was the storage of formulas as functions and subroutines. A similar system using the relational data model was developed by Bandyopadhyoy et al (11, 12) for storage and manipulation of structured data and algebraic formulas. All these systems facilitate storage of both data and formulas. This project is a new attempt to develop the above ideas further, in an object-oriented environment which provides a uniform paradigm to represent quantities, formulas, units and geometry which was lacking in our earlier work (10, 12).

4. Object Oriented Knowledge Representation

A Class Hierarchy diagram showing the relationship between the various entities in the object-oriented knowledge base is shown in Figure 1. Each entity is implemented as a class in C++. For example the object Quantity represents the attributes common to all scientific quantities. Each instance of a class represents a real-world object, for example Force is an instance of Quantity and Newton is an instance of the class Unit.

Inheritance is used to allow classes to inherit data and methods from a more general class. For example classes Physical Property and Physical

Constant share common attributes like dimensions, but differ in the type of data that needs to be stored by each instance.

In addition, the classes Formula and Geometry are described in terms of other system objects; Formulas are composed of several Quantity instances. Geometries are represented by a set of Geometrical Quantity instances, which define the shape, and a set of Formula instances which relate the Geometrical Quantities. The Geometry model is a hierarchical one which, through the use of inheritance, is capable of describing three dimensional structures in terms of their cross section and the extra dimension of depth. Consequently there is almost no redundant data stored in the knowledge base.[2]

The QPS system itself has also been constructed in an hierarchical fashion. The lowest level being the definitions and methods of the primitive data structures used universally within the system, for example *list* and *set*. Also at this level are the objects that implement the system's datatypes, currently real numbers, intervals and triangular fuzzy numbers (13). The next level defines the physical schema, using a filing system based on B-Trees for efficiency.

A layer of abstraction above the physical schema is the logical or data model, this schema defines the classes representing the scientific data. These classes are encapsulated into an object oriented knowledge base by the layer above, this binds the methods which index and search the knowledge base with the data files. A level devoted to the storage of the complex system objects is necessary because the physical schema is designed only for the manipulation of the most primitive classes.

The objects defined in the level above the Knowledge Base exist to perform the problem solving process. Amongst them is an object which co-ordinates the systematic search for a solution which possesses several heuristic methods and an object to evaluate equations arithmetically. There is also an object to intelligently translate equations and quantities from the symbolic format an engineer or scientist employs into the internal format used by QPS.

All the functions provided by the QPS system entities are encapsulated inside an Interface, whose methods are invoked from the Graphical User Interface. One of the major strengths of this system is that the GUI is completely independent of the underlying implementation.

[2] See Figure 1 for the Class Hierarchy

5. Manipulation of Data

The problems we aim to solve are common problems for physical chemists, the computation of the value of a goal quantity by applying formulas. This is simple when there is a single formula to apply and the values of all other quantities in the formula are known, i.e. either specified by the user or available in the knowledge base. The process becomes complex when more than one formula is applicable and when the values of some of the quantities in the formulas are unknown. Unknown quantity values may be computed from other formulas. Then the formulas should be used in a correct sequence.

We use an Artificial Intelligence technique called the Problem Decomposition Strategy (14, 15) to tackle this problem. We divide the problem of computing a quantity into a number of sub-problems, each involving the computation of a formula with several sub-quantities. When more than one formula is applicable, they are tried one by one. The entire problem space can be represented as an AND/OR tree, and a Depth-first Recursive Search is employed to traverse the tree. The leaf nodes represent quantities whose values are known. The search terminates at the leaf nodes and returns the value to the level above. When a dead-end is reached, the system progressively backtracks to the levels above in an attempt to select another formula. If the complete search space is exhausted, the system reports that the problem is unsolvable and prompts the user for more information.

6. Example of AI Technique

The system's search strategy is illustrated below with a simple problem involving the kinetic theory of gases. Problem solving by QPS is a three stage process, first the problem is specified, then the inference engine searches the stored knowledge set for a solution, and finally the value of the answer is evaluated. The latter two stages are automatic and require no intervention by the user, whilst problem specification entails describing the initial problem state to the system. The system's interface has been designed to allow scientifically literate users to enter problem parameters in terms of standard scientific symbols and units.

The handling of uncertainty is an important aspect of the QPS system. All scientists accept that values are never discrete but have a degree of

error. Consequently our system allows the user to specify the estimated or known errors for each quantity. If a quantity is entered without an error, for example 1.2 units, the system will assume an error of 50% of the least significant figure. This allows the user to keep a crisp modal value in mind, whilst the underlying system uses fuzzy logic to store a measure of the inherent uncertainty.

Example :

A cylinder has been measured using a millimeter graduated ruler, and found to be 3 cm in diameter and 10 cm in length. The cylinder has been filled with helium at temperature of 293 K. If the gas has a pressure of 2 10^5 Pa, what is the mass of the gas?

This problem is typed into the system in the following natural format :

Geometry : Cylinder
Material : Helium
$d = 3$ cm
$l = 10$ cm
$P = 2\ 10^5$ Pa
$T = 293$ K

The QPS system solves this problem using the strategy shown by the search tree in Figure 2. Answers are produced by the QPS system in LaTeXformat, and the solution report for the above example is shown in Figure 3.

The solution shows that an AI system can be used to solve simple problems in Chemistry. Other examples using QPS in stress engineering have shown that problems of considerable complexity can be solved by this method. We have found that scaling up the size of the knowledge base does not present a problem.

7. Application to Molecular Computations

The example in section 6 is a very simple, almost trivial example of the application of AI techniques to solve a problem using formulas. However, the same process (without change) could be used on problems of much greater complexity.

An example would be to enhance the OPENMOL system for molecular

computations as proposed by Diercksen(1). OPENMOL consists of a number of abstract data types, equivalent to objects in our QPS system, which can be manipulated along with data and wave functions to compute different molecular properties. These abstract types are pieces of code which calculate values of variables from a set of formulas. Being objects, these abstract data types could replace the objects representing formulas in QPS without any change to the logic of the system.

In addition, the object-oriented knowledge base of QPS would be able to store atomic or molecular wave functions as data objects and manipulate these using the code objects of the OPENMOL system. This was already envisaged by Diercksen in the OPENMOL system and now the design of QPS provides a mechanism to enable the AI aspects of OPENMOL to be implemented.

Acknowledgements

Thanks are due to Short Brothers Plc, and the Department of Education, N. Ireland who helped support this research.

References

(1) H. F. Diercksen, G. Hall, Intelligent Software: The OpenMol Program, Computers in Physics pp 215-222, 1993

(2) J. Larkin , J. McDermott , D. P. Simon and H. A. Simon Expert and Novice Performance in Solving Physics Problems, Science 208, 20, pp 1335-1342, 1980

(3) A. Bundy, Solving Mechanics Problems Using Meta-Level Interface. Expert Systems in Micro Electronic Age, Ed. D Michie Edinburgh University Press, Edinburgh, Scotland, pp50-64, 1979

(4) J. R. Rumble, and F. J. Smith, Database Systems in Science and Engineering. Adam Hilger, Bristol, United Kingdom, pp 120-121, 1988.

(5) E. Tyugu, Knowledge Based Programming, Addison Wesley, Workinghom, United Kingdom, pp 120-121, 1988

(6) F. J. Smith, and M. V. Krishnamurthy, Integration of Scientific Data and Formulas in an Object-Oriented Knowledge Based System. Knowledge Based Systems, Journal 7, pp 135-141, 1994.

(7) G.S. Novak, Representation of Knowledge in a Program for Solving Physics Problems. Proc. of 5th International Joint Conference on Artificial Intelligence, pp 286-291, 1977.

(8) B. Welham, Geometry Problem Solving Technical Report, Department of Artificial Intelligence, University of Edinburgh, Scotland, 1977

(9) G. Mints, and E. Tyugu, The Programming System PRIZ. Journal of Symbolic Computation 5, pp 286-291, 1988

(10) F. J. Smith, and J. G. Hughes, The Belfast Scientific Database System. The Role of Data in Scientific Progress Ed. PS Glaeser North Holland, Amsterdam, pp 435-437, 1985

(11) S. Bandyopadhyay, and J. S. Devitt, A Symbolic Information Management System. Journal of Symbolic Computation Vol 4, pp397-408, 1987

(12) S. Bandyopadhyay, J. G. Hughes, F. J.Smith, and K. Sen, A Generalised Scientific Information System. Comp Phys Comm 33, pp 49-53, 1994.

(13) A. Kaufmann, M. M. Gupta, Introduction to Fuzzy Arithmetic : Theory and Applications, Van Nostrand Rentold, New York, 1991

(14) J. N. Nilsson, Principles of Artificial Intelligence. Springer International , Berlin, Germany, Chapter 3, 1980.

(15) E. Rich, K. S. Knight, Artificial Intelligence, 2nd Ed. McGraw Hill, New York, USA, Chapter 3, 1991

Artificial Intelligence Support for Computational Chemistry

Włodzisław Duch

Department of Computer Methods,
Nicholas Copernicus University,
ul. Grudziądzka 5, 87–100 Toruń, Poland.

Abstract

Possible forms of artificial intelligence (AI) support for quantum chemistry are discussed. Questions addressed include: what kind of support is desirable, what kind of support is feasible, what can we expect in the coming years. Advantages and disadvantages of current AI techniques are presented and it is argued that at present the memory-based systems are the most effective for large scale applications. Such systems may be used to predict the accuracy of calculations and to select the least expensive methods and basis sets belonging to the same accuracy class. Advantages of the Feature Space Mapping as an improvement on the memory based systems are outlined and some results obtained in classification problems given. Relevance of such classification systems to computational chemistry is illustrated with two examples showing similarity of results obtained by different methods that take electron correlation into account.

ADVANCES IN QUANTUM CHEMISTRY, VOLUME 28

0065-3276/97 $25.00

1. Introduction

Progress in theory, availability of software and development of computer technology have created highly sophisticated systems for performing complex calculations on various chemical compounds. Computational methods are routinely used nowadays not only by theoretical chemists but also by experimentalists (cf. QCLDB bibliography [1]). There is no doubt that the future of computational methods is bright. However, two fundamental problems face further development of computational chemistry.

First, programs used in molecular physics and quantum chemistry became very large (hundreds of thousands of lines of code), hard to maintain, extend or use in conjunction with other programs. Several different sets of programs, often repeating identical calculations, are used to take advantage of the specialized capabilities of different quantum chemistry packages. The developers of these software packages create many software patches, adding to the complexity of the existing systems. New computer architectures and network environments become additional complication for the software developers working with old codes. Recently, two new approaches were proposed to address these problems. The OpenMol project [2] is based on the abstract data type model, defining precisely the types of data used by the program by the collection of operations which access, generate and update this data. Abstract data types are easy to implement in most computer languages and they preserve important features of objects without introducing unnecessary complications of the full object-oriented programming paradigm. Another interesting approach to the development of computational chemistry systems was taken in the CACTVS project [3]. It uses concepts of dataflow processing and visual programming to create a distributed client/server network environment for the computation, management, analysis and visualization of diversified chemical data. CACTVS project addresses also the problem of integration of various types of chemical knowledge.

While software engineering techniques may help to change the monolithic, state-of-the-art, mutually incompatible programs into cooperating, extensible supersystems of programs, and thus solve the first problem, the second problem is much harder. Computational chemistry methods and programs are based almost entirely on the numerical techniques. Despite high sophistication these programs are deceptively easy to use and the trend towards visual user interfaces will only aggravate this problem. A few lines of input may keep a supercomputer busy for many hours and produce garbage since computational chemistry programs have absolutely no knowledge of what they compute. Asked to compute the dipole moment of a molecule they do not check for inversion symmetry first but immediately start computations. These programs have no memory to store and to

analyze previous results, they are not able to notice similarities with the previous runs, in short they do not have any general intelligence. Some specific intelligence is easy to built into the software, for example the rules determining the use of damping factors during SCF calculations. Tutorials and help files may assist the user in answering such questions as: What can we expect from calculations at the minimal basis set level? What are the traps of using MP2 perturbation theory? When to use different computational methods? This knowledge, based on experience of computational chemists, is not readily available and is not yet contained in systems of programs for computational chemistry support.

Numerical orientation of quantum chemists seems to be the main reason for this lack of intelligence in computational chemistry codes. Since the times when only experts (quantum chemists) were using these codes are over, and the complexity of the computational tools have greatly increased, more effort should be devoted to developing intelligent systems. The OpenMol project [2] has explicitly addressed this problem, proposing to use a rule-based expert system to control the flow of calculations and to search the databases for previous calculations on the same system. The QCLDB database [1] contains only names of molecules, methods used and properties calculated, but it does not contain the results of calculations. The availability of a large collection of such data is a necessary prerequisite to test various rules and to experiment with systems capable of learning from examples. In contrast to computational systems which are able to solve completely novel problems, predictions and estimations of intelligent software is based on empirical knowledge, partially capturing the experience of human expert, and are thus limited to classes and problems broadly similar to the problems encountered before.

Such an approach has obviously some limitations but the machine learning techniques [4] developed in artificial intelligence (AI) go much beyond the database lookups. The main goal of this paper is to discuss the AI techniques helpful in creation of intelligent software for support of computational chemistry. In the second section knowledge-based and other AI techniques will be evaluated from the point of view of their suitability for computational chemistry. In particular the memory-based systems will be briefly discussed. In the third section recent results obtained with the Feature Space Mapping (FSM) system [5] for classification problems are described and compared with results obtained by expert systems and simple memory-based techniques. Similarity and clusterization of results obtained by many computational methods used to calculate electric properties of ozone and hydrogen chloride are visualized using multidimensional scaling techniques in the fourth section. These results illustrate how classification systems may be used to predict the cheapest method capable of calculations at a specified level of accuracy. A short discussion closes this paper.

2. What can AI offer ?

In the context of Artificial Intelligence (AI) "intelligence" is defined as the ability to use knowledge in form of facts and rules [6]. Artificial Intelligence has unfortunately more critics that associate its goals with creation of artificial humans than enthusiasts trying to use its techniques to solve practical problems. Today, even some house appliances use fuzzy logic and neural networks to improve their performance. To compare such devices a Machine Intelligence Quotient (MIQ) is sometimes given. Computational chemistry programs may also be compared according to their intelligence. Programs that require an input from the user whenever the same information may be computed from the previously given input data are less intelligent than programs that are able to draw more conclusions from their input. For example, some programs require symmetry of orbitals as inputs, more intelligent programs require only specification of the symmetry group and most intelligent programs (in this particular respect) use geometry input data to determine automatically all symmetry-related information. Yet even at this simple level there is a lot to be done and computational chemistry packages are far from drawing all possible conclusions from symmetry arguments. Users of more intelligent programs have less chances to commit errors – many quantum chemists certainly recall runs aborted due to the errors in orbital symmetry assignment.

Another simple tasks where more intelligence is desired is input checking. A database of a typical bond length and bond angles in different environments would be very useful to alert the users to potential errors. The more knowledge the program has the more intelligence it may show. The trouble is that the computational chemistry programs have no knowledge at all, they are capable only of running numerical algorithms. What is strongly desired in such programs is general intelligence that should help their users to avoid simple errors. Intelligence build in the numerical software is not sufficient, knowledge-based programs should be separated from the numerical software [2].

Whenever there is knowledge in form of rules one can use the expert system technology. More expert systems are used now in industry than in science. The expert system technology is widely used in symbolic algebra systems and in the support of chemical analysis and synthesis [7], but not in molecular physics or computational chemistry. A good example of the possibilities of expert system technology is provided by the KAM system developed by Yip at MIT [8]. Equations describing a dynamical system are set up starting from verbal description and solved by performing numerical simulations. Phase space portraits are obtained and graphically displayed. Visual data are analyzed by a camera and finally a verbal description of results, similar to an analysis by a human expert, generated.

Expert systems have many advantages: they are based on a technology that has proved to be useful, there are many expert systems used routinely, for some applications they are quite reliable, their reasoning is relatively easy to understand and they are able to explain how and why specific conclusions have been reached. There is no doubt that many expert systems should be created to support computational chemistry, as advocated by the OpenMol project [2]. The use of a rule-based expert system requires thorough understanding of the problem domain allowing for a formulation of the set of rules useful for reasoning. This is not a trivial task and it contributes significantly to the costs and long development time of the expert systems. There is already a lot of experience in computational chemistry, related to the selection of the basis sets, expected accuracies of calculations at different levels of approximations etc. Certainly it is worthwhile to work on such systems collecting the expertise in the form of rules and building systems to support decisions during input specification (for example in selection of methods and basis sets) and during output analysis (looking for possible inconsistencies, evaluating accuracy of the results).

Decision support systems may be based on expert systems, statistical techniques such as decision trees, belief spaces, probabilistic reasoning, chain graphs and many others [4, 8]. There are many machine learning systems, including rule-based systems [6], that are capable of improving their performance by learning from examples. In particular, neural networks have become popular in recent years, since they do not require explicit formulation of rules (logical rules may be derived automatically from a trained network) but may learn from examples. Neural networks find many applications in chemistry [9]. For real world problems, when a large number of data has to be analyzed, one has to be careful using neural network techniques [10]. Most neural systems learn slowly and new facts may interfere with facts already learned leading to catastrophic forgetting [11]. To focus the discussion a particular classification system that should be able to classify the goals – calculations proposed by the user – into three classes will be considered. The classes are: "high", "low" accuracy expected, and "no opinion". These classes obviously depend on the property calculated, therefore a separate classification subsystems should be used for each property. The classification system obtains the input data to the computational chemistry package and attempts to correlate this data with the computed output data and with accuracy (estimated by the user) of computed results. Initially the system does not know much so it will usually have no opinion. After processing a large number of cases it should be able to generalize its knowledge sufficiently well to predict with some confidence the quality of calculations on unknown chemical systems.

Two questions arise here. Is such a classification system feasible? If it is feasible, what are the best tools to build it? The answer to the first

question is not clear and requires empirical investigations. It all depends on how well this system would be able to generalize. Even with a minimal ability to predict accuracy of calculations in new situations, provided for example by a fuzzy look-up table containing compressed representation of input-output data, such classification system should be valuable, since it would be able to recall results of all calculations already performed, saving time (at least for calculations requiring considerable time) and preventing repetition of the same calculations. Poor generalization is expected whenever the outputs are very sensitive to small changes in the inputs. Consider for example semiempirical methods. Their reliability is restricted to a well defined classes of molecules because the results of calculations are too sensitive to the parameters used, types of bonds, atoms and geometry. In the worst case, the classes in the parameter space may have fractal boundaries. Stability of *ab initio* methods is generally better and there is hope that a useful classification system is feasible. In some cases it may even be possible to have a system capable of approximating results and thus of predicting the actual values of properties without performing the calculations or using the predicted values for initialization in iterative procedures. Classification is easier than approximation, therefore it should be attempted first.

Such classification system should "express opinions" recommending methods of computation and basis sets for a given molecule. Lack of a recommendation is then treated as a warning that the case is very different from all those attempted before. All these considerations are purely theoretical, because unless such a system is actually constructed and tested it would not be possible to predict its performance. The key issue is whether it is possible to find a small number of features that will allow for good classification. It is relatively easy to define the similarity of different basis sets and in some cases also of the molecules: adding one more carbon group to a long polyen does not lead to a dramatic change of the accuracy of calculations. On the other hand adding a heavy metal atom without a proper extension of the basis set may lead to a drastic decrease of accuracy. Similarity of computational methods is harder to define and extensive empirical studies are required to determine it. Similarity of molecules is also hard to define. Here similarity is regarded only from the point of view of the similarity of accuracy of computed properties. The indices of Quantum Molecular Similarity [12] define similarity between molecules by integration of electronic densities. This requires availability of densities and optimization of rotational and translational positions of the two molecules that are compared. These indices, obtained from CNDO calculations, were used for prediction of various properties, such as the extracting constants of Cu(II) from β-diketone systems, biological activity of retinoid compounds and steroid hormones, and classification of odor intensity of chemical compounds [12]. In all these cases clusterization of the results may be observed, indicating that there

is sufficient information in the Quantum Molecular Similarity indicators to distinguish between different classes of molecules from the point of view of investigated properties. The main problem in such applications is to find good features that allow for classification. Electron density may not be the best choice because CNDO densities are not accurate and the procedure for calculation of quantum similarity indices from densities is computationally expensive. Simpler input information, based on the types of bonds, deviation from the typical bond length and description of electron shells involved in bonds may also be sufficient to achieve similar clusterization or good classification of the accuracy of computations.

Since it is quite probable that a classification system useful for computational chemistry is feasible, the second question should be considered: what are the best tools to build it? Many techniques useful for classification have been devised by proponents of machine learning (a branch of artificial intelligence), statistics, pattern recognition, and neural networks. There are several problems to be considered. First problem is the selection of features that are sufficient for classification. Features should include description of molecules – atoms, bonds, electron shells, molecular states, geometry, symmetry, basis sets, methods and programs used, other input parameters given to computational packages, properties calculated, estimation of accuracy and timing. Second problem is the lack of a large database of data to train the classifier using examples containing both high and low accuracy results. Without knowledge contained in such database it is not possible to develop a proper "judgment" of how to perform good calculations. To create such a database results of calculation of various molecular properties using available methods for many molecules should be compiled. Third, a reliable classification system is needed, a system that should be able to compress the input data by forming prototype cases and predicting new results on the basis of similarity of inputs. does not seem to be the best solution. General rules may be derived analyzing the performance of memory based classifier, but *a priori* it is not clear

Computational chemistry may produce almost an infinite amount of data, therefore one has to select classification system that would be able to cope with large, real world problems. One of the AI techniques that does not require formulation of general rules, but is rather based on memory, is called Case Based Reasoning (CBR) [13]. The study of CBR was motivated by cognitive science. A particular subtype of CBR, well suited for classification of large, loosely structured data, is called Memory Based Reasoning (MBR) [14]. These methods belong to the family of the nearest-neighbor-like methods introduced in pattern recognition [8]. Memory-based reasoning has been applied to a typical benchmark database tests as well as to the object recognition and classification of free text samples taken from very large databases. There is no learning phase and there are no adaptive

or learning parameters to manipulate. Results are better than or comparable to those obtained by neural networks. In general, memory based methods seem to be better suited to industrial, large scale applications than are the neural methods.

As an example consider the 1990 U.S. Census classification task. Free text samples from 22 million citizens were classified by assigning industry and occupation codes, based on job descriptions given in questionnaires [14]. An expert system called AIOCS was used. The rules were laboriously derived from a training data base consisting of 132 247 cases classified by human experts. The time required for the development of this system was equivalent to 192 month/person (16 years/person). Still, accuracy is rather low (Table 1). An alternative memory based system called PACE was developed in just 4 months/person and efficiently implemented on CM-2 parallel computer.

Table 1
Comparison of an expert system and a memory based system.

Name	% of industry codes assigned	% of occupation codes assigned	Development month/person
AIOCS	57%	37%	192
PACE	73%	57%	4

Memory based reasoning has some disadvantages: generalization and interpolation is not as good as in neural networks, therefore a large number of good examples is needed, there is no data compression and thus computational demands and memory requirements are high, making these methods unsuitable for on-line learning. Clearly a combination of the memory-based methods (developed by the pattern recognition community) and methods based on adaptive systems (developed by the neural networks community) is desired. Below, a recently developed universal neurofuzzy system [5] that may be viewed as an improvement of the MBR methods is described.

3. Feature Space Mapping

Instead of storing all training facts, as the memory based methods do, it is desirable to form prototypes by remembering a number of facts clustered near each other as one memory object. Neural networks that use localized functions, such as the RBF networks [11], are capable of such a representation. However, their classification decisions are based only on the output values of the network, not on the distance between the data and the known prototype clusters. The theory behind RBF and similar networks [15] does not help to see the problem as that of a geometrical description of complex

memory objects in the multidimensional feature spaces, and it does not distinguish between the local generalization based on interpolation, and the probabilistic, nearest-neighbor generalization based on distances from the input data to the borders of memory objects representing the data clusters.

The Feature Space Mapping (FSM) neurofuzzy network [5] is based on fuzzy memory traces. Changing the parameters of FSM network allows for trading the memory requirements and computational demands for accuracy of data description. The incoming data vectors provide the values of the features (via pre-processing of the raw data, if necessary) of internal representations X_i suitable for classification. A coordinate system based on these features $\{X_i\}$ defines a multidimensional feature space. Since the features may be of different types (logical, integer, continuous, symbolic) partial classifications are performed in local feature spaces while the final classification is performed in the space that is highest in the hierarchy (Fig. 1). The system learns by creating and modifying memory traces (clusters) in these spaces. Memory traces are described using memory function $M(X)$ as the fuzzy areas in the feature space where the function has non-zero values. This function is a linear combination of localized separable functions:

$$M(\mathbf{X}, \mathbf{D}, \mathbf{\Delta}) = \sum_p W_p \; s(\mathbf{X}; \mathbf{D^p}, \mathbf{\Delta^p}) = \sum_p W_p \; \prod_i g\,(X_i; D_i^p, \Delta_i^p) \qquad (1)$$

Memory function does not vanish only around the data vectors $\mathbf{D}$ stored in the M function. The "weights" W_p and the "dispersions" $\mathbf{\Delta}$ are the adaptive parameters defining the memory function for a given set of input values. Each multidimensional function $s()$ is a product of one-dimensional component functions $g()$. If the input data is noisy or if there is too many data items to store the centers $\mathbf{D}$ are also treated as adaptive parameters. In the learning process the shapes of the memory objects and their mutual positions are adjusted by the local learning procedures which estimate the probability density of the incoming data. Local maxima of the memory function are prototypical (fuzzy) representations of the training data. Such system may learn in supervised as well as unsupervised mode and may use fuzzy reasoning in the process of classification or decision making [5]. FSM provides logical rules in fuzzy form:

$$\text{IF } (\mathbf{X} \in P_k) \text{ THEN } \mathbf{X} \text{ is of class } C_k \qquad (2)$$

where P_k is the memory object created in adaptive process. Such rules provide discretization of the feature space into areas labeled by linguistic variables (names of classes). Crisp (classical) logical rules are obtained if the shape of the memory objects is restricted to a sum of cuboids

$\sum_{m=k,l..}[X_1^{m_1}...X_1^{m'_1}] \times [X_2^{m_2}...X_2^{m'_2}] \times ...$, equivalent to alternative of conjunctions of linguistic variables $(s_1^{k_1} \wedge s_2^{k_2} \wedge ..) \vee (s_1^{l_1} \wedge s_2^{l_2} \wedge ..) \vee ....$

Localized description of the input data leads to network output that is effectively zero except for small regions of the input space around the training data vectors. On the other hand, delocalized functions, such as sigmoidal functions used in the popular backpropagation (multilayered perceptron) networks, create boundaries between classes dividing the input space with hyperplanes. Such networks may extrapolate far beyond the input regions where reliable data exists. Memory based systems using k-nearest-neighbors rule (k-NN) [11] may warn the user that the reliability of the answer is low when the distance to the nearest memory trace is large. In FSM the representation of the data is compressed by clustering, therefore the k-NN approach should not be used directly for centers of the clusters, because in such a case the data that are close to the border of a large cluster would be wrongly assigned to a small cluster whose center is closer. FSM networks compute gradients and use them to find the cluster with the "largest influence" on a given position in the data space. If gradients and the network outputs are too small, the fuzziness of the network nodes is temporarily increased (by increasing the dispersion parameters) until gradients become sufficiently large to point towards the most important cluster in the neighborhood.

The FSM system was tested [16] on many datasets. In case of Glass Identification Database created by Forensic Science Service direct comparison with rule-based expert system was possible. The database contains information about 7 types of glasses that may be identified by 10 chemical and physical properties. A total of 214 samples are provided, out of which 21 vectors were selected randomly as the test base and the rest was taken as the training base. After initialization the network had 7 nodes and accuracy of 88% (since the results depend slightly on order in which the training data is presented all accuracies are average from 10 runs). This accuracy was improved to 96% by adding 12 new nodes. The network with a total of 19 nodes achieved 94.5% accuracy on the test set. Further increase of accuracy for the training set to 100% (FSM may always learn the training data perfectly) resulted in worse generalization and accuracy decreased to 88.5% on the test set. For this database the accuracy of a rule-based system (BEAGLE system), the nearest-neighbor algorithm (simple and frequently used memory-based algorithm) and discriminant analysis is 82%, 83% and 74%, respectively, much worse than the FSM results.

The Shuttle dataset from NASA contains 9 numerical attributes, 43500 training vectors and 14500 test vectors. There are 6 classes. FSM initialization gives 7 network nodes and 88% accuracy. Increasing the accuracy on the training set to 94%, 96% and 98% requires a total of 15, 18 and 25 net-

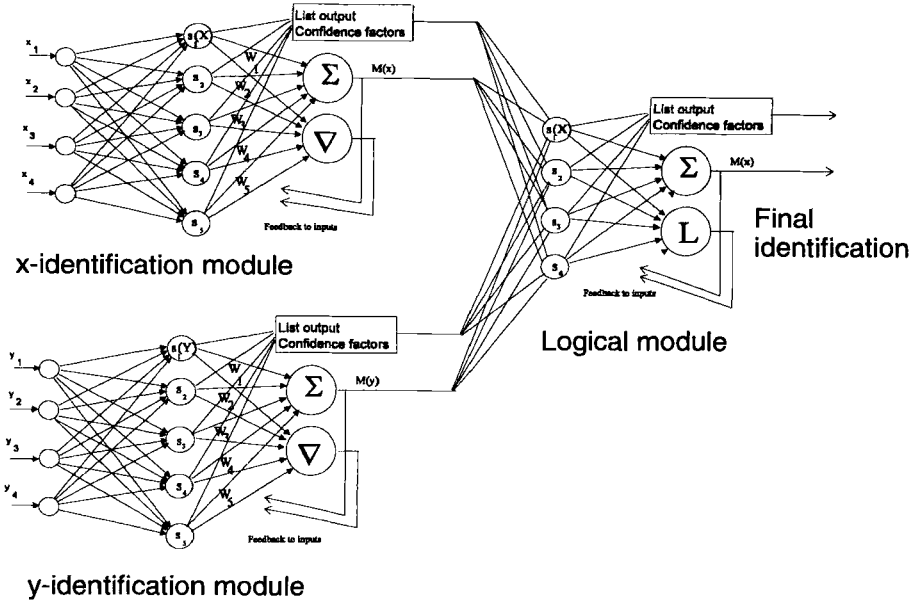

Figure 1: Two recognition and one logical module of FSM network.

work nodes and gives accuracies on the test set of 95.5%, 97.8% and 98.5%. Backpropagation network reached an accuracy of 95.5% on the training set. Memory based methods such as k-NN require all 43500 vectors as the reference memory traces. FSM demonstrates in this case a significant data compression with quite good generalization.

4. Classification of computational chemistry results.

In a recent paper Maroulis [17] has evaluated the performance of correlated methods in molecular property calculations using pattern recognition and clustering in feature spaces. Four series of calculations were considered, each time using just one basis set. SCF and 7 correlated methods were applied to calculation of 23 properties (electric properties – multipole moments, polarizabilities and hyperporalizabilities) of HCl molecule and 11 properties of N_2 molecule. Two series of calculations were performed on ozone, in the first series 16 properties were studied by 7 methods, in the second series 6 properties were studied by 11 methods. The results were analyzed by looking at the similarity matrices and producing the minimum spanning trees. Features used in this study are restricted to the values $Q_{m\alpha}$ of property α computed with method m. First the matrix D_{ij} mea-

suring the distances between different methods is computed and then the similarity matrix S_{ij}:

$$D_{ij} = \left(\sum_{\alpha} |Q_{i\alpha} - Q_{j\alpha}|^2 \right)^{1/2} ; \qquad S_{ij} = 1 - D_{ij} / \max_{ij} D_{ij} \tag{3}$$

Each method is represented here by a vector of calculated properties. Since there are no reference values for the computed properties it is impossible to define absolute accuracies. The procedure defined by Maroulis is still useful, defining a global similarity of various computational methods. If specific questions are admitted by the classification system non-averaged similarity matrices S_{ij}^{α} should be used. The two-dimensional graphical representation of the multidimensional data used by Carbó *et.al.* [12] and by Maroulis [17] is based on the spanning trees, preserving only a local information about the distances and thus also about similarities. Given a matrix of distances D_{ij}, $i, j = 1, .., n$, the minimum spanning tree is defined as the acyclic connected graph (each pair of nodes i and j has just one route connecting them) with the shortest overall distance between its nodes. In this case the nodes represent methods while the distances between connected vertices are elements of the distance matrix D_{ij}.

A better representation of the multidimensional data is based on the minimization of the overall measure of topographical distortion, i.e. placing the original, multidimensional vectors (treated as points in the feature space) in a low-dimensional (usually two-dimensional) target space. This procedure is known as the multidimensional scaling (MDS) and has been used predominantly in mathematical psychology [18]. Similar procedures were introduced by Sammon [19] and Duch [20]. One useful measure of topographical distortions is:

$$0 \leq A(D;d) = \frac{\sum_{i>j} (D_{ij} - d_{ij})^2}{\sum_{i>j} (D_{ij}^2 + d_{ij}^2)} \leq 1 \tag{4}$$

where target space distances d_{ij} are free parameters that are minimized to reduce $A(D;d)$. This measure is equal to zero if the original distances D_{ij} are perfectly reproduced in the target space without errors and grows to one with growing topographical distortion.

Two and three-dimensional results of the MDS treatment of the similarity data derived from calculations described by Maroulis [17] are given in Figure 2 (for HCl) and Figure 3 (for O_3). One-dimensional MDS map of HCl calculations shows just two clusters, SCF and all other methods. Thus one dimensional MDS maps differentiate between SCF and methods that take electron correlation into account. Two-dimensional MDS (Fig. 2) shows

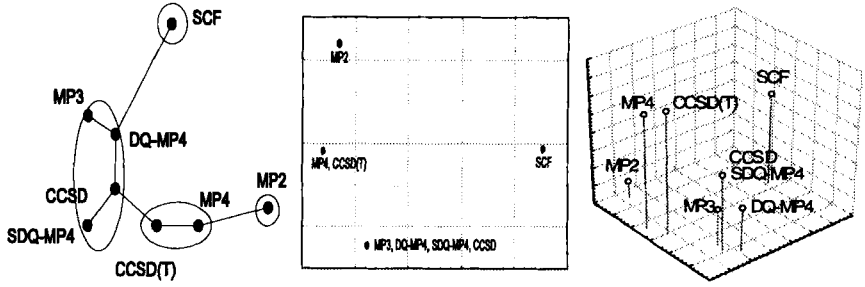

Figure 2: Minimal spanning tree and MDS configurations in two and three dimensions for calculation of 23 properties of HCl with 8 computational methods

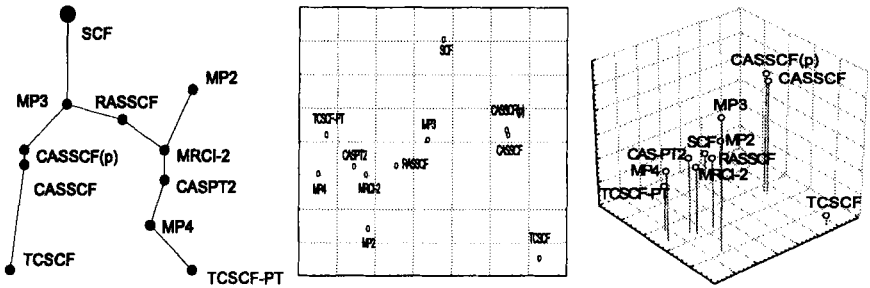

Figure 3: Minimal spanning tree and MDS configurations in two and three dimensions for calculation of 6 properties of O_3 with 11 computational methods

four clusters of methods: SCF; MP2; (MP3,DQ-MP4,SDQ-MP4,CCSD) and (MP4,CCSD(T)). In this case results of MP3, DQ-MP4, SDQ-MP4 and CCSD methods are hard to distinguish from each other, results of MP4 and CCSD(T) are quite similar while MP2 method and MP3 group are about at the same distance from the MP4 group. Three-dimensional MDS picture shows more detailed relations preserving this clusterization. One conclusion that may be drawn from Fig. 2 is that the electric properties of HCl may be calculated with about the same accuracy using MP3 or CCSD method and, at higher level of accuracy, with MP4 or CCSD(T). Results for the ozone molecule (Fig. 3) show less pronounced clustering of the methods (properties of this molecule are more difficult to compute), with CASPT2 and MRCI-2 methods quite close to each other, MP4 and RASSCF giving somewhat worse results.

5. Summary

Although it is not possible to draw any conclusions from the illustrations given in the previous section, it would be useful to have a classification system which, on the basis of many such results, would recommend the cheapest method of calculation for a specified level of accuracy. Certainly HCl molecule is not the only example for which results of calculations with MP4 (cheaper method) and CCSD(T) (more expensive) methods are similar. Classification systems have memory and use examples stored in the database to form a model of the multidimensional data in the space of selected features. There is hope that the classification basins in the feature space are sufficiently regular to support generalization to cases that were not yet encountered. In some cases explicit rules may be formulated. However, rule-based systems are usually less accurate than memory based adaptive systems and, for large number of rules and large number of variables appearing in rule conditions, reasoning with rules may simply be too complex.

In this paper the need for an intelligent support of computational chemistry software packages was stressed and the memory-based classification systems suitable for this task recommended. More experiments with selection of relevant features to determine similarity of molecules and methods from the point of view of calculation of molecular properties are needed. Classification systems, such as the FSM, are ready to handle the data, but the task of collecting large amount of data to create a useful system is quite demanding.

Acknowledgements

This paper is dedicated to Geerd Diercksen on the occasion of his 60th birthday. I am grateful to him and other colleagues who took part in the discussions of the applications of AI in computational chemistry at the Max Planck Institute for Astrophysics in the summer of 1994, and to Mariusz Kłobukowski for critical reading of the manuscript. Support by the Polish Committee for Scientific Research, grant 8T11F 00308, is gratefully acknowledged.

References

(1) QCLDB 12: Quantum Chemistry Literature Data Base Bibliography of Ab Initio Calculations for 1993 Guest-Editors: H. Hosoya, S. Yamabe, U. Nagashima, M. Togasi, T. Matsushita, N. Koga, M. Hada, H. Matsuzawa and S. Yabushita.

(2) G.H.F. Diercksen and G.G. Hall, Comp. in Phys. **8** (1994) 215–222

(3) W.D. Ihlenfeldt, Y. Takahashi, H. Abe, S. Sasaki, *J. Chem. Inf. Comput. Sci* **34** (1994) 109–118

(4) Machine learning resources are collected at the WWW page: http://www.aic.nrl.navy.mil/~aha/research/machine-learning.html

(5) W. Duch, G.H.F. Diercksen, Comp. Phys. Comm. **87** (1995) 341–371; W. Duch, Neural Network World **4** (1994) 645-654.

(6) A. Newell, H.A. Simon, Communic. ACM **19** (1976) 113–126; A. Newell, *Unified theories of cognition.* (Harvard Univ. Press, Cambridge, MA 1990)

(7) Z. Hippe, *Artificial Intelligence in Chemistry: Structure Elucidation and Syntheses Design* (Elsevier/PWN 1991)

(8) P. H. Winston, *Artificial Intelligence* (Addison Wesley 1992, 3rd ed.)

(9) J. Zupan, J. Gasteiger, *Neural networks for chemists: an introduction* (VCH, Weinheim, Germany 1993)

(10) W. Duch, G.H.F. Diercksen, Comp. Phys. Comm. **82** (1994) 91–103

(11) J. A. Anderson, *An Introduction to Neural Networks* (MIT Press 1995)

(12) R. Carbó, B. Calabuig, L. Vera, E. Basalú, Adv. in Quantum Chem. **25** (1994) 253–313

(13) D. Leake, ed. *Case-Based Reasoning: Experiences, Lessons and Future Directions* (AAAI Press, Menlo Park 1996)

(14) D.L. Waltz, *Memory-based reasoning*, in: M. A. Arbib, *The Handbook of Brain Theory and Neural Networks* (MIT Press 1995), pp. 568–570

(15) J. Platt, Neural Comput. **3** (1991) 213–225; V. Kadirkamanathan, M. Niranjan, Neural Comput. **5** (1993) 954–975

(16) W. Duch, R. Adamczak, N. Jankowski and A. Naud, Engineering Applications of Neural Networks (EANN), Helsinki 1995, pp. 221–224; Duch W, Adamczak R, Jankowski N, *Improved memory-based classification*, EANN'96, London (in print)

(17) G. Maroulis, Int. J. Quantum Chem. **55** (1995) 173–180

(18) J.C. Lingoes, E.E. Roskam, I. Borg (Eds.), *Geometric representation of relational data.* (Ann Arbor: Mathesis Press 1979).

(19) J.W. Sammon Jr., IEEE Trans. on Comp. **C-18** (1969) 401–409.

(20) W. Duch, Open Systems and Information Dynamics **2** (1995) 295–302

Abstract Data Types In The Construction Of Knowledge-Based Quantum Chemistry Software

P. L. Kilpatrick and N. S. Scott

Department of Computer Science, The Queen's University of Belfast, Belfast BT7 1NN, N. Ireland

Abstract

Recently, Diercksen and Hall (1) presented the OpenMol Program: a proposal for an open, flexible and intelligent software system for performing quantum chemical computations. Central to their proposal was the observation that there is a close relationship between an abstract data type operation and a production rule in a rule-based expert system. The aim of this paper is to explore the establishment of a sound theoretical foundation for this relationship.

ADVANCES IN QUANTUM CHEMISTRY, VOLUME 28

0065-3276/97 $25.00

1 Introduction

In a recent paper (1), entitled "Intelligent software: The OpenMol program", Diercksen and Hall expounded their vision of an open, flexible and intelligent software system for performing quantum chemical calculations. They advocated the use of abstract data types (ADTs) as a means of developing well engineered numerical software. However, rather than create a large inflexible monolithic program they proposed that the implementation of the ADTs should be treated as a structured collection of reusable software components. Given some quantum chemical property or process as a goal, a rule-based expert system would devise a computational strategy. The strategy would be embodied in a "macrofile" containing a sequence of ADT operations which, when executed, would compute the required property or process. In essence, the synthesis of ADTs and a rule-based expert system would provide the means of developing an intelligent goal driven software system for performing quantum chemical calculations.

Central to the OpenMol proposal is the postulate that there is a close relationship between an ADT and a production rule in a rule-based expert system: a relationship which forms the natural basis for the synthesis of knowledge and numerical data processing. The aim of this paper is to explore the postulated relationship in greater depth and to move towards a theoretical foundation for it. Without a sound theoretical base it is impossible to exploit the relationship envisaged in the OpenMol system.

In section 2 we consider the nature of ADTs and production rules. In particular, we illustrate how the syntax and semantics of ADT operations can be rigorously specified using a formal specification notation based on predicate logic. By specifying ADT operations using pre- and post-conditions we show that a mapping can be established between a formally specified ADT and the antecedent and consequent parts of a production rule. In section 3 we specify some operations of an ADT for matrices. We show the corresponding production rules and illustrate the execution of an idealised inference engine. Through this simple example we show that a set of production rules which capture knowledge about ADT operations is unlikely to be sufficient to provide a useful knowledge-base. Further rules are required which embody knowledge about the algebra of the abstract type itself. Finally, in section 4 we summarise our investigation.

2 Abstract data types and production rules

Abstract data types have been established in computer science for many years (2). Indeed they are at the heart of the object-oriented programming paradigm. However, their use in scientific programming has been limited - probably because, prior to FORTRAN 90, FORTRAN provided no direct

language support for ADTs (3). It is appropriate, therefore, to begin by briefly reviewing the nature of an ADT.

2.1 The nature of an ADT

Informally, an ADT is a data type together with an associated collection of operations on the type. These operations are the only operations permitted for manipulation of objects of the type. Variables of the type record the state of the ADT, while the operations define the behaviour of the ADT. For instance, a matrix is an example of a type which is commonly used in quantum chemical computations. Associated operations could include: constructing a matrix; adding two matrices; producing the inverse of a matrix; and diagonalising a matrix to find its eigenvalues and eigenvectors.

ADTs are abstract in the sense that they are specified without regard for the way in which they will be implemented. In effect, the specification describes a list of services available on the data type, and the formal properties of these services. Clients of the ADT may only access its data structure through the advertised services which are independent of the ADT's implementation (however, note reference (4)). This facilitates the construction of well engineered software which is easy to maintain and modify. Most modern programming languages provide direct support for ADTs either through modules/packages (e.g. FORTRAN 90, Ada) or classes (e.g. C++).

The rigorous specification of an ADT requires a type specification and, for each operation, the operation's name, signature, pre-condition and post-condition. The signature may be considered to convey the syntax of the operation while the pre- and post-conditions convey its semantics. As an illustration consider an ADT which manipulates real square matrices.

First, using a notation in the style of VDM-SL (5) we rigorously specify the type Matrix, which represents real square matrices. **Throughout the remainder of this article the term matrix will refer to a real square matrix.**

$$\begin{aligned}
&\text{MatrixRow} = \text{Seq}_1 \text{ of Real}\\
&\text{Matrix} = \text{Seq}_1 \text{ of MatrixRow}\\
&\\
&\text{inv-Matrix(M:Matrix) :Boolean}\\
&\text{post } (\forall\, i, j \in \text{inds(M)} \cdot \text{len(M[i])} = \text{len(M[j])}\ ) \wedge\\
&\qquad (\text{len(M)} = \text{len(M[1])})
\end{aligned}$$

A variable of type Matrix is a sequence or list of one or more elements (Seq_1), each of type MatrixRow. A variable of type MatrixRow is a sequence of one or more real numbers. An invariant, expressed through a function inv-Matrix, constrains each row in the matrix to be of equal length

and the number of rows (len(M)) to be equal to the number of columns (len(M[1])).

Next we consider one of the ADT's operations. We choose an operation whose purpose is to tridiagonalise, by means of an orthogonal transformation, a symmetric matrix.

Tridiagonalise: A:Matrix → T:Matrix X P:Matrix
pre Symmetric(A:Matrix)
post $P^TP = I \wedge$
$P^TAP = T \wedge$
Tridiagonal(T:Matrix) ∧
Symmetric(T:Matrix)

The signature of the operation, A:Matrix → T:Matrix X P:Matrix, indicates that Tridiagonalise takes as input a matrix A and returns two matrices T and P. The pre- and post-conditions are predicates which specify the semantics of the operation. **Provided** A is a symmetric matrix, the implementation of the operation **is guaranteed** to return a symmetric and tridiagonal matrix T and an orthogonal matrix P, with the property that T, P and A are related through the orthogonal transformation, $P^TAP = T$. It is important to note that the specification informs us **what** the operation does but not **how** it is effected. The specification describes the properties of the operation's output parameters but does not impose an algorithm whereby the orthogonal matrix P and the tridiagonal matrix T may be computed.

In this example we have augmented VDM-SL with conventional matrix notation. In addition, we have made use of two auxiliary functions to hide the lower level details of the specification. For example, the auxiliary function Symmetric may be expressed as

Symmetric(S:Matrix) :Boolean
post $(\forall i, j \in inds(S) \cdot S[i][j] = S[j][i])$

All auxiliary functions need to be specified in a similar manner to complete the specification. However, because of space constraints, we exclude such lower level details from this article.

2.2 Rigorously specified ADTs and production rules

Production rules are a formalism commonly used in expert systems but which have their origin in automata theory and formal grammars. Each rule consists of an antecedent-consequent pair, for example:

Rule 1: if

A_1 and A_2 and A_3 and ... A_n

then

C_1 and C_2 and C_3 and ... C_m

Rule 1 has the meaning that **provided** the antecedents A_1 and .. A_n are true, then the consequents C_1 and ... C_m **are guaranteed** to be true.

It is clear from the above description and the discussion in section 2.1 that the semantics of a production rule are very similar to the interpretation of a rigorously specified ADT operation. Thus any rigorous ADT specification may be recast in the form of a set of production rules. For example, the specification of the ADT operation Tridiagonalise becomes :

Tridiagonalise: if

A:Matrix and Symmetric(A:Matrix)

then

T:Matrix and P:Matrix and
$P^TP = I$ and
$P^TAP = T$ and
Tridiagonal(T:Matrix) and
Symmetric(T:Matrix)

This can be interpreted as meaning that provided the operation Tridiagonalise is given a variable A of type Matrix such that A has the property of being symmetric then the operation guarantees to produce two variables, T and P, both of type Matrix, such that P has the property of being orthogonal, T has the properties of being tridiagonal and symmetric, and A, T , and P have the property of being related through the orthogonal transformation, P^TAP. The rule does not tell us anything about the values of A, T and P - rather it provides us with a description of their properties.

Informally, any rigorously specified ADT operation can be recast as a production rule as follows:

1. The rule is given the same name as the operation.
2. The operation's input variables (including their type details) and the operation's pre-condition are conjoined to give a rule antecedent.
3. The operation's output variables (including their type details) and the operation's post-condition are conjoined to give a rule consequent.

The general connection between an ADT and a production rule set was observed by Diercksen and Hall (1). However, they did not emphasise the need for a production rule to encapsulate **both** an ADT operation's syntactic and semantic content.

3 An ADT and its associated production rule set for a simple configuration interaction expansion problem

As stated in the introduction, one of the novel features of the OpenMol program is that its numerical software has been developed in accordance with the ADT model. It is proposed that knowledge about each ADT be recorded in the rule set of an expert system. Then, given some quantum chemical property or process as a goal, the function of the expert system is to construct a directed graph: the nodes of the graph are ADT operations while the directed arcs denote the order in which the implemented operations should be invoked to achieve the goal. In this section we illustrate how such a directed graph might be constructed. We begin by considering a simple configuration interaction (CI) expansion problem.

3.1 A simple CI expansion problem

Assume that we have a database which contains, for each neutral atom, a list of configurations. We denote the configuration list for the atom with atomic number i by $[\psi_{1i}, \psi_{2i}, ...\psi_{ni}]$. For example, the first configuration for the carbon atom, ψ_{14}, might be $1s^2 2s^2 {}^1S^e$. We wish to construct a CI expansion for each atomic state of a specified atom. For example, the i^{th} atomic state of atom j, Ψ_{ij}, is represented by a linear combination of the atom's configurations

$$\Psi_{ij} = a_{i1j}\psi_{1j} + a_{i2j}\psi_{2j} + ... \; a_{inj}\psi_{nj} \tag{1}$$

with the property that

$$<\Psi_{ij} \mid H \mid \Psi_{kj}> = E_{ij}\,\delta_{ik} \tag{2}$$

where H is the atomic Hamiltonian operator. The CI expansion coefficients, a_{ijk}, are simply the eigenvectors obtained by diagonalising the Hamiltonian matrix,

$$<\psi_{ij} \mid H \mid \psi_{kj}> \tag{3}$$

3.2 Specification of the available operations

We assume that we have available FORTRAN implementations of the following operations:

Multiply: Given two conformant matrices this operation returns their product.

Tridiagonalise: Given a symmetric matrix this operation returns a similar symmetric tridiagonal matrix and the corresponding orthogonal transformation matrix.

Householder: Given a symmetric tridiagonal matrix this operation returns its eigenvalues.
InverseIteration: Given a symmetric matrix and its eigenvalues this operation returns the eigenvectors of the matrix.
GetAtomBasisSet: Given an atom i this operation searches the database and returns the list of configurations $[\psi_{1i}, \psi_{2i}, ...\psi_{ni}]$.
CreateHamiltonian: Given a list of configurations, $[\psi_{1i}, \psi_{2i}, ...\psi_{nj}]$, this operation constructs and returns the Hamiltonian matrix, $<\psi_{ij} \mid H \mid \psi_{kj}>$.

In figure 1 we show how these operations are specified with the required degree of rigour. The auxiliary functions necessary to complete the specification are informally described in figure 2.

3.3 The production rules

Using the informal mapping described in section 2.2 the operations specified in figure 1 can be recast as production rules. These operation rules are shown in figure 3. Although we have sufficient operations to achieve the goal of determining a CI expansion for a given atom we have no convenient means of specifying such a goal nor do we have, with the current rule set, a means of achieving it in an automated way. As the rule set stands the goal would have to be specified in the following cumbersome manner:

Given,
A:Atom = Hg
if instantiations of the following can be found
ABS:AtomBasisSet, H:Matrix, P:Matrix, T:Matrix, Q:Matrix,
D:Matrix and E:Matrix
such that
(AtomBasis(A:Atom; ABS:AtomBasisSet) and
HamiltonianMatrix(ABS:AtomBasisSet; H:Matrix) and
Symmetric(H:Matrix) and $P^TP = I$ and $Q^TQ = I$ and
$P^THP = T$ and $Q^TTQ = D$ and Diagonal(D:Matrix) and
E=PQ) is true
then
ABS:AtomBasisSet and E:Matrix can be used to construct a CI expansion of Hg.

This goal cannot be achieved because, although implicit in the mathematics, no rule explicitly specifies the relative size of its matrix parameters. Thus the antecedent of the rule Multiply cannot be satisfied and the operation to compute E=PQ can never be invoked.

Figure 1

A rigorously specified ADT for matrices.

Types
MatrixRow = Seq1 of Real
Matrix = Seq_1 of MatrixRow
inv-Matrix(M:Matrix) :Boolean
post $(\forall i, j \in inds(M) \cdot len(M[i]) = len(M[j])) \wedge$
$(len(M) = len(M[1]))$

Atom = {H, He, ...Hg...Ha}
AtomBasisSet = to be defined

Operations
Multiply: A:Matrix X B:Matrix → C:Matrix
pre $len(A) = len(B)$
post $AB = C$

Tridiagonalise: A:Matrix → T:Matrix X P:Matrix
pre Symmetric(A:Matrix)
post $P^TP = I \wedge$
$P^TAP = T \wedge$
Tridiagonal(T:Matrix) ∧
Symmetric(T:Matrix)

Householder: T:Matrix → D:Matrix
pre Tridiagonal(T:Matrix) ∧ Symmetric(T:Matrix)
post $\exists Q \in Matrix \cdot (Q^TQ = I \wedge Q^TTQ = D) \wedge$
Diagonal(D:Matrix)

InverseIteration: T:Matrix X D:Matrix → Q:Matrix
pre Symmetric(T:Matrix) ∧ Diagonal(D:Matrix) ∧
$\exists R \in Matrix \cdot (R^TR = I \wedge R^TTR = D)$
post $Q^TQ = I \wedge$
$Q^TTQ = D$

GetAtomBasisSet: A:Atom →ABS:AtomBasisSet
post AtomBasis(A:Atom; ABS:AtomBasisSet)

CreateHamiltonian: ABS:AtomBasisSet → H:Matrix
post HamiltonianMatrix(ABS:AtomBasisSet; H:Matrix) ∧
Symmetric(H:Matrix)

The operation rules are, therefore, insufficient in themselves to produce a flexible expert system. They need to be augmented by type rules which express more general knowledge about the algebra of the data types. Seven such type rules are given in figure 4 and are described below:

Figure 2

An informal description of the auxiliary functions needed to complete the specification given in figure 1.

Auxiliary Functions

AtomBasis(A:Atom; ABS:AtomBasisSet) :Boolean
returns true iff ABS is the configuration list associated with atom A

HamiltonianMatrix(ABS:AtomBasisSet; H:Matrix) :Boolean
returns true iff H is the Hamiltonian matrix constructed from the configuration list ABS according to eq(3).

Symmetric(A:Matrix) : Boolean
returns true iff A is symmetric.

Tridiagonal(A:Matrix) :Boolean
returns true iff A is tridiagonal.

Diagonal(D:Matrix) : Boolean
returns true iff D is diagonal

CIExpan expresses the fact that if an atomic basis set for a specified atom is used in the construction of a Hamiltonian matrix and the eigenvectors of that matrix are found, then the atomic basis and the eigenvectors can be used to construct a CI expansion for the specified atom.
EValue expresses the fact that if an orthogonal transformation is applied to a matrix, resulting in a diagonal matrix, then the diagonal matrix contains, on its diagonal, the eigenvalues of the original matrix.
EVector expresses the fact that if an orthogonal transformation is applied to a matrix, resulting in a diagonal matrix, then the columns of the orthogonal matrix contain the eigenvectors of the original matrix.
Otransform expresses the fact that applying two orthogonal matrices P and Q to a matrix A in sequence is the same as applying the product of P and Q to the matrix A.
Oproduct expresses the fact that the product of two orthogonal matrices is orthogonal.
Osize expresses the fact that if the matrices A, P and T are related through an orthogonal transformation then they are all of the same size.
Asize expresses the associative property that if matrix A is the same size as matrix B and matrix B is the same size as matrix C then matrix A is the same size as matrix C.

Figure 3

The production rule set for the operations rigorously specified in figure 1.

Multiply:
  if
    A:Matrix and B:Matrix and len(A:Matrix) = len(B:Matrix)
  then
    C:Matrix and AB = C

Tridiagonalise:
  if
    A:Matrix and Symmetric(A:Matrix)
  then
    T:Matrix and P:Matrix and
    $P^TP = I$ and $P^TAP = T$ and
    Tridiagonal(T:Matrix) and Symmetric(T:Matrix)

Householder:
  if
    T:Matrix and
    Tridiagonal(T:Matrix) and Symmetric(A:Matrix)
  then
    D:Matrix and
    $\exists Q \in \text{Matrix} \cdot (Q^TQ = I \text{ and } Q^TTQ = D)$ and Diagonal(D)

InverseIteration:
  if
    T:Matrix and D:Matrix and Symmetric(T) and Diagonal(D) and
    $\exists R \in \text{Matrix} \cdot (R^TR = I \text{ and } R^TTR = D)$
  then
    Q:Matrix and $Q^TQ = I$ and $Q^TTQ = D$

GetAtomBasisSet:
  if
    A:Atom
  then
    ABS:AtomBasisSet and
    AtomBasis(A:Atom; ABS:AtomBasisSet)

CreateHamiltonian:
  if
    ABS:AtomBasisSet
  then
    H:Matrix and HamiltonianMatrix(ABS:AtomBasisSet; H:Matrix)
    and Symmetric(H:Matrix)

Figure 4
Type rules required to augment the rule set.

CIExpan:
  if
    AtomBasis(A:Atom; ABS:AtomBasisSet) and
    HamiltonianMatrix(ABS:AtomBasisSet; H:Matrix) and
    EigenVectorOf(H:Matrix; E:Matrix)
  then
    CIExpansion(A:Atom; ABS:AtomicBasisSet; E:Matrix)
EValue:
  if
    $X^TX = I$ and $X^TAX = D$ and Diagonal(D:Matrix)
  then
    EigenValueOf(A:Matrix; D:Matrix)
EVector:
  if
    $X^TX = I$ and $X^TAX = D$ and Diagonal(D:Matrix)
  then
    EigenVectorOf(A:Matrix; X:Matrix)
Otransform:
  if
    $P^TP = I$ and $Q^TQ = I$ and
    $P^TAP = T$ and $Q^TTQ = R$ and $E = PQ$
  then
    $E^TAE = R$
Oproduct:
  if
    $P^TP = I$ and $Q^TQ = I$ and $E = PQ$
  then
    $E^TE = I$
Osize:
  if
    $E^TAE = R$
  then
    len(A:Matrix) = len(E:Matrix) and
    len(A:Matrix) = len(R:Matrix)
ASize:
  if
    len(A:Matrix) = len(B:Matrix) and
    len(B:Matrix) = len(C:Matrix)
  then
    len(A:Matrix) = len(C:Matrix)

3.4 The production system

A production system consists of a rule set, a rule interpreter which decides which rules to apply and when, and a working memory (WM) to hold data, goals and intermediate results. In this section we illustrate the execution of an idealised production system. The strategies used by rule interpreters are well known and will not be considered here (see for example (6)). Rather, we concentrate on what happens to the WM as each rule is fired and show how the initial goal is achieved. The rule set is defined by the rules given in figures 3 and 4. The goal we wish to achieve is expressed by the rule

```
goal:
    if
        CIExpansion(A:Atom; ABS:AtomicBasisSet; E:Matrix)
    then
        HALT
```

which is added to the rule set. The command HALT terminates execution of the inference engine. The WM is initialised with the fact A:Atom = Hg. Throughout we underline an item to indicate it is the variable's instantiated value. The contents of the WM during execution is illustrated by figure 5. It is partitioned into two sections: one holding facts and the other holding properties. Each fact and property is numbered to identify the step at which it was added to the WM.

In step 1 the WM is initialised. When execution begins only the antecedent of the rule, *GetAtomBasisSet*, can be matched by the single fact in the WM. This causes the rule to fire and its consequents to be added to the WM. The instantiated value of ABS is an example of a *Skolem* constant. (A Skolem constant is normally used to replace an existentially quantified variable in a predicate.) The actual value of ABS is of no interest to us. We choose to instantiate it to the unique but arbitary value ABS1.

Next to fire is rule *CreateHamiltonian*, the antecedent of which is matched by fact 2. The consequents of this rule cause fact 3 and properties 3a and 3b to be added to the WM.

The current state of the WM permits only rule *Tridiagonalise* to fire next, its antecedent being matched by fact 3 and property 3b. When the rule is fired facts 4a and 4b and properties 4a, 4b, 4c, and 4d are added to the WM.

At this point it is possible for the rules *Osize* and *Householder* to fire. We assume that rule interpreter's conflict resolution strategy causes the *Householder* rule to fire first. *Householder*'s antecedent is matched by fact 4a and properties 4c and 4d. The second consequent of this rule states the property of some matrix Q. It is important to note that Q is not computed by the operation nor is it passed as output.

Figure 5
The Working Memory (WM) partitioned into facts and properties

	Facts		Properties
1	A:Atom = Hg	2	AtomBasis(Hg; ABS1)
2	ABS1:AtomBasisSet	3a	HamiltonianMatrix(ABS1; H1)
3	H1:Matrix	3b	Symmetric(H1)
4a	T1: Matrix	4a	$P1^T P1 = I$
4b	P1: Matrix	4b	$P1^T H1 P1 = T1$
		4c	Tridiagonal(T1)
		4d	Symmetric(T1)
5	D1: Matrix	5a	$Q1^T Q1 = I$ and $Q1^T T1 Q1 = D1$
		5b	Diagonal(D1)
6	Q2: Matrix	6a	$Q2^T Q2 = I$
		6b	$Q2^T T1 Q2 = D1$
		7a	len(P1) = len(H1)
		7b	len(H1) = len(T1)
		8a	len(Q2) = len(T1)
		8b	len(T1) = len(D1)
		9	len(P1) = len(T1)
		10	len(Q2) = len(P1)
		11	len(P1)=len(Q2)
12	C1: Matrix	12	C1 = P1Q2
		13	$C1^T H1 C1 = D1$
		14	$C1^T C1 = I$
		15	EigenVectorOf(H1; C1)
		16	CIExpansion(Hg; ABS1; C1)

However, it is required in order to establish a property of the output matrix D. As such, this existentially quantified matrix, which is another example of a Skolem constant, is not recorded in the facts part of the WM, but only in the properties part.

The state of the WM now makes it possible for rule *InverseIteration* to fire. The antecedents of this rule are matched by: fact 4a and property 4d; fact 5 and property 5b; and by property 5a. The consequents cause fact 6 and properties 6a and 6b to be added to the WM.

Next to fire is type rule *Osize*. First, it fires using property 4b to establish properties 7a and 7b. Then using property 6b, properties 8a and 8b are established. The type rule *Asize* now fires three times. First, using properties 7a and 7b, and then using properties 8a and 8b the properties 9 and 10 are added to the WM. On the third firing property 11, that P1 and Q2 are the same size, is deduced. Facts 4b and 6 and property 11 permit ***Multiply*** to be invoked, resulting in fact 12 and property 12 being added to

the WM.

The antecedents of *Otransform* are matched by properties 4a, 6a, 4b, 6b, and 12 and result in property 13 being added to the WM.

The type rule *Oproduct* uses properties 4a, 6a, and 12 to establish property 14. The antecedents of the type rule *EVector* can now be matched by properties 14, 13, and 5b. This causes the rule to fire and add property 15 to the WM. The penultimate rule to be matched is *CIExpan*. Its antecedents are matched by properties 2, 3a and 15 resulting in property 16 being added to the WM. Finally, property 16 causes the goal rule to fire and execution to terminate.

By recording each rule which successfully fires, together with those rules whose consequents enable it to fire, we can construct a directed graph of operations which, if executed, will compute the specified goal. In this simple example the graph is a straight line of operations resulting in the following procedure calling sequence:

GetAtomBasis(Hg, ABS)→ CreateHamiltonian(ABS, H)→
Tridiagonalise(H, T, P)→ Householder(T, D)→
InverseIteration(T, D, Q)→ Multiply(P, Q, E)

The instantiated varaibles ABS and E can then be used to construct the CI expansion for Hg.

4 Summary

In the OpenMol program (1) proposed by Diercksen and Hall numerical software is developed using the ADT model. This methodology facilitates the construction of well engineered software which is relatively easy to maintain and extend. In addition, Diercksen and Hall argued that it has a further advantage. They observed that there is a close relationship between an ADT and a production rule. They suggested that by capturing knowledge about ADTs in a production rule set it would be possible to develop a rule-based expert system which, given some quantum chemical property or process as a goal, could devise a strategy to compute the desired property or process.

In this paper we have explored their observation in greater depth. We have shown that this relationship must involve both the syntactic and semantic information of an ADT operation. We have illustrated that a convenient way to capture the syntax and semantics of an ADT operation is to use a formal specification notation based on predicate logic. By specifying ADT operations using pre- and post-conditions we have shown informally that a mapping can be established between a formally specified ADT and the antecedent and consequent parts of a production rule. We have further shown that including only rules which correspond to each of an ADTs op-

erations is unlikely to produce a useful and flexible expert system. Further type rules are required which represent knowledge about the algebra of the ADT types.

Finally, we illustrated the operation of a goal directed inference system. We showed how its WM must be partitioned into two parts. One partition contains instantiated variables which represent the current state of the ADTs while the other records currently established properties. The role of Skolem constants in the WM was also highlighted.

Throughout this paper we have used an idealised notation for both the ADT operations and the production rules. In the formal specification of the ADT operations we have used a notation in the style of VDM-SL (5) but supplemented it with conventional mathematical notation. We have also made liberal use of auxiliary functions to mask inessential detail. Further work is underway to explore in detail the development of a suitable and consistent notation which will permit ADT specifications to be recast in the notation of a powerful expert system such as CLIPS (6); and to investigate a means of constructing and analysing the directed graph referred to in section 3.

5 Acknowledgements

NSS wishes to thank GHF Diercksen for stimulating discussions on the use of ADTs in the OpenMol project and for his encouragement and support while NSS was an AvH Research Fellow at the Max-Planck Institut für Astrophysik, München during which the seeds of this paper were developed. NSS gratefully acknowledges a Research Fellowship from the Alexander von Humboldt Foundation and support from the EPSRC (grant GR/J70307) and the British Council/DAAD ARC programme. The authors wish to thank Professor M Clint for stimulating and elucidating conversations on numerous aspects of formal specification notations.

References

[1] G. H. F. Diercksen and G. G. Hall, Computers in Physics **8**, 215 (1993).

[2] J. Guttag, Commun. ACM **20**, 396 (1977).

[3] N. S. Scott, P. L. Kilpatrick and D. Maley, Comp. Phys. Commun. **84**, 201 (1994).

[4] D. Maley, P. L. Kilpatrick, E. W. Schreiner, N. S. Scott and G. H. F. Diercksen, D. Comp. Phys. Commun. In press (1996).

[5] J. Dawes. *The VDM-SL Reference Guide*, Pitman: London, 1990.

[6] L. Brownston, R. Farrell, E. Kant and N. Martin, *Programming expert systems in OPS5*, Addison-Wesley: Reading, Mass, 1985.

Index

C

D

E

F

G

H

I

K

L

M

N

Q

R

S

T

U

V

W